Processing of oxide bonded porous silicon carbide ceramic membrane for microfiltration applications

Thesis Submitted to Jadavpur University in Partial Fulfilment of the Requirements for the Degree of Doctor of Philosophy (Science)

By
Dulal Das
(Index No. 20/19/Chem./26 dated 14.08.2019)

Membrane and Separation Technology Division
CSIR-Central Glass and Ceramic Research Institute
196, Raja S. C. Mullick Road, Jadavpur,
Kolkata-700 032, India
2022

सीएसआईआर - केन्द्रीय काँच एवं सिरामिक अनुसंधान संस्थान
196, राजा एस सी मल्लिक रोड, कोलकाता - 700 032, भारत
CSIR - CENTRAL GLASS & CERAMIC RESEARCH INSTITUTE
196, Raja S C Mullick Road, Kolkata - 700 032, India

CERTIFICATE FROM THE SUPERVISOR

This is to certify that the thesis entitled "**Processing of oxide bonded porous silicon carbide ceramic membrane for microfiltration applications**" submitted by Mr. Dulal Das who got his name registered on 14th August, 2019 (Ref. No. D-7/SC/784/19 and Index no. 20/19/Chem./26) for the award of Ph.D. (Science) degree of Jadavpur University, is absolutely based upon his own work under the supervision of Dr. Nijhuma Kayal and that neither this thesis nor any part of it has been submitted for either any degree/diploma or any other academic award anywhere before.

Nijhuma Kayal 19/04/2022

(Dr. Nijhuma Kayal)
Principal Scientist
Membrane & Separation Technology Division
CSIR-Central Glass and Ceramic Research Institute
196, Raja S. C. Mullick Road, Kolkata-700032

Dr. Nijhuma Kayal
Principal Scientist
CSIR- Central Glass and Ceramic Research Inst.
196, Raja S.C. Mullick Road
Kolkata-700032

.....

(Signature of Supervisor date with official seal)

Declaration

I, Dulal Das, declare that the work contained in this thesis is original and has been done by myself under the guidance of Dr. Nijhuma Kayal at CSIR-CGCRI Kolkata. The work has not been submitted to any other Institute for degree or diploma. I have followed the Institute norms and guidelines and abide by the regulation as given in the Ethical Code of Conduct of the Institute. Whenever I have used materials (data, theory and text) from other sources, I have given due credit to them by citing them in the text of the thesis and giving their details in the reference section.

Date: 19/04/2022

Dulal Das
Dulal Das

DEDICATED TO MY FAMILY

Acknowledgement

This thesis is a testament to my long, strenuous journey towards receiving the Ph.D. degree. The journey was not solely an individual effort, but nurtured in the reinforcing interactive medium made by numerous people including my family, well-wishers, friends and colleagues of different organizations. Accordingly, at the onset, it is a pleasant task to express my thanks to all those who contributed in many ways to the success of this endeavour and made it a memorable experience for me.

Firstly, I would express my sincere gratitude to my research supervisor, Dr. Nijhuma Kayal, Principal Scientist, CSIR-Central Glass and Ceramic Research Institute (CSIR-CGCRI), Kolkata for giving me an opportunity to work under her guidance. I greatly appreciate her tireless support and encouragement throughout the research work. Her valuable guidance, constant encouragement, novel scientific ideas, inspiration, keep interest and good wishes are going to be a monitoring tool throughout my life. This feat was possible only because of the unconditional support provided by Mam. I believe that her spacious guidance and consistent way of thinking will help me throughout my research work.

I would also like to thank my Research Advisory Committee (RAC) members Dr. Subrata Dasgupta, Dr. Chittaranjan Sinha, Dr. Swapan Kumar Bhattacharya for their valuable time, suggestion and helpful discussions. I would like to thank former and present head of Membrane & Separation Technology Division, CGCRI.

I take this opportunity to gratefully acknowledge the Department of Science and Technology (DST), Government of India, for providing financial assistance which helped me to perform my work comfortably.

I must express my gratitude to former director Dr. K. Muraleedharan, and present director Dr. Suman Kumari Mishra, CSIR-Central Glass and Ceramic Research Institute for their continuous support and constant encouragement.

I thank Prof. M.D.M. Innocentini, (University of Ribeirao Preto, Brazil) for the help with the air permeation and water filtration experiments.

I would like to thank all the scientific and technical staff at NOCCD, CMD and MSTD divisions, CSIR-CGCRI, for their kind support on experimental set up which helped me to complete the thesis successfully. I have been extremely fortunate to have lab mates and friends especially Sanchita Di, Hasmat Da, Srikrishna, for their encouragements, spontaneous cooperation and sharing of knowledge have been instrumental in shaping my efforts into success. I wish all of them every success in their days ahead.

I gratefully acknowledge the service rendered by the technical staff especially Nitai Da, Ashoke Da, Dolui Da, of Material Characterization Division, CSIR-CGCRI, Kolkata.

My special thanks go to my best friends Aloke, Prabhas, Arup, Biswajit, Uma, Ipsita, Surajit, Tapas, Malobi for their valuable suggestions in difficult times, precious motivations and everlasting support.

Finally, special thanks are due to my family for their cooperation, encouragement and constant prayer for my success. Words cannot articulate how appreciative I am to my mother Manju Bala Das, my father Ratan Das, my sister Dipti, my brother Srimanta and Basudev for all the sacrifices they made on my behalf.

I apologize for inadvertent omission of reference of any one, who has contributed directly or indirectly towards the completion of my thesis work.

List of Author's Publications

List of publication included in this thesis

1. D. Das, N. Kayal, G.A. Marsola, D.G.P. Filho, M.D.M. Innocentini, Recycling of coal fly ash for fabrication of elongated mullite rod bonded porous SiC ceramic membrane and its application in filtration, J. Euro. Ceram. Soc., 40(5), 2163-2172, 2020. (IF- 5.302)
2. D. Das, N Kayal, M.D.M. Innocentini, Permeability behavior and wastewater filtration performance of mullite bonded porous SiC ceramic membrane prepared using coal fly ash as sintering additive, Trans. Ind. Ceram. Soc., 80(3), 186-192, 2021. (IF-1.729)
3. D. Das, N. Kayal, G.A. Marsola, D.G.P. Filho, M.D.M. Innocentini, Permeability behavior of silicon carbide-based membrane and performance study for oily wastewater treatment, Int. J. App. Ceram. Tech., 17(3), 893-906, 2020. (IF-1.968)
4. D. Das, N. Kayal, D.G.P. Filho, M.D.M. Innocentini, Effect of processing parameters on mullite bonded SiC membrane for turbid water filtration, Membr. Water Treat., 12(3), 133-138, 2021. (IF-1.0)
5. D. Das, S. Baitalik, N. Kayal, Properties of multiple oxide- bonded porous SiC ceramics prepared by an infiltration technique, Int. J. App. Ceram. Tech., 17(2), 476-483, 2020. (IF-1.968)
6. D. Das, N. Kayal, The Effect of Bond Phase Additive and Sintering Temperature on the Properties of Mullite Bonded Porous SiC Ceramics, Mat. Sci. Forum, 978, 2020. (IF-0.55)
7. D. Das, N. Kayal, Influence of fly ash and steam on microstructure and mechanical properties of oxide bonded porous SiC ceramics, Bol. Soc. Esp. Ceram. V, 58(6), 255-262, 2019. (IF-2.383)
8. D. Das, N. Kayal, Thermal shock resistance of porous silicon carbide ceramics prepared using clay and alumina as additives, Trans. Ind. Ceram. Soc., 78(3), 165-172, 2019. (IF-1.729)

List of publications not included in thesis

1. D. Das, N. Kayal, Permeability and dust filtration behavior of porous SiC ceramic candle filter, Mat. Today Proceed., 39, 1235-1240, 2021. (IF- 1.24)

2. D. Das, N. Kayal, Influence of clay content on microstructure and flexural strength of in situ reaction bonded porous SiC ceramics, Mat. Today Proceed., 33, 5150-5155, 2020. (IF-1.24)
3. P. Sardar, D. Das, N. Kayal, Processing of Si-Mo-SiC composite by infiltration of silicon metal alloy into coir fiber derived bio-preform, Mat. Today Proceed., 21, 1069-1077, 2020. (IF-1.24)
4. D. Das, N. Kayal, Review on oxide bonded porous SiC ceramics: processing, properties and applications, J. Mater. Sci. Res. Rev., 1-25, 2018.
5. D. Das, N. Kayal, Advancement of oxide bonded porous SiC ceramics, Edited by Y. Gan, New Advances in Materials Science and Engineering Vol. 2, Book Publisher International, 2020.

List of abstracts/full paper presented in Conferences

1. D. Das, N. Kayal, Acid and alkali corrosion of porous silicon carbide ceramic membrane (CORCON-2018), 30th Sept.- 3rd Oct. 2018 at Jaipur, Rajasthan, India.
2. D. Das, N. Kayal, The effect of bond phase additive and sintering temperature on the properties of mullite bonded porous SiC ceramics (ICPCM–2018), December 6th - 8th, 2018 at NIT Rourkela, Orissa, India.
3. D. Das, N. Kayal, Thermal shock resistance of porous silicon carbide ceramics prepared using clay and alumina as additives, 82th Annual Session of Indian Ceramic Society, January 9th - 10th, 2019 at Jamshedpur, India.
4. P. Sardar, D. Das, N. Kayal, Processing of Si-Mo-SiC composite by infiltration of silicon metal alloy into coir fibre derived bio-preform (ICRACM-2019), February 25th- 28th, 2019 at IIT BHU, Varanasi, India.
5. D. Das, N. Kayal, Influence of clay content on micro structure and flexural strength of in situ reaction bonded porous SiC ceramics (ICPCM–2019), December 12th-14th, 2019 at NIT Rourkela, Orissa, India.
6. D. Das, N. Kayal, Fabrication of porous SiC ceramic membrane utilizing waste fly ash (RECYCLE-2020), February 12th-13th, 2020 at IIT Guwahati, Assam, India.
7. D. Das, N. Kayal, Processing of oxide bonded porous silicon carbide ceramic membrane for treatment of oily waste water, International Online Congress on Membranes and Membrane Assisted Processes (ICMMAP 2021) from 12th -14th February 2021 held in Mahatma Gandhi University, Kottayam, Kerala, India.

Table of Contents

Cover page

Certificate from the supervisor

Acknowledgement *i-ii*

List of publications *iii-iv*

List of contents *v-vii*

List of figures *ix-xiv*

List of Tables *xv-xvi*

List of symbols and abbreviations *xvii-xviii*

Abstract *1-4*

Chapter 1: Introduction *5-11*

Chapter 2: Literature Review *12-69*

2.1. Overview on porous materials *14*

2.2. Properties and application of porous ceramics *14-15*

2.3. Properties of ceramic materials *16*

2.3.1. Silicon Carbide (SiC) *16-17*

2.3.1.1. Structure of SiC (polymorphs and polytypes) *17-19*

2.3.1.2. Properties of SiC materials *19*

2.3.1.3. Effect of impurities on the properties of SiC materials *20*

2.4. Sintering methods for fabrication of dense SiC ceramics *21-22*

2.5. Processing routes of fabrication of porous SiC ceramics *22-26*

2.5.1. Partial Sintering *26-29*

2.5.2. Replica Method *29-33*

2.5.3. Sacrificial template method *33-35*

2.5.4. Direct foaming method *35-36*

2.5.5. Reaction Bonding Method *36-40*

2.6 Secondary Bonding Phase *41*

2.6.1. Mullite *41*

2.6.1.1. Preparation of mullite by powder mixing method *41*

2.6.1.2. Sol-gel method *41*

2.6.1.3. Structure of mullite *42*

2.6.1.4. Properties of mullite *43*

2.6.2. Cordierite ($5SiO_2.2Al_2O_3.2MgO$) *44*

2.6.2.1. Preparation of cordierite by powder mixing method *44*

2.6.2.2. Sol-gel method *44*

2.6.2.3. Structure of cordierite *44-45*
2.6.2.4. Properties of cordierite *45*
2.7. Application of oxide bonded porous SiC ceramics *46*
2.7..1. Hot Gas Filtration *46-47*
2.7..2. Wastewater Filtration *47-50*
2.7.2.1. Dead-end Filtration *50*
2.7.2.2. Cross-flow Filtration *50*
2.7.3.3. Hybrid-flow Filtration *51*
Chapter 3: Objectives *70-72*
Chapter 4: Experimental Procedure *73-101*
4.1. Selection of raw materials and their characterizations *75*
4.1.1. Selection of SiC powder *75*
4.1.2. Alumina *76*
4.1.3. Fly ash *76-77*
4.1.4. Selection of pore formers *78-80*
4.2. Preparation of porous SiC ceramics *80*
4.2.1. Preparation of porous SiC powder compacts by powder mixing methods *80*
4.2.2. Selection of secondary oxide bond phases *81*
4.3. Preparation of secondary cordierite bond phase precursor in sol form *82*
4.3.1. Cordierite sol preparation and Methods and Instruments used to characterize precursor sol *82*
4.3.1.1. Zeta sizer for measurement of particle size and Zeta potential *83*
4.3.1.2. Rheometer for measurement of rheological properties *83*
4.3.2. Incorporation of secondary bond phase into SiC ceramics by infiltration technique *83-84*
4.4. Preparation of samples for mechanical analyses *84*
4.5. Corrosion study *84*
4.6. Thermal shock study *85*
4.7. Methods and Instruments used to characterize ceramic powder and ceramic materials *85*
4.7.1. Determination of dimensional changes *85*
4.7.2. Determination of density and porosity *85-86*
4.7.3. Estimation of % SiC oxidation degree and theoretical calculation the amount of different phases for oxide bonded porous SiC ceramic samples *86*

4.7.3.1. Estimation of % SiC oxidation degree *86*
4.7.3.2. Prediction of porosity and amount of bond phases present in oxide bonded porous SiC ceramic sample *86-87*
4.7.4. X-ray diffraction (XRD) analysis *87-88*
4.7.5. Field Emission Scanning Electron Microscopy (FESEM) and elemental mapping and Energy Dispersive X-ray Spectroscopy (EDS) analyses *88*
4.7.6. Three point flexural bending strength and Young modulus measurement *88-89*
4.7.7. Pore size distribution (PSD) analysis *89*
4.7.8. Differential scanning calorimetric (DSC), differential thermal (DTA) and thermogravimatric (TG) analyses. *89*
4.8. Experimental procedure for measurement of air permeability *90*
4.8.1. Theoretical Background *90-91*
4.8.2. Experimental procedure *92*
4.9. Experimental procedure for measurement of water permeability *92*
4.9.1. Theoretical Background *92-95*
4.9.2. Experimental procedure for water filtration *95-96*
4.10. Preparation and Filtration of Kaolinite turbid water *97*
4.11. Collection and characterization of wastewater *98*
4.11.1. Determination of Chemical Oxygen Demand (COD) *98*
4.11.2. Measurement of TSS and TDS *98*
4.11.3. Quantitative estimation of oil and grease in sample water and permeate *99*
Chapter 5: Results and Discussions *102-189*
Chapter 5.1: Fabrication of mullite bonded porous SiC ceramic membrane utilizing solid waste fly ash as a source of bond phase additives
5.1.1. Effect of MoO_3 addition in the formation of secondary phases, porosity and density of mullite bonded porous SiC ceramics *106*
5.1.2. XRD analysis *107-109*
5.1.3. SEM analysis *109-112*
5.1.4. PSD analysis *112-113*
5.1.5. Mechanical properties *114*
5.1.6. Air permeability *114-116*
5.1.7. Water permeation study *116-118*
5.1.6. Waste water filtration study *118-120*

Chapter 5.2: Mullite bonded porous SiC ceramic membranes prepared using alumina as a bond forming additive and clay as sintering aid.

5.2.1.Effect of clay as a sintering additive in final SiC ceramics *124-127*

5.2.2. XRD study *127*

5.2.3. Microstructure analysis *128-129*

5.2.4. PSD analysis *130*

5.2.5. Air permeability behaviour of the porous SiC membrane *130-132*

5.2.6. Water permeability behaviour of the SiC membrane *132-133*

5.2.7. Wastewater filtration studies *134-135*

5.2.8. Turbidity removal studies from kaolinite water *136-138*

Chapter 5.3: Properties of multiple oxide - bonded porous SiC ceramics prepared by an infiltration technique

5.3.1. Characteristics of cordierite sol *142-144*

5.3.2. Cordierite sol infiltration *144*

5.3.3. Structural and physical characterization of porous ceramics *144-145*

5.3.4. XRD analysis *145-147*

5.3.5. SEM analysis *147*

5.3.6. Flexural strength analysis *148-149*

5.3.7. Permeability coefficients and pore related characteristics of porous SiC ceramics *149-151*

5.3.8. Filtration performance *151-155*

Chapter 5.4: The effect of sintering temperature and additives content on the chemical corrosion and thermal shock resistance properties of mullite bonded porous SiC ceramics.

5.4.1. Material properties of the porous SiC ceramic samples *158*

5.4.2. XRD analysis *159-162*

5.4.3. SEM analysis *162-164*

5.4.4. Pore size distribution analysis *165*

5.4.5. Mechanical strength analysis *165-167*

5.4.6. Effect of Thermal Shock on Mechanical Strength *167-171*

5.4.7. Effect of thermal shock on microstructure of porous materials *171-174*

5.4.8. Corrosion studies in presence of fly ash and steam *174-181*

Chapter 6: Conclusions and future scope *190-196*

6.1. Conclusions *192-195*

6.2. Future scope *196*

List of Figures

Figure 2.1.	*Typical images of (a) open-cell and (b) closed-cell configured porous ceramics*	*16*
Figure 2.2.	*Lattice sites of C of crystalline SiC viewed from [0001] direction. A, B, C represent positions in different bilayers.*	*18*
Figure 2.3.	*Stacking sequences of SiC polytypes in the [1120] plane.*	*19*
Figure 2.4.	*Schematic of sintering process in ceramics*	*21*
Figure 2.5.	*Schematic diagram of freequently used processing methods (a) partial sintering, (b) replica, (c) sacrificial template, (d) direct foaming, and (e) bonding techniques*	*24*
Figure 2.6.	*FESEM image of porous SiC ceramics showed the interconnected huge plate like grains produced by partial sintering method*	*28*
Figure 2.7.	*A radial (a) and an axial (b) microstructural view of the surface of typical wood-like porous SiC ceramic fabricated by partial sintering*	*29*
Figure 2.8.	*Typical SEM image of highly porous SiC ceramics fabricated via the replica technique: (a) Impregnated polyurethane sponges with SiC slurry to produce SiC foams (b) SiC foams produced by CVD process*	*31*
Figure 2.9.	*Image of SiC foams fabricated by chemical vapour deposition (CVD) of SiC on polymeric foams (Duocell ®, Auckland)*	*32*
Figure 2.10.	*Microstructures of highly porous SiC ceramics prepared with sacrificial templates: (a) SiC foams produced using polymer beads and SiC powders (b) SiC foam produced using polymer beads and polycarbosilane as a SiC precursor*	*34*
Figure 2.11.	*A representative microstructure of macro porous SiC ceramic prepared by direct foaming in which (a) azodicarbonamide is used as a blowing agent, (b) water vapour is used as a blowing agent*	*36*
Figure 2.12.	*Microstructures of oxide bonded porous SiC ceramics bonded through (a) silica and (b) mullite at the neck region.*	*38*
Figure 2.13.	*Projection of the ideal orthorhombic mullite unit cell which is associated with the formation of an oxygen vacancy and readjustment of oxygen in the O(3) positions.*	*42*

Figure 2.14.	*Three dimensional network of cordierite structure*	*45*
Figure 2.15.	*Efficiency of various separation processes*	*47*
Figure 2.16.	*Schematic diagrams of microfiltration, ultrafiltration, nanofiltration and reverse osmosis*	*49*
Figure 2.17.	*Photographs of commercially available flat sheet, tubular and hollow-fibre geometries for ceramic membranes.*	*50*
Figure 4.1	*SEM micrographs of two different SiC powders having different particle sizes.*	*75*
Figure 4.2	*XRD patterns of two different green SiC powders*	*75*
Figure 4.3	*Particle size distribution pattern of two different SiC powders used in this study*	*76*
Figure 4.4	*XRD pattern of industrial waste fly ash used in this study*	*77*
Figure 4.5	*(a) Particle size distribution, (b) TG-DTA and (c) XRD pattern of graphite powder used in this work.*	*79*
Figure 4.6	*TG-DTA pattern of (left) Polyvinyl chloride (PVC) and (right) Poly methyl methacrylate (PMMA) powder used in this work during air sintering.*	*80*
Figure 4.7	*(a) Pressing machine used for ceramic sample preparation (b) electrically heated high temperature used for preparation of ceramic samples*	*81*
Figure 4.8	*Sintering schedule of different powder compacts*	*81*
Figure 4.9	*Schematic flow chart of infiltration process used in present work*	*84*
Figure 4.10	*Three point bending flexural strength measurement test setup*	*89*
Figure 4.11	*Scheme of airflow permeation apparatus.*	*92*
Figure 4.12	*Details of the sample holder used in the airflow experiments.*	*92*
Figure 4.13	*Scheme of the water flow permeation apparatus.*	*96*
Figure 4.14	*Picture of the water permeation setup.*	*96*
Figure 5.1.1.	*XRD plot of SiC ceramics prepared using SiC and fly ash with (a) 0 (b) 1 (c) 3 and (d) 5 wt% MoO_3.*	*109*
Figure 5.1.2	*SEM micrographs of porous SiC samples prepared with different pore formers showing a) internal morphologies at low magnification and (b) mullite rods at high magnification.*	*111*

Figure 5.1.3	*EDX results showing elemental information of different phases obtained during SEM microscopy of sample without pore former (SF).*	*112*
Figure 5.1.4.	*Pore size distribution pattern of porous SiC ceramic membrane prepared with and without pore formers.*	*113*
Figure 5.1.5	*Permeation curves for SiC ceramic membranes with different porosities measured with airflow.*	*115*
Figure 5.1.6	*Maps of properties and applications of porous ceramics with location of SiC membranes SF, SF-G and SF-P: (a) porosity map adapted from Okada et al. (b) permeability map adapted from Vakifahmetoglu et al.*	*115*
Figure 5.1.7	*Plot of pure water flux against TMP for porous SiC membranes of different porosities.*	*117*
Figure 5.1.8	*Relative contribution on membrane resistance in the interval 0.3–2.5 bar*	*118*
Figure 5.1.9	*Evaluation of the effectiveness of different ceramic membranes for removing pollutant contaminants from wastewater*	*118*
Figure 5.1.10	*Photograph of wastewater filtered through porous ceramic membranes with varying porosities before and after filtering*	*119*
Figure 5.2.1.	*XRD pattern of porous SiC ceramics sintered at 1400℃ showing the effect of clay addition on phase formation*	*125*
Figure 5.2.2.	*XRD pattern of mullite bonded SiC ceramics*	*127*
Figure 5.2.3.	*Representative microstructures of SiC microfiltration membrane prepared at 1400°C in (A) low and (B) high magnification*	*129*
Figure 5.2.4	*EDX analysis of the marked region of fish scale shaped (A) cristobalite needle shaped (B) mullite crystal in SiC membranes*	*129*
Figure 5.2.5.	*Distribution of pores in mullite-bonded porous SiC sintered at 1400°C*	*130*
Figure 5.2.6	*Experimental air permeation curves for SiC membranes prepared with different pore formers*	*131*
Figure 5.2.7.	*Location of experimental k_1 and k_2 data of SiC membranes obtained in this work in a comprehensive permeability map, adapted from references*	*132*

Figure 5.2.8.	*Experimental water permeation curves for SiC membranes prepared with different pore formers*	*134*
Figure 5.2.9.	*Photographs of the permeate water after filtration through porous SiC membranes*	*135*
Figure 5.2.10.	*Photographs of different membranes after 300s of turbid water filtration.*	*136*
Figure 5.2.11.	*Variation of turbid water flux as a function of filtration time for porous SiC membranes*	*136*
Figure 5.2.12.	*Turbidity level for all membranes before and after 300s of filtration*	*137*
Figure 5.3.1	*Particle size distribution of cordierite sol*	*142*
Figure 5.3.2	*Viscosity v_s shear rate changes of cordierite sol*	*142*
Figure 5.3.3	*TG-DTA pattern of cordierite gel during heat treatment in air up to 1450°C*	*143*
Figure 5.3.4	*XRD pattern of cordierite powders obtained at 1400°C*	*144*
Figure 5.3.5.	*The pore size distribution patterns of SiC ceramics sintered in different temperatures with multiple oxide bonds*	*145*
Figure 5.3.6.	*XRD pattern of multiple oxide bonded SiC ceramics sintered at various temperature*	*146*
Figure 5.3.7.	*Microstructural view of multiple oxide bonded porous SiC ceramics sintered at 1400C showing porous network at lower magnification (L) and various morphologies at different areas at high magnification (R) and their EDX analysis results*	*147*
Figure 5.3.8.	*Flexural strength as a function of open porosity for the as prepared SiC ceramics sintered at various temperature*	*149*
Figure 5.3.9.	*Permeation curves for multiple oxide bonded porous SiC ceramics prepared at (a) 1300°C and (b) 1400°C*	*151*
Figure 5.3.10.	*Effect of individual collection mechanisms on collection efficiencies with dust particle sizes for the porous SiC ceramics prepared at 1400°C*	*154*
Figure 5.3.11.	*An estimate of the total single collector efficiency curve for porous SiC ceramics prepared at 1400°C*	*155*

Figure 5.4.1.	*Photograph of sintered SiC ceramics [MSC2 sintered at (a) 1500 (c) & (e) at 1400] and [MSC3 sintered at (b) 1500 (d) 1400 (e) 1450 ℃]*	*159*
Figure 5.4.2.	*XRD diffraction patterns of oxide bonded porous SiC ceramics prepared without, with alumina additives sintered at 1400 ℃ and pure SiC powder*	*160*
Figure 5.4.3.	*XRD pattern of mullite bonded porous SiC ceramic (MSC3) sintered at different temperature*	*161*
Figure 5.4.4.	*Microstructures of oxide bonded porous SiC ceramic (MSC3) sintered at (a) 1400 and (b) 1450 ℃*	*162*
Figure 5.4.5.	*High resolution microstructural view of oxide bonded porous SiC ceramic (MSC3) sintered at (a) 1400 and (b) 1450 ℃*	*163*
Figure 5.4.6.	*EDS analysis of different crystal phases formed different region (a) needle and (b) fish scale in MSC3 sample sintered at 1400 ℃*	*164*
Figure 5.4.7.	*Pore size distribution pattern of MSC1 and MSC2 ceramics sintered at 1400 ℃ in air*	*165*
Figure 5.4.8.	*Pore size distribution pattern of oxide bonded porous SiC ceramics of (a) MSC1 sintered at 1500^{o}C and (b) MSC3 sintered at 1300^{o}C*	*165*
Figure 5.4.9.	*Effect of alumina content on the mechanical strength of the oxide bonded porous SiC ceramics*	*166*
Figure 5.4.10	*Effect of quenching cycle on the flexural strength of (a) MSC2 and (b) MSC4 ceramic sample quenched at 1000 ℃ in presence of air medium*	*168*
Figure 5.4.11.	*Variation of mechanical strength with quenching cycles for MSC2 sample by air quenching method heated at 1000°C*	*169*
Figure 5.4.12.	*Flexural strength of (▽) MSC4 and (♦) MSC5 sample as a function of quenching cycle due to cooling in water at room temperature from 1000^{o}C*	*169*
Figure 5.4.13.	*Change of flexural strength for MSC1 sample as a function of quenching temperature in (♦) air and (▽) water medium*	*171*
Figure 5.4.14.	*Microstructural view of (a) MSC4 and (b) MSC2 samples after 4th thermal cycle of cooling in water from 1000^{o}C*	*172*

Figure 5.4.15.	*Fracture surface of MSC sample quenched in water from (a) 1000℃ and (b) 1200℃ to room temperature*	*172*
Figure 5.4.16.	*Fracture surface of (a) MSC1 and (b) MSC2 sample after 5th cycle of air quenching at 1000℃*	*173*
Figure 5.4.17.	*Effect of air quenching on XRD patterns of (a) MSC1 and (b) MSC5 samples quenched at 1000^{o}C.*	*174*
Figure 5.4.18.	*XRD pattern of fly ash received from industries (a) and calcined for 96 hours at 1000℃ (b)*	*175*
Figure 5.4.19.	*XRD pattern of MSC1 sample after corrosion with (a) steam, (b) ash, and (c) steam and ash. (Cr#cristobalite; m#mullite; s#SiC; C#alkaline alumina silicate)*	*176*
Figure 5.4.20.	*XRD pattern of MSC2 sample after corrosion for 96 h with (a) steam, (b) fly ash, (c) fly ash and steam*	*176*
Figure 5.4.21.	*XRD plot of (a) MSC1 and (b) MSC2 samples after corrosion for 240 h with steam and fly ash*	*177*
Figure 5.4.22.	*XRD pattern of (a) MSC1 and (b) MSC2 samples after corrosion for 240 h with steam*	*177*
Figure 5.4.23.	*SEM images of top surface of sample (a) MSC1 and (b) MSC2 after exposure at 1000℃ for 96 h covered with fly ash*	*178*
Figure 5.4.24.	*SEM images of corroded sample (a) MSC1 and (b) MSC2 in presence of steam for 96 h*	*179*
Figure 5.4.25.	*Microstructural view of top surfaces of filter material (a) MSC1 and (b) MSC2 after corrosion in presence of fly ash and steam for 96h*	*179*
Figure 5.4.26.	*Pore size distribution pattern of MSC1 sample after corrosion in presence of (a) fly ash and steam, and (b) steam*	*180*

List of Tables

Table 2.1.	*Different SiC polytypes stacked in the C-direction with their respective physical parameters.*	*18*
Table 2.2.	*General properties of SiC bulk materials*	*19*
Table 2.3.	*Different sintering techniques were used to fabricate dense SiC ceramics by several researchers.*	*22*
Table 2.4.	*The conventional processing techniques, sintering conditions and characteristics of the porous SiC ceramics*	*25*
Table 2.5.	*Influence of sintering additives and processing parameters on the properties of porous SiC ceramics obtained by reaction bonding technique*	*40*
Table 2.6.	*Refractory properties of mullite*	*43*
Table 2.7.	*Refractory properties of cordierite*	*45*
Table 4.1.	*Characteristics of raw powders used in the present work*	*78*
Table 4.2.	*The basic properties of the SiC and the secondary bond phases used to bind the SiC particles*	*82*
Table 4.3.	*The raw materials used for the preparation of cordierite sol*	*83*
Table 4.4.	*Test conditions used for corrosion analyses*	*85*
Table 5.1.1.	*Characteristics of mullite bonded SiC ceramic membranes sintered at 1000°C*	*107*
Table 5.1.2.	*Effect of MoO_3 content on crystalline phases of porous SiC ceramic membranes prepared using SiC and fly ash in a weight ratio of 0.8:0.2*	*109*
Table 5.1.3.	*Comparison of airflow permeability and pore size data for the samples prepared with different pore formers*	*116*
Table 5.1.4.	*Comparison of the performance of the ceramic membrane reported in the literature*	*120*
Table 5.2.1.	*Effect of clay content on phase composition and flexural strength*	*124*
Table 5.2.2.	*Characteristics of porous SiC ceramic membranes*	*126*
Table 5.2.3.	*Rietveld analysis results of porous SiC ceramics*	*128*
Table 5.2.4.	*Effect of various pore former on the permeability coefficient value and pore size for as prepared SiC membranes obtained during air permeation*	*131*

Table 5.2.5.	*Specific permeability (SP), membrane resistance (R_m) and permeability values obtained for tested membranes in the water flow experiments*	*133*
Table 5.2.6.	*Characterization of wastewater before and after filtration by the ceramic membranes*	*135*
Table 5.2.7.	*Performance parameters of prepared SiC membranes for turbidity removal*	*138*
Table 5.3.1.	*Rietveld phase analysis of multiple oxide bonded porous SiC ceramics sintered at 1300-1400°C*	*147*
Table 5.4.1.	*Final composition of different samples*	*158*
Table 5.4.2.	*Rietveld analysis data of sintered SiC ceramics*	*160*
Table 5.4.3.	*Calculation of the crystalline phases for sintered samples at variable temperatures*	*162*
Table 5.4.4.	*Effect of corrosion media on the mass and porosity of the filter materials*	*175*
Table 5.4.5.	*Quantitative estimation of the crystalline phases after corrosion with steam in presence or absence of fly ash for 96 h*	*178*
Table 5.4.6.	*Effect of corrosion on the room temperature mechanical strength of the filter materials after corrosion for 96 h*	*181*

List of Abbreviations

ADCA	*Azodicarbonamide*
CFV	*Cross flow velocity*
CIP	*Cold isostatic pressing*
COD	*Chemical oxygen demand*
COF	*Covalent organic framework*
CVD	*Chemical vapour deposition*
GOF	*Goodness of the fit*
IGCC	*Integrated gasification combined cycle*
MF	*Microfiltration*
MOF	*Metal organic framework*
NF	*Nanofiltration*
PCS	*Poly carboxysiloxane*
PD	*Pressure decay*
PFBC	*Pressurized fluidized bed combustion*
PMMA	*Poly methyl methacrylate*
PVC	*Poly vinyl chloride*
RO	*Reverse osmosis*
SiC	*Silicon carbide*
SOFC	*Solid oxide fuel cell*
SP	*Specific permeability*
TDS	*Total dissolved solid*
TMP	*Transmembrane pressure*
UF	*Ultrafiltration*

List of Symbols

A_{flow}	*Flow area (m^2)*
A_S	*Happel's parameter*
d_{pi}	*Nanoparticle dust size (m)*
d_{pore}	*Average fluid dynamic pore size (m)*
E	*Collection efficiency*
F_o	*Forchheimer number*
J	*Flux ($Lm^{-2}h^{-1}$)*
k_1	*Darcian permeability constant (m^2)*
k_2	*Non-Darcian permeability constant (m)*
k_B	*Boltzmann constant ($m^2\ kg\ s^{-2}\ K^{-1}$)*
L	*Sample thickness (m)*
MM_{air}	*Molar mass of dry air*
N_{Pe}	*Peclet number*
N_R	*Interception parameter*
N_{Re}	*Reynolds number*
N_{St}	*Stokes' number*

$N_{St,eff}$	*Effective Stokes number*
ΔP	*Pressure drop*
P_i	*Absolute fluid pressures at the entrance of the medium*
P_o	*Absolute fluid pressures at the exit of the medium*
Q	*Flow rate (m^3/s)*
R″	*Resistance to thermal shock damage*
R_h	*Hydraulic radius (m)*
R_m	*Membrane resistance*
T	*Absolute temperature (℃)*
TMP_i	*Initial transmembrane pressure*
v_s	*Fluid velocity ($m\ s^{-1}$)*
v_t	*Terminal settling velocity ($m\ s^{-1}$)*
x_{clay}	*Weight fraction of clay*
x_{pf}	*Weight fraction of pore former*
x_{SiC}	*Weight fraction of SiC*
Γ_f	*Critical strength of materials*

List of Greek Letters

ε	*Porosity (vol%)*
η	*Coefficient of viscosity (cP)*
η_D	*Single collector efficiency due to diffusion*
η_{DI}	*Single collector efficiency due to direct interception*
η_E	*Single collector efficiency due to electrophoresis*
η_G	*Single collector efficiency due to gravity*
η_I	*Single collector efficiency due to inertia*
η_T	*Total single collector efficiency*
λ	*Mean free path of gas molecules (m)*
μ	*Fluid viscosity ($kg\ m^{-1}\ s^{-1}$)*
ρ	*Fluid density ($kg\ m^{-3}$)*
σ	*Flexural strength (MPa)*
θ	*Contact angle (°)*
τ	*Tortuosity of the porous wick*
γ	*Surface energy or surface tension of the liquid (N/m)*

Abstract

Porous silicon carbide (SiC) ceramics has been considered as an excellent engineering materials for various industrial application such as diesel particulate filter, mechanical seals, petroleum refining, catalytic supports, chemical refining, hot gas & molten metal filters, gas turbine system, heat exchanger, wastewater filtration etc. due to its excellent porous structure with narrow pore size distribution, high temperature mechanical strength, high hardness, high thermal conductivity value, low thermal expansion coefficient, good thermal shock resistance, excellent corrosion resistance and thermal shock value etc. However, a major problem with SiC based non-oxide ceramic materials is their low sinterability due to their strong covalent bonds between C and Si. Depending on the application of porous SiC ceramics, various methods were used to fabricate porous SiC ceramics. In most of these methods SiC need to be sintered at very high temperatures using selective sintering additives, expensive atmospheres, costly equipment and delicate instrumentation. Recently porous SiC ceramics are produced by most simple and cost effective oxide bonding method. In oxide bonding technique porous SiC compact is heat treated in presence of air and during heat treatment the oxidised silica coming from the surface of SiC reacts with oxide additives (such as Al_2O_3, MgO, CaO etc.) to form secondary bond phases between SiC particles. Considering the cost of raw materials, ease and repeatability of formation including low temperature formation possibility of the bond phases the oxide bonds are very popular for SiC systems of materials, substantial research work has been initiated all over the globe for the development of oxide bonded porous SiC ceramics; still there are many unresolved issues that need further attentions. For example, the evolution of the bond phase and the chemical reactions responsible for bond phase formation and the influence of burning of any carbonaceous pore former on bond phase formation of SiC and the cost of the final ceramics are the major global unresolved issues. Finally, effects of the processing parameters on the material and mechanical properties, permeation behaviour and waste water filtration behaviour of porous SiC ceramics need systematic investigations. The beginning materials must be well dispersed with the sintering additive and the pore former in order to achieve significant filter performance improvements.

Inspired by these possibilities in this present thesis work, porous SiC ceramics bonded with silica and mullite phases were prepared by oxide bonding method at low temperature. In this work, SiC powder compact were prepared by taking desired amounts of SiC, Al_2O_3, Clay, Fly ash (source of bond phase additives) etc. powders. Different volume fractions of pore former

were used for generation of porosity. Sintering involves burning out the pore former at a temperature higher than that at which it burns (mostly at 800°C) in order to create pores. Temperature higher than 700°C, the SiC particles under slow oxidation, leading to formation of silica and with increase in temperature, the process become fast. At temperatures (1000 to 1400°C) oxidation derived silica reacted with Al_2O_3 to form silica, mullite, which bonds SiC particles together and produced a rigid porous body. Also in this study, cordierite precursor were incorporated in porous SiC compacts by using an infiltration technique and developed of oxide bonded porous SiC ceramics following a low temperature sintering method. The reasons behind the selection of these bond phase systems are their useful properties, such as high refractoriness, low thermal expansion coefficient nearly with SiC, low oxygen diffusion coefficient, low dielectric constant, good thermal and chemical stability etc. The effect of amount of sintering additives, metal catalyst, sintering temperatures, pore formers, on the bonding phase formation and the properties of the final ceramics are evaluated. Air permeability, pure water permeability and waste water filtration studied were also studied by using this ceramic membrane. The thermal shock and corrosion resistance properties were evaluated.

Mullite bonded SiC ceramic membranes were synthesized by recycling industrial waste fly ash as a source of bonding phase, SiC as raw materials, and MoO_3 as sintering catalyst for growth of mullite at 1000°C by oxide bonding method. To investigate the effect of MoO_3 catalyst on the mullitization reaction, microstructural and mechanical properties of the final ceramics, four different SiC ceramics compositions having different amount of MoO_3 content were prepared. In the final mixture three different pore forming agent were used to increase the porosity of the ceramics and observed its effects on the permeability parameters and filtration characteristics. To characterise material properties of the final ceramics porosity, density and % oxidation were evaluated. XRD, Rietveld, SEM mechanical properties and pore size distribution pattern were analysed in order to identify major phases with their content, morphologies, mechanical strength and pore diameters of porous SiC ceramics. The porosity, flexural strength and the pore size of the final ceramics were varied from ~36-45 vol%, ~38-28 MPa, and ~2.9-4.0 µm respectively. TG-DTA data indicated that the mullitization reaction had occurred at comparatively lower temperature at 1000°C in presence of MoO_3. From the air & water permeation study, the ceramics prepared in this work showed coefficient value k_1, k_2 and specific water permeability (SP) value in the range of 7.30×10^{-15} to 2.66×10^{-13} m^2, 1.18×10^{-11} to 2.63×10^{-8} m, and 1532 to 6113 $Lm^{-2}h^{-1}bar^{-1}$ respectively. The

membranes showed a high separation efficiency of oil, COD, TDS and turbidity of ~93-89%, ~92-82%, ~91-89% and ~94-91% from kitchen wastewater and also it showed high turbidity removal efficiency >99.5% from synthetically prepared kaolinite turbid water.

In another approach mullite-bonded porous SiC ceramics membranes also prepared using commercial SiC powder, alumina, alkaline oxide clay as sintering additives, and different sacrificial pore formers. The effect of pore formers on materials, microstructural properties, and air and water permeability of porous ceramic were investigated. A variation in porosity from 38-50 vol%, pore diameter 3.7- 6.5 μm, and flexural strength 28-38 MPa of the final ceramics were observed depending on the characteristics of the pore former. The Darcian (k_1) and non-Darcian (k_2) permeability evaluated from air permeation behaviour at room temperature was found to vary from 1.48×10^{-13} to 4.64×10^{-13} m^2 and 1.46×10^{-8} to 6.51×10^{-8} m, respectively. High oil rejection rates (89%-93%) were obtained by all membranes from feed wastewater containing 1557 mg/L oil. A very high pure water permeability of 13298 $Lm^{-2}h^{-1}bar^{-1}$ was obtained with membrane having porosity of 48 vol% and mechanical strength of 31.5 MPa.

To avoid the agglomeration of bond phase additives during powder processing method, another infiltration assisted method was considered to develop porous ceramics with homogeneous distribution of bond phases. Following infiltration technique, multi-oxide bonded porous SiC ceramics were prepared at 1300- 1400°C by sintering a powder compact of SiC and Al_2O_3, infiltrated with cordierite sol. The microstructures, phase components, mechanical properties and air permeation characteristics of multi-oxide bonded porous SiC ceramics were examined and compared with materials obtained via a powder processing route. A variation in sintering temperature affected porosity, average pore diameter, and flexural strength of the ceramics. For instance, porosity varied from 33 to 37 vol%, average pore diameter was ~12- 14 μm, and strength varied from 23-39.6 MPa. According to the X-ray diffraction results, both cordierite and mullite content increased with the increase in sintering temperature. Furthermore, the presence of alumina powder in the final ceramics improved strength due to the formation of mullite in the bond phase in contrast to the samples prepared without alumina. A single collector efficiency model was used to theoretically determine the particulate filtration efficiency of the developed ceramics. The result indicated that the material developed in this study have strong application possibilities in pollution control.

The impact of the amount of bond phase alumina additive and the sintering temperature on phase evolution, microstructure, pore size distribution, flexural strength, thermal shock resistance, and corrosion resistance properties of the in-situ mullite bonded porous SiC ceramics were also studied. The alumina content was varied from 5-10 wt%, and porous SiC ceramics were fabricated via reaction sintering at 1300-1500°C for 4h. Porous mullite bonded SiC ceramics prepared at 1400°C with 10 wt% alumina additive exhibited highest mechanical strength of ~ 58 MPa at porosity level ~27 vol%. Temperature-dependent thermal shock resistance of porous SiC ceramics due to cooling was evaluated as a function of quenching temperature (from 0°-1200°C) and quenching frequency (up to 10 cycles) using the air and water-quenching technique. A laboratory corrosion study of SiC ceramics was conducted at 1000°C for 96–240 hours in presence of steam, coal ash, and both steam and coal ash. With corrosion duration and medium, the apparent change in mass, porosity, and density was recorded. The corroded samples were evaluated with SEM, XRD, and mechanical tests and the results indicated water vapour is the perpetrator for strength degradation. Thermal and other corrosion results indicated that the material has strong application possibilities in hot gas filtration.

The oxide bonding technique and the utilization low cost starting materials were found to be an effective way synthesizes cost effective porous SiC membrane at lower temperature with improved mechanical, corrosion and thermal shock resistance properties. The methods developed in this study can be effectively utilized in the fabrication of porous SiC ceramics for various applications such as hot-gas filtration, wastewater filtration, catalytic support, etc.

Chapter 1

Introduction

Introduction

The combination of a large specific surface area, good mechanical properties, high thermal conductivity, and good chemical stability makes porous silicon carbide (SiC) ceramics an attractive material for structural and functional applications. Applications of porous SiC ceramics in some areas (such as porous burner, diesel particulate filtration in honeycomb structures, hot gas and molten metal filtration etc.) has been already exploited by industries or by researchers [1-3] but in some areas include wastewater filtrations, catalytic supports, acoustic and thermal insulators, high temperature structural materials, thermoelectric energy convertor, as a membrane for separation and in reinforcement of composites [4-9] etc. are still under research. However, one of the major obstacles to the widespread use of silicon carbide is the sinterability of SiC ceramics. Due to strong covalent nature of the C-Si bond, the diffusive process of sintering of SiC requires a very high temperatures (1800-2000°C) to sinter. Other difficulties includes requirement of complex precursors many of which are very expensive and not easily available, expensive atmosphere, costly dedicated instrumentation, etc. Recently porous SiC ceramics are produced using reaction bonding technique at low temperatures (800-1500°C). Various oxide as well as non-oxide bonds such as clays, phosphates, frits, alkali oxides, Si_3N_4 etc., are used for SiC ceramics and their uses are practiced in industries since long. However, oxide bonds are more popular than non-oxide bonds due to its processing advantages and cost factor. The common oxide bonds often suffers from softening at low temperatures, depletion and destabilization during service, cracking or spalling in very long processing times, etc. There is a possibility of binding SiC grains by secondary phases made of oxidation derived silica to form rigid porous ceramic bodies. The SiC ceramics synthesized by this technique exhibit good thermal and chemical stability because of formation of protective silica layer on SiC; the method requires low processing temperatures and air as the firing atmosphere and uses cheap commercial SiC powders of coarse grains in the starting mixtures; the method hence becomes very cost effective. In this technique formation of different types of oxide bonds for SiC is possible [10-11]. Silica becomes the most common bond for SiC [12]. Mullite ($3Al_2O_3.2SiO_2$) bonds for SiC can impart good thermal shock resistance, better high temperature stabilities and high oxidation and corrosion resistance [13-14]. The inexpensive cordierite ($2MgO.2Al_2O_3.5SiO_2$) with a low thermal expansion coefficient (~1.5×10^{-6}/°C) may also be an important bond for SiC [15-16]. In addition to the ability to synthesize the material at low temperatures, the material also has a low dielectric constant, good thermal stability, and good chemical stability [17].

Substantial research work has been initiated all over the globe for the development of oxide bonded porous SiC ceramics; a survey of literature indicates that the process of oxide bonding of porous SiC ceramics has many issues still not explored. The effects of bond phase compositions on the materials and mechanical properties of the porous SiC ceramics require systematic investigation; existing published literature does not reveal the specific role that the bond phase composition can play to control the microstructure, mechanical properties and water permeability behaviour. The relations between pore related characteristics of the oxide bonded porous SiC are not studied in depth. The effects of materials parameters (bond phase compositions, porosity, pore size and pore size distribution) on permeation behaviour of the SiC membranes prepare at low temperature requires to be studied. In the published literature, no research studies published in these directions. In literature very few studies are available on oxide bonded SiC MF membrane for wastewater treatment and hot gas filtration.

In this backdrop, in this present thesis work, a systematic investigations were carried out on the fabrication of porous oxide bonded SiC ceramics using optimum amount and cost effective raw materials, bonding additives and suitable pore former at comparatively lower sintering temperature. This investigation systematically investigated the morphology, the size distribution of pores, the air permeability, the corrosion resistance, the thermal shock resistance, and the filtration of SiC membranes. The proposed research also intends to harness the advantages of the low temperature oxide bonding technique for synthesis SiC MF membrane at low temperature with variations in pore sizes for oily wastewater filtration applications. For systematic description and discussion of entire work, the thesis has been divided into five chapters. The brief contents of different chapters have been described below:

Chapter-2	Literature Review	Introduction about porous ceramics and their properties and applications, Importance of porous SiC ceramics, a brief description on methods of processing porous SiC ceramics and their drawback, Importance of oxide bonding method and their limitations, Secondary oxide bond phases and their properties. Short description on different application areas.
Chapter-3	Objectives	Highlights the objectives of the thesis work
Chapter-4	Experimental Procedures	Detailed discussions on experimental procedure including selection of raw materials and their characteristics, Detail procedure of powder processing method and sol infiltration technique for development of oxide bonded SiC ceramics. Detail procedure and method of air and water permeation study. Wastewater filtration method and characterisation before and after filtration. Detail procedure and method of corrosion and thermal shock study.
Chapter-5	Results and Discussions	Material properties of oxide bonded (mullite, cordierite) porous SiC ceramics including porosity, density, volume change, pore diameter and degree of SiC oxidation; Microstructural and mechanical properties and their correlations; Identification and quantification of the crystalline phase in the final ceramics and their role on properties; Performance evaluation of the SiC membrane for treatment of wastewater treatment, air and pure water permeation behaviour; Evaluation of corrosion and thermal shock resistance properties of porous SiC ceramics
Chapter-6	Conclusions and future scope	Final conclusions of present study and future scope

References

1. J. Adler, Ceramic diesel particulate filters, Int. J. Appl. Ceram. Technol., 2 (2005) 429-439.
2. C.C. Agrafiotis, I. Mavroidis, A.G. Konstandopoulos, B. Hoffschmidt, P. Stobbe, M. Romero, V.F. Quero, Evaluation of porous silicon carbide monolithic honeycombs as volumetric receivers/collectors of concentrated solar radiation, Sol. Energy Mater Sol. Cells, 91 (2007) 474-488.
3. A. Ortona, S. Pusterla, P. Fino, F. Mach, A. Delgado, S. Biamino, Aging of reticulated Si-SiC foams in porous burners, Adv. Appl. Ceram., 109 (2010) 246-251.
4. K. Koumoto, M. Shimohigoshi, S. Takeda, H. Yanagida, Thermoelectric energy conversion by porous SiC ceramics, J. Mater. Sci. Lett., 6 (1987) 1453-1455.
5. T. Matsumoto, J. Takahashi, T. Tamaki, T. Futagi, H. Mimura, Y. Kanemitsu, Blue- green luminescence from porous silicon carbide, Appl. Phys. Lett., 64 (1994) 226-228.
6. A. Konstantinov, C. Harris, A. Henry, E. Janzen, Fabrication and properties of high-resistivity porous silicon carbide for SiC power device passivation, Mater. Sci. Eng. B, 29 (1995) 114-117.
7. N. Keller, C.P. Huu, S. Roy, M. Ledoux, C. Estournes, J. Guille, Influence of the preparation conditions on the synthesis of high surface area SiC for use as a heterogeneous catalyst support, J. Mater. Sci., 34 (1999) 3189-3202.
8. V. Suwanmethanond, E. Goo, P.K. Liu, G. Johnston, M. Sahimi, T.T. Tsotsis, Porous silicon carbide sintered substrates for high-temperature membranes, Ind. Eng. Chem. Res., 39 (2000) 3264-3271.
9. M. Dröschel, M.J. Hoffmann, R. Oberacker, H. Both, W. Schaller, Y.Y. Yang, D. Munz, SiC ceramics with tailored porosity gradients for combustion chambers, Key Eng. Mater., 175 (2000) 149-162.
10. P. Greil, Advanced engineering ceramics, Adv. Mater., 14 (2002) 709-716.
11. F. Schüth, Engineered porous catalytic materials, Annu. Rev. Mater. Res., 35 (2005) 209-238.
12. R. Mouazer, I. Thijs, S. Mullens, J. Luyten, SiC foams produced by gel casting: synthesis and characterization, Adv. Eng. Mater., 6 (2004) 340-343.
13. K. Ishizaki, S. Komarneni, M. Nanko, Porous materials: Process technology and applications, Springer Science & Business Media, 2013.

14. J.H. Eom, Y.W. Kim, S. Raju, Processing and properties of macroporous silicon carbide ceramics: A review, J. Asian Ceram. Soc., 1 (2013) 220-242.
15. L.S. Sigl, H.J. Kleebe, Core/rim structure of liquid- phase- sintered silicon carbide, J. Am. Ceram. Soc., 76 (1993) 773-776.
16. M.E. Davis, Ordered porous materials for emerging applications, Nature, 417 (2002) 813-821.
17. C.D. Chang, A.J. Silvestri, The conversion of methanol and other O-compounds to hydrocarbons over zeolite catalysts, J. Catal., 47 (1977) 249-259.

Chapter 2

Literature Review

2.1. Overview on porous materials

Porous materials that contain voids, channels, holes or basically pores has gained enormous interest in different scientific areas. Due to its highly porous nature and homogeneous pore structure, porous materials (micro or macro) can be used in several application field such as filtration, adsorption, heterogeneous catalysis, sensor device etc. [1-2]. Since last two decades, a number of literatures have been reported on different type of porous materials like zeolites, metal-organic frameworks (MOFs), covalent organic frameworks (COFs) and porous organic polymers etc. that have made the large contribution to society so far [3-7]. Any single category of porous material cannot be serve all purposes. However, due to their long range structure, crystallinity etc. COFs, MOFs or other porous polymers shows enhanced functionality in various applications such as, selectivity for a molecular separation, selective carbon dioxide capture, wastewater treatment and air permeation applications and catalysis etc. but also carries some limitations. The characteristics of active sites are difficult to control while modifications to local structures are difficult and the thermal and hydrothermal stability of the sites is poor [8-11]. To have an impact on real applications, the mandatory criteria for porous materials are their scalable and multiple functional capability enhancements such as long term stability, selectivity, adsorption kinetics, and processing at a reasonable cost envelope. Porous ceramic materials exhibit outstanding thermal shock resistance, high thermal insulation capability, and superior corrosion resistance compared to other porous materials like polymers, metals, or even their denser counterparts. A new generation of porous ceramics has been developed using a variety of inorganic materials, including alumina (Al_2O_3), silicon carbide (SiC), clay, silicon nitride (Si_3N_4), zirconia (ZrO_2), cordierite ($5SiO_2.2MgO.2Al_2O_3$), mullite ($3Al_2O_3.2SiO_2$), and also silicate glass, carbon as well as concrete [12]. Recently in most of the applications, porous ceramics were exposed to harsh environments (high temperature, in presence of corrosive media etc.). The application of porous ceramics in energy related field (such as catalyst or absorption supports for chemical reactions, ion exchange materials, molecular sieves, controlled release materials), filtration field (hot gas filtration, waste water filtration, molten metal filtration, diesel particulate filters etc.) has gained increasing interest in recent years as a support materials or a filter material [13-21].

2.2. Properties and application of porous ceramics

Practical implementation of the porous ceramics based technology had been started in 1930s in Russia and other countries [22]. In recent years, the development of advanced porous

ceramics have been increased significantly for their advantages as engineering materials in a wide range of fields. Various application areas of interest include:

- Porous ceramics as a filters for removal of particulate matters, dust from hot gas generated in various industrial processes and diesel engines exhaust.
- Porous ceramic based membrane for filtration of wastewater by removing oil, toxic metal, heavy metal, suspended contaminants, virus etc.
- Porous ceramics as a catalyst support for dehydrogenation of formic acid, recombination of methane, oxidation of ammonia, decomposition of organics by photo catalysis, and destruction of volatile organic compounds by incineration.
- Porous ceramics as a heat insulator in spacecraft, heat exchanger in steel billet heating furnaces, and sound absorber for subways, tunnels for fire proofing and TV emission centre, cinemas etc.
- Porous ceramics as molten metal filter to obtain highly pure metals by removing non-metallic particles in foundry industries.
- Porous ceramics as electrolytes in Solid oxide fuel cells (SOFCs) and also as energy storage components in concentrated solar power configurations and batteries.
- The shielding effect of porous material is extremely beneficial for modern aircraft, automobiles, and commercial wireless communication devices.

The applications of porous ceramics are possible due to their exceptional properties, including their high melting temperature, large specific surface area with narrow pore size distribution, excellent thermal shock properties, high toughness, good thermal insulation capability, and low dielectric constant value etc. Based on each specific application area, the right composition and microstructure of the porous ceramics can be selected to provide these properties. An important factor influencing a material's properties is its porosity, pore size distribution, and pore morphology. These properties of the porous materials are largely influenced by the processing route those are used in the production of the porous ceramics. Depending on the pore size, porous materials are classified into three different categories. These are macro porous ($d < 2$ nm), meso-porous ($2 \text{ nm} < d < 50$ nm) and micro porous ($d < 200$ nm). Porous ceramics can also be categorised by their basic porous configuration such as open-cell (or reticulated) and closed-cell which is shown in Figure 2.1 and this salient features plays a crucial role in determining the functionalities of various materials [23]. A structure with open cells and connected pores has high permeability, making it suitable for

applications where fluid transfer is important. While a closed-cell structure with isolated pores offers potential advantages for use as insulation materials, since a restricted flow of fluid is required [24-25]. The choice of the right ceramic matrix is therefore vital for a given application, based on the desired pore size and open or closed pore configuration. Porous ceramics are characterized by these structural features which determine their mechanical properties and advanced functionalities.

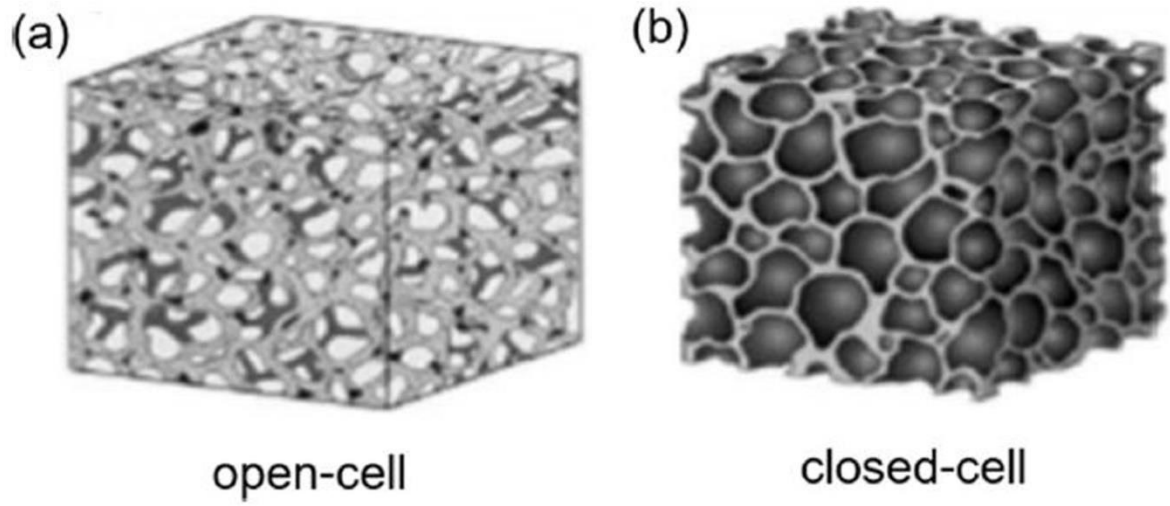

Figure 2.1. Typical images of porous ceramics with (a) open-cell and (b) closed-cell configuration [26].

2.3. Properties of ceramic materials

Generally porous ceramic filter are made of by two different categorised ceramic materials such as non-oxide and oxide ceramic materials. Selection of the most common, appropriate, reliable filter has been made depending on some important features such as strength, durability in harsh condition, thermal conductivity, and thermal shock resistance etc. Literature study indicated that various oxide ceramic materials (like Al_2O_3, TiO_2, ZrO_2, mullite, etc.) and few non-oxide ceramic materials (SiC, Si_3N_4, SiAlONs etc.) are also used to fabricate porous ceramic. Among all the oxide and non-oxide membrane, SiC membrane are considered as one of the best material for hot gas filtration and wastewater treatment. But rare reports are available on oxide bonded SiC ceramic membrane for such kind of application.

2.3.1. Silicon Carbide (SiC)

Silicon carbide is rare in nature & was discovered by the American inventor Edward G. Acheson in 1891. He found new green crystals attached to the electrodes as a result of

heating of clay and coke in an iron bowl in the presence of arc-light served as the electrodes for the preparation of artificial diamonds. He named the newly formed compound as carborandum, as it is coming from the alumina whose natural form is known as corundum. α-SiC can be synthesized via the Acheson process at ~2000°C by the following reaction steps (carbothermal reaction of quartz) [27].

$$2\ SiO + C = SiO + CO \quad (1)$$

$$SiO + 2C = SiC + CO \quad (2)$$

The reaction process generally occurs in between 1600°C to 2500°C which produces SiC grains, are subsequently milled and purified to obtain a commercial SiC powder of different grades. *Shi et al.* reported that Acheson process consists with solid state materials (sand and petrol coke) which require high temperature and long reaction time and also limits the extent of reaction and marked as non-suitable method to prepare ultrafine SiC powder [28]. Several other methods have been reported by researchers to synthesize nano-scale SiC powder for various application purposes. Chemical vapour deposition (CVD) [29], sol-gel process [30], plasma technique [31], combustion synthesis [32] and micro wave heating technique [33] have been reported to synthesize nano-scale β-SiC powder.

2.3.1.1. Structure of SiC (polymorphs and polytypes)

SiC devices can exist in various crystal structures called polytype. Different polytypes have their own unique ionization rates, charge carrier mobility and field/velocity properties [34-35]. Only a few SiC polytypes are commonly acceptable for electronic semiconductors among the over 170 existing polytypes. At present, the most common polytypes are cubic (C) 3C-SiC, the hexagonal (H) 4H-SiC and 6H-SiC, and the rhombohedral (R) 15R-SiC. With the development of manufacturing techniques, the first used polytype 3C was quickly replaced by the 6H polytype [36]. Around mid-1990s, the growth of 4H had surpassed the growth of 6H, becoming the dominant polytype for SiC in almost all devices. Currently, only 4H and 6H-SiC are commercially available [35]. In addition to the geometry of the lattice structure, polytypes are distinguished by the stacking sequences of successive bilayers of Carbon and Si [35, 37]. The latter can be demonstrated in Figure 2.2 whereby the tetrahedrally bonded C atoms are linked to three Si atoms within the bilayer and to a single Si atom in the layer below, i.e. in the [0001] direction of the lattice structure. Considering the location of C atoms within a bilayer, they form a hexagonal structure, as shown in Figure 3.3 with label “A”. The next

bilayer then has the option of positioning its Si atoms in the "B" or "C" lattice sites, thus, forming different polytypes. By permutation, the different polytypes can be constructed in the three foregoing geometries. For instance, 4H-SiC has a stacking sequence of ABCBABCB and 3C-SiC has a stacking sequence of ABCABC. In this way, the numerical designators preceding each structure type (geometry) are a function of the periodicity of stacking. The stacking sequences and respective material properties of the most commonly known polytypes are listed in Table 2.1. It should be noted that all polytypes except the cubic are anisotropic, i.e. they vary in their properties depending on the direction in which the crystal grows.

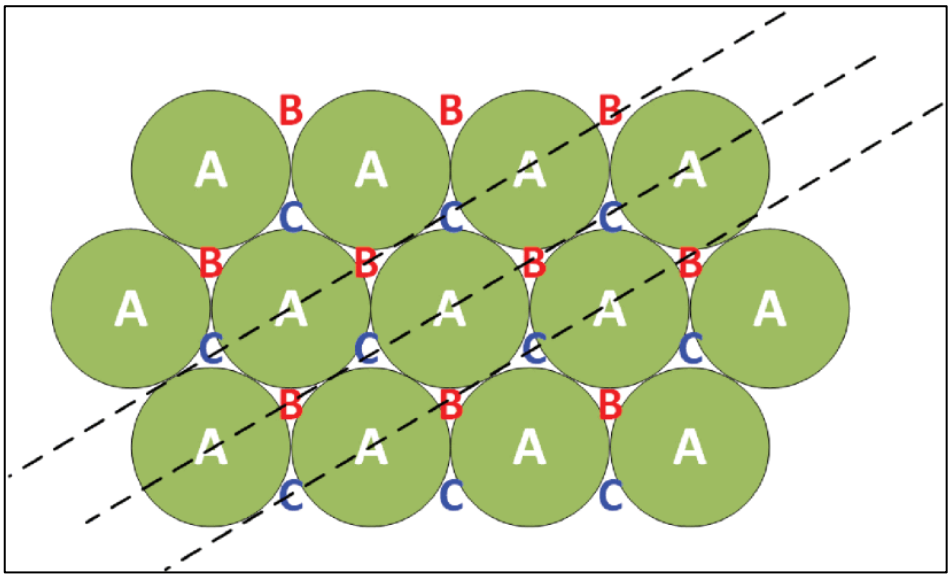

Figure 2.2. Lattice sites of C of crystalline SiC viewed from [0001] direction. A, B, C represent positions in different bilayers [37].

Table 2.1. Different SiC polytypes stacked in the C-direction with their respective physical parameters.

Polytype	Stacking Sequence	Density (gm/cc)	Lattice α(Å)	Lattice c(Å)
2H	AB	3.2	3.08	5.04
3C	ABC	3.2	4.36	4.36
4H	ABCB	3.2	3.08	10.05
6H	ABCACB	3.2	3.08	15.12
15R	ABCACBCABACABCB	3.2	3.08	37.8

It can be simply considered that each bilayer is composed of a planar sheet of Si atoms coupled with a planar sheet of C atoms, whereas different polytypes of SiC are composed of different stacking sequences of the Si-C bilayers. The plane formed by a bilayer sheet of Si and C atoms is commonly referred to as the basal plane. Figure 2.3 represents the stacking sequence of different polytypes. The crystallographic c-axis direction is defined normal the Si-C bilayer plane (the [0001] direction in Figure 2.2). According to *Inomata et al.* 2H-SiC is stable below 1400°C, 3C between 1400 and 1600°C, 4H between 1600 and 2100°C, 6H above 2100°C and 15R above 2200°C [38].

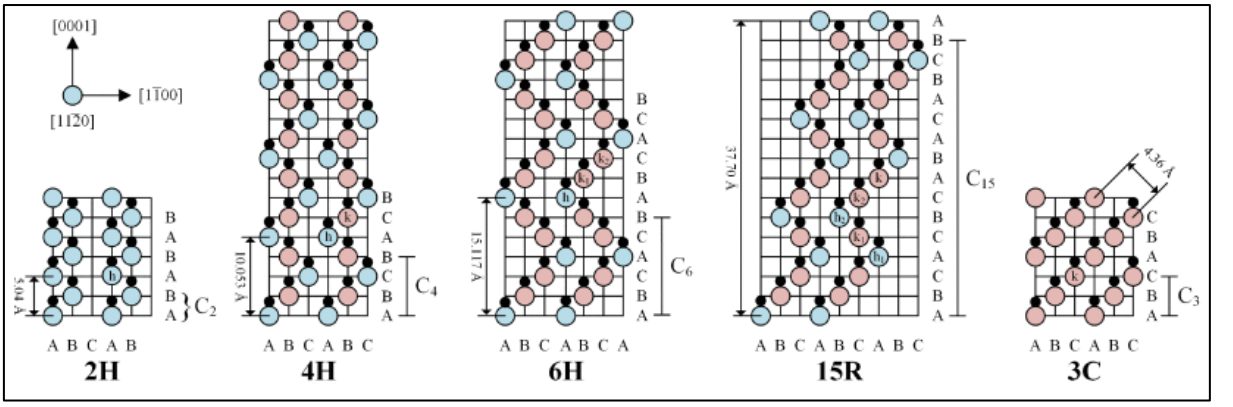

Figure 2.3. Stacking sequences of SiC polytypes in the [1120] plane [38].

2.3.1.2. Properties of SiC materials

SiC bulk material consists with excellent mechanical and physical properties, such as high fracture toughness, thermal conductivity, low thermal expansion and high strength which make them suitable in applications for severe environments. The properties of SiC bulk materials are given in Table 2.2.

Table 2.2. General properties of SiC bulk materials

Properties	SI unit	SI/Metric
Melting point	°C	2730
Density	g/cc	3.1
Flexural strength	MPa	550
Elastic modulus	GPa	410
Compressive strength	MPa	3900
Hardness	Kg/mm^2	2800

Fracture toughness K_{IC}	$MPa•m^{1/2}$	4.6
Maximum use temperature	°C	1650
Thermal conductivity	W/m•°K	120
Coefficient of thermal expansion	10^{-6}/°C	4.0
Specific heat	J/Kg•°K	750

2.3.1.3. Effect of impurities on the properties of SiC materials

Industrially synthesized SiC materials contain impurities such as Al and Fe comes from the raw materials silica and coke. The synthesis atmosphere is kept as nitrogen which is also found to be incorporated during crystal formation. Henceforth, in this method purity level is to be maintained approximately 98-99·9%. SiC powders were categorised in to two sections depending on the purity level i.e., the high purity SiC powder is known as green SiC, while the less pure SiC known as black SiC. The general impurities are present in SiC raw powders are free carbon; free metallic Si, SiO_2, Fe in free or oxide state, N_2 and O_2 etc. *Heuer et al.* systematically investigated the effects of impurity such as Si, on the oxidation kinetics of SiC powder where inward oxygen diffusion occurred which resulted in nucleation reaction and produced spherulitic particles of silica that were found to be deposited on SiC surface [39]. They have suggested that vitreous SiO_2 phase is recrystallized in melted free Si at low temperature ~1400°C. Nitrogen and aluminium are common impurities that affect the electrical conductivity of SiC. *Asgharzadeh et al.* investigated on the densification and microstructural evolution of reaction bonded SiC-Si-C system within the sintering temperature range of 1400-1600°C with detrimental effects of free Si and C, on the formation of final ceramic product [40]. They reported that if content of Si is greater than 2.5wt% in SiC powder mixture then densification of SiC ceramics are decreased with increasing sintering temperatures. Densification is also retarded with increase of carbon content and during oxidation reaction of C-SiC powder mixture porous ceramics are formed with burning of carbon. The presence of free Si in SiC powder also caused micro cracks in the final ceramics due to huge difference in thermal expansion co-efficient and crystallographic mismatch [41]. It is also mentioned a decrease of mechanical strength value with increase of free silicon and carbon content in SiC powder. *Gou et al.* reported oxygen removal technique which was present as inherent impurity in SiC powder by adding carbon as external impurity to get

phase pure SiC for further ceramic fabrication at comparatively lower sintering temperature [42].

2.4. Sintering methods for fabrication of dense SiC ceramics

Sintering of ceramic materials is the process of heating the green ceramic compacts at high temperature below its melting temperature. This process involves connecting ceramic particles to each other by simple neck formation and grow at these contact points by some different reaction mechanism and becomes hard structural materials. The mechanism of sintering process in ceramics is shown in Figure 2.4 in schematic view.

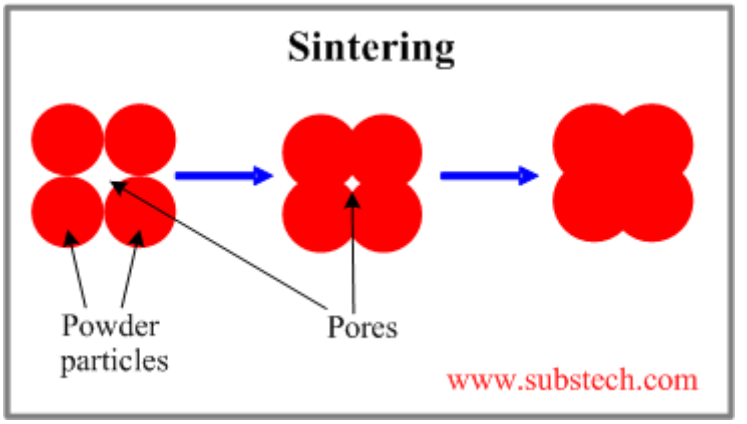

Figure 2.4. Schematic of sintering process in ceramics [43].

The practical application of SiC ceramics in different field is restricted due to its high sintering temperature coming from its strong covalent nature of Si-C bond and low oxygen diffusion properties. The SiC materials has 88% covalent and 12% ionic bond with each other. So the pure SiC ceramics can only be densified by sintering at very high temperature (> 2000°C) under ultrahigh pressure. In presence of impurities or additives, SiC ceramics can sintered at comparatively lower temperature than the sintering temperature of pure SiC ceramics. The sintering temperature and the properties of SiC ceramic largely depend on the additive used for densification. The addition of sintering additives increases shrinkage rate and density after sintering at relatively low temperatures. However, the presence of sintering additives can result in the segregation of secondary phases at grain boundaries, which adversely impacts high-temperature performance. Another factor plays an important role during sintering process that is pressure, which can also reduce the sintering temperature and time. Different sintering techniques with various sintering additives have been used for sintering SiC ceramics by several researches, these are mainly (1) solid state sintering (2)

liquid phase sintering (3) reaction bonding, (4) sintering via solid solution formation etc. The sintering techniques were developed to prepare dense SiC ceramics by adding different sintering aids as listed in Table 2.3. The reported literatures have given knowledge of sintering techniques of dense SiC ceramics which has further been improvised by several researchers to develop porous ceramics with modified processing routes.

Table 2.3. Different sintering techniques were used to fabricate dense SiC ceramics by several researchers.

Sintering Techniques	Sintering types	Sintering Temp^{r} (°C)	Sintering medium	Ceramic system	Ref.
Solid state sintering	Pressureless sintering	2150	Argon	S-SiC	[44]
	Pressureless sintering	1850-2000	Argon	S-SiC	[45]
	Gel casting	2150	Argon	SiC	[46]
	Pressureless sintering	2050	Argon	SiC-B_4C	[47]
	Gel casting	1900-2030	Argon	SiC-Al_2O_3-Y_2O_3	[48]
	Pressureless sintering	2150-2200	Argon	SiC-B_4C	[49]
Liquid phase sintering	Pressureless sintering	1875	Argon	Si-SiC	[50]
	Pressureless sintering	1800-2000	Argon		[51]
	Pressureless sintering	1900-2100	Vacuum	SiC- B_4C	[52]
	Spark plasma sintering	1700-1800	Vacuum	SiC- Al_2O_3-CaO	[53]
Reaction bonding	Infiltration of molten Si	1500	Vacuum	Dense SiC	[54]
	Robocasting	1850	Nitrogen	C/SiC	[55]
	Laser sintering,		Vacuum	Si-SiC	[56]
	Infiltration of molten Si into SiC	1850	Argon	Dense SiC	[57]
	Infiltration of a silicon melt into charcoal	1500	Argon	Si-SiC	[58]
Sintering via solid	Spark plasma sintering	1600-1800	Argon	ZrB_2–SiC	[59]
	Pressureless sintering	2100-2150	Argon	ZrB_2–SiC-	[60]

solution formation				$MoSi_2$	
	Hot pressing	2050-2150	Argon	SiC-AIN	[61]
	Spark plasma sintering	1800	Argon	$(Zr,Ti)B_2$–ZrC–SiC	[62]
	Hot-Pressing	1800	Argon	SiC-AIN Solid	[63]

2.5. Processing routes of fabrication of porous SiC ceramics

Literature study indicates that the increasing demand of porous SiC ceramics in different industrial application pushed the researchers to fabricate porous SiC ceramics by numerous processing routes using various natural or artificial materials as raw, resulted to a variety of porous structure and pore morphologies. Each processing route is targeted for specific applications and the SiC ceramics have a specific range of porosity, microstructure, and pore size distribution [64]. The fabrication processes that have been used frequently to fabricate porous SiC ceramics are (1) partial sintering, (2) replica method, (3) sacrificial template, (4) direct foaming, and (5) bonding technique. As can be seen in Figure 2.5, the main principles for these processing routes are illustrated schematically.

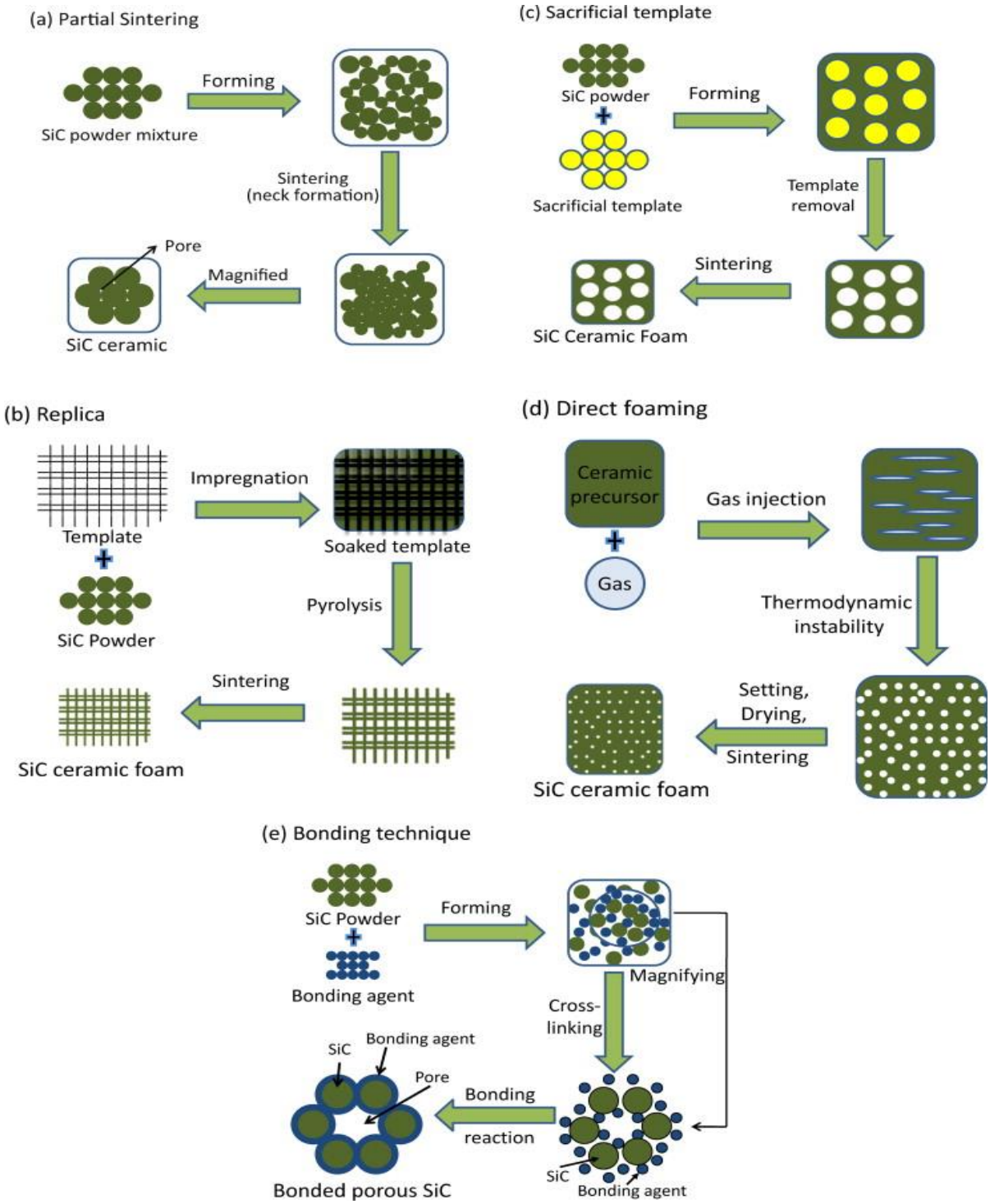

Figure 2.5. Schematic diagram of freequently used processing methods (a) partial sintering, (b) replica, (c) sacrificial template, (d) direct foaming, and (e) bonding techniques [64].

In onward section, a detailed discussion is given of each processing route, including the effects on the material, and microstructural properties of SiC ceramics. Table 2.4 shows the sintering parameters and the materials properties of some SiC ceramics prepared by several researchers.

Table 2.4. The conventional processing techniques, sintering conditions and characteristics of the porous SiC ceramics

Processing techniques		Sintering conditions	Ceramic properties
Partial sintering	Liquid phase sintering	1400-1950°C in Ar med [65-68]	Porosity: 4-64 vol% Pore size: 0.1-2.5 µm
	Pressureless sintering	1450-2000°C in air/vacuum med. [69-72]	Porosity: 30–65vol% Pore size: 0.19–8.16 µm
	Recrystallization	1650-2300°C in Ar med. [73-74]	Porosity: 55–65 vol% Pore size: 1–20 µm
	Sintering multisized SiC powder	1500-2150°C Ar med.[75-76] Cold isotactic pressing (CIP) at 220 MPa, 1500°C in Ar med. [77]	Porosity: 1-76.3 vol%
	Sintering Nano sized SiC powder	Cold isotactic pressing (CIP) at 260 MPa, 1200°C-1800°C in Ar med.[78]	Pore size: 0.035-5 µm
Replica	SiC powder slurry	1400°C in air med. [79]	Porosity: 60–96 vol% Cell size: 1µm–5mm
	Precursor solution Open cells	900-1300°C in N_2 med. [80]	Porosity: 60–89 vol% Cell size:0.2 – 1mm
	Chemical vapor deposition of SiC	1000-1450°C in Ar med. [81-82]	Porosity: 85–95 vol% Cell size: 200–500 µm
	Natural wood-derived carbon foam	1000-1650°C in inert med/vacuum [83-85]	Porosity: 43-92 vol% Cell size: 1-200 µm
	Artificial carbon foam	Infiltration of liquid Si at 1550°C under vacuum then heated upto 1700°C [86]	Porosity: 94-97 vol% Cell size: 50-350 µm
Sacrificial template	Synthetic organics [nylon, PMMA]	1400-2050°C in Ar/air med. [87-91]	Porosity: 15-88 vol% Pore size: 1-150 µm
	Natural organics[wax, yeast, dextrin]		Porosity: 27-70 vol% Pore size: 100-700µm
	Liquids [water, camphene]		Porosity: 74-87 vol% Pore size: 12-147 µm
	Salt [NaCl]		Pore size: 10-40µm

	Metal/ceramic [silicon, carbon, silica]		Porosity: 30-64 vol% Pore size :0.5-150 µm
Direct foaming	Chemical blowing agent	Pyrolyzed at 1000°C [92] 1100-1700°C, N_2 med [93]	Porosity: 59-91 vol% Pore size: 5 µm-10 mm
	Physical blowing agent	Pyrolyzed at 1200°C, N_2 med [94] 1850°C, Ar med. [95]	Porosity: 40-62 vol% Pore size: 2-20 µm
Reaction bonding	**Bonding agent**	Sintered at various temperature at 800-1500°C in air [96-100]	Open cell porosity: 15-80 vol%, pore size: 0.5-50 µm
	Silica, mullite, cordierite, YAG etc.		

2.5.1. Partial sintering

Partial sintering is the well accepted method to fabricate porous SiC ceramics. Partial sintering involves bonding powder particles together by simple surface diffusion, evaporation–condensation, recrystallization or re-precipitation of solutions. A unique homogeneous porous structure can be seen in Figure 2.5(a) when sintering temperature is lower than full densification temperature. By lowering sintering temperature, it is possible to avoids additive addition and possible to construct a constrained network structures by coarser powders followed by recrystallization. In partial sintering, the size of starting powders and degree of sintering can determine the porosity and pore size of ceramics. Generally, most of studies used the powder having particle size three to five time larger than the pore size required for particular application [101]. Previous studies have shown bending strength is directly associated with the neck radius to particle radius ratio, and neck formation is directly related to sintering temperature. Using slip casting of submicron SiC powder and alumina additive mixtures at 1450–1800°C, *Lin et al.* have fabricated macro porous SiC ceramics with the porosity composed of 29–39%, the pore size of 0.10–2.33 µm, by varying alumina content (3–8wt%) respectively [102]. In order to fabricate porous SiC ceramics, *Fukushima et al.* used cold isostatic pressing (CIP) to press submicron powders of SiC under different alumina additive concentrations, CIP pressures and sintering temperatures between 1500 and 1800°C [103-104]. They have found that the sample without alumina additive, the pore size and particle size of the porous SiC membrane was increased but there was a decrease in pores size in the final ceramics after addition of 4% alumina. The reduction of pore size is believed to be due to the formation of a liquid SiO_2–Al_2O_3 phase on SiC surfaces. However they have also seen a reduced size of pores in the ceramics after fabrication of ceramics at higher CIP

pressure. *Zhao et al.* [105] processed porous SiC ceramics with porosity in the range of 66–70%, using Al_2O_3–SiO_2–Y_2O_3 additives sintered at 1350–1750°C by pressure less sintering. To prohibit the densification in the final ceramic, *Kim et al.* used large SiC particles or whiskers (65μm) with submicron SiC particles during fabrication of porous SiC ceramics [106]. They observed variation of 0.30% to 0.39% porosity of the porous SiC ceramics by variation of amount of large SiC particles or whiskers and the applied pressure during sintering. *Zhou et al.* [107] fabricated porous SiC tubes with homogeneous and defect-free microstructures by partial sintering methods sintered at 1800-1900°C. With variation of sintering temperature, they observed variation of porosity, pore size and mechanical strength from 40-46%, 0.19-1.70 μm and 47-110 MPa respectively. *Kawamura et al*. produced porous β-SiC ceramics by synthesising SiC particles using powdered mixtures of Si and fullerene or Si and amorphous carbon at a 1000K temperature in presence of sodium vapour [108]. Microstructural studies of final ceramics prepared with Si and fullerene showed that there was a formation of agglomerates of submicron sized SiC particles and open spaces in fracture surface while for the ceramic with amorphous carbon, the surface was quite smooth with cavities and voids. *Hotta et al.* processed porous SiC ceramics using with Al_2O_3 or AlN–Y_2O_3 additives at 1900-2000°C at heating rate 50-200°C/min by spark plasma sintering [109]. The size of the SiC grains in the final ceramics decreased with increase in the heating rate and porosity of the ceramic also increased. However the mechanical strength of the ceramics increased with increase in the sintering temperature. The SiC ceramics sintered at 1950°C showed a high mechanical strength of 95 MPa with open porosity of 42%. Additionally, the addition of additives resulted in the inhibition of grain growth and the reduction of pore size in the samples. *Kim et al.* [110] developed porous SiC ceramics using B_4C additives and they have seen that there was a formation of interconnected huge plate like grains in SiC ceramics due to recrystallization between β-SiC and B_4C. At higher temperature 2100°C, the phase transformation (α→β) occurred and the gas phase reaction, such as an evaporation–condensation reaction influenced rapid grain growth of β-SiC that consumed the unstable SiC matrix resulting in an interconnected network structure with huge plate like grains which is shown in Figure 2.6.

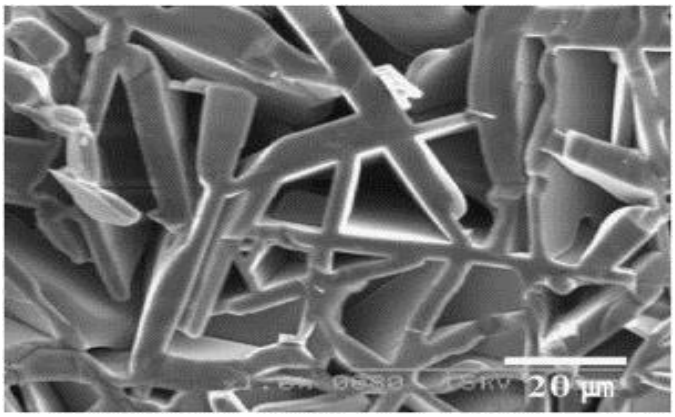

Figure 2.6. FESEM image of porous SiC ceramics showed the interconnected huge plate like grains produced by partial sintering method [110].

Using a high temperature recrystallization process, *Liu et al.* [111] created porous ceramics with wood like structures by mimicking the formation mechanism of wood cellular structures. At higher than 1800°C, SiC produces the gas mixture of Si, Si_2C and SiC_2 by simple decomposition and the Si gas acted as a transport medium for carbon and SiC. Porous green body is caused by the directional flow of gas mixture, which results in the surface ablation of SiC grains, the rearrangement of SiC grains, and the recrystallization of SiC grains, which leads to the formation of aligned columnar fibrous SiC crystals and tubular pores in the axial direction. Sintering temperature and pressure also play an important role in determining the formation of fibrous columns in the columnar direction. Typical microstructure of wood like porous SiC ceramics are shown in Figure 2.7 [111].

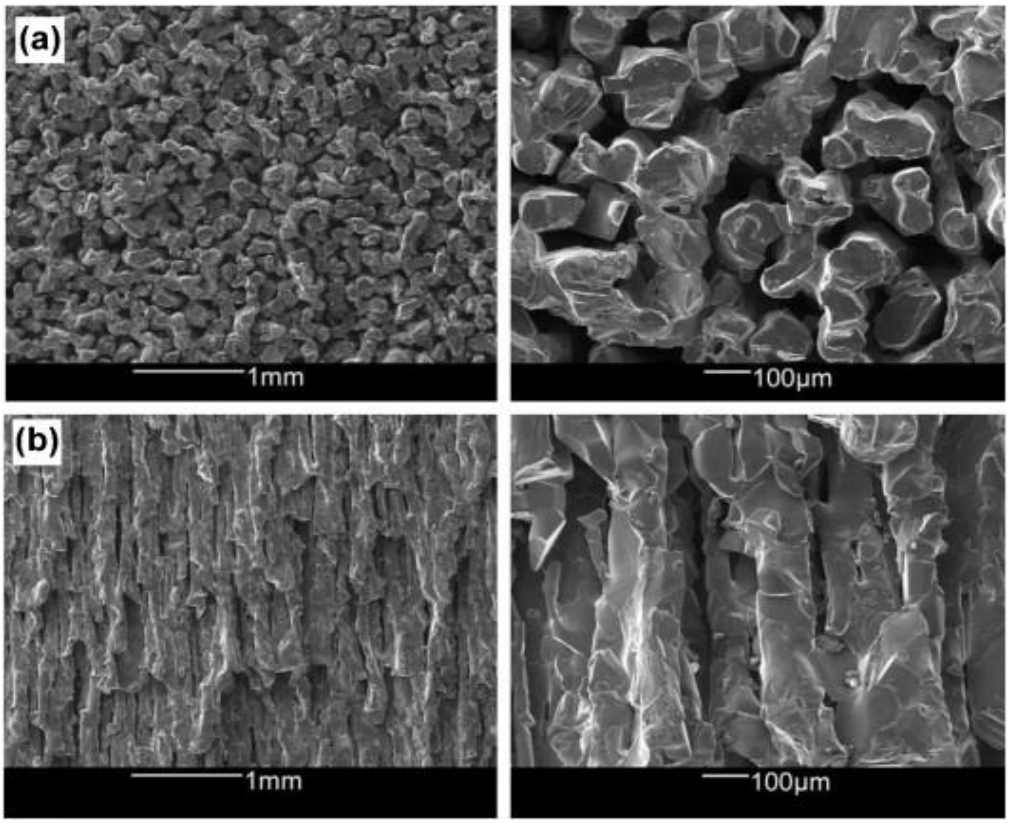

Figure 2.7. A radial (a) and an axial (b)microstructural view of the surface of typical wood-like porous SiC ceramic fabricated by partial sintering [111].

In summary, this processing route is the simplest method to fabricate porous SiC ceramics with homogeneous porous structure with narrow pore size distribution. The porosity and the pore size can be controlled and porosity can varied below 68% and with pore size ranging from 0.1 to 10 μm. Due to SiC's high covalent bonding strength, it is possible to obtain grains of varying size without shrinkage and densification, which facilitates easy dimensional control during this process. However, despite of these advantages of this processing technique, there are few disadvantages which can retard its practical applications in different areas. These are mainly requirements of high purity raw materials, requires a very high sintering temperature, necessity to maintain whole process in special atmosphere, complexity of production of big parts etc.

2.5.2. Replica method

A second widely used method for the fabrication of porous SiC ceramics is replica method, which is based on a copy of the original foams and a strut structure that follows the shape of the pore. This method involves mainly three different techniques to produce porous SiC

ceramics. These are (1) impregnation of polymer foams with SiC suspension or precursor solution, (2) chemical vapour deposition (CVD) of SiC on polymeric foams and (3) infiltration of natural wood derived or artificial carbon foams with Si sources. A very high porosity more than 90% with open cell pore size ranging from 100 μm to millimetres in porous SiC ceramics can be achieved by this replica method. In various application (molten metal filtration) the produced SiC filters by this method, is being widely used. The first method based on impregnation of polymer foams with a SiC suspension or precursor solution involves following steps, firstly the cellular or porous structure are saturated with SiC suspension or precursor sol then removes the excess sol by simple centrifuges followed by air drying the coated cellular or porous structure. After that the structure were heated at certain temperature to remove the polymer sponge by decomposition and finally sintered at optimum temperature [112-117]. In this way, macroporous SiC ceramics can be produced that exhibit the same morphology as their original porous substrate. After the organic sponge is burned out, reticulated porous SiC ceramics processed by the above method contain triangular pores inside struts that make them sensitive to structural stresses and limit their structural applications. The mechanical strength of the reticulated porous SiC ceramics was improved through the simple recoating method used by *Zhu et al.* [118]. They coat the sponge preform uniformly with a thicker slurry of SiC in their study. After burning out the sponge from the reticulated preform by heating, they have recoated the reticulated preform with thinner slurry by centrifugal method. After densification process, they have noticed that the mechanical strength of the porous SiC ceramics has been improved significantly. Researchers also have observed the same type of phenomenon in reticulated porous SiC ceramics and have speculated that the strength of such ceramic improves considerably when the solid content of the slurries increases [112-113]. In one study, *Mouazer et al.* [114] developed porous SiC ceramics by replica method with B_4C as a sintering aid, gelatine as a gelling agent, and polyurethane foam as a template for the replication process. In their study, a very stable aqueous SiC slurry were prepared by adding appropriate amount of gelling, anti-foaming and dispersing agents and filled all the pores of polyurethane foam. In order to ensure that the sponge is completely filled with slurry, it is compressed and rolled on to remove excess slurry. They have seen that after sintering at 2120°C for 1 h in argon, the porosity of the SiC ceramic foams lies between 78-88 vol%. *Yao et al.* [115] processed reticulated porous SiC ceramics with polyurethane sponges by using mixture of $MgO–Al_2O_3–SiO_2$ as a sintering additives sintered at 1000–1450°C. They have seen that the optimum sintering temperature can be lowered by 100°C by adding $MgO–Al_2O_3–SiO_2$ additives compared to $Al_2O_3–SiO_2$ additives. A ceramic slurry

consisting of SiC powders and bentonite was used by *Soy et al.* [116] for fabrication of reticulated porous SiC ceramics as a binder and sintering additive. They observed that with the increase in the amount of bentonite content from 1 wt% to 10 wt% in the starting composition, porosity decreased from 86% to 84% while the mechanical strength of final ceramics is increased. A reticulated porous SiC ceramic was developed by *Bao et al.* [117] by soaking polyurethane foams in polysilane precursor solutions and heating those at 900-1300°C in nitrogen. In this way, the SiC foam showed a well-defined open cell structure with no voids between the struts. By using two types of polymeric precursor, *Nangrejo* and *Edirisinghe* [118] also prepared reticulated porous SiC ceramics. A literature review suggests that varying polymeric precursor and/or second phase filler concentrations can control the sintering shrinkage of SiC ceramics [119-122]. The microstructure of reticulated SiC ceramics with well-defined open-cell structures prepared using this method can be seen in Figure 2.8(a).

The second method involves the deposition of SiC coating on the polyurethane foams by chemically vapour deposition (CVD) method. Figure 2.8(b) shows the strut-based open cell microstructure of the porous SiC ceramic prepared in this way, which consists of polyhedral cells with 12–14 faces. The company named as Duocell® (Oakland, California), they have prepared SiC foams by this method and the image of the prepared SiC ceramics shown in Figure 2.9.

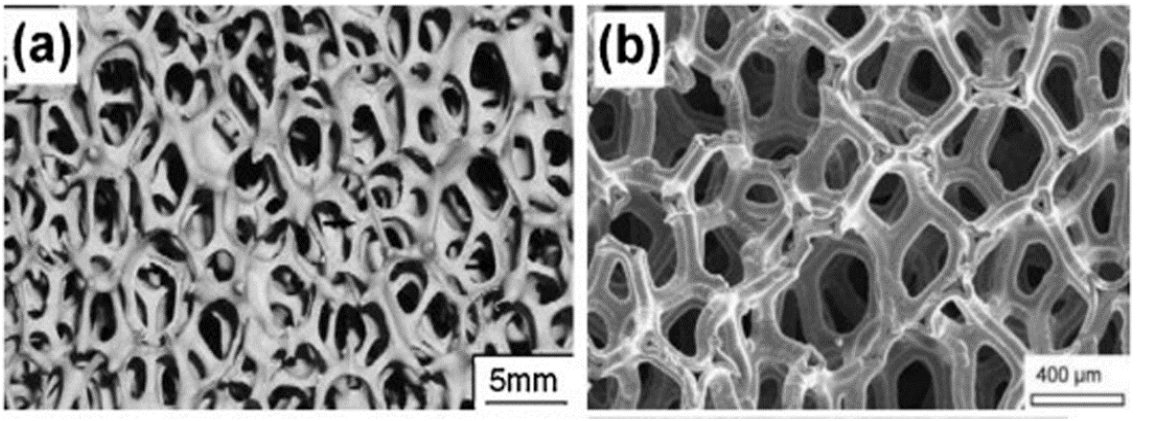

Figure 2.8. Typical SEM image of highly porous SiC ceramics fabricated via the replica technique: (a) Impregnated polyurethane sponges with SiC slurry to produce SiC foams [120] (b) SiC foams produced by CVD process [123].

Figure 2.9. Image of SiC foams fabricated by chemical vapour deposition (CVD) of SiC on polymeric foams (Duocell ®, Auckland) [118].

The third method proposed the infiltration of liquid or gaseous Si or Si source (such as SiO_2, or TEOS) in to carbon foams which are prepared by pyrolysis of woods, to form SiC or Si-SiC ceramics [113, 124-126]. By infiltrating liquid Si into carbonized wood and then reacting to form SiC, *Greil et al.* first created cellular SiC ceramics that have homogeneous pore structures [125]. Their process involves pyrolyzing wood to decompose poly-aromatic components in wood to form carbon preforms at temperatures between 800 and 1800°C under inert atmosphere. For cellular SiC and Si/SiC ceramics, the preforms of biological carbon were infiltrated with gaseous or liquid Si. Literature study also indicates that the anisotropic pore structures of SiC ceramics strongly depends on the initial cellular structure of different kinds of wood uses in this method. *Herzog et al.* [127] modified porosity and pore size of porous wood derived SiC ceramics which was produced by carbothermal reduction between the carbonized wood-based material and an infiltrated silica sol. The obtained structural properties of the materials were isotropic and porosities were in the range of 55–74%.

From the literature study, it can be concluded that replication is the most advisable method for the production of open-cell SiC ceramics with pores varying from 10 μm to 5 μm, with porosities between 60% and 95%. The polymer replica technique is entirely dependent on adhesion between an impregnating suspension and a polymeric sponge. Although this

technique has many advantages, the mechanical strength and reliability of porous structures produced by this method is improved by the formation of hollow and crack struts during pyrolysis of the polymer sponge but one disadvantage of this technique is the formation of rigid struts in the reticulated structure during pyrolysis of the polymeric template, a condition that significantly weakens the mechanical strength of the porous ceramic [128]. Additionally, the technique requires several steps, prolonging its duration and increased its cost.

2.5.3. Sacrificial template method

Another common technique for fabricating porous SiC ceramics is sacrificial template method by using a sacrificial template, which can be either natural or synthetic organics, liquids, salts, metals, or ceramics. The process involves mixing SiC powders or SiC precursors with a suitable amount of sacrificial template and creating a biphasic composite by using the template SiC powders or precursor mixtures, and then removing the template before or during sintering to create pores. With various sacrificial templates, ceramics showed a range of flexural strengths between 170 and 2.4 MPa and a range of porosities from 35-77 vol% [129]. The type of pore former used impacts the extraction of sacrificial templates from the biphasic composites. The most common and frequently used pore former for sacrificial template method are polymer micro beads and microspheres. As an example, *Kim et al.* [130-133] achieved tailorable porosity of 16% to 69% by using polymer micro beads as a pore forming agent coupled with a controlled micro bead content and sintering temperature. SiC can be synthesized by adding additional carbon sources along with a higher temperature (>1400°C) to the polysiloxane [134-135]. This study also suggested that the porosity of the composites was adjusted by adjusting the template, inert filler, additive content, and sintering temperature so that it ranged from 40% to 95%. *Eom et al.* [132, 136-137] reported that by controlling the amount of additive, SiC powder, and sintering temperature, it is possible to control the microstructure of SiC ceramics prepared by sacrificial method. According to their study, when sintering temperature increased from 1750 to 1950°C, grain size grew to a large extent and grain morphology changed from equiaxed to cubic to hexagonal platelets [136]. In addition, Al_2O_3–Y_2O_3–CaO additives were observed to provide low viscosity liquid phase and β-α phase transformation of SiC, resulting in porous SiC ceramics with toughened strut microstructures. α-SiC grains have also been observed to form at 1950°C when powders or a mixture of α/β powders containing small amounts (≤10%) of β powders were used. Figure 2.10 (a) illustrates the typical microstructure of porous SiC ceramics obtained from 1% α-SiC

and 99% β-SiC powders. Porous SiC ceramics with typical pore size distribution were produced by *Bereciartu et al.* [138] using Y_2O_3 and Al_2O_3 as sintering additives and mesocarbon micro beads as a sacrificial template. Studying the effects of particle size on porosity and mechanical properties, they found that a nanometre-size powder of SiC and C resulted in higher porosity in SiC ceramics than micrometre-sized powder. *Jin* and *Kim* [139] pyrolyzed a polycarbosilane (PCS) and polymer microbead cross-linked body at 1100-1400°C in an atmosphere of argon to produce highly porous SiC ceramics. Experimental findings suggest a range of tailored porosities between 56% and 88% can be achieved in SiC ceramics by controlling microbead content and pyrolysis temperature. The microstructure obtained from the process is depicted in Figure 2.10 (b). Using Si grains as Si sources and templates as carbon sources, *Yamane et al.* [140] fabricated porous SiC ceramics. This was heated at 900°C for 24 hours in the presence of Na vapour, leading to 55-59% porosity. By infiltrating polymethylsilane solution into a colloidal silica template and then pyrolyzing them, *Sung et al.* [141] developed highly porous SiC ceramics with pore array microstructure.

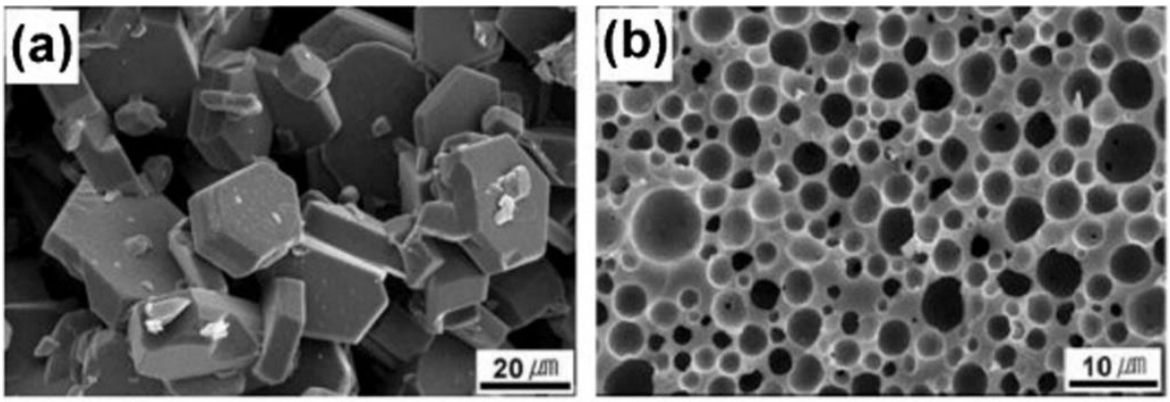

Figure 2.10. Microstructures of highly porous SiC ceramics prepared with sacrificial templates: (a) SiC foams produced using polymer beads and SiC powders [136] (b) SiC foam produced using polymer beads and polycarbosilane as a SiC precursor [139].

Therefore, sacrificial template method is one of the suitable method for controlling porosity, pore size distribution, and pore morphology of the porous SiC ceramics by choosing an appropriate sacrificial template, because the size, shape, and content of the template determine pore size, pore shape, and porosity. It is possible to achieve porous SiC with a high porosity ranging from 10 to 90% and wide pores size of up to 750 μm by varying the template content and sintering temperature by this sacrificial template method. Compared to replica method, this sacrificial template method is preferred to produce highly porous SiC

ceramics with interconnected porous structure where as in replica method SiC ceramics produced with open cell porous structure [142-143]. However, the removal of the organic template material can be very time consuming and generates harmful by-products.

2.5.4. Direct foaming method

In direct foaming method, porous SiC ceramics are normally developed by generating bubbles inside SiC ceramic slurries or in polymeric precursor solution to create stabilized foam in SiC with the help of blowing agent, dried and finally sintered at optimum temperature. The schematic of processing method is shown in Figure 2.5(d). The nucleation and growth of the bubbles are strongly depends on the viscosity of the precursor or ceramic slurry and the particle size of the SiC powders. The most common blowing agents are liquids that can become gaseous upon evaporation, solids that can produce gas upon combustion, or gases introduced into the liquid mixture by mechanical stirring or bubbling (gas injection). Based on their properties, blowing agents are classified into two section i.e. physical and chemical agents. Physical blowing agents does not interact with the materials present in the slurry whereas the chemical agents reacts with the materials and produces gaseous compounds. *Fukushima* and *Colombo* [144] fabricated macro-cellular porous silicon carbide foams using PCS polymeric precursor with a chemical blowing agent (azodicarbonamide, ADCA) by direct foaming method. The foamed PCS were pyrolyzed at 1000°C in presence of N_2 atmosphere and obtained highly porous SiC having porosity 59 to 85% and pore size varied 416 to 1455 µm as can be seen in the microstructure of SiC foams obtained by direct blowing of PCS (Figure 2.11(a)) [144]. Decomposition of polymeric precursor leading to the formation of volatile species which act as a pore former during fabrication of porous SiC foam with porosity ranging from 50 to 60% [145]. According to several research studies, it is possible to manipulate the porosity of SiC ceramics in part by controlling the gas evaporation process by tailoring the polymeric precursor composition and structure. *Kim et al.* [146] proposed a new approach to fabricate porous SiC with high cell density $>10^9$cells/cm^3 and cells <10 µm through direct foaming using a preceramic mixture of poly-carbosilane and polysiloxane from preceramic precursors and CO_2 as a blowing agent. The process involves several steps, in the 1st step gas, liquid or supercritical CO_2 are used to saturate preceramic polymer then bubbles are generated by heating by which thermodynamic instability are created due to pressure drop. Finally the bubbles forms and then the polymers are converted into micro-cellulosic ceramics by pyrolysis and sintering [146-149]. As a result of the

experiment, it was discovered that porous ceramics with a very fine and homogenous cell structure can be produced if the microcellular structures are preserved during the transformation from preceramic to ceramic. Also they have developed porous SiC foams having uniform cellular structure with open cells produced by the steam chest molding method and the microstructure was given in Figure 2.11(b).

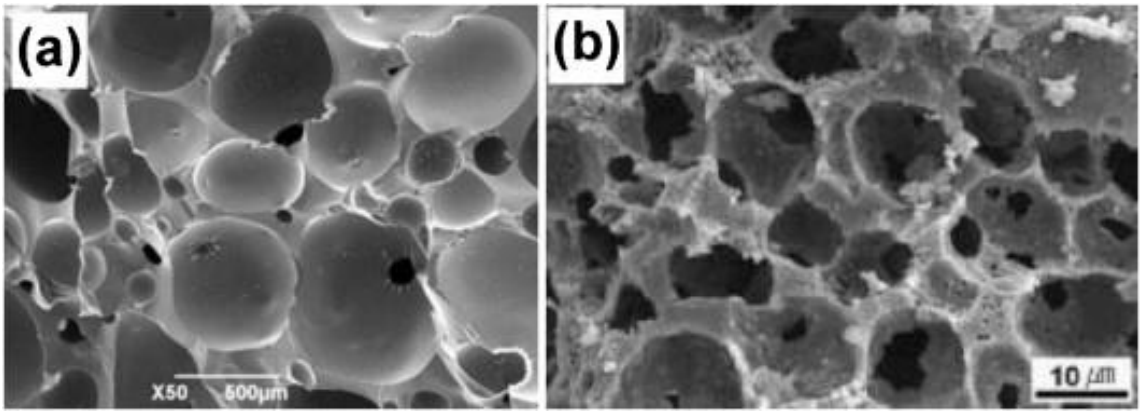

Figure 2.11. A representative microstructure of macro porous SiC ceramic prepared by direct foaming in which (a) azodicarbonamide is used as a blowing agent [144], (b) water vapour is used as a blowing agent [148].

In summary, the direct foaming technique is an easy processing route to prepare highly porous SiC ceramics up to 95% with both open and closed-cell structures [101,129,142]. These ceramics have a well-connected porosity with unique permeability that enables them to regulate fluid transport in finer detail within the structure [142, 150]. Incorporation of gas into the suspension or liquid slurry makes the SiC ceramic porous and the porosity is depends on the amount of gas incorporated during foaming process. A stronger foam can be produced in this method as compared to other methods due to the ability to create dense ceramic struts and defects-free struts. However, the problem with the process is that these bubbles are likely to coalesce and then result in large pores in porous ceramics due to thermodynamic instability. Thus one major drawback of this method is a difficult process for producing ceramics with narrow pore size distributions despite all of its advantages [129, 146, 151].

2.5.5. Reaction bonding method

All of the above-discussed processing methods, such as partial sintering, replica, sacrificial template, and direct foaming, are very easy and suitable for fabricating highly porous SiC ceramics but efforts are going on to reduce fabrication cost. Most of these mentioned

methods requires very high sintering temperatures of ≥1800°C for the processing of SiC ceramics due its strong covalent bonding characteristic, costly equipment, inert atmosphere for sintering. Therefore, one of the major concerns concerning the processing of porous SiC ceramics is how to achieve porous SiC ceramics at low firing temperatures. There have been several studies conducted to reduce the processing temperature of porous SiC ceramics, and it has been suggested that processing temperature can be lowered by using polymer precursors as a precursor for SiC, and one of the most prominent ways to lower the processing temperature could be the choice of suitable bonding materials. The schematic presentation of the reaction bonding process for low-temperature fabrication of porous SiC ceramics is provided in Figure 2.5(e) [152-153]. Various bonding materials such as silica (SiO_2), mullite ($3Al_2O_3.2SiO_2$), alkali, cordierite ($2MgO{\cdot}2Al_2O_3{\cdot}5SiO_2$), Si, SiC, silicon nitride (Si_3N_4), silicon oxycarbide (SiOC), and frit etc. were used as bonding materials by several researchers for porous SiC ceramics. Depending on the processing parameters, the material and mechanical properties of obtained for oxide bonded SiC ceramics by various researcher are summarized in Table 2.5. The ceramic prepared by oxide bonding method obtained good thermal shock resistance, chemical stability, and high specific strength at low cost compared to other processing methods. *She et al.* [154-155] firstly developed SiO_2 bonded porous SiC ceramics by a simple oxidation bonding technique and they have seen that during heating/sintering of SiC ceramics in presence of air, SiC got oxidised and the SiC particles were bonded with each other through the oxidation derived silica. The Figure 2.12(a) shows an example of a typical microstructure of the silica bonded porous SiC ceramics [156]. The results indicated that the porosity of the SiC ceramic decreases with increase in processing temperature and decrease in particle size of SiC and the ceramics sintered at 1100–1400°C showed porosity in the range of 28-40%. By manipulating the graphite content and/or the size of graphite particles, this same group has successfully controlled both the porosity and the pore size of porous silica-bonded SiC ceramics [158]. Based on the processing parameters, porosities of final ceramics ranged from 32 to 50% and pore diameters ranged from 3.4 to 7.6 μm. *Chan* and *Kim* [157] prepared highly porous silica bonded SiC ceramics at 1300-1400°C in air with polymer micro beads as an intermediary material to form spherical pores in final ceramics. Through the control of the sacrificial template content and sintering temperature, they have varied the porosity of the ceramic from 19 to 77%. The prepared ceramics showed high flexural strength of 60 MPa with porosity 40%. *Choi et al.* [158-159] investigated the effect of alkaline earth material on the mechanical strength of mullite bonded porous SiC ceramics

at temperatures ranging from 1350 to 1450°C. Their results showed that the addition of alkaline earth materials to ceramic compositions lowered the mullitization temperature from 1550°C to 1250°C and ceramic showed improved mechanical strength. *Dey et al.* [160] developed typical needle shaped mullite bonded porous SiC ceramics by infiltrating silica sol into SiC–Al_2O_3 powder compact sintered at 1500°C in presence of air and the ceramics with porosity ~ 30% showed 51 MPa strength. A typical microstructure of mullite bonded SiC ceramics is shown in Figure 2.12 (b) showing formation of rod/needle type mullite crystal at the neck region of SiC ceramics. *Kayal et al.* [161-162] prepared the porous SiC compact by burning out the petroleum coke and infiltrated mullite sol into powder compact and finally sintered at 1300-1500°C in air to prepare mullite bonded porous SiC ceramics. Based on an XRD analysis, they have found that SiC ceramics are predominantly composed of SiC, cristobalite and mullite. The porosity of the final ceramics varied between 31-49% depending on the petroleum coke content, infiltration step, and sintering temperature, with an average pore diameter of 8 μm for all the ceramics.

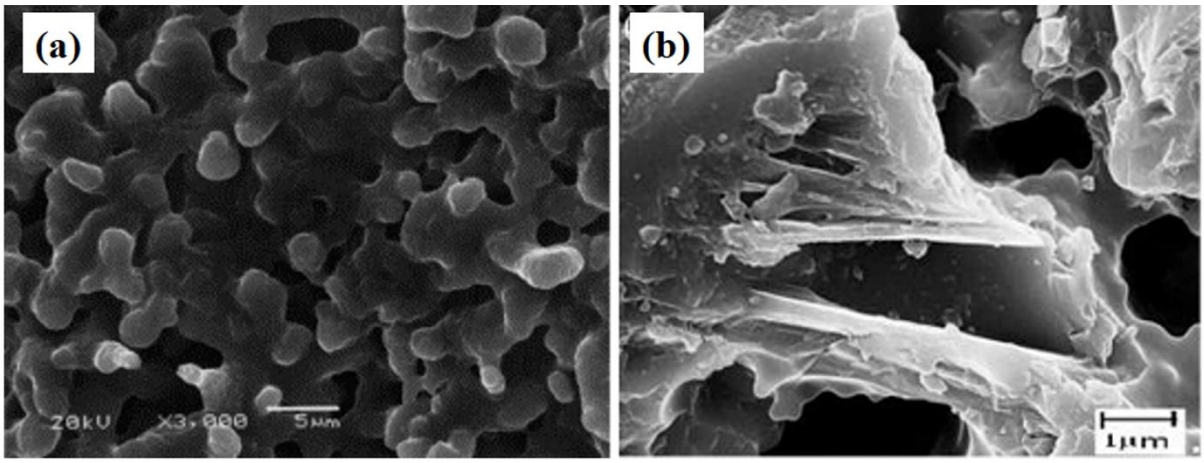

Figure 2.12. Microstructures of oxide bonded porous SiC ceramics bonded through (a) silica [156] and (b) mullite [160] at the neck region.

It was found that additive composition influenced the flexural strength of porous SiC ceramics processed by reaction bonding method, as studied by *Eom et al.* [163-164]. The various additives resulted in a wide range of porosities between 56 to 72% as well as a wide range of flexural strengths from 8 MPa to 122 MPa. However, some specimens showed different flexural strengths at the same porosity. In contrast, the flexural strength of porous SiC ceramics sintered with 3 wt% Al_2O_3–2wt% Y_2O_3 was 55 MPa at 62% porosity, whereas it was 45 MPa at the same porosity when sintered with 3wt% Al_2O_3–1wt% Y_2O_3–1wt% CaO

[163]. Porous mullite bonded SiC ceramics were fabricated by *Choi et al.* [165] using 4 wt% alkaline earth oxide additive. As a result of the addition of alkaline earth oxides to SiC ceramic, the mullitization temperature was lowered considerably, from 1450-1550°C to 1350-1450°C, and the flexural strength was significantly improved. The mullite bonded SiC ceramic sintered with 4 wt% SrO had a flexural strength of 44 MPa at a porosity of 46% while the ceramics prepared without SrO showed flexural strength of 6 MPa at 49% porosity. The results revealed that selecting the sintering additive composition judiciously is an efficient way to improve the mechanical properties of porous SiC ceramics. Using in situ reaction bonding method, *Zhu et al.* prepared cordierite bonded SiC ceramics using clay, talc, and Al_2O_3 as a bonding additives along with SiC powders [166]. During sintering, pores are created by the burning out of pore former while at the same time, the oxidised silica coming from SiC surface reacted with the clay, talc, and Al_2O_3 to form cordierite phase. In the final ceramics, SiC particles were bonded by the in situ reaction derived cordierite and the porosity were varied from 28% to 60% depending on the amount of pore former.

From literature reports, it is very clear that bonding technique is low-temperature processing route for fabrication of porous SiC ceramics with porosity ranging from 15% to 87 vol% and is a cheaper method compare to the other processing methods. The processing temperature generally varies in a range of 800–1550°C that depends on the composition of the bonding material. Therefore reaction bonding technique can be considered as an innovative, simple, cost effective method for processing of porous SiC ceramics at lower temperature with homogeneous porous structure with high mechanical strength which can be controlled by suitable selection of bonding additives, pore former, sintering temperature, duration of sintering, etc. In order to fabricate of oxide bonded porous SiC ceramic materials for specific applications as catalytic support, hot gas, water filter membrane; the selection of secondary refractory materials by observing their compatibility with SiC bulk material properties such as, thermal shock resistance, strength, thermal expansion fracture toughness, chemical reactivity, thermal conductivity etc. are necessary. Among various oxide refractory materials mullite, cordierite are very common because of exceptional refractory properties that make possible their huge applications in material and metallurgical field.

Table 2.5. Influence of sintering additives and processing parameters on the properties of porous SiC ceramics obtained by reaction bonding technique.

Bonding phase	SiC(d_{50}) (µm)	Additives source	Pore former	Sintering Temp^r (°C)	Porosity(%)	Pore dia (µm)	Strength (MPa)	Ref.
Silica	0.6-2.3	SiC	---	1100-1400	28-41	---	60-190	[149]
	0.3-58		Graphite	1400-1500	31-36	2.5-12	40-133	[152]
	0.34		Microbead	1400	40	25-30	65	[153]
Mullite	2.3	Al_2O_3	Graphite	1400	36-75	2.5-12	10-52	[151]
	20	Al_2O_3, Y_2O_3	Graphite	1300-1550	34-57	1.6-8	5-28	[154-156]
	10	Al_2O_3, MgO, CaO, SrO	---	1350-1550	35-53	1.6-4	14-87	[167]
	90 & 0.5	do	---	1450	44-49	---	6-44	[168]
	65 &0.5	ALN,Al_2O_3, Al, $Al(OH)_3$	---	1450-1500	35-46	---	---	[169]
	2.4	Al_2O_3	Graphite	1300-1500	30-47	---	22-56	[170]
	---	Red mud, $Al(OH)_3$	Graphite	1350	31.4	---	49.4	[222]
	---	Bauxite	Graphite	1350-1500	31.4-47.8	---	36.6-85.2	[223]
Cordierite	20	Al_2O_3, talc, clay	Graphite	1360	28-60	1.9-4.9	10-55	[165]
	10	Al_2O_3, MgO	Graphite	1200-1400	28-66	2-8	3-71	[163]
	10	Al_2O_3, MgO, CeO_2	Graphite	1250-1400	28-56	2.4-3.2	4-36	[164]
SiC	65 & 0.7	Si (1)	Carbon black	1700-1800	38-46	5-25	3-42	[171]
Si_3N_4	---	Nitridation reagents Y_2O_3+Al_2O_3	---	1360-1430	30	---	1-62	[172-173]
Alkali aluminosilicates	---	Alkali (metakaolin, KOH/K_2SiO_3 mixture)	---	1200	78-87	---	0.9	[174]

2.6. Secondary bonding phase

2.6.1. Mullite

Mullite is a rarely available mineral consisting of alumina silicate ($3Al_2O_3.2SiO_2$). It is considered as an emerging engineering materials for both traditional and advanced application due to its high melting temperature, low thermal expansion coefficient and conductivity value (close to the value of SiC), excellent thermal and chemical stability etc. In 1924, mullite was first discovered in volcanic rocks in Isle of island Mull, Scotland [175] occurred at the contact zone of a hot magma with Al_2O_3 rich clay sediments. Since the first citation in 1924, a number of study have been carried out on the synthesis, properties, phase equilibrium and crystal chemistry of mullite ceramics and matrix composites [176-177].

2.6.1.1. Preparation of mullite by powder mixing method

Since 1959, dense mullite ceramic materials have been prepared using decomposition of mullite, kaolinite powders [178] at high temperature and later on, alumina and silica powder have been chosen to prepare mullite at high sintering temperatures [179]. *Wahl et al.* reported about several powders as source of mullite formation [180]. *Otani et al.* prepared mullite by thermal decomposition of methyl siloxy aluminium compounds [181]. *Sainz et al.* prepared mullite by the reaction sintering of kaolinite-alumina mixtures at the various sintering temperatures ranged from 1150 to 1700°C [182].

2.6.1.2. Sol-gel method

Highly pure and homogeneous phase of mullite was synthesized by sol-gel route [183-185]. The literature reports showed that mixing of aluminium and silicon sources in atomic level produced monophasic gel and mixing of precursors within 1 to 100 nm scale produced diphasic gel, water content, pH, presence of organic and inorganic additives, starting materials etc. are important factors to determine the properties of final mullite ceramics. The calcination of mullite gels at low and moderate temperatures have influenced on their behaviour at high temperatures especially on their crystallization temperature. Therefore, sol-gel method has shown beneficial route to prepare mullite ceramics at comparatively low temperatures which makes it cost effective material. On the other hand several other methods like, co-precipitation [186], hydrothermal [187], and chemical vapour deposition [188] processes, have also been reported to prepare mullite by aiming specific applications.

2.6.1.3. Structure of mullite

Mullite has an orthorhombic crystal structure with the space group 'Pbam' and unit cell dimensions of a = 0.7540 nm, b = 0.7680 nm, and c = 0.2885 nm for the stoichiometric composition [189]. On Figure 2.13, a [001] projection of an ideal unit cell is shown, from which it is obvious that mullite is made of chains of AlO_6 octahedra at the edges and centre of the unit cell, running parallel to the c-axis. These chains are joined by $(Al,Si)O_4$ tetrahedra forming double chains, which also run parallel to the c-axis. Mullite possesses a defect crystal structure [190] consisting of chains of slightly distorted Al-O octahedra which run parallel to the c axis of the orthorhombic unit cell. These chains are linked by discontinuous double chains of Al-O and Si-O tetrahedra with randomly distributed aluminium and silicon atoms. The discontinuities in the latter chains are caused by the movement of some of the aluminium (and possibly silicon) ions into normally unfilled tetrahedral positions because of insufficient oxygen atoms present to bond to them in the normal positions. The occupation of these new sites also increases the coordination of the remaining oxygen atoms and forces them into new positions that are slightly different from their original locations. The connection of octahedral and tetrahedral chains produces relatively wide structural channels that also run parallel to the c axis.

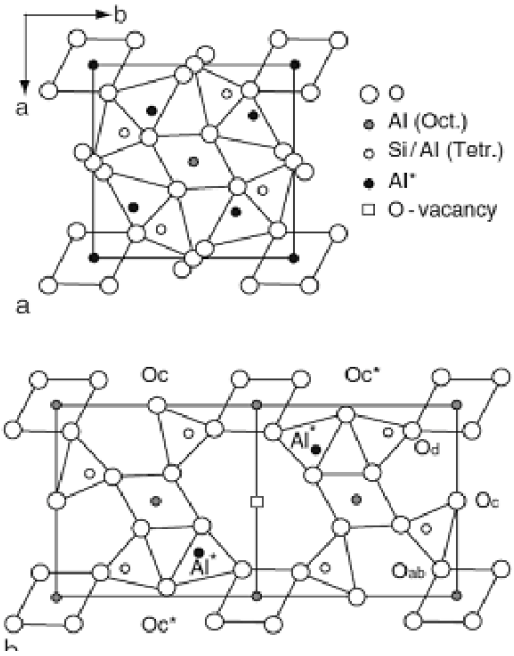

Figure 2.13. Projection of the ideal orthorhombic mullite unit cell which is associated with the formation of an oxygen vacancy and readjustment of oxygen in the O(3) positions [189].

2.6.1.4. Properties of mullite

A large number of technological applications are associated with the mullite refractory system due to its physical and chemical properties, including its low thermal expansion, low density, low thermal conductivity, its strong mechanical strength, good creep resistance, and its stability in harsh chemical environments [191]. The refractory properties are summarized in Table 2.6.

Table 2.6. Refractory properties of mullite

Properties	
Melting point (°C)	1840
Density (g/cc)	3.17
Thermal conductivity (W/m.K)	6
Thermal expansion co-efficient (1/K)	5.3×10^{-6}
Oxygen diffusion co-efficiency (m^2/s)	8.6×10^{-20} at 1000-1300°C
Flexural strength (MPa)	180
Compressive strength (MPa)	1310
Fracture toughness ($MPa.m^{1/2}$)	2.5-3.1 (RT to 1225°C)

2.6.2. Cordierite ($5SiO_2.2Al_2O_3.2MgO$)

Cordierite was discovered in 1813, in specimens from Níjar, Almería, Spain, is named after the French geologist Louis Cordier (1777–1861). Cordierite ($2MgO–2Al_2O_3–5SiO_2$) is another important kind of ceramic materials having $MgO–SiO_2–Al_2O_3$ systems that have a wide range of applications in various industrial areas due to its specific properties such as low thermal expansion (kiln furniture), high thermal resistance, high chemical durability, low dielectric constant, and interesting mechanical properties. Several processing methods have been accepted on cordierite refractory materials related to their preparation as arcing plate materials [192], synthesis from a mixture of talc, clay, calcined kyanite, alumina to get cordierite as the major crystalline phase with minor mullite phase [193-194] and on honey comb cordierite structures [195] etc. To prepare cordierite ceramic materials several methods have been reported till date using powder mixing, sol-gel, chelating ligation and colloidal mixing etc. methods at low sintering temperatures.

2.6.2.1. Preparation of cordierite by powder mixing method

Literature study indicated that several efforts are reported for the synthesis of cordierite ceramics by powder mixing methods [196-199]. *Grosjean* [197] studied the talc-clay reaction of different sources and he found 30 mass% talc and 70 mass% clay to be the most suitable composition as it showed minimum thermal expansion at 1000°C in all test samples fired at 1330 °C. *Boccaccini et al.* [199] fabricated cordierite glass matrix composites from fly ash and waste glass. Commercial alumina platelets were reinforced to improve the wear resistance of the material. For fly ash contents up to 20 mass%, nearly fully dense compacts could be fabricated at a low sintering temperature (650°C). Higher fly ash content hampered the densification process because other alkaline oxide impurities in the fly ash set up dangers for viscous flow to occur.

2.6.2.2. Sol-gel method

Han and *Park* [200-202] synthesized and sintered cordierite from metal alkoxides, using $Si(OC_2H_5)_4 \cdot Al(OC_3H_7)_3 \cdot Mg(OC_2H_5)_2$ by the sol-gel method. Densification of this powder compact, which was studied by using the precursor powders calcined at 900°C for 2h, improved at the sintering temperature of 800–900°C. An alkoxide sol-gel route was developed by *Tsai* [202] to prepare cordierite ceramics. From XRD results, they observed that up to temperature of 800°C, the cordierite ceramics remained amorphous but above this temperature, phase transition occurs from amorphous to crystalline. The μ-cordierite and α-cordierite phase was formed at 900°C and 1050°C respectively.

2.6.2.3. Structure of cordierite

According to the classification of silicates, cordierite belongs to the class of silicates and subclass of cyclosilicates. Cordierites containing the hexagonal and orthorhombic magnesium/alumina silicate frameworks consist of tetrahedral units $[(Si/Al)O_4]$, forming Si_6O_{18} six membered rings (Figure 2.14). The rings are stacked one above the other and successively rotated about 30° relatively to each other. These rings are linked together laterally and vertically by tetrahedra and $[MgO_6]$ octahedra. The ring stacking produces large hexagonal channels parallel to the c-axis, in which various cation or small molecular units can be inserted. The crystal structure of cordierite was investigated by several researchers.

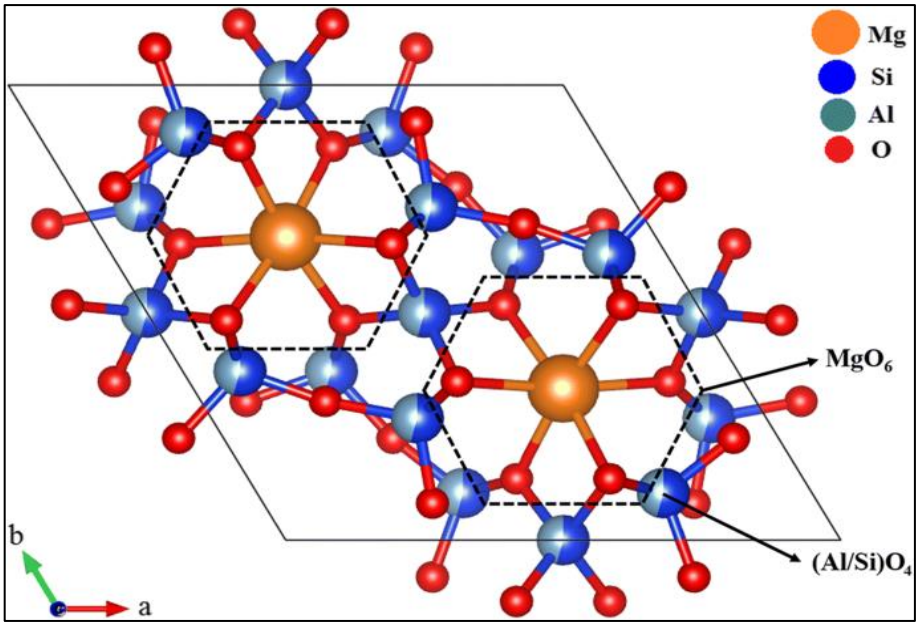

Figure 2.14. Three dimensional network of cordierite structure [203].

2.6.2.4. Properties of cordierite

The cordierite has been used as major phase of many ceramics and glass-ceramics due to their unique electrical and thermal properties which has made them versatile in different branches of industry [204]. Cordierite has very low thermal expansion coefficient close to that of silicon carbide, a high chemical resistivity, less volume expansion nature, a low dielectric constant, a high refractoriness with a high mechanical strength [205-206]. The details of their refractory properties are summarized in Table 2.7.

Table 2.7. Refractory properties of cordierite

Properties	
Melting point (°C)	1435
Density (g/cc)	2.63
Thermal conductivity (W/m.K)	3.0 @ RT
Thermal expansion co-efficient (1/K)	2.5×10^{-6}
Oxygen diffusion co-efficiency (m^2/s)	1.27×10^{-18} at 826-880°C
Specific heat (J/Kg.K)	350
Flexural strength (MPa)	~117 @ RT
Compressive strength (MPa)	350
Fracture toughness ($MPa.m^{1/2}$)	1.8-3.1 (RT to 1250-1300°C)

2.7. *Application of oxide bonded porous SiC ceramics*

2.7.1. Hot gas filtration

Since the late ninety's, several dust removal and gas treatment applications have relied on the use of highly porous ceramic membranes with narrow pore size distribution, especially where hot gases are present [207]. Hot gas filters are commonly used in industries like radioactive waste, biomass gasification [208], metal refining, incineration [209], coal gasification [210], biomass pyrolysis, integrated gasification combined cycle (IGCC) [211], metal recycling, and pressurized fluidized bed combustion (PFBC) [208, 212]. The asymmetric structure of the ceramic membrane element has the structural characteristics of small pore size of the membrane separation layer and large pore size of the support layer. One of the purposes of this design is to reduce the resistance during filtration, because it is the membrane that really plays the role of filtration and separation. Secondly, the pore size gradient is changed so that most of the soot particles are trapped when they pass through the membrane surface. The particles passing through the separation layer are getting larger and larger due to the size of the channel, and the adsorption force is getting smaller and smaller, so it is not easy to be blocked by adsorption in the channels of the support layer, so as to achieve the purpose of efficient separation. The porous ceramic membrane filter has outstanding advantages such as high temperature resistance, corrosion resistance, high mechanical strength, stable structure and no deformation, long service life, and it can achieve functional regeneration through many times of cleaning, so it is considered as one of the best choices of dust removal in high temperature flue gas. Compared with cyclone dust collectors, wet dust collectors, bag dust collectors and high-efficiency electrostatic precipitators, the porous ceramic filter has a higher dust removal efficiency, exceeding 99.9%, and its filtration performance, especially the filtration efficiency for ultrafine dust particles below PM2.5 is superior to other dust collectors. In addition, the porous ceramic filter material will not cause secondary pollution, and it is one of the most suitable and promising materials for the deep purification of high-temperature dust-containing flue gas. The efficiency of ceramic filter test results versus particle size is compared to other particulate filters in Figure 2.15.

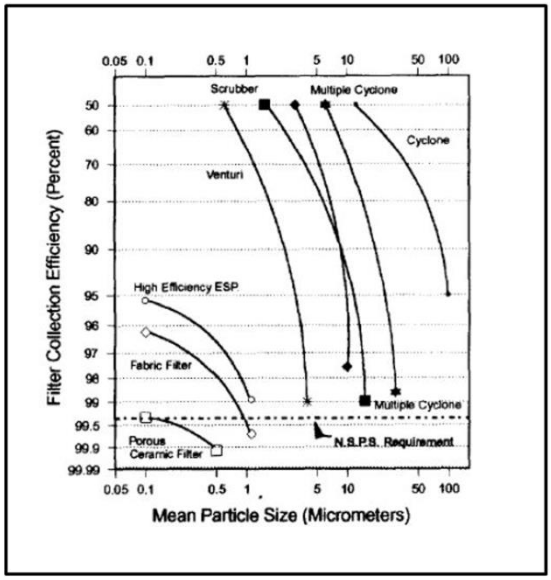

Figure 2.15. Efficiency of various separation processes [213].

With the development of coal gasification, coal liquefaction, fluidization, clean coal, and powder engineering technology, ceramic membranes for purification of high-temperature dusty gas are under urgent demand. For this, the further development of new ceramic membrane filter material technology research, improvement of product quality, and reduction of production costs are of great significance to the improvement of industrialization level. The development of ceramic membrane purification technology for industrial high-temperature dust-containing flue gas can effectively reduce the emission concentration of smoke and dust, reduce PM2.5 particulate matter emissions in industrial flue gas, and recover high-grade heat energy in the flue gas which can increase life time of turbine, increase energy efficiency and reduce atmospheric pollution. Enhancing the level of coordination between industrial development and the environment and making positive contributions to sustainable development and the construction of an environmentally friendly society are required in order to improve the quality of atmospheric environment.

2.7.2. *Wastewater filtration*

Wastewater is known as the polluted form of water that generated specifically, as domestic sewage, industrial sewage, or storm sewage [214]. The polluted water contains high amount of impurities so that it is unfit for any particular use and the discharge of these waste water into the environment, can disturb the balance of the ecosystem. There are various sources which generated large amount of wastewater and each wastewater contain its own combination of pollutants [215]. Depending on the source of wastewater, the pollutants mainly presents are

heavy metals, oil particle, colouring agents, micro plastics, bacteria, virus etc. The oil contaminated wastewater are generated in different industrial process, such as petrochemical, refinery processing, metallurgical industries, dairy industries [216], tanning and leather processing [217] and also from household usages. Discharge of this type of wastewater into sea or river will inhibit the self-purification processes and adversely affect the physicochemical and organoleptic properties of water. Therefore, these pollutants need to be efficiently treated to prevent intoxication of the environment and aquatic life. In addition, due to rapid industrialisation and urbanisation, there will be a water shortage in near future. Since the pure water is not found in nature, so wastewater must be treated before being discharged into the environment and for the reuse in the process that has been accepted as a sustainable option to address these problems [218]. Several conventional technologies has been used to separate oil from the oily wastewater. Membrane based filtration treatment considered as one of the emerging technologies for treating of wastewater due to its advantageous properties. Membranes are mainly polymeric or ceramic based and the ceramic units offer many advantages over polymeric ones, such as superior permeability, durability, easier cleaning, superior chemical, mechanical, and thermal stability [219-221]. In spite of these advantages, there are still several challenges for this technology that need to be addressed. These are mainly the fabrication cost, antifouling properties, selective separation, and utilization of this technology to large scale applications [222-223]. Porous SiC membranes are considered as suitable filter for water filtration and purification due to their advantageous properties compared to the other oxide and non-oxide ceramic membranes or polymeric membrane, those are: (i) higher porosity with narrow pore size distribution (ii) high chemical stability (iii) high mechanical stability and (iv) high hydrophilicity resulting in high fluxes at low pressures. Although SiC membranes are more vulnerable to breakage than polymeric membranes, but they are more suitable to withstand backwash pressures due to their mechanical stability [224-225] as well as their greater hydrothermal stability [226].

Membrane-based separation processes can be further classified according to the driving force and pressure driven membrane processes are the most commonly used. According to the membrane pore size, pressure driven membrane filtration can be divided into four methods: microfiltration (MF), ultrafiltration (UF), nanofiltration (NF) and reverse osmosis (RO). Pore size range and the separation characteristic of these four methods are shown in Figure 2.16 respectively.

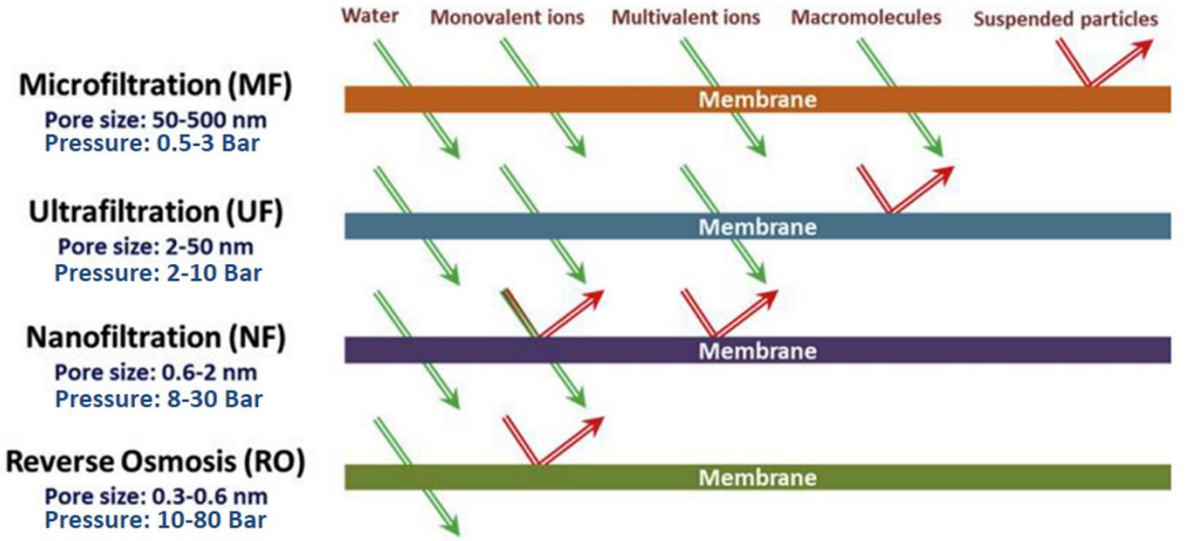

Figure 2.16. Schematic diagrams of microfiltration, ultrafiltration, nanofiltration and reverse osmosis [227].

For practical applications, membranes need to have a large surface area for effective filtration of wastewater [228]. Different configuration of ceramic membrane such as flat geometry (disc shaped, plate shaped) or cylindrical (single and multichannel tubes, hollow fibres tube) are fabricated and used to address different operational situations. Literature study indicated that the cylindrical configured membrane are more suitable because of easier sealing of the elements, high separation efficiency, higher permeability, and better capability to handle higher cross-flow velocities compared to flat geometry [223, 229] for wastewater filtration. However, researchers and ceramic membrane manufacturers in particular are concerned that ceramic brittleness may make it difficult for them to optimize the packing densities of ceramic modules in order to reduce the overall footprint of an installed treatment system in the field [229]. Figure 2.17 shows some photographs of commercially available flat sheet, tubular and hollow-fibre geometries for ceramic membranes.

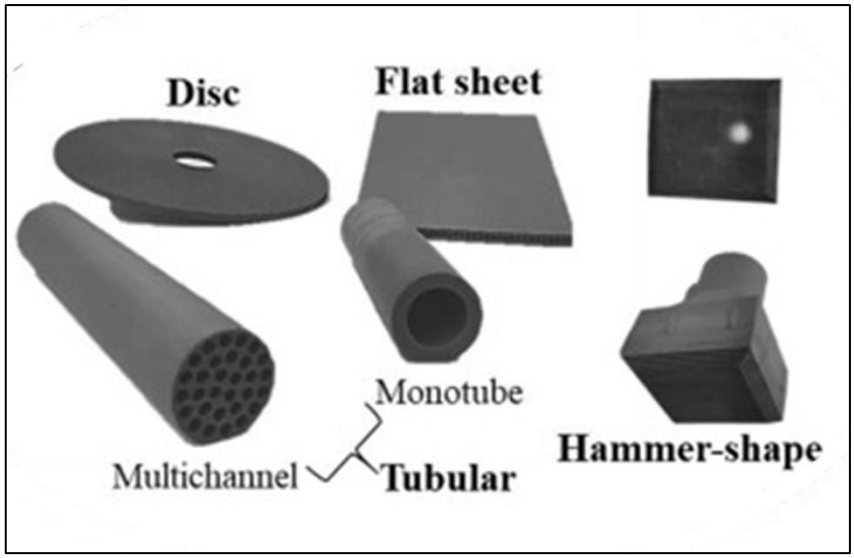

Figure 2.17. Photographs of commercially available flat sheet, tubular and hollow-fibre geometries for ceramic membranes.

Besides that, there are various configurations of operating a filtration process:

2.7.2.1. ***Dead-end filtration***

Dead-end filtration is the most simple, basic and cost effective method of filtration. In this method the particles/pollutants accumulated water is forced through the membrane. As a results the particles are accumulated, forms a cake layer on the membrane surface and this will increases the resistance of filtration. Hence the pressure loss above the filter medium. For this reason, the filter cake must be removed. The filters are cleaned at a regular intervals by backwashing or the filter material is replaced by a new, depending on the solid concentration in feed water. The membranes used in this process commonly flat shaped membrane.

2.7.2.2. Cross-flow filtration

This is the most convenient and commonly used filtration method. A fluid flows across the surface of the membrane rather than directly down onto it in cross-flow filtration. The high flow rates across the membrane surface decreases the fouling tendency of the membranes. Typically, tubes with a membrane layer on the interior wall of the tube are used in this process. This process is termed "cross-flow" because the flow directions of the feed and filtration are at a 90 degree angle. The cross-flow filtration process is an excellent method of filtering liquids with high levels of filterable matter.

2.7.2.3. Hybrid-flow filtration

This filtration method is the combination of the dead-end and the cross-flow filtration. Hybrid-flow filtration process has two phases of filtration. In first phase i.e., in production phase, one side of the membrane tubes are closed and the dead-end type filtration is performed and in the next step, in the flushing phase the membrane tube remains open in both side and cross-flow type filtration is carried out. This type of filtration is very much suitable for treating water streams containing suspended solids in low concentrations (polishing).

The literature review indicates that fabrication of porous SiC ceramics by oxide/reaction bonded method has become a globally popular choice; however many aspects of the processing method have not been at all studied or limited investigations were carried out. Moreover the possible application areas of oxide bonded macroporous SiC membrane are not fully explored. The following lists highlight the lacuna of research done so far:

1) The role of additives contents/ types of additive on formation of crystalline bond phases and the chemical reactions responsible for bond phase formation are not investigated in depth.

2) The utilizations of industrial waste on fabrication of porous SiC membranes at a significantly low temperature are not explored. Very limited reports are available on the effects of the bond phase composition on the materials and mechanical properties of the porous SiC ceramics which require systematic investigation.

3) Permeation behaviour of the macroporous SiC membrane prepared using industrial waste or optimum amount of clay/ alumina based sintering additives needs to be studied. Effects of fluid (gas) properties and flow conditions on the permeation behaviour are required to be investigated. In the published literature, very limited studies are available in these directions.

4) In order to determine the applicability of the porous SiC ceramics in particulate filtration or hot gas filtration it is essential to know particle capture efficiencies of the material. No report is published on evaluation of particulate filtration efficiency theoretically using experimental air permeation results though it is very important aspects.

5) The application of oxide bonded SiC ceramic membrane in wastewater filtration is current area of research, there are several issues (fabrication cost, water permeability, filtration efficiency, chemical corrosion resistance properties, fluid flow characteristics, reusability, fouling behaviour, etc.) which needs to be explored for commercialization.

6) To determine the application of SiC membrane in treatment of industrial wastewater, hot gas filtration, etc., it is essential to know the chemical and thermal shock resistance properties of the material. Literature review indicate a very few studies are carried out in this direction and there are many issues which needs further research.

The research work of the current thesis has been undertaken to address these issues. The objectives of the current research are mentioned in the next chapter.

References

1. M.E. Davis, Ordered porous materials for emerging applications, Nature, 417 (2002) 813-821.
2. J.P.F. Debruijn, A.Venegas, J.A. Martinez, Ultrafiltration performance of Carbosep membranes for the clarification of apple juice, LWT-Food Sci. Technol., 36 (2003) 397-406.
3. C.D. Chang, A.J. Silvestri, The conversion of methanol and other O-compounds to hydrocarbons over zeolite catalysts, J. Catal., 47 (1977) 249-259.
4. P.B. Venuto, E.T. Habib, Fluid catalytic cracking with zeolite catalysts, United States, (1979).
5. S.V. Donk, A.H. Janssen, J.H. Bitter, K.P. Jong, Generation, characterization, and impact of mesopores in zeolite catalysts, Catal. Rev., 45 (2003) 297-319.
6. T. Ben, H. Ren, S. Ma, D. Cao, J. Lan, X. Jing, W. Wang, J. Xu, F. Deng, J.M. Simmons, Targeted synthesis of a porous aromatic framework with high stability and exceptionally high surface area, Angewandte Chemie, 121 (2009) 9621-9624.
7. A.G. Slater, A.I. Cooper, Function-led design of new porous materials, Science, 348 (2015) 8075.
8. X. Qu, P.J. Alvarez, Q. Li, Applications of nanotechnology in water and wastewater treatment, Water Res., 47 (2013) 3931-3946.
9. Z. Ding, J.T. Kloprogge, R.L. Frost, G. Lu, H. Zhu, Porous clays and pillared clays-based catalysts. Part 2: a review of the catalytic and molecular sieve applications, J. Porous Mater., 8 (2001) 273-293.
10. S. Aguado, A.C. Polo, M.P. Bernal, J. Coronas, J. Santamar, Removal of pollutants from indoor air using zeolite membranes, J. Membr. Sci., 240 (2004) 159-166.
11. C. Perego, R. Millini, Porous materials in catalysis: challenges for mesoporous materials, Chem. Soc. Rev., 42 (2013) 3956-3976.
12. T. Ohji, Porous Ceramic Materials, Handbook of Advanced Ceramics, Elsevier Inc., 2013.
13. T. Konegger, L.F. Williams, R.K. Bordia, Polysilazane derived porous ceramic supports for membrane and catalysis applications, J. Am. Ceram. Soc., 98 (2015) 3047-3053.
14. L. Gauckler, M. Waeber, C. Conti, M.J. Duliere, Ceramic foam for molten metal filtration, J. Miner. Met. Mater. Soc., 37 (1985) 47-50.

15. G.B. Merrill, J.A. Morrison, High temperature insulation for ceramic matrix composites, US 6287511, 2000.
16. R.L. Helferich, R.C. Schenck, Porous ceramic article for use as a filter for removing particulates from diesel exhaust gases, US4976760A, 1990.
17. F. Rezaei, A. Mosca, P. Webley, J. Hedlund, P. Xiao, Comparison of traditional and structured adsorbents for CO_2 separation by vacuum swing adsorption, Ind. Eng. Chem. Res., 49 (2010) 4832-4841.
18. A. Corma, From microporous to mesoporous molecular sieve materials and their use in catalysis, Chem. Rev., 97 (1997) 2373-2420.
19. G. Nordlund, J.B. Sing Ng, L. Bergstrom, P. Brzezinski, A membrane reconstituted multisubunit functional proton pump on mesoporous silica particles, ACS nano, 3 (2009) 2639-2646.
20. J. Andersson, J. Rosenholm, S. Areva, M. Lindén, Influences of material characteristics on ibuprofen drug loading and release profiles from ordered micro-and mesoporous silica matrices, Chem. Mater., 16 (2004) 4160-4167.
21. M. Twigg, J. Richardson, Theory and applications of ceramic foam catalysts, Chem. Eng. Res. Des., 80 (2002) 183-189.
22. I.Y. Guzman, Highly Refractory Porous Ceramics, Metallurgiya, Moscow, (1971) 181-199.
23. M.V. Twigg, J.T. Richardson, Fundamentals and applications of structured ceramic foam catalysts, Ind. Eng. Chem. Res., 46 (2007) 4166-4177.
24. C. Galassi, Processing of porous ceramics: Piezoelectric materials, J. Eur. Ceram. Soc., 26 (2006) 2951-2958.
25. J.H. Eom, Y.W. Kim, S. Raju, Processing and properties of macroporous silicon carbide ceramics: A review, J. Asian Ceram. Soc., 1 (2013) 220-242.
26. P.V. Kumar, G.S. Gupta, Study of formation of silicon carbide in the Acheson process, Steel Res. Int., 73 (2002) 31-38.
27. F.V. Dijen, R. Metselaar, The chemistry of the carbothermal synthesis of β-SiC: Reaction mechanism, reaction rate and grain growth, J. Eur. Ceram. Soc., 7 (1991) 177-184.
28. W. Zhu, M. Yan, Effect of gas flow rate on ultrafine SiC powders synthesized through chemical vapor deposition in the SiH_4-C_2H_4-H_2 system, Scr. Mater., 39 (1998) 1675-1680.

29. J. Li, J. Tian, L. Dong, Synthesis of SiC precursors by a two-step sol–gel process and their conversion to SiC powders, J. Eur. Ceram. Soc., 20 (2000) 1853-1857.
30. B. Ravi, O. Omotoye, T. Srivatsan, M. Petrorali, T. Sudarshan, The microstructure and hardness of silicon carbide synthesized by plasma pressure compaction, J. Alloys Compd., 299 (2000) 292-296.
31. A. Huczko, M. Bystrzejewski, H. Lange, A. Fabianowska, S. Cudziło, A. Panas, M. Szala, Combustion synthesis as a novel method for production of 1-D SiC nanostructures, J. Phys. Chem. B, 109 (2005) 16244-16251.
32. D. Changhong, Z. Xianpeng, Z. Jinsong, Y. Yongjin, C. Lihua, X. Fei, The synthesis of ultrafine SiC powder by the microwave heating technique, J. Mater Sci., 32 (1997) 2469-2472.
33. K. Järrendahl, R.F. Davis, Materials properties and characterization of SiC, Semicond. Semimet., 52 (1998)1-20.
34. T. Ayalew, SiC semiconductor devices technology modeling and simulation, 2004.
35. H.A. Mantooth, M.D. Glover, P. Shepherd, Wide bandgap technologies and their implications on miniaturizing power electronic systems, IEEE J. Emerg. Sel. Top. Power Electron, 2(2014) 374-385.
36. S. Tian, Monte Carlo simulation of ion implantation in crystalline SiC with arbitrary polytypes, IEEE Trans. Electron Devices, 55 (2008) 1991-1996.
37. Y. Inomata, Z. Inoue, M. Mitomo, H. Suzuki, Relation between growth temperature and the structure of SiC crystals grown by the sublimation method, apps.dtic.mil., 1969.
38. A. Heuer, L. Ogbuji, T. Mitchell, The microstructure of oxide scales on oxidized Si and SiC single crystals, J. Am. Ceram. Soc., 63 (1980) 354-355.
39. H. Asgharzadeh, N. Ehsani, Densification and Microstructural Evolutions during Reaction Sintering of SiC-Si-C Powder Compacts, ISRN Mater. Sci., 2011 (2011).
40. M. Wilhelm, W. Wruss, Influence of annealing on the mechanical properties of SiC–Si composites with sub-micron SiC microstructures, J. Euro. Ceram. Soc., 20 (2000) 1205-1213.
41. W.M. Guo, Z.G. Yang, G.J. Zhang, Effect of carbon impurities on hot- pressed ZrB2–SiC ceramics, J. Am. Ceram. Soc., 94 (2011) 3241-3244.
42. I. Levin, D. Brandon, Metastable alumina polymorphs: crystal structures and transition sequences, J. Am. Ceram. Soc., 81 (1998) 1995–2012.

43. Y. Li, H. Wu, X. Liu, Z. Huang, D. Jiang, Microstructures and properties of solid-state-sintered silicon carbide membrane supports, Ceram. Int., 45 (2019) 19888-19894.
44. G. Magnani, G. Sico, A. Brentari, P. Fabbri, Solid-state pressureless sintering of silicon carbide below 2000°C, J. Euro. Ceram. Soc., 34 (2014) 4095-4098.
45. D.C. Jana, G. Sundararajan, K. Chattopadhyay, Effect of monomers content in enhancing solid-state densification of silicon carbide ceramics by aqueous gelcasting and pressureless sintering. Ceram. Int., 43 (2017) 4852-4857.
46. M.S. Datta, A.K. Bandyopadhyay, B. Chaudhuri, Sintering of nano crystalline a silicon carbide by doping with boron carbide, Bull. Mater. Sci., 25 (2002) 181–189.
47. J. Zhang, D. Jiang, Q. Lin, Z. Chen, Z. Huang, Gelcasting and pressureless sintering of silicon carbide ceramics using Al_2O_3–Y_2O_3 as the sintering additives, J. Eur. Ceram. Soc., 33 (2013) 1695-1699.
48. W. Guo, H. Xiao, X. Yao, J. Liu, J. Liang, P. Gao, G. Zeng, Tuning pore structure of corrosion resistant solid-state-sintered SiC porous ceramics by particle size distribution and phase transformation, Mater. Des., 100 (2016) 1-7.
49. C.Y. Liu, W.H. Tuan, S.C. Chen, Ballistic performance of liquid-phase sintered silicon carbide, Ceram. Int., 39 (2013) 8253-8259.
50. Y.W. Kim, H. Tanaka, M. Mitomo, S. Otani, Influence of powder characteristics on liquid phase sintering of silicon carbide, J. Ceram. Soc. Jpn., 103 (1995) 257-261.
51. A. Malinge, A. Coupé, Y.L. Petitcorps, Pressureless sintering of beta silicon carbide nanoparticles, J. Eur. Ceram. Soc., 32 (2012) 4393-4400.
52. U. Sabu, B. Majumdar, B.P. Saha, Spark plasma sintering of silicon carbide with Al_2O_3 and CaO: Densification behaviour, phase evolution and mechanical properties, Trans. Indian Ceram. Soc., 77 (2018) 4.
53. S. Aroati, M. Cafri, H. Dilman, M.P. Dariel, Preparation of reaction bonded silicon carbide (RBSC) using boron carbide as an alternative source of carbon, J. Eur. Ceram. Soc., 31 (2011) 841-845.
54. L. Wahl, M. Lorenz, J. Biggemann, N. Travitzky, Robocasting of reaction bonded silicon carbide structures, J. Eur. Ceram. Soc., 39 (2019) 4520-4526.
55. S. Meyers, L.D. Leersnijder, J. Vleugels, Direct laser sintering of reaction bonded silicon carbide with low residual silicon content, J. Eur. Ceram. Soc., 38 (2018) 3709-3717.

56. N.L. Zhang, J.F. Yang, Y.C. Deng, B. Wang, P. Yin, Preparation and properties of reaction bonded silicon carbide (RB-SiC) ceramics with high SiC percentage by two-step sintering using compound carbon sources, Ceram. Int., 45 (2019) 15715-15719.

57. D.W. Shin, S.S. Park, Y.H. Choa, Silicon/silicon carbide composites fabricated by infiltration of a silicon melt into charcoal, J. Am. Ceram. Soc., 82 (1999) 3251-3253.

58. C. Hu, Y. Sakka, J. Gao, H. Tanaka, S. Grasso, Microstructure characterization of ZrB_2–SiC composite fabricated by spark plasma sintering with $TaSi_2$ additive, J. Eur. Ceram. Soc., 32 (2012) 1441-1446.

59. S. Jafari, M.B. Vandchali, M. Mashhadi, Effects of HfB_2 addition on pressureless sintering behavior and microstructure of ZrB_2-SiC composites, Int. J. Refract. Hard Met., 94 (2021)105371.

60. M. Landon, F. Thevenot, The SiC–AlN system: Influence of elaboration routes on the solid solution formation and its mechanical properties, Ceram. Int., 17 (1991) 97-110.

61. A.S. Namini, S.A. Delbari, M.S. Asl, Q.V. Le, Characterization of reactive spark plasma sintered (Zr,Ti)B_2–ZrC–SiC composites, J. Taiwan Inst. Chem. Eng., 119 (2021) 187-195.

62. R. Ruh, A. Zangvil, Composition and properties of hot-pressed SiC-AIN solid solutions, J. Am. Ceram. Soc., 65 (1982) 260-265.

63. V. Suwanmethanond, E. Goo, P.K. Liu, G. Johnston, M. Sahimi, T.T. Tsotsis, Porous silicon carbide sintered substrates for high temperature membranes, Ind. Eng. Chem. Res., 39 (2000) 3264-3271.

64. J. Ihle, M. Herrmann, J. Adler, Phase formation in porous liquid phase sintered silicon carbide: Part III: Interaction between Al_2O_3–Y_2O_3 and SiC, J. Eur. Ceram. Soc., 25 (2005) 1005-1013.

65. C. Wang, J. Wang, C. Park, Y.W. Kim, Cross linking behavior of a polysiloxane in preceramic foam processing, J. Mater. Sci., 39 (2004) 4913-4915.

66. T. Shimonosono, S. Ikeyama, Y. Hirata, S. Sameshima, Compressive deformation of liquid phase-sintered porous silicon carbide ceramics, J. Asian Ceram. Soc., 2 (2014) 422-428.

67. Z.Y. Deng, J. She, Y. Inagaki, J.F. Yang, T. Ohji, Y. Tanaka, Reinforcement by crack tip blunting in porous ceramics, J. Eur. Ceram. Soc., 24 (2004) 2055-2059.

68. E.S. Kang, Y.W. Kim, W.H. Nam, Multiple thermal resistance induced extremely low thermal conductivity in porous SiC-SiO_2 ceramics with hierarchical porosity, J. Eur. Ceram. Soc., 41 (2021) 1171-1180.

69. B.K. Jang, Y. Sakka, Influence of microstructure on the thermo-physical properties of sintered SiC ceramics, J. Alloys Compd., 463 (2008) 493-497.

70. B.K. Jang, Y. Sakka, Thermophysical properties of porous SiC ceramics fabricated by pressureless sintering, Sci. Technol Adv. Mater., 8 (2007) 655-659.

71. J.F. Zhang, X.N. Zhou, Q. Zhi, S. Zhao, X. Huang, N.L. Zhang, Microstructure and mechanical properties of porous SiC ceramics by carbothermal reduction and subsequent recrystallization sintering, J. Asian Ceram. Soc., 8 (2020) 255-264.

72. J. Hvam, P. Morgen, E.M. Skou, U.G. Nielsen, T. Wolff, T.E. Warner, The role of aluminium as an additive element in the synthesis of porous 4H-silicon carbide, J. Eur. Ceram. Soc., 36 (2016) 3267-3278.

73. C. Reynaud, F. Thevenot, Porosity dependence of mechanical properties of porous sintered SiC: Verification of the minimum solid area model, J. Mater. Sci. Lett., 19 (2000) 871-874.

74. M. Fukushima, Y. Zhou, Y.I. Yoshizawa, Fabrication and microstructural characterization of porous silicon carbide with nano-sized powders, Mater. Sci. Eng. B, 148 (2008) 211-214.

75. P. Wan, J. Wang, Highly porous nano SiC with very low thermal conductivity and excellent high temperature behaviour, J. Eur. Ceram. Soc., 38 (2018) 463-467.

76. P. Wan, Z. Wu, H. Zhang, L. Gao, J. Wang, Porous nano-SiC as thermal insulator: wisdom on balancing thermal stability, high strength and low thermal conductivity, Mater. Res. Lett., 4 (2016) 104-111.

77. X. Zhu, D. Jiang, S. Tan, The control of slurry rheology in the processing of reticulated porous ceramics, Mater. Res. Bull., 37 (2002) 541-553.

78. J.M. Qian, J.P. Wang, G.J. Qiao, Z.H. Jin, Preparation of porous SiC ceramic with a woodlike microstructure by sol-gel and carbothermal reduction processing, J. Eur. Ceram. Soc., 24 (2004) 3251-3259.

79. X. Yuan, J. Lü, X. Yan, L. Hu, Q. Xue, Preparation of ordered mesoporous silicon carbide monoliths via preceramic polymer nanocasting, Micropor. Mesopor. Mat., 142 (2011) 754-758.

80. J.H. Eom, Y.W. Kim, C.B. Park, C. Wang, Effect of forming methods on porosity and compressive strength of polysiloxane-derived porous silicon carbide ceramics, J. Ceram. Soc. Jpn., 120 (2012) 199-203.

81. P. Greil, T. Lifka, A. Kaindl, Biomorphic cellular silicon carbide ceramics from wood: I. Processing and microstructure, J. Eur. Ceram. Soc., 18 (1998) 1961-1973.

82. Y. Yang, Q. Guo, S. Li, S. Zhao, J. Shi, L. Liu, Silicon carbide foams produced by siliciding carbon foams derived from mixtures of mesophase pitch and nano-SiC particles, Mater. Sci. Eng. A, 488 (2008) 514-518.

83. G.A. Labat, C. Zollfrank, A. Ortona, S. Pusterla, A. Pizzi, V. Fierro, A. Celzard, Structure and oxidation resistance of micro-cellular Si–SiC foams derived from natural resins, Ceram. Int., 39 (2013) 1841-1851.

84. T. Xue, Z.J.W. Wang, Preparation of porous SiC ceramics from waste cotton linter by reactive liquid Si infiltration technique, Mater. Sci. Eng. A, 527 (2010) 7294-7298.

85. S. Roy, K.G. Schell, E.C. Bucharsky, Processing and elastic property characterization of porous SiC preform for interpenetrating metal/ceramic composites, J. Am. Ceram. Soc., 95 (2012) 3078-3083

86. W. Chi, D. Jiang, Z. Huang, S. Tan, Sintering behaviour of porous SiC ceramics, Ceram. Int., 30 (2004) 869-874.

87. S. Ying, T.S. Hong, J.D. Liang, J. Inorg. Mater., 18 (2003) 830-83.

88. T.J. Fitzgerald, V.J. Michaud, A. Mortensen, Processing of microcellular SiC foams, J. Mater. Sci., 30 (1995) 1037-1045.

89. T.H. Yoon, H.J. Lee, J. Yan, D.P. Kim, Fabrication of SiC-based ceramic microstructures from preceramic polymers with sacrificial templates and lithographic techniques-A review, J. Ceram. Soc. Jpn., 114 (2006) 1330.

90. P. Colombo, Engineering porosity in polymer-derived ceramics, J. Eur. Ceram. Soc., 28 (2008) 1389-95.

91. A. Shimamura, M. Fukushima, M. Hotta, T. Ohji, N. Kondo, Fabrication and characterization of porous alumina with denser surface layer by direct foaming,J. Ceram. Soc. Jpn., 125 (2017) 7-11.

92. Y.W. Kim, S.H. Kim, C. Wang, C.B. Park, Fabrication of microcellular ceramics using gaseous carbon dioxide, J. Ame. Ceram. Soc., 86 (2003) 2231-2233.

93. Y.W. Kim, C.B. Park, Processing of microcellular preceramics using carbon dioxide, Compos. Sci. Technol., 63 (2003) 2371-2377.

94. B.V.M. Kumar, J.H. Eom, Y.W. Kim, Effect of filler addition on porosity and strength of polysiloxane-derived porous silicon carbide ceramics, J. Ceram. Soc. Jpn., 119 (2011) 48–54.

95. S. Liu, Y.P. Zeng, D. Jiang, S. Liu, Effects of preheat- treated aluminosilicate addition on the phase development, microstructure, and mechanical properties of mullitized porous OBSC ceramics, Int. J. Appl. Ceram. Technol., 6 (2009) 617–625.

96. S. Zhu, S. Ding, H. Xi, R. Wang, Low-temperature fabrication of porous SiC ceramics by preceramic polymer reaction bonding, Mater. Lett., 59 (2005) 595–597.

97. S. Liu, Y.P. Zeng, D. Jiang, Fabrication and characterization of cordierite-bonded porous SiC ceramics, Ceram. Int., 35 (2009) 597–602.

98. I.H. Song, M.J. Park, H.D. Kim, Y.W. Kim, J.S. Bae, Microstructure and permeability property of Si bonded porous SiC with variations in the carbon content, J. Korean Ceram. Soc., 47 (2010) 546–552.

99. S. Wood, A.T. Harris, Porous burners for lean-burn applications, Prog. Energy Combust. Sci., 34 (2008) 667-684.

100. T. Ohji, M. Fukushima, Macro-porous ceramics: processing and properties, Int. Mater. Rev., 57 (2012) 115–131.

101. P.K. Lin, D.S. Tsai, Preparation and analysis of a silicon carbide composite membrane J. Am. Ceram. Soc., 80(1997) 365–372.

102. M. Fukushima, Y. Zhou, H. Miyazaki, Y. Yoshizawa, K. Hirao, Y. Iwamoto, S. Yamazaki, T. Nagano, Microstructural characterization of porous silicon carbide membrane support with and without alumina additive, J. Am. Ceram. Soc., 89 (2006) 1523–1526.

103. M. Fukushima, Y. Zhou, Y. Yoshizawa, K. Hirao, Oxidation behavior of porous silicon carbide ceramics under water vapor below 1000°C and their microstructural characterization, J. Ceram. Soc. Jpn., 114 (2006) 1155–1159.

104. H.S. Zhao, Z.G. Liu, Y. Yang, X.X. Liu, K.H. Zhang, Z.Q. Li, Preparation and properties of porous silicon carbide ceramics through coat-mix and composite additives process Trans. Nonferrous Met. Soc. China, 21 (2011) 1329–1334.

105. S.H. Kim, Y.W. Kim, J.Y. Yun, H.D. Kim, Manufacture and Characteristics of Porous Silicon Carbide Ceramics by Partial Sintering Process, J. Korean Ceram. Soc., 41 (2004) 541–547.

106. Y. Zhou, M. Fukushima, H. Miyazaki, Y. Yoshizawa, K. Hirao, Y. Iwamoto, K. Sato, Preparation and characterization of tubular porous silicon carbide membrane supports, J. Membr. Sci., 369 (2011) 112–118.

107. F. Kawamura, H. Yamane, T. Yamada, S. Yin, T. Sato, Low temperature fabrication of porous β- SiC ceramics in sodium vapor, J. Am. Ceram. Soc., 91 (2008) 51–55.

108. M. Hotta, H. Kita, H. Matsuura, N. Enomoto, J. Hojo, Pore size control in porous SiC ceramics prepared by spark plasma sintering, J. Ceram. Soc. Jpn., 120 (2012) 243–247.

109. Y. Kim, K. Min, J. Shim, D.J. Kim, Formation of porous SiC ceramics via recrystallization, J. Eur. Ceram. Soc., 32(2012) 3611–3615.

110. G. Liu, P. Dai, Y. Wang, J. Yang,Y. Zhang, Fabrication of wood-like porous silicon carbide ceramics without templates, J. Eur. Ceram. Soc., 31(2011) 847–854.

111. X. Zhu, D. Jiang, S. Tan, Microwave absorbing property of SiC reticulated porous ceramics, Mater. Res. Bull., 37 (2002) 541–553.

112. X. Zhu, D. Jiang, S. Tan, Preparation of silicon carbide reticulated porous ceramics, Mater, Sci. Eng. A, 323 (2002) 232–238.

113. R. Mouazer, S. Mullens, I. Thijs, J. Luyten, A. Beukenhoudt, Silicon carbide foams by polyurethane replica technique, Adv. Eng. Mater., 7 (2005) 1124–1128.

114. X. Yao, S. Tan, X. Zhang, Z. Huang, D. Jiang, Low temperature sintering of SiC reticulated porous ceramics with $MgO–Al_2O_3–SiO_2$ additives as sintering aids, J. Mater. Sci., 42 (2007) 4960–4966.

115. U. Soy, A. Demir, F. Caliskan, Effect of bentonite addition on fabrication of reticulated porous SiC ceramics for liquid metal infiltration, Ceram. Int., 37 (2011) 15–19.

116. X. Bao, M.R. Nangrejo, M.J. Edirisinghe, Preparation of silicon carbide foams using polymeric precursor solutions, J. Mater. Sci., 35, 4365–4372 (2000).

117. M.R. Nangrejo, M.J. Edirisinghe, Porosity and strength of silicon carbide foams prepared using preceramic polymers, J. Porous Mater., 9 (2002) 131–140.

118. X. Yao, S. Tan, Z. Huang, D. Jiang, Effect of recoating slurry viscosity on the properties of reticulated porous silicon carbide ceramics Ceram. Int., 32 (2006) 137–142.

119. X. Zhu, D. Jiang, S. Tan, Z. Zhang, Improvement in the strut thickness of reticulated porous ceramics, J. Am. Ceram. Soc., 84 (2001) 1654–1656.

120. M.R. Nangrejo, X. Bao, M.J. Edirisinghe, The structure of ceramic foams produced using polymeric precursors, J. Mater. Sci. Lett., 19 (2000) 787–789.

121. M.R. Nangrejo, X. Bao, M.J. Edirisinghe, Preparation of silicon carbide–silicon nitride composite foams from pre-ceramic polymers, J. Eur. Ceram. Soc., 20 (2000) 1777–1785.

122. A. Zampieri, H. Sieber, T. Selvam, G.T.P. Mabande, W. Schwieger, F. Scheffler, M. Scheffler, P. Greil, Zeolite covered polymer derived ceramic foams: novel hierarchical pore systems for sorption and catalysis, Adv. Mater., 17 (2005) 344–349.

123. V.S. Kaul, K.T. Faber, R.E. Sepulveda, A.R.A. Lopez, J.M. Fernandez, Precursor selection and its role in the mechanical properties of porous SiC derived from wood, Mater. Sci. Eng. A, 428 (2006) 225–232.

124. P. Greil, Advanced engineering ceramics, Adv. Mater., 14 (2002) 709–716.

125. K.E. Pappacena, K.T. Faber, Thermal conductivity of porous silicon carbide derived from wood precursors, J. Am. Ceram. Soc., 90 (2007) 2855–2862.

126. A. Herzog, U. Vogt, O. Kaczmarek, R. Klingner, K. Richter, H. Thoemen, Porous SiC ceramics derived from tailored wood- based fibreboards, J. Am. Ceram. Soc., 89 (2006) 1499–1503.

127. A.R. Studart, U.T. Gonzenbach, E. Tervoort, L.J. Gauckler, Processing routes to macroporous ceramics: a review, J. Am. Ceram. Soc., 89 (2006) 1771–1789.

128. S.H. Lee, Y.W. Kim, Processing of cellular SiC ceramics using polymer microbeads, J. Korean Ceram. Soc., 43 (2006) 458–462.

129. J.H. Eom, Y.W. Kim, Effect of template size on microstructure and strength of porous silicon carbide ceramics, J. Ceram. Soc. Jpn., 116 (2008) 1159–1163.

130. J.H. Eom, Y.W. Kim, I.H. Song, Effects of the initial α-SiC content on the microstructure, mechanical properties, and permeability of macroporous silicon carbide ceramics, J. Eur. Ceram. Soc., 32 (2012) 1283–1290.

131. J.H. Eom, Y.W. Kim, Effect of initial α-phase content on microstructure and flexural strength of macroporous silicon carbide ceramics, Met. Mater. Int., 18 (2012) 379–383.

132. Y.W. Kim, S.H. Kim, I.H. Song, H.D. Kim, C.B. Park, Fabrication of open- cell, microcellular silicon carbide ceramics by carbothermal reduction, J. Am. Ceram. Soc., 88 (2005) 2949–2951.

133. G.T. Burns, R.B. Taylor, Y. Xu, A. Zangvil, G.A. Zank, High temperature chemistry of the conversion of siloxanes to silicon carbide, Chem. Mater., 4 (1992)1313–1323.

134. J.H. Eom, Y.W. Kim, M. Narisawa, Microstructural development of macroporous silicon carbide ceramics during annealing, J. Ceram. Process. Res., 2 (2008) 176–179.

135. J.H. Eom, Y.W. Kim, M. Narisawa, Processing of porous silicon carbide with toughened strut microstructure, J. Ceram. Soc. Jpn., 118 (2010) 380–383.

136. A. Bereciartu, N. Ordása, C.G. Rosales, A. Morono, M. Malo, E.R. Hodgson, J. Abellà, L. Sedano, Manufacturing and characterization of porous SiC for flow channel inserts in dual-coolant blanket designs, Fusion Eng. Des., 86 (2011) 2526–2529.

137. Y.J. Jin, Y.W. Kim, Low temperature processing of highly porous silicon carbide ceramics with improved flexural strength, J. Mater. Sci., 45 (2010) 282–285.

138. H. Yamane, T. Shirai, H. Morito, T. Yamada, Y. Hasegawa, T. Ikeda, Fabrication of porous SiC ceramics having pores shaped with Si grain templates, J. Eur. Ceram. Soc., 31 (2011) 409–413.

139. K. Sung, S.B. Yoon, J.S. Yu, D.P. Kim, Fabrication of macroporous SiC from templated preceramic polymers, Chem. Commun., (2002) 1480–1481.

140. B.V.M. Kumar, Y.W. Kim, Processing of polysiloxane-derived porous ceramics: a review, Sci. Technol, Adv. Mater., 11 (2010) 044303.

141. Y.W. Kim, J.H. Eom, C. Wang, C.B. Park, Processing of porous silicon carbide ceramics from carbon- filled polysiloxane by extrusion and carbothermal reduction, J. Am. Ceram. Soc., 91(2008) 1361–1364.

142. M. Fukushima, P. Colombo, Silicon carbide-based foams from direct blowing of polycarbosilane, J. Eur. Ceram. Soc., 32 (2012) 503–510.

143. X. Bao, M.R. Nangrejo, M.J. Edirisinghe, Synthesis of silicon carbide foams from polymeric precursors and their blends, J. Mater. Sci., 34 (1999) 2495–2505.

144. Y.W. Kim, S.H. Kim, C. Wang, C.B. Park, Fabrication of microcellular ceramics using gaseous carbon dioxide, J. Am. Ceram. Soc., 86 (2003) 2231–2233.

145. Y.W. Kim, C.B. Park, Processing of microcellular preceramic using carbon dioxide, Compos. Sci. Technol., 63 (2003) 2371–2377.

146. Y.W. Kim, C. Wang, C.B. Park, Processing of porous silicon oxycarbide ceramics from extruded blends of polysiloxane and polymer microbead, J. Ceram. Soc. Jpn., 115 (2007) 419–424.

147. Y.W. Kim, S.H. Kim, X. Xu, C.H. Choi, C.B. Park, H.D. Kim, Fabrication of porous preceramic polymers using carbon dioxide, J. Mater. Sci. Lett., 21 (2002) 1667–1669.

148. P. Colombo, E. Bernardo, Macro and micro-cellular porous ceramics from preceramic polymers, Compos. Sci. Technol., 63 (2003) 2353–2359.

149. P. Colombo, Conventional and novel processing methods for cellular ceramics, Philos. Trans. R. Soc., 364 (2006) 109–124.

150. S. Ding, Y.P. Zeng, D. Jiang, In-situ reaction bonding of porous SiC ceramics Mater. Charact., 59 (2008) 140–143.

151. J.H. She, Z.Y. Deng, J.D. Doni, T. Ohji, Oxidation bonding of porous silicon carbide ceramics, J. Mater. Sci., 37 (2002) 3615–3622.

152. J.H. She, J.F. Yang, N. Kondo, T. Ohji, S. Kanzaki, Z.Y. Deng, High- strength porous silicon carbide ceramics by an oxidation- bonding technique, J. Am. Ceram. Soc., 85 (2002) 2852–2854.

153. J.H. She, T. Ohji, Z.Y. Deng, Thermal shock behaviour of porous silicon carbide ceramics, J. Am. Ceram. Soc., 85 (2002) 2125–2127.

154. J.H. She, T. Ohji, S. Kanzaki, Oxidation bonding of porous silicon carbide ceramics with synergistic performance, J. Eur. Ceram. Soc., 24 (2004) 331–334.

155. Y.S. Chun, Y.W. Kim, Processing and mechanical properties of porous silica bonded silicon carbide ceramics, Met. Mater. Int., 11(2005) 351–355.

156. Y.H. Choi, Y.W. Kim, I.S. Han, S.K. Woo, Effect of alkaline earth metal oxide addition on flexural strength of porous mullite-bonded silicon carbide ceramics, J. Mater. Sci., 45 (2010) 6841–6844.

157. Y.H. Choi, Y.W. Kim, S.K. Woo, I.S. Han, Effect of template content on microstructure and flexural strength of porous mullite bonded silicon carbide ceramics, J. Korean Ceram. Soc., 47 (2010) 509–514.

158. A. Dey, N. Kayal, O. Chakrabarti, Preparation of mullite bonded porous SiC ceramics by an infiltration method, J. Mater. Sci., 46 (2011) 5432–5438.

159. N. Kayal, A. Dey, O.P. Chakrabarti, Incorporation of mullite as a bond phase into porous SiC by an infiltration technique, Mater. Sci. Eng. A, 535(2012) 222–227.

160. N. Kayal, A. Dey, O.P. Chakrabarti, Synthesis of mullite bonded porous SiC ceramics by a liquid precursor infiltration method: Effect of sintering temperature on material and mechanical properties, Mater. Sci. Eng. A, 556 (2012) 789–795.

161. J.H. Eom, Y.W. Kim, Effect of additive composition on microstructure and strength of porous silicon carbide ceramics, J. Mater. Sci., 44 (2009) 4482–4486.

162. J.H. Eom, Y.W. Kim, Effect of additives on mechanical properties of macroporous silicon carbide ceramics, Met. Mater. Int., 16 (2010) 399–405.

163. M.G. Kakroudi, N.P. Vafa, M.S. Asl, M. Shokouhimehr, Effects of SiC content on thermal shock behavior and elastic modulus of cordierite–mullite composites, Ceram. Int., 46 (2020) 23780-23784.

164. S. Zhu, S. Ding, H. Xi, Q. Li, R. Wang, Preparation and characterization of SiC/cordierite composite porous ceramics, Ceram. Int., 33 (2007) 115–118.

165. S.B. Hanna, M. Awaad, N.A. Ajiba, E.A. Saad, Characterization of porous alumino-silicate bonded SiC-ceramics prepared by hand-pressing and extrusion methods, Silicon, 2017.

166. B.V.M. Kumar, J.H. Eom, Y.W. Kim, I.H. Song, H.D. Kim, Effect of aluminum hydroxide content on porosity and strength of porous mullite bonded silicon carbide ceramics, J. Ceram. Soc. Jpn., 119 (2011) 367–370.

167. Y. Jing, X. Deng, J. Li, C. Bai, W. Jiang, Fabrication and properties of SiC/mullite composite porous ceramics, Ceram. Int., 40 (2014) 1329-1334.

168. B. Wang, H. Zhang, H.T. Phuong, F. Jin, J.F. Yang, K. Ishizaki, Gas permeability and adsorbability of the glass-bonded porous silicon carbide ceramics with controlled pore size, Ceram. Int., 41 (2015) 2279-2285.

169. G.P. Kennedy, K.Y. Lim, Y.W. Kim, Effect of additive composition on porosity and flexural strength of porous self-bonded SiC ceramics, J. Ceram. Soc. Jpn., 118 (2010) 810–813.

170. H.F. Lopez, W. Phoomiphakdeephan, High temperature oxidation of nitride bonded SiC-ceramics, Mater. Lett., 36 (1998) 65–69.

171. Y. Zhang, Microstructures and mechanical properties of silicon nitride bonded silicon carbide ceramic foams, Mater. Res. Bull., 39 (2004) 755–761.

172. J. Ihle, M. Herrmann, J. Adler, Phase formation in porous liquid phase sintered silicon carbide: Part I: Interaction between Al_2O_3 and SiC, J. Eur. Ceram. Soc., 25 (2005) 987–995.

173. M.A. Alvin, T.E. Lippert, J.E. Lane, Assessment of Porous Ceramic Materials for Hot Gas Filtration Applications. Am. Ceram. Soc. Bull., 70 (1991) 1491-1498.

174. E. Simeone, M. Siedlecki, M. Nacken, S. Heidenreich, W. de Jong, High temperature gas filtration with ceramic candles and ashes characterisation during steam-oxygen blown gasification of biomass, Fuel, 108 (2013) 99-111.

175. S. Heidenreich, W. Haag, M. Salinger, Next generation of ceramic hot gas filter with safety fuses integrated in venturi ejectors, Fuel, 108 (2013) 19-23.

176. X. Guan, B. Gardner, R.A. Martin, J. Spain, Demonstration of hot gas filtration in advanced coal gasification system. Powder Technol., 180 (2008) 122-128.

177. Y. Ohtsuka, N. Tsubouchi, T. Kikuchi, H. Hashimoto, Recent progress in Japan on hot gas cleanup of hydrogen chloride, hydrogen sulfide and ammonia in coal-derived fuel gas, Powder Technol., 190 (2009) 340-347.

178. S. Heidenreich, B. Scheibner, Hot gas filtration with ceramic filters: Experiences and new developments, Filtr. Separat., 39 (2002) 22-25.

179. T. Mushiri, K. Manjengwa, C. Mbohwa, Advanced Fuzzy Control in Industrial Wastewater Treatment (pH and Temperature Control), Proceedings of the World Congress on Engineering, London, UK, I, 2014.

180. S. Hanchang, Industrial wastewater-types, amounts and effects, Point Sources of Pollution: Local Effects and their Control-Volume II, (2009) 19-202.

181. E Ankyu, R Noguchi, Economical evaluation of introducing oil-water separation technology to wastewater treatment of food processing factory based on separation engineering, Agric. Agric. Sci. Procedia, 2 (2014) 67–73.

182. J. Coca, G. Gutierréz, J.M. Benito, Treatment of oily wastewater, Water Purification and Management, (2010) 1–55.

183. S.A. Deowan, S.I. Bouhadjar, J. Hoinkis, Membrane bioreactors for water treatment, Advances in Membrane Technologies for Water Treatment, Wood head Publishing, Oxford, (2015) 155-184.

184. T.T. More, S. Yan, R.D. Tyagi, R.Y. Surampalli, Applications of membrane processes for concentrated industrial wastewater treatment, Membr. Technol. Environ. App., (2012) 217-238.

185. R.W. Baker, Membrane technology and applications, John Wiley & Sons, Ltd, (2004) 96-103.

186. S. Luque, D. Gómez, J.R. Álvarez, Industrial applications of porous ceramic membranes (pressure- driven processes), Membr. Sci. Technol., 13 (2008) 177-216.

187. P. Sanciolo, S. Gray, Outcomes of membrane research: Impacts on the australian and international water industry, Institute for Sustainability and Innovation Victoria University, 2014.

188. A.K. Pabby, Handbook of Membrane Separations Chemical, Pharmaceutical, Food and Biotechnological Applications, Second Edition, Hoboken, 2015.

189. A. Lerch, S. Panglishch, P Buchta, Y. Tomitac, H. Yonekawa, K. Hattori, R. Gimbel, Direct river water treatment using coagulation/ceramic microfiltration, Desalination, 179 (2005) 41-50.

190. N. Shirasaki, T. matshushita, Y. matsui, K. Ohno, Effects of reversible and irreversible membrane fouling on virous removal by a coagulation microfiltration system, J. Water Supply Res. T. AQUA, 57 (2008) 501-506.

191. A. Buekenhoudt, Stability of porous ceramic membranes, Membr. Sci. Technol., 13 (2008) 1-31.

192. A.G.T. Fane, R Wang, Y Jia, Membrane technology: Past, present and future, Membr. Desalination Technol., 13 (2011) 1-45.

193. M. Lee, Z. Wu, K. Li, Advances in ceramic membranes for water treatment, Advances in Membrane Technologies for Water Treatment, (2015) 43-82.

194. N. Bowen, J. Greig, The system: Al_2O_3. SiO_2, J. Am. Ceram. Soc., 7 (1924) 238-254.

195. H. Schneider, K. Okada, J.A. Pask, Mullite and Mullite Ceramics, John Wiley & Sons, (1994) 1-251.

196. J. Pask, Critical review of phase equilibria in the Al_2O_3-SiO_2 system, in: Mullite and mullite matrix composites, 1990.

197. G. Brindley, M. Nakahira, The kaolinite- mullite reaction series: II, metakaolin, J. Am. Ceram. Soc., 42 (1959) 314-318.

198. L.B. Pankratz, W.W. Weller, K.K. Kelley, Low-temperature heat capacity and high-temperature heat content of mullite, US Dept. of the Interior. Bureau of Mines, 1963.

199. F. Wahl, R. Grim, R. Graf, Phase transformations in silica-alumina mixtures as examined by continuous X-ray diffraction, Am. Mineral., 46 (1961) 1064-1076.

200. A.K.S. Otani, Thermal transformation of SiO_2-Al_2O_3, gels prepared from methylsiloxyaluminum compounds, Kogyo Kagaku Zasshi, 67 (1964) 1509-1512.

201. M. Sainz, F. Serrano, J. Amigo, J. Bastida, A. Caballero, XRD microstructural analysis of mullites obtained from kaolinite–alumina mixtures, J. Eur. Ceram. Soc., 20 (2000) 403-412.

202. H. Schneider, D. Voll, B. Saruhan, J. Sanz, G. Schrader, C. Rüscher, A. Mosset, Synthesis and structural characterization of non-crystalline mullite precursors, J. NonCryst. Solids, 178 (1994) 262-271.

203. D. Amutharani, F. Gnanam, Low temperature pressureless sintering of sol-gel derived mullite, Mater. Sci. Eng. A, 264 (1999) 254-261.

204. E. Tkalcec, H. Ivankovic, R. Nass, H. Schmidt, Crystallization kinetics of mullite formation in diphasic gels containing different alumina components, J. Eur. Ceram. Soc., 23 (2003) 1465-1475.

205. S. Chaudhuri, S. Patra, Preparation and characterisation of transition metal ion doped mullite, Br. Ceram. Trans., 96 (1997) 105-111.

206. S. Somiya, M. Yoshimura, M. Suzuki, T. Yamaguchi, Mullite powder from hydrothermal processing, Mullite and Mullite Matrix Composites, 6 (1987) 287-310.

207. Y. Hirata, I.A. Aksay, Processing of mullite with powders processed by chemical vapor deposition, Ceram. Trans., 6 (1990) 23.

208. R.J. Angel, C.T. Prewitt, Crystal structure of mullite: A re-examination of the average structure, Am. Min., 71 (1986) 1476–1482.

209. D.L. Hamilton, C.W. Burnham, E.F. Osborn, The solubility of water and effects of oxygen fugacity and water content on crystallization in mafic magmas, J. Petrol., 5 (1964) 21–39.

210. P. Dokko, J.A. Pask, K. Mazdiyasni, High temperature mechanical properties of mullite under compression, J. Am. Ceram. Soc., 60 (1977) 150-155.

211. A.E. Stringfellow, Ceramic arcing plate material, US2864919A, 1958.

212. A.V. Somers, M. Berg, A.A. Shukle, Cordierite refractory compositions and method of forming same, US3954672A, 1976.

213. H.J. Choi, J.U. Kim, S.H. Kim, M.H. Lee, Preparation of granular ceramic filter and prediction of its collection efficiency, Aerosol Sci. Tech., 48 (2014) 1070-1079.

214. T. Matsuhisa, S. Soejima, N. Yamamoto, Cordierite ceramic honeycomb and a method for producing the same, US4295892A, 1981.

215. K. Sumi, Y. Kobayashi, E. Kato, Low temperature fabrication of cordierite ceramics from kaolinite and magnesium hydroxide mixtures with boron oxide additions, J. Am. Ceram. Soc., 82 (1999) 783-785.

216. P. Grosjean, Cordierite ceramics, Interceram, 42 (1993) 11–15.

217. S. Taruta, T. Hayashi, K. Kitajima, Preparation of machinable cordierite/mica composite by low temperature sintering, J. Eur. Ceram. Soc., 24 (2004) 3149-3154.

218. A.R. Boccaccini, M. Bucker, J. Bossert, K. Marszalek, Glass matrix composites from coal fly ash and waste glass, Waste Manage., 17 (1997) 39–45.

219. M.H. Han, K.C. Park, A study on the synthesis and sintering of cordierite powder from metal alkoxide (I): Synthesis of cordierite powder from metal alkoxide, J. Korean Ceram. Soc., 27 (1990) 625–630.

220. M.H. Han, K.C. Park, Synthesis and sintering of cordierite from metal alkoxides (II) sintering, J. Korean Ceram. Soc., 27 (1990) 777–782.

221. M.T. Tsai, Alkoxide sol gel processed cordierite fiber, J. Am. Ceram. Soc., 85 (2002) 1637–1639.

222. W. Wang, W. Chen, H. Liu, Recycling of waste red mud for fabrication of SiC/mullite composite porous ceramics, Ceram. Int., 45 (2019) 9852-9857.

223. C. Bai, Y. Li, Z. Liu, P. Liu, X. Deng, J. Li, J. Yang, Fabrication and properties of mullite-bonded porous SiC membrane supports using bauxite as aluminum source, Ceram. Int., 41 (2015) 4391-4400.

Chapter 3

Objectives

The literature review revealed that porous SiC ceramics has been applied in significant versatile industrial areas due to its excellent properties. Oxide bonding technique is recommended as suitable and simple method of fabrication of porous SiC ceramics at low temperature using commercial SiC powder and hence the method is economic compared to other processing route. Porous SiC ceramics bonded with corrosion resistant oxide bond phases have great potential to become attractive material due to their high chemical and oxidation resistance, and also high thermal and mechanical stability. Advanced oxide systems, mullite ($3Al_2O_3.2SiO_2$) and cordierite ($2Al_2O_3.2MgO.5SiO_2$) etc. can form cohesive bonds with SiC, and it can be possible to develop corrosion resistance SiC microfiltration membrane bonded by these oxides at low temperature. The content of total porosity, pore size and pore connectivity of the ceramics bonded by these oxides can also be possible to alter by suitable use of pore formers. Despite of these various advantages of this oxide bonding technique, there are few issues which are needs to be investigated. These are mainly the cost of the ceramics, homogeneous microstructures with narrow pore size distribution of porous ceramics having optimum strength etc. Literature study indicated very few reports are available on study the application possibilities of oxide bonded SiC ceramic membrane in wastewater purification, particulate filtration from air, etc. The self-bonded or reaction bonded SiC ceramics prepared at high temperature >1800°C in air atmosphere showed that the SiC membrane can be used in treatment of produced water.

Therefore this research work is formulated with following aims/objectives

(1) Development of micro porous SiC membrane at low temperature by oxide bonding route using suitable low cost oxide additives, metal catalyst, etc.

(2) Evaluation of material, structural, air permeability characteristics of the filter and mechanical properties of SiC membrane.

(3) Mechanism of oxide bond formation and find out the pore related characteristics.

(4) Effect of processing parameters on the bond phase and on properties of membrane.

(5) Evaluation of chemical corrosion resistance properties of the SiC membrane in different corrosive medium and thermal shock resistance of the SiC ceramic membrane.

(6) Performance evaluation of the SiC membrane for treatment of dairy wastewater, refinery wastewater etc. and evaluate the effect of different operating condition including TMP, CFV on the flux rate.

(7) Reusability study of the SiC membrane after wastewater treatment.

Chapter 4

Experimental Procedure

4.1. Selection of raw materials and their characterizations

4.1.1. Selection of SiC powder

In the present study, commercially available SiC powder of two different grade sizes (400 grit, and 80S, α-SiC powder: Grindwell Norton, India) were used. For possible industrial applications of the developed material in the present research work, commercial SiC powders were chosen. Microstructure examinations showed that the particles were of irregular in shape as well as non-uniform distribution in sizes as shown in Figure 4.1. To identify their crystalline phase, XRD analysis was carried out and the results indicated the presence of α-phase in 400 and 80S grit SiC powders of Grindwell Norton as shown in Figure 4.2. The particle size distribution pattern of two different SiC powders were shown in Figure 4.3. Chemical analysis of the SiC powder was done and the results have been presented in Table 4.1.

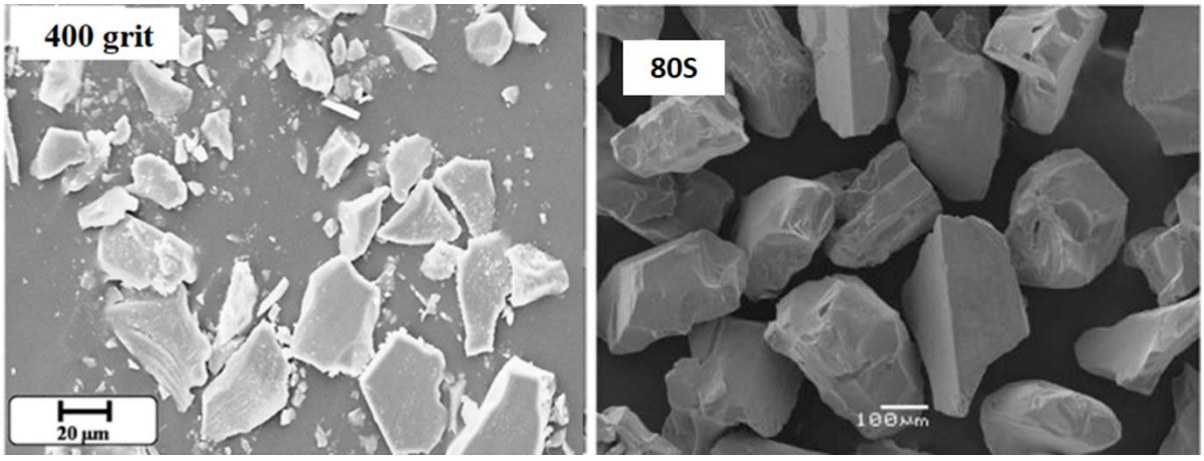

Figure 4.1. SEM micrographs of two different SiC powders having different particle sizes.

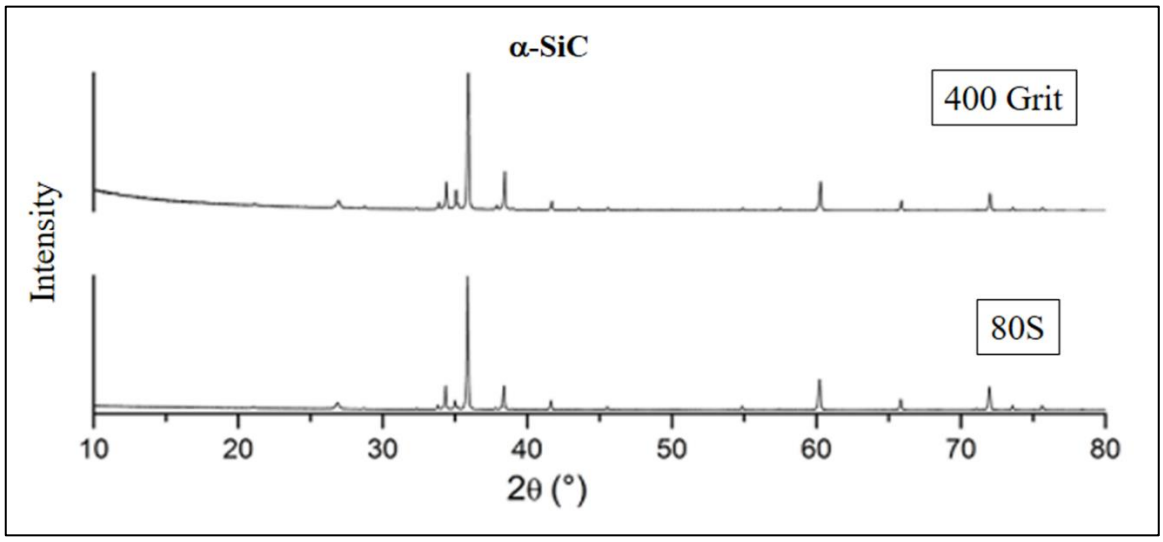

Figure 4.2. XRD patterns of two different green SiC powders

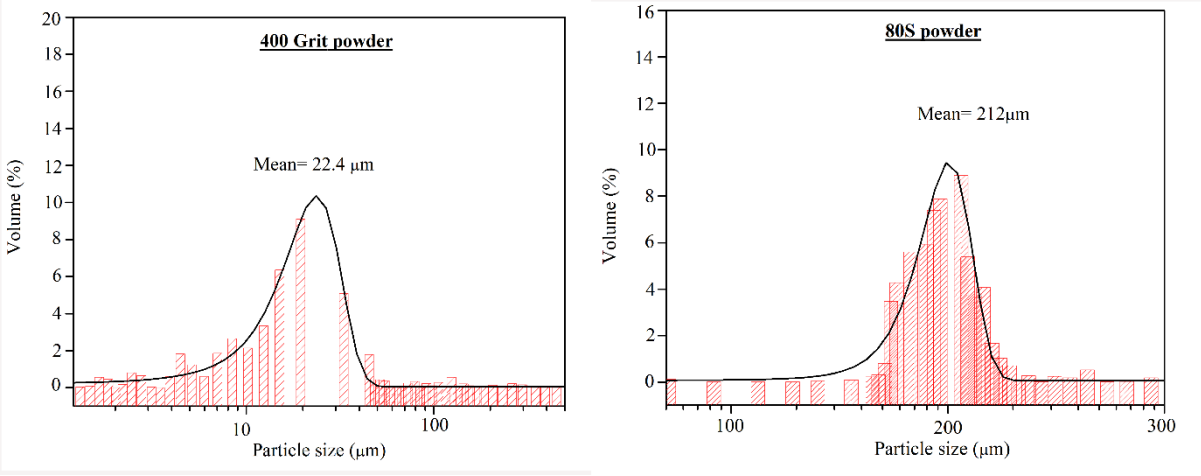

Figure 4.3. Particle size distribution pattern of different SiC powders used in this study.

4.1.2. Alumina

According to literature, various types of pure Al_2O_3 powders such as (Al_2O_3, AlN, $Al(OH)_3$) were used by different authors [1-3]. The sizes of alumina powders in the reported studies varied from 0.6 to 15 µm. It is reported that fine powders almost totally reacted with SiO_2, while the coarse powders remained unreacted Al_2O_3. On the basis of this information, in the present work Al_2O_3 powders of α-type, commercial grade and moderate particle size (d_{50}=6.5 µm) was selected. The XRD analysis indicated the alumina powder was of α-form with rhombohedral crystal structure. (JCPDS No. 46-1212). Chemical analysis of the alumina powder was done following ASTM standard: C 573-81 and the results have been presented in Table 4.1.

4.1.3. Fly ash

Fly ash is the by-product from the combustion of coal used as fuel in power plants, and it is a cheap and abundant raw material. However, it is a major source of air pollution, lead contamination, and other environmental problems. Therefore utilization of fly ash can reduce the environmental pollution as well as the cost of the products. Recently several researchers have used industrial solid waste fly ash to fabricate value added porous ceramic membrane [4-9]. *Agarwal et al.* fabricated low cost kaolin-fly ash based microfiltration membrane for oily wastewater filtration [7]. *Fu et al.* fabricated mullite based ceramic membrane by recycling fly ash as source of silica and alumina for microfiltration application [8]. *Zhu et al.* developed low cost cordierite ceramic membrane using fly ash for oil-in-water emulsion treatment [9]. But no

work has been reported on the utilization of fly ash as a source of bond phase additives for fabrication of oxide bonded porous SiC ceramics membrane at low temperature. Fly ash contain high amount of silica and alumina along with other alkaline oxides depending on the sources. So in this work, fly ash is used as source of bond phases for formation of secondary bonding phase in SiC ceramics. In this present work industrial waste fly ash was collected from (CESC Budge Budge, Kolkata, India, softening temperature 1380°C; bulk density 0.8 g/cm^3; d_{50} =16 μm) and used for the preparation of mullite/cordierite bonded porous SiC ceramic membranes. Chemical analysis of the alumina powder was done and the results have been presented in Table 4.1. To identify their crystalline phase, XRD analysis was carried out and the results indicated the presence major phase mullite and quartz phase shown in Figure 4.4.

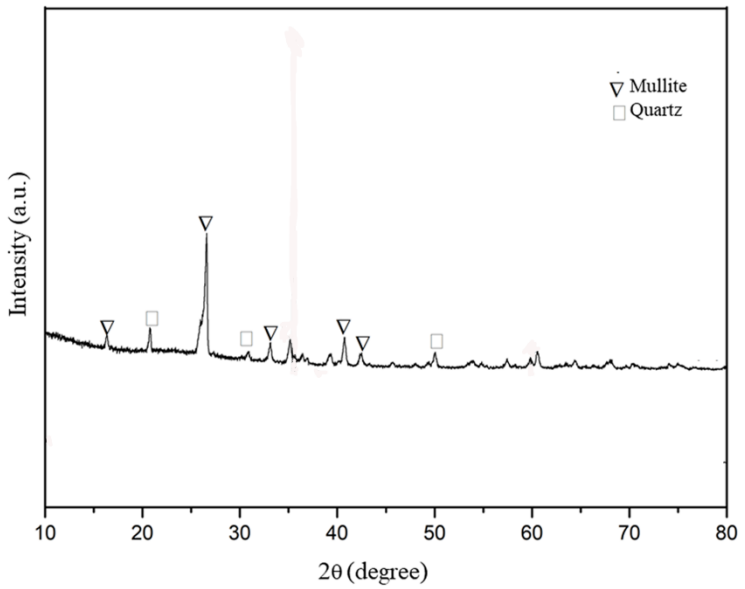

Figure 4.4. XRD pattern of industrial waste fly ash used in this study

Table 4.1. Characteristics of raw powders used in the present work

Powders	Compositions (W/W)	Source	Particle size (µm)		
			d_{10}	d_{50}	d_{90}
α-SiC 400 grit	SiC:98.74% SiO_2:0.52% Al_2O_3:0.08% TiO_2:0.23% Fe_2O_3:0.23% CaO:0.06% MgO: trace, Na_2O:0.35% K_2O: trace	M/S Grindwell Norton, India	9.48	22.48	43.11
α-SiC 80S	SiC: 98.78% SiO_2:0.48% Al_2O_3:0.09% TiO_2:0.23% Fe_2O_3:0.23% CaO:0.05% MgO: trace, Na_2O:0.35% K_2O: trace	M/S Grindwell Norton, India	126.07	212.1	334.28
α- Al_2O_3	Al_2O_3: 98.76%, Fe_2O_3: 0.03% Na_2O : 0.50%, K_2O :0.07%, SiO_2:trace, MgO: trace, CaO: trace TiO_2 :trace, LOI : 0.33%	Indian Aluminium Co. Ltd., India	2.69	6.49	13.08
Fly ash	SiO_2: 52.3%, Al_2O_3: 28.6%, CaO: 5.8%, Fe_2O_3:4.1%, Ti_2O_3: 2.4% MgO: 1.6%, Na_2O: 0.40%, K_2O: 0.06%, LOI: 4.6%	CESC Budge Budge, Kolkata, India	7.34	16	39.13

4.1.4. Selection of pore formers

Generally the pore size, porosity and mechanical strength of a porous SiC membrane are controlled by the particle size of the SiC and also on the amount and size of pore former. A suitable pore former are used in order to increase the pore volume. But a primary challenge during development of membrane is to achieve controllable or tailored pore size and porosity of the membranes using pore formers. Reported literature data indicated that different authors used different types of pore former having different particles size [10-14]. Therefore, pore former selection needs to be targeted to sustain the low cost SiC membrane with high porosity for commercial application. Graphite (Kanodia Minerals & Chemical Co., Howrah, India) as inorganic pore former, polyvinyl chloride (PVC, Loba Chemie, India), and poly-methyl methacrylate micro beads (PMMA, Sigma-Aldrich Inc., St. Louis, MO, USA) as organic pore former are used in this study. During sintering process, the pore former

undergoes decomposition and create well defined pores in the final ceramics [15-16]. Therefore, it was necessary to observe thermal combustion temperature and decomposition pattern of the pore former. The pore formers were characterised by measuring (i) particle size (ii) response during thermal heating and (iii) XRD pattern. In the present work, thermal analysis of pore forming agents were carried out with the help of thermo gravimetric-differential thermal analysis (TG-DTA) in dry air at 10°C/min heating rate. The particle size distribution pattern, crystalline phase by X-ray diffractometry technique and thermal history with the help of heat flow and mass retention analysis of the graphite powder was done as shown in Figure 4.5. Polymer micro beads and PVC were non-crystalline definite sized powder which were further characterised by their thermal analysis as shown in Figure 4.6.

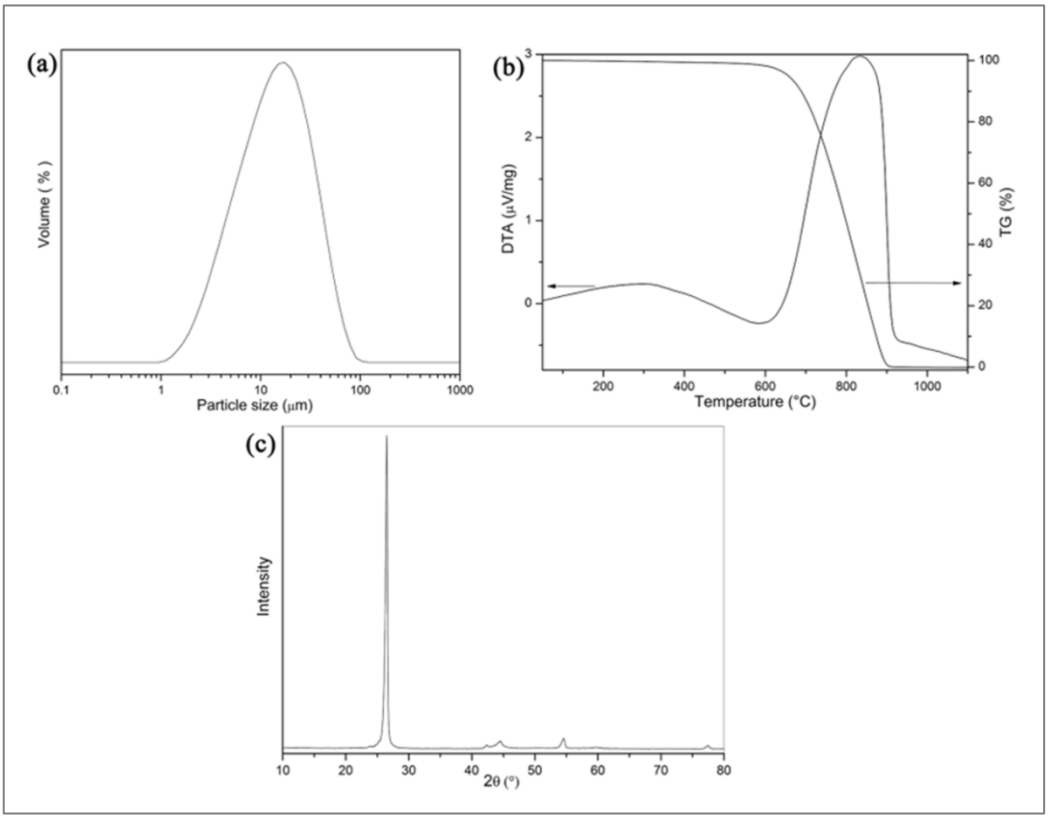

Figure 4.5. (a) Particle size distribution, (b) TG-DTA and (c) XRD pattern of graphite powder used in this work.

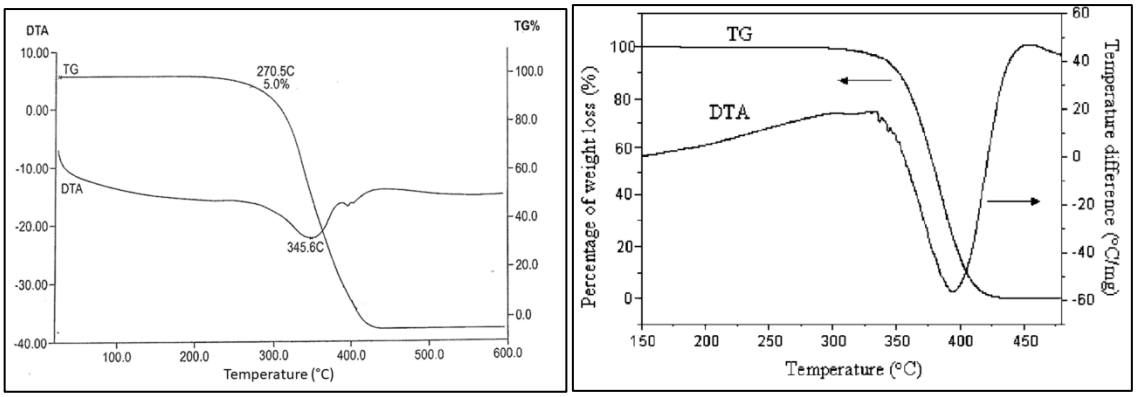

Figure 4.6.TG-DTA pattern of (left) Polyvinyl chloride (PVC) and (right) Poly methyl methacrylate (PMMA) powder used in this work during air sintering.

4.2. Preparation of porous SiC ceramics

4.2.1. Preparation of porous SiC powder compacts by powder mixing methods

α-SiC powders with different amount of oxide additives, catalyst, with or without pore formers (10-20%) were mixed in a acetone medium and the mixtures were ball milled for 24 h for homogeneous mixing. The powder mixture was dried in air followed by further drying at 80°C for 24 h. The dry powder mixtures was then mixed with 10 wt% polyvinyl alcohol (Loba Chemie, India) solution, which was used as adhesive, then pressed in a hydraulic pressing machine (Figure 4.6) (Brilliant Hydraulic, India) at 23 MPa gauge pressure to produce rectangular bar samples ($5\times40\times16$ mm^3) and circular disc sample (40×10 mm^2). The bar samples were employed for the evaluation of materials properties, determination of structural (crystalline) parameters, microstructure and mechanical properties and the circular discs were used to study air and water permeation behaviour and wastewater filtration tests. The pressed green samples were kept under 100°C for 24h to remove all the water molecules form the sample. The well dried green compacts were subsequently heated as 850°C for 1h to burn out the pore former. They were further heat treated at higher temperature (1000-1500°C) for 1-4h in presence of air in a high temperature ceramic tube furnace (Figure 4.7) (Model no. TE-3499-2, M/s Therelek Engineers (P) Ltd, Bangalore, India) depending on the compositions to produce oxide bonded porous SiC ceramics. Figure 4.8 presents the firing schedules used for preparation of oxide bonded porous SiC from different powder systems.

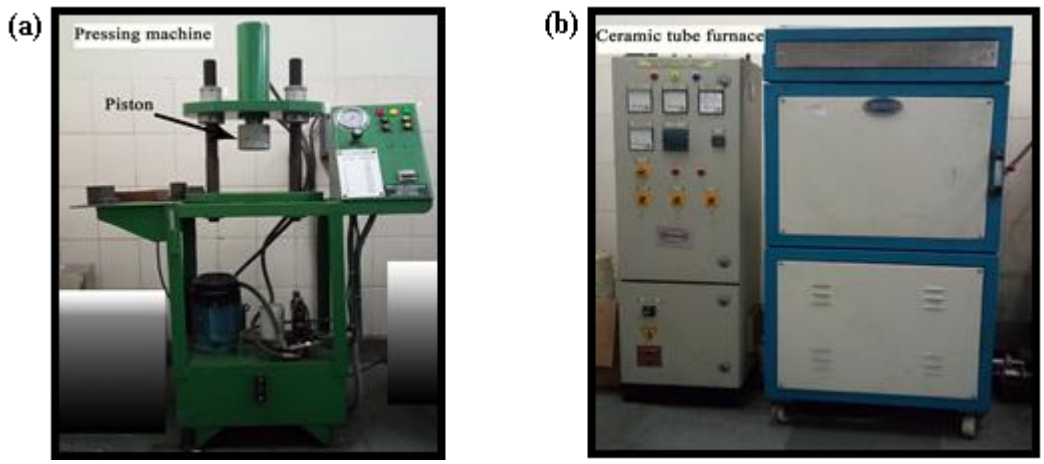

Figure 4.7. (a) Pressing machine used for ceramic sample preparation (b) electrically heated high temperature used for preparation of ceramic samples

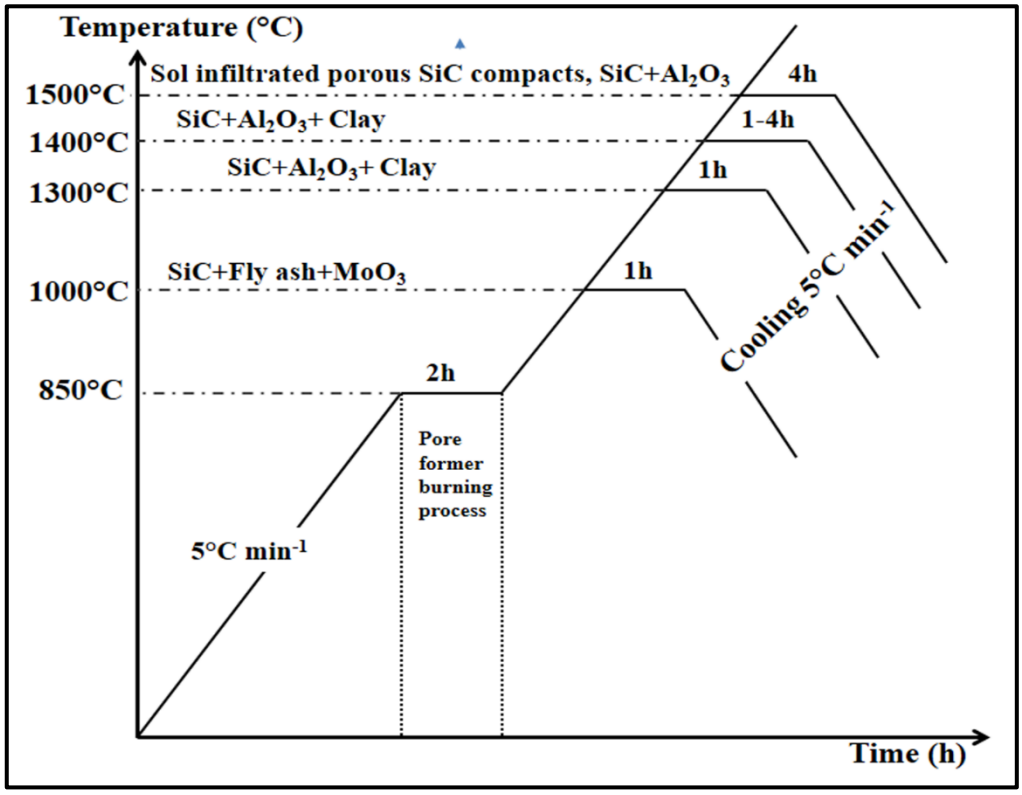

Figure 4.8. Sintering schedule of different powder compacts

4.2.2. Selection of secondary oxide bond phases

The selection of secondary oxide bond phases was done on the basis of compatibility of the following parameters with SiC:

- ❖ High melting point
- ❖ Low thermal expansion co-efficiency

- Low oxygen diffusion co-efficiency
- High temperature strength
- High mechanical stability

Table 4.2. The basic properties of the SiC and the secondary bond phases used to bind the SiC particles.

Refractory properties	SiC	Oxide bond phases	
		Mullite	Cordierite
Melting Point (°C)	2730	1840	1435
Thermal expansion co-efficiency (CTE) (/K)	4.7×10^{-6}	5.3×10^{-6}	2.5×10^{-6}
Oxygen diffusion co-efficiency (m^2/s)	---	8.6×10^{-20} at 1000-1300°C [17]	1.27×10^{-18} at 826-880°C [18]
Fracture toughness (K_{IC}) ($MPa.m^{1/2}$)	2.71@RT	2.5-3.1 (RT to 1225°C) [19]	1.8-3.1 (RT to 1250-1300°C) [20]

4.3. Preparation of secondary cordierite bond phase precursor in sol form

Cordierite sol was prepared individually by using various salt precursors. The precursor salts, acid and organic polymer compounds used for sol preparation are enlisted in Table 4.3.

Table 4.3. The raw materials used for the preparation of cordierite sol

Name of Sol	Required materials/salts	Sources
Cordierite	• Aluminium Nitrate Nonahydrate ($Al(NO_3)_3.9H_2O$) (ANN) • Magnesium Nitrate Hexahydrate $Mg(NO_3)_2.6H_2O$) (MNH) • Tetraethyl Orthosilicate ($Si(OC_2H_5)_4$), (TEOS)	• >95% pure; (Merck Specialties Pvt. Ltd., Mumbai, India) • (Sigma Aldrich Pvt. Ltd., USA) • Purity 98%; (Acros Organics, NJ, USA)

4.3.1. Cordierite sol preparation and Methods and Instruments used to characterize precursor sol

Cordierite sol was prepared by two step processes, at first step, MNH and ANN were dissolved in ethanol in 2:4 molar ratio and the solution was stirred for 30 min in warm condition for complete dissolution of salts in the solvent [21]. The transparent colloidal solution was kept as precursor (A). In the second step, TEOS was added in ethanol in 1:3

molar ratio at room temperature (RT) and marked as precursor B. Precursor A was added drop wise into B at room temperature with continuous stirring for 6-7 h to form transparent sol in which stoichiometric molar ratio 2:4:5 of Mg:Al:Si was strictly maintained.

4.3.1.1. Zeta sizer for measurement of particle size and Zeta potential

In order to observe the particles size distribution pattern of colloidal sol, DLS particle size analyser (Zetasizer; ZEN 3690, Malvern Instrument Ltd. Worcestershire, UK) was used. To measure surface potential changes of SiC powder dispersed in DI water and in secondary bond phase precursor sol as a function of *p*H, zeta/surface potential was measured using Zetasizer.

4.3.1.2. Rheometer for measurement of rheological properties

To study the deformation and flow behaviour of precursor sol, rheometer was used as an effective tool. In the present work, viscosity, hysteresis nature of the precursor sol of secondary bond phase was measured using modular based rotational viscometer (MCR-102, Anton Paar GmbH, Graz, Austria, Europe) with cup and stirrer geometry (ST-24-2D/2V/2V-30).

4.3.2. Incorporation of secondary bond phase into SiC ceramics by infiltration technique

The green SiC powder (d_{50}= 22.4 µm) compact prepared following the method as described earlier section [4.2.1]. The pressed green samples prepared without pore formers kept under 100°C and subsequently heat treated at 1100°C in air medium for 4 h to obtain porous SiC structure with sufficient handling strength in ceramic tube furnace. The samples were prepared using pore forming agents were heat treated at 750°C and 850°C for PMMA and graphite respectively to remove volatile agents and the samples were further heat treated at 1100°C to obtain porous SiC structures. After that porous SiC compacts were kept into an evacuator and evacuated until internal pressure reduced up to 0.5 mm of Hg and kept for two hours under the evacuated condition. After reaching to the desired evacuation level which was monitored using manometer attached to the evacuator, sol was added through an inlet, which was designed to disperse the sol in the porous compacts under the capillary action of the bulk SiC pores. As soon as the sol was incorporated, the samples were taken out and kept under RT for 24 hours and then at 100°C for 24 hours. During this step, the incorporated sol was transformed into gel state due to evaporation of solvent part. This led to weight gain of porous SiC compact which was measured using electrical weighing machine (Sartorius,

India). Infiltration technique was repeated for several times until the weight gain of sol-gel incorporated porous SiC compacts became constant.

The final saturated sol-gel incorporated SiC compacts were sintered at 1300-1400°C with a hold at temperatures at which the maximum conversion of gel to crystalline bond phase could take place. The basic laboratory set up used for infiltration is presented in Figure 4.9. The holding temperatures were decided from thermal and thermo gravimetric analyses of each sol-gel of secondary bond phases. The mass loss from the gel and mass gain by oxidation derived silica from SiC resulted in a porous SiC bulk material with sufficient handling strength.

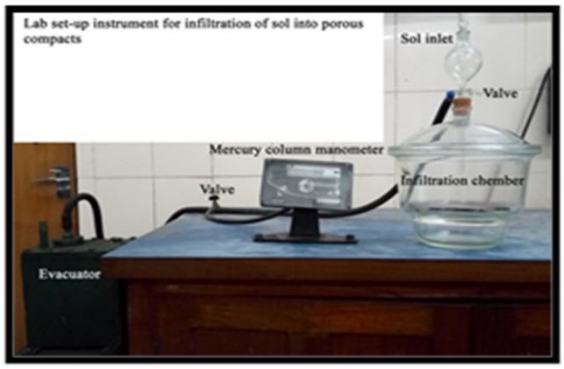

Figure 4.9. Schematic flow chart of infiltration process used in present work

4.4. Preparation of samples for mechanical analyses

For mechanical study, the SiC powder mixture was pressed in a hydraulic pressing machine with dimension of 40×4.75×3.5 mm^3 and then each stick was ground and polished up to 10 µm followed by sintered in various temperature according to the composition. After sintering, the sintered stick sample were used for mechanical (3-point bending strength) testing.

4.5. Corrosion study

Corrosion experiments were conducted using samples covered with fly ash and placed in aluminium oxide boats, which were then heated at 1000°C for 24-96 hours. A second set of corrosion experiments were conducted in the presence of steam for 96-240 hours. Water was injected at a rate of 15 ml/min through the water dosing pump into the furnace when the temperature reached 700°C for steam generation. Then furnace temperature was allowed to increase up to 1000°C and was kept for 96–240h. The corroded samples were measured for

mass, porosity, and density changes. Pore size, XRD analysis, microstructure and room temperature flexural strength of the corroded samples were studied. The details of corrosion conditions used for analysis of corrosion resistance properties of SiC samples are summarized in Table 4.4.

Table 4.4. Test conditions used for corrosion analyses

Secondary bond phases used	Corrosion temperature (°C)	Corrosion medium
Mullite	1000	Steam, Fly ash, Steam +Fly ash

4.6. Thermal shock study

To investigate the effect of thermal shock, the prepared stick samples (mentioned in 4.4 paragraph) were heated at a rate of 5°C/min to the preset temperature (800-1200°C) and held for 30 min and then the samples were cooled to room temperature in presence of air. The process was repeated for 10-12 cycles. Thermal shock resistance to cooling was also tested by water quenching technique, in which the heat treated samples at the preset temperature for 30 min were dropped into a water bath at room temperature and the process was repeated for 10 times. Then the following characterisation flexural strength and SEM study were carried out.

4.7. Methods and instruments used to characterize ceramic powder and ceramic materials

Detailed characterisations were carried out to observe analytical, structural, material and mechanical behaviour of the sintered final products in the present work. The details of characterisation instruments used for characterization of pre-ceramic materials and ceramic materials after sintering and the samples after corrosion test are described below

4.7.1. Determination of dimensional changes

The dimensional changes of the porous ceramic samples were determined by a digital slide calliper (Digimatic calliper, Mitutoyo Corporation, Japan).

4.7.2. Determination of density and porosity

The density and the porosity of the porous ceramic samples were determined following the water immersion method. The weight of a piece of the fired sample was measured in air. The piece was then boiled in de-ionised water for 2 h and allowed to cool to room temperature in the submerged condition and the suspended weight was taken. Then the piece was taken out,

surfaces were cleaned carefully with a piece of moistened cloth and the soaked weight was measured. The density (g cm^{-1}) and the porosity (in volume %) were estimated using the following equations:

$$BD = \frac{W_1}{W_3 - W_2} \tag{3}$$

$$P = \frac{W_3 - W_1}{W_3 - W_2} \tag{4}$$

Where W_1, W_2 and W_3 were the dry weight, suspended weight and soaked weight, respectively.

4.7.3. Estimation of % SiC oxidation degree and theoretical calculation the amount of different phases for oxide bonded porous SiC ceramic samples

4.3.7.1. Estimation of % SiC oxidation degree

The mass as well as volume contributions of different phases which were found to be developed in porous ceramics was calculated with the help of stoichiometric mass conversion fraction of SiC to SiO_2 during air oxidation reaction.

Considering the initial mass of pressed green SiC composite sample = $M_1\, g$

Mass of SiC composite samples after sintering =$M_2 g$

The mass of SiC in SiC composite green ceramics = M_{SiC}

Then according to mass change the % of SiC oxidation rate (*f*) is

$$f = 2[\frac{(M_2 - M_1)}{M_{SiC}}] \times 100\% \tag{5}$$

4.7.3.2. Prediction of porosity and amount of bond phases present in oxide bonded porous SiC ceramic sample

The equation derived for prediction of porosity are based on the assumption that (a) no significant volume change occurs on oxide bonding of porous SiC ceramics, (b) SiC powders (of density ρ_{SiC}) are almost pure, (c) alumina (of density $\rho_{alumina}$) and oxidation derived silica (of density ρ_{silica}) react to form mullite (of density $\rho_{mullite}$) and no alumina left in the final ceramics and (d) residue from clay remain as burnt clay (of density $\rho_{burntclay}$) in the final product.

The starting powder compact (of green weight W_g) is made of SiC (of weight fractions x_{SiC}), alumina (of weight fraction $x_{alumina}$), clay (of weight fraction x_{clay}) and pore former (of weight fraction x_{pf} and density ρ_{pf}). The experimental porosity and bulk density of the oxide bonded SiC ceramics (of fired weight W_f) are ε and ρ_f, respectively. The respective fractional masses retained after TG heating for clay and pore former are x'_{clay} and x'_{pf}.

The weight gain due to formation of silica by SiC oxidation is given by

$$\Delta W = (W_f - W_g) + W_g[x_{clay}(1 - x'_{clay}) + x_{pf}(1 - x'_{pf})] \quad (6)$$

The weight of residual SiC is given by

$$W_{SiC} = W_g x_{SiC} - 2\Delta W \quad (7)$$

The weight of burnt clay is given by

$$W_{burntclay} = W_g x_{clay} x'_{clay} \quad (8)$$

The weight of residual pore former is given by

$$W_{pf} = W_g x_{pf} x'_{pf} \quad (9)$$

From the TG experiments we observed that practically no masses were left for the pore former after sintering. So, x'_{pf}=0

The weight of mullite is given by

$$W_{mullite} = W_g x_{alumina} \times \frac{M_{mullite}}{3M_{alumina}} \quad (10)$$

Where $M_{mullite}$ and $M_{alumina}$ are the molar masses of mullite and alumina respectively.

The weight of the residual silica (as cristobalite) is given by

$$W_{silica} = 3\Delta W - W_g x_{alumina} \times \frac{2M_{silica}}{3M_{alumina}} \quad (11)$$

Where M_{silica} is the molar mass of silica.

The porosity of the oxide bonded porous SiC ceramics can be predicted by the following equation:

$$\varepsilon_{model} = \frac{\frac{W_f}{\rho_f} - \left[\frac{W_{SiC}}{\rho_{SiC}} + \frac{W_{silica}}{\rho_{silica}} + \frac{W_{burntclay}}{\rho_{burntclay}} + \frac{W_{mullite}}{\rho_{mullite}}\right]}{\frac{W_f}{\rho_f}} \quad (12)$$

4.7.4. X-ray diffraction (XRD) analysis

An effective and rapid method of identifying the crystal phases present in a sample is powder X-ray diffraction (PXRD). Only a small amount of sample is needed for the analysis. In the present work, the ceramics before and after low and high temperature corrosion, thermal shock tests were characterised by powder XRD analysis using X-ray diffractometer with CuKα radiation (λ=1.5418 Å) (PW1710; Philips, Boynton Beach, FL) and a scan rate of 0.02°/minute from 0° to 90°. The quantitative phase determination was done from XRD line profile analysis using Rietveld technique with the help of High Score Plus software (version 3.0e; PAN analytical B.V., Almelo, the Netherlands). The Rietveld refinement was reported with the help of the reliability parameters like profile residual factor (Rp), expected residual factor (R_{exp}) and goodness-of-fit (GOF) from the calculated fitting curves.

4.7.5. Field Emission Scanning Electron Microscopy (FESEM) and elemental mapping and Energy Dispersive X-ray Spectroscopy (EDS) analyses

Morphology of a synthesized sample surface and cross section can be seen in details using FESEM. An electron beam is bombarded on the sample surface by the SEM, and electrons are emitted from the surface that is interacting with the beam, creating a picture of the sample surface. A scanning electron microscope (SEM; SE-440, Leo-Cambridge, Cambridge, UK) (SE-440, Leo-Cambridge, Cambridge, UK) was used to examine the microstructure and elemental composition of porous SiC ceramics before and after corrosion and thermal shock analyses. The starting SiC powder size distribution, secondary phase formation and fracture surfaces analyses of ceramic materials after mechanical testing were also examined by FESEM analyses.

4.7.6. Three point flexural bending strength and Young modulus measurement

Flexural strength is the amount of force an object can take without breaking or permanently deforming. The flexural strength (σ) of the porous SiC bar samples were calculated by three point bending method, using the following equation

$$\sigma = \frac{3FL}{2bd^2} \qquad (13)$$

where F is the load at a given point on the load deflection curve in N unit, L is the Support span in mm, b is the width of test beam in mm unit, d is the depth or thickness of tested beam in mm unit. A three-point flexural test was conducted on a Universal Testing Machine (with a

span of 40 mm and crosshead speed of 0.5 mm/min) to determine the room temperature flexural strength (UTM) (Model 1123, Instron, Canton, MA, USA). In addition to the load deflection data, a LVDT was used with a resolution of 0.05% of full scale deflection. The ceramic samples of 40×4.75×3.5 mm^3 dimension were placed on the supporting pin with (L) 40 mm apart and loading pin was set in the middle top of the samples maintaining L/2 distance from both pin supports as shown in Figure 4.10, where the sample breaking load in terms of stress was measured with respect to strain of the sample during testing. A standard software (Instron Bluehill-2, UK) was used to calculate Young's modulus of porous SiC. An average has been reported for the mechanical property data based on five readings.

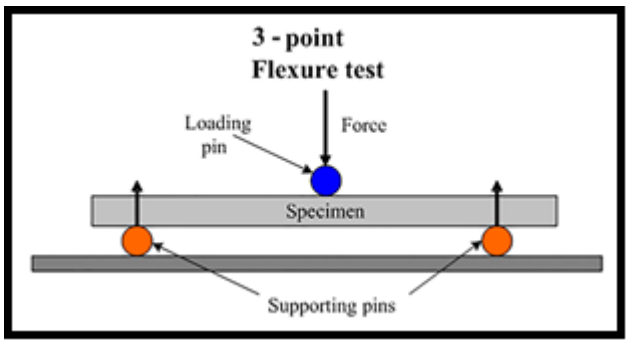

Figure 4.10. Three point bending flexural strength measurement test setup

4.7.7. Pore size distribution (PSD) analysis

Mercury porosimetry is an established technique for determining pore size, porous volume, and pore size distribution. Due to Mercury's non-wetting properties, when pressure is applied it is forced into pores. In the present work, PSD analysis was carried out using technique which is based on the simple phenomenon of the capillary depression of Hg under pressure (50,000Psi). This method is suitable for determination of pore size distribution pattern of macro porous materials. The analysis was carried out using mercury (Hg) intrusion porosimeter (Quanta chrome Instruments, FL) to determine the pore size distribution, pore volume and bulk porosity of the porous SiC bulk ceramics following the working principle proposed by Washburn equation as mentioned below.

$$h = \left(\frac{R_h \gamma \cos\theta}{2\tau^2 \mu} \right)^{1/2} \sqrt{t} \qquad (14)$$

Where h is the rise of liquid to the capillary channel as a function of time t, R_h is hydraulic radius, γ is the surface energy or surface tension of the liquid, θ is contact angle, μ is the viscosity of liquid, and τ is the tortuosity of the porous wick.

4.7.8. Differential scanning calorimetric (DSC), differential thermal (DTA) and thermogravimatric (TG) analyses.

To study reaction mechanisms during heat treatment of SiC powder composite or infiltrated SiC and to examine formation of phase in presence of catalyst, DTA/DSC and TG analyses were carried out using simultaneous thermal analyzer (STA 490C; Netzcsh-Geratebau, GambH, Selb, Germany). To understand the reaction mechanism, kinetics of crystallization process of oxide bond formation; the dry powders were heat treated up to 1500°C in dry air medium at variable heating rate of 10°C/min. A derivative weight loss curve (DTG) was used to understand the point at which weight loss was most apparent.

4.8. Experimental procedure for measurement of air permeability

4.8.1. Theoretical Background

The experimental relationship between the fluid pressure applied through a porous medium (ΔP) and the resulting superficial fluid velocity (v_s) permeated through the medium can be well represented by Forchheimer's equation: (15-19)

$$\frac{\Delta P}{L} = \frac{\mu}{k_1} v_s + \frac{\rho}{k_2} v_s^2 \qquad (15)$$

in which L is the medium length or thickness along the macroscopic flow direction, and μ and ρ are respectively the viscosity and density of the fluid. The parameters k_1 and k_2 are respectively known as Darcian and non-Darcian permeability coefficients, in reference to Darcy's law, which establishes a linear dependence between ΔP and v_s. These coefficients are only dependent of the porous structure and weigh the contributions of viscous and inertial losses on the total pressure drop. Notably, k_1 is expressed in square length dimensions, while k_2 is expressed in length dimensions to maintain dimensional consistency in Equation (15).For compressible flow of gases, ΔP in Equation (15) must be calculated by:

$$\Delta P = \frac{P_i^2 - P_o^2}{2P} \qquad (16)$$

in which P_i and P_o are, respectively, the absolute fluid pressures at the entrance and exit of the medium. P is the pressure for which v_s, μ and ρ are measured or calculated. In this work $P = P_o \approx P_{atm}$ and the viscosity μ (in Pa.s) and density ρ (in kg/m^3) of air were estimated as a function of temperature T (in °C) and pressure P_o (in Pa) by:

$$\mu = 1.73\times10^{-5}\left(\frac{T+273}{273}\right)^{1,5}\left(\frac{273+125}{T+273+125}\right) \quad (17)$$

$$\rho = \frac{P_o MM_{air}}{8.314(T+273)} \quad (18)$$

in which MM_{air} is the molar mass of dry air (0.028965 kg/mol).

If the open porosity (ε) and the Darcian permeability coefficient (k_1) of the medium are known, then the average fluid dynamic pore size (d_{pore}) can be estimated by the following Ergun-related equation: (15-17):

$$d_{pore} = \left(\frac{150k_1}{2.25\varepsilon}\right)^{0.5} \quad (19)$$

4.8.2. Experimental procedure

Experimental evaluation of permeability was carried out in a laboratory made apparatus, with tests performed in steady-state regime with dry airflow at room conditions. The test sample was sealed with annular rubber rings within a cylindrical sample holder that provided a useful medium diameter of 2.03 cm a circular flow area (A_{flow}) of 3.24 cm^2. The pressure gradient across the specimen ($P_i - P_o$) was measured by a digital manometer (*Sper Scientific, model 840083, Scottsdale-AZ, U.S.A.*) in response to variations in the air volumetric flow rate Q, controlled by a needle valve and measured with a lab-made soap bubble flowmeter open to the atmosphere. Flow rate (Q) was corrected to the value at sample exit (Q_o) and finally converted to superficial velocity by $v_s = Q_o/A_{flow}$.

The collected data set (P_i, P_o and v_s) for each test was fit treated according to the least-square method using a parabolic model of the type: $y = ax + bx^2$, where y is ΔP (from Equation 17) and x is the fluid velocity v_s. The permeability parameters were then calculated from the fitted constants a ($k_1=\mu/a$) and b ($k_2=\rho/b$) of Equation (15). The apparatus used for permeation tests is schematized in Figures 4.11 and 4.12.

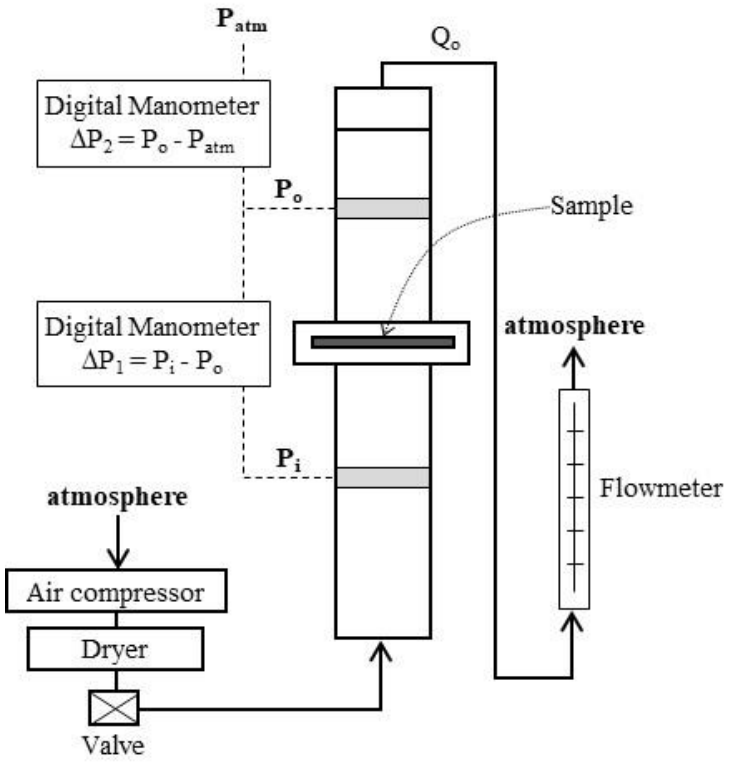

Figure 4.11. Scheme of airflow permeation apparatus.

Figure 4.12. Details of the sample holder used in the airflow experiments.

4.9. Experimental procedure for measurement of water permeability

4.9.1. Theoretical Background

For membranes used in liquid filtration operations, the nomenclature of variables is slightly different. The flux (J) of water permeated through the filter is usually correlated to the transmembrane pressure (TMP). Therefore, Equation (17) can be rewritten as:

$$\frac{TMP}{L} = \frac{\mu}{k_1} J + \frac{\rho}{k_2} J^2 \quad (20)$$

Inversely, to obtain the flux J as a function of the transmembrane pressure TMP:

$$J = \frac{-\left(\frac{\mu}{k_1}\right) + \left(\left(\frac{\mu}{k_1}\right)^2 + 4\left(\frac{\rho}{k_2}\right)\left(\frac{TMP}{L}\right)\right)^{0.5}}{2\left(\frac{\rho}{k_2}\right)} \quad (21)$$

It is worth noting that both v_s (Equation 17) and J (Equation 18) are equivalent in dimensions, except that v_s is given usually in m/s while J is given in L/m^2.h. Experimentally, J or v_s can be obtained by any of the following relationships:

$$J = v_s = \frac{Q}{A_{flow}} = \frac{V}{tA_{flow}} = \frac{w}{\rho A_{flow}} = \frac{M}{t\rho A_{flow}} \quad (22)$$

in which Q is the volumetric flow rate of permeated fluid (in m^3/s or L/h), A_{flow} is the superficial area of the medium exposed to flow (in m^2), V is the volume of fluid (m^3 or L) permeated in a given time t (in s or h), w is the mass flow rate of permeated fluid (in kg/s), M is the mass of fluid (in kg) permeated in a given time t (in s or h). Similarly, for incompressible flow ΔP = TMP (in Pa or bar).

In cases in which only the viscous contribution on pressure drop is relevant (validity of Darcy's law), Equations (15) and (20) can be respectively simplified to: (17-26)

$$\frac{TMP}{L} = \frac{\mu}{k_1} J \quad (23)$$

Inversely: $J = \frac{k_1}{\mu L} TMP$ (24)

The resistance of the membrane to flow R_m is defined then as:

$$R_m = \frac{L}{k_1} \quad (25)$$

and Equation (16) is rewritten as:

$$J = \frac{TMP}{\mu R_m} \tag{26}$$

The specific permeability (SP) of the membrane (based on the validity of Darcy's law) can be defined as:

$$SP = \frac{J}{TMP} \tag{27}$$

or:

$$SP = \frac{1}{\mu R_m} \tag{28}$$

It is important to observe in Equations (23-24) that the membrane resistance R_m and the specific permeability SP are only constant if the experimental relationship between TMP and J is also constant. Depending on the pressure applied, however, a parabolic relationship between TMP and J is observed (Equation 28) and SP may vary. In this case, description of the membrane permeation performance with clean fluids is better represented by k_1 and k_2 coefficients and by Equation (25). The linearity of the J × TMP and the validity of Equations (20-25) can be verified through the dimensionless parameter F_o (Forchheimer number) defined as:

$$Fo = \frac{\rho J(k_1 / k_2)}{\mu} \tag{29}$$

Equation (3) can be then rewritten as:

$$\frac{TMP}{L} = \frac{\mu}{k_1} J(1 + Fo) \tag{30}$$

The relative contributions of viscous and inertial resistances on TMP are then calculated by:

$$\text{Viscous (\%)} = 100\left(\frac{1}{1+Fo}\right) \tag{31}$$

$$\text{Inertial (\%)} = 100\left(\frac{Fo}{1+Fo}\right) \tag{32}$$

If F_o <<1, then Viscous (%) → 100% and Equation (19) reduces to Equation (16). Otherwise, the flux J will not vary linearly with TMP and R_m and SP will be variable according to the TMP applied.

For water, the viscosity μ (in Pa.s) and density ρ (in kg/m^3) can be estimated as a function of temperature (in °C) in the interval 0 to 100°C by:

$$\mu = \frac{0.1}{2.1482\left[(T-8.435)+\sqrt{8078.4+(T-8.435)^2}\right]-120} \tag{33}$$

$$\rho = 1.4887\times10^{-5}T^3 - 5.7544\times10^{-3}T^2 + 1.0541\times10^{-2}T + 1000.1 \tag{34}$$

If the open porosity (ε) and the Darcian permeability coefficient (k_1) of the medium are known, then the average pore size (d_{pore}) can be estimated by the following Ergun-related equation:

$$d_{pore} = \left(\frac{150k_1}{2.25\varepsilon}\right)^{0.5} \tag{35}$$

4.9.2. Experimental procedure for water filtration

Experimental evaluation of water permeability was carried out in a laboratory made apparatus, with tests performed in steady-state regime with distilled water flow at room conditions. The test sample was sealed with annular rubber rings within a cylindrical sample holder that provided a useful medium diameter of 2.4 cm a circular flow area (A_{flow}) of 4.52 cm^2. Distilled water stored in a 10 L tank was pumped through the sample. The pressure gradient (ΔP_i) across the sample was measured with a pressure transducer (0–10 bar) and controlled by a needle valve and the resulting water flow rate Q = V/t was obtained by volume (V) and time (t) measurements with a graduated tube test. Superficial water velocity was calculated by $v_s = Q/A_{flow}$.

The collected data set (ΔP and v_s) for each test was fit treated according to the least-square method using a parabolic model of the type: $y = ax + bx^2$, where y is ΔP and x is the water velocity v_s permeated through the sample. The permeability parameters were then calculated from the fitted constants a (k_1=μ/a) and b (k_2=ρ/b).

Similarly, J and TMP were used to calculate the resistance (R_m) and the specific permeability (SP) of each sample by Equations (27-28). The apparatus used for permeation tests is schematized in Figures 4.13 and 4.14.

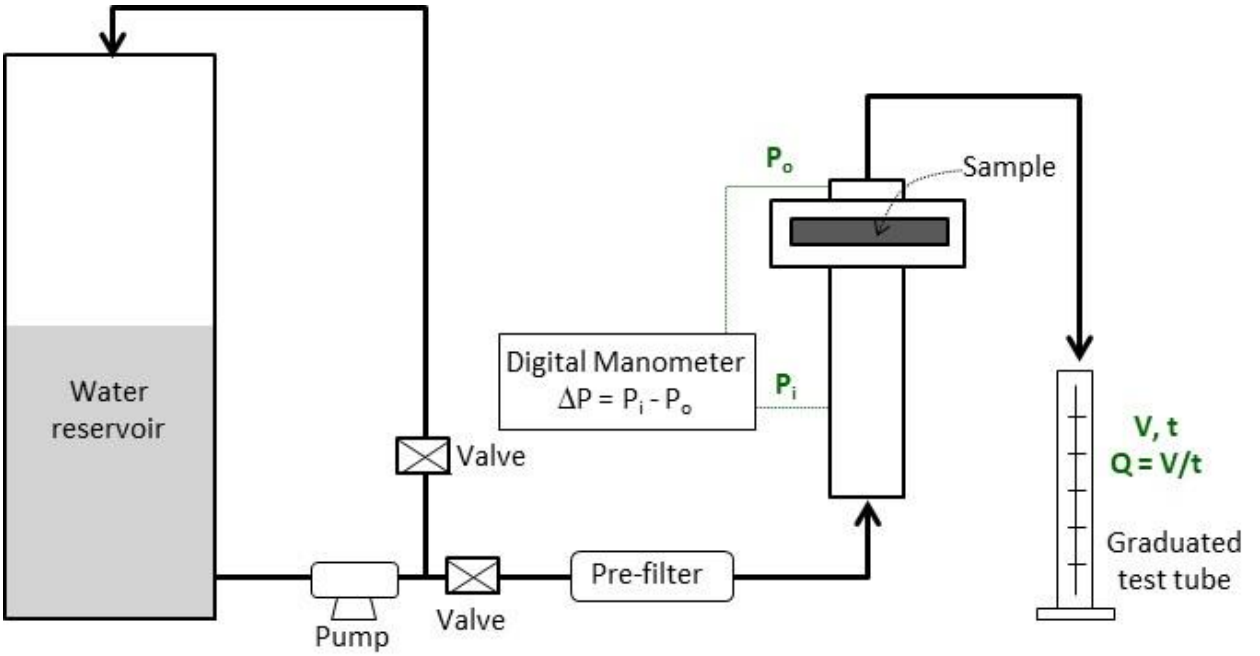

Figure 4.13. Scheme of the water flow permeation apparatus.

Figure 4.14. Picture of the water permeation setup.

4.10. Preparation and Filtration of Kaolinite turbid water

The turbid water was prepared by adding 200 g of kaolinite (powder) in 8 L of chlorine free water under 300 rpm agitation for 2 h. The mixture was settled by 48 h under room conditions and the supernatant water was collected for the experiments, with a turbidity level in the range 104 –166 NTU. For each membrane sample, two tests were run: first with distilled water to acquire the permeation profile and then with the turbid water containing kaolinite particles to verify the retention ratio and fouling of the membrane. During the test, a volume of distilled water ($V_{w,i}$) of 200 ml was fed in the reservoir above the sample of total volume (V_t) of 448 mL. Therefore, an initial volume of air ($V_{air,i}$) of 248 ml was kept above the water level. The air pressure (P) in the reservoir was raised to provide an initial transmembrane pressure ($TMP_i = P_f - P_{atm}$) of ≈ 900 mbar (90 kPa) relative to the atmosphere. The valve between the reservoir and the sample was then open and the water was allowed to permeate downward through the sample, being collected in a test tube for analysis. The air pressure inside the reservoir continuously decreased due to the reduction in the water level caused by the permeation through the membrane. The TMP data was collected in a data logger at each 1s and a mass balance inside the reservoir allowed to estimate the cumulated volume of water permeated through the membrane (V_p) as a function of time by:

$$V_p = V_{air,i}\left(\frac{TMP_i - TMP}{TMP + P_{atm}}\right) \tag{36}$$

The decay in the transmembrane pressure along time (PD) was obtained by:

$$PD = \left(\frac{TMP_i - TMP}{TMP}\right)100\% \tag{37}$$

The same procedure was carried out with the same membrane, but this time with replacement of clean water by turbid water (diluted kaolinite suspension). The retention ratio was evaluated after 300s of test by measuring the turbidity of water in the feed and in the permeate using a portable turbidimeter (*HACH, model 2100p, Loveland, CO – USA*). The atmospheric pressure at the laboratory conditions (P_{atm}) was in the range 935 – 942 mbar (93.5 – 94.2 kPa) and temperature between 21 and 24°C. The reduction of flow caused by fouling was obtained by comparing the volumes of permeate of clean and turbid water after 300 s of test:

$$FR = \left(\frac{V_{p,\ clean\ water} - V_{p,\ turbid\ water}}{V_{p,\ clean\ water}} \right) 100\% \quad (38)$$

4.11. Collection and characterization of wastewater

First the kitchen waste water was collected from canteen at three different times and mixed the water. The heavier contaminants or particles were allowed to sediment and separated from kitchen waste water by settling the water for 10 days. The supernatant water was characterized by measuring total suspended solids (TSS) [Tarsons, India], and COD [Spectra lab, India], total dissolved solids (TDS), pH, and conductivity [Multiparameter Sension 156, Hach], turbidity [2100ANIS Turbidimeter, Hach] etc.

4.11.1. Determination of Chemical Oxygen Demand (COD)

The chemical oxygen demand (COD) of a measured solution is an indicator of how much oxygen the reactions are capable of consuming. Oxygen consumption is commonly measured in mass of oxygen consumed per volume of solution, expressed in SI units as milligrams per litre (mg/L). The amount of organics present in the solution can be easily detect by this COD method. In first step 1.5 ml of digestion mixture 0.25(N) $K_2Cr_2O_7$ solution + Ag_2SO_4) and 3.5 ml of reagent mixture (Conc. H_2SO_4 + $HgSO_4$) are taken in a COD digester tube. To this tube 2.5 ml of sample water is added and taken for 2 h at 120^oC in a COD Digester [Spectra lab, India] machine. After the tube was cooled down, the solution in the tube carefully transferred to conical flask, titrating with the standard Mohr's solution using ferroine as an indicator.

Molarity of Mohr's solution= vol^m of dichromate sol^n ×0.25(N) / vol^m of Mohr^s sol^n

$$COD\ (mg/L) = \frac{(A-B)\times M\times 8000}{volume\ of\ sample\ taken} \quad (39)$$

A is the volume of Mohr's solution require for blank titration, B is the volume of the Mohr's solution require for sample titration, M is the molarity of Mohr's solution and 8000= mili equivalent weight of oxygen × 1000 ml.

4.11.2. Measurement of TSS and TDS

Total suspended solid (TSS) is referred to the amount of solid and liquid present in solution in suspended condition and this materials are non-filterable in nature. While total dissolved solid refers to the amount of materials are completely dissolved in solution & these are filterable in nature. The well mixed sample is filtrated through the whatmann 42 paper and

the residue retained on the filter is dried at 100^{o}C for the complete removal of water. The increase of filter weight after filtration represents TSS. After filtration permeate was taken in teflon pot, and dried at 120^{o}C until the complete removal of water. The increase of teflon pot weight after evaporation, refers to the TDS in water

$$TSS\ \left(mg/L\right)=\frac{\left(W_2-W_1\right)\ \times 1000}{V} \tag{40}$$

W_2 is the wt. of filter paper after filtration, W_1 is the wt. of filter paper before filtration. V is the volume of sample taken

$$TDS\ \left(mg/L\right)=\frac{\left(M_2-M_1\right)\ \times 1000}{V} \tag{41}$$

M_2 is the wt. of teflon pot after filtration, M_1 is the wt. of teflon pot before filtration. V is the volume of sample taken.

4.11.3. Quantitative estimation of oil and grease in sample water and permeate

Quantitative estimation of oil in oil-water emulsion is generally carried out by Spectrophotometric method. In this method optical density of sample oil dissolved in n-hexane is measured using spectrophotometer at maximum absorbance at a particular wavelength. Then concentration of oil is determined with respect to standard curve. But for kitchen water, even though complete mass transfer of oil from waste water to n-hexane was carried out but determination of concentration of oil by spectrophotometric method was not possible as oil extracted from kitchen waste water contains different types of oil. In this work the determination of concentration of oil in waste water was carried out by solvent evaporation method. In this method extracted oil in hexane solution was evaporated by rotary evaporating process. From difference of weight oil concentration was measured.

References

1. S. Ding, S. Zhu, Y. Zeng, D. Jiang, Fabrication of mullite-bonded porous silicon carbide ceramics by in situ reaction bonding, J. Eur. Ceram. Soc., 27 (2007) 2095–2102.
2. B.V.M. Kumar, J.H. Eom, Y.W. Kim, I.S. Han, S.K. Woo, Effect of aluminum source on flexural strength of mullite-bonded porous silicon carbide ceramics, J. Ceram. Soc. Jpn., 118 (2010) 13–18.
3. W.G. Chi, D.L. Jiang, Z.R. Huang, S.J. Tan, Sintering behaviour of porous SiC ceramics, Ceram. Int., 30 (2004) 869–874.
4. Z. Xing, Y. Hu, D. Xiang, Y. Ma, Porous SiC-mullite ceramics with high flexural strength and gas permeability prepared from photovoltaic silicon waste, Ceram. Int., 46 (2020) 1236-1242.
5. J.H. Li, H.W. Ma, W.H. Huang, Effect of V_2O_5 on the properties of mullite ceramics synthesized from high-aluminium fly ash and bauxite, J. Hazard Mater. 166 (2009) 1535–1539.
6. Y. Dong, S. Hampshire, J. Zhou, Z. Ji, J. Wang, G. Meng, Sintering and characterization of fly ash based mullite with MgO addition, J. Eur. Ceram. Soc., 31 (2011) 687–695.
7. S. Ding, Y.P. Zeng, D. Jiang, In-situ reaction bonding of porous SiC ceramics, Mater. Charact., 59 (2008) 140–143.
8. S. Ding, S. Zhu, Y. Zeng, D. Jiang, Fabrication of mullite-bonded porous silicon carbide ceramics by in situ reaction bonding, J. Eur. Ceram. Soc., 27 (2007) 2095–2102.
9. Y.S. Chun, Y.W. Kim, Processing and mechanical properties of porous silica-bonded silicon carbide ceramics, Met. Mater. Int., 11 (2005) 351–355.
10. G.G. Gnesin, L.A. Shipilova, L.I. Chernyshev, V. Loikovskii, A. Prez, Formation of highly-porous ceramic based on silicon carbide, Powder Metall. Met. Ceram., 33 (1994) 262-267.
11. S. Liu, Y.P. Zeng, D. Jiang, Fabrication and characterization of cordierite-bonded porous SiC ceramics, Ceram. Int., 35 (2009) 597–602.
12. B.A. Horri, C. Selomulya, H. Wang, Characteristics of Ni/YSZ ceramic anode prepared using carbon microspheres as a pore former, Int. J. Hydrogen Energy, 37 (2012) 15311–15319.

13. A. Haugen, A. Geffroy, A. Kaiser, V. Gil, MgO as a non-pyrolyzable pore former in porous membrane supports, J. Euro. Ceram. Soc., 38 (2018) 3279–3285.
14. J. Depasse, Silica hydrosols: Influence of the refractive index of the electrolyte solution on the turbidity and on the interparticle interactions, J. Colloid Interface Sci., 188 (1997) 229-231.
15. W.J. Moore, Basic physical chemistry, Prentice Hall, 1983.
16. M.R.B. Romdhane, S. Boufi, S. Baklouti, T. Chartier, J.F. Baumard, Dispersion of Al_2O_3 suspension with acrylic copolymers bearing carboxylic groups, Colloids Surf, A Physicochem. Eng. Asp., 212 (2003) 271-283.
17. K.C. Song, Preparation of mullite fibers from aluminum isopropoxide–aluminum nitrate–tetraethylorthosilicate solutions by sol–gel method, Mater. Lett., 35 (1998) 290-296.
18. S. Wang, F. Kuang, Sol gel preparation and infrared radiation property of boron-substituted cordierite glass-ceramics, J. Mater. Sci. Technol., 26 (2010) 445-448.

Chapter 5

Results and Discussions

Chapter 5.1

5.1. Fabrication of mullite bonded porous SiC ceramic membrane utilizing solid waste fly ash as a source of bond phase additives

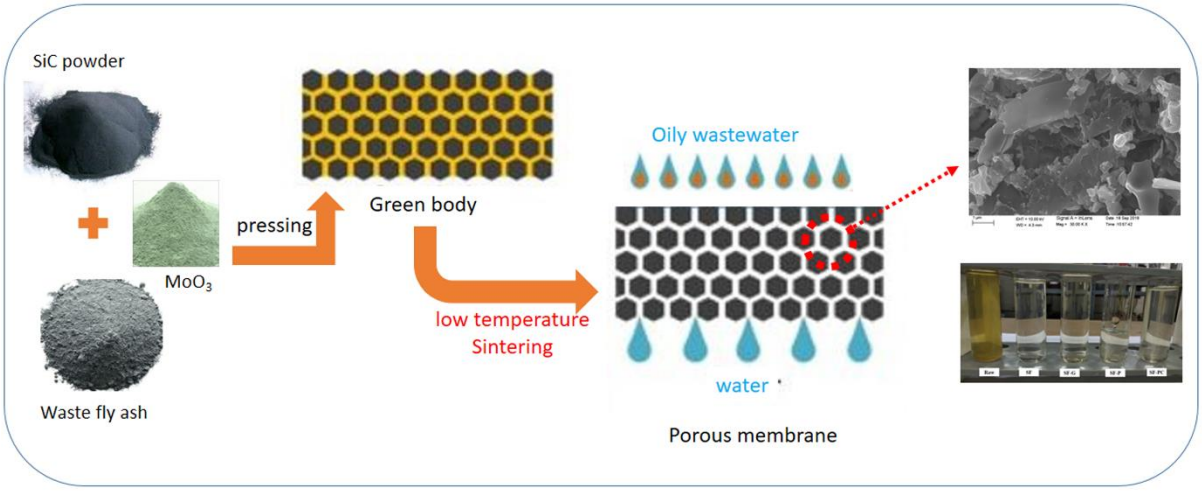

In this chapter, efforts are made to fabricate mullite bonded porous SiC ceramics by facile solid-state reaction process using SiC as raw materials, industrial waste fly ash as a source of bond phase additives at 1000°C. MoO_3 was used as sintering catalyst to lower the mullite formation and the effects of MoO_3 catalyst on mullitization reaction and mullite morphology was investigated in detail. In order to increase the porosity of the ceramics, three different pore forming agent such as graphite, PVC and PMMA were used. The effects of pore formers addition on the materials, mechanical, pore size, air & water permeation, and wastewater filtration properties of the porous ceramics also investigated. The porous SiC ceramics with addition of 5 wt% MoO_3 exhibited a flexural strength of 38.4 MPa at porosity 36.4 vol% and showed 92% oil removal efficiency from oily wastewater. This technique, combining low-cost materials and the co-sintering at low temperature, can serve as a cost-effective method for the production of high-performance porous SiC ceramic membranes for filtration application.

Publications

1. D. Das, N. Kayal, G.A. Marsola, D.G.P. Filho, M.D.M. Innocentini, J. Euro. Ceram. Soc., 40 (2020) 2163-2172.
2. D. Das, N. Kayal, M.D.M. Innocentini, Trans. Indian Ceram. Soc., 80 (2021) 186-192.

5.1.1. Effect of MoO_3 addition in the formation of secondary phases, porosity and density of mullite bonded porous SiC ceramics

The role of the MoO_3 on the binder phase formation was further studied by synthesizing porous SiC ceramic samples at 1000°C for 1 h, using SiC powder (d_{50}= 22.4 µm) and industrial waste fly ash powder with varying amount of MoO_3. It was observed for the sample prepared without MoO_3 that, loose particles were seen coming out from the surface of the ceramics, indicated weak bonding between particles, while with increase in the amount of MoO_3 from 1 wt% to 3 wt%, porosity decreased from 41.3 to 37.2 vol%, indicated densification. The samples prepared with 5 wt% MoO_3 were found to be strong enough and obtained with ~36.4 vol% porosity and negligible dimensional change (<~1%). From XRD analysis, it was also found that mullite bond phase was formed when amount of MoO_3 was 5 wt% in the ceramic. Therefore, 5 wt% MoO_3 was selected as an optimum amount for the preparation of mullite bonded porous SiC ceramics. To observe the effect of pore forming agent on properties of final ceramics, three types of sacrificial pore forming agents (polymer microbead, PVC and graphite) were used to develop porous SiC structure. The samples obtained using graphite, PVC and polymer microbead named as SF-G, SF-PC and SF-P respectively. The addition of the pore former increased the porosity of the membranes and reduced the density of the ceramics. As a result of using graphite, porosity was increased to ~42 vol% and reached to 44.7 and 46 vol% for the sample prepared with PVC and PMMA respectively. The general characteristics of sintered SiC ceramics prepared using 5 wt% MoO_3, with and without pore formers is given in Table 5.1.1. After sintering, the SiC ceramics showed a very small volume change (less than 1%). In terms of oxidation, the degree of SiC oxidation varies from ~16.3–19.6% according to the size and amount of pore former used. PMMA was burned out at comparatively lower temperature than graphite and PVC, as a result more silica was produced in the sample prepared with PMMA.

Table 5.1.1. Characteristics of mullite bonded SiC ceramic membranes sintered at 1000°C.

Sample code	Linear dimensional change (%)			Porosity (%)	Flexural strength(MPa)	Degree of oxidn. of SiC
	length	width	thickness			
SF	0.05	0.12	0.13	36.36±0.14	38.40±0.09	16.3
SF-G	0.16	0.14	0.31	42.03±0.11	34.31±0.05	17.2
SF-P	0.21	0.16	0.34	44.68±0.18	27.92±0.18	19.6
SF-PC	0.23	0.16	0.35	44.70±0.09	28.60±0.03	17.8

5.1.2. XRD analysis

XRD profiles of mullite bonded SiC ceramics with varying amount of MoO_3 are presented in Figure 5.1.1. The ceramics prepared with 5 wt% of MoO_3 showed major crystalline phases of α-SiC (crystal system: hexagonal; space group: P63mc; a=b=3.0817 Å, c=15.1183 Å and α=β=90°, γ=120°; JCPDS 74–1302), cristobalite (crystal system: tetragonal; space group: P41212; a=b=4.9934 Å, c=7.0055 Å and α=β=γ=90°; JCPDS 76-0939), mullite (crystal system: orthorhombic; space group: Pbam; a=7.5539 Å, b=7.6909 Å, c=2.8839 Å and α=β=γ=90°; JCPDS 79–1455) and Mo_8O_{23} (crystal system: monoclinic; space group: P1c1; a=13.39 Å, b=8.06 Å, c=16.82 Å and α=γ=90° and β=106.02°; JCPDS 152–9952).While the sample prepared with 1−3 wt% of MoO_3, no characteristic peak of mullite was observed, instead of sillimanite (Al_2SiO_5) (crystal system: orthorhombic; space group: Pbnm; a=7.4345 Å, b=7.5989 Å, c=5.7507 Å and α=β=γ=90°; JCPDS 788-0892) was found. The sample prepared without MoO_3 showed a small peak of alumina (crystal system: hexagonal; space group: R-3c; a=b=4.7606 Å, c=12.994 Å and α=β=90° γ=120°; JCPDS 77–2135) and quartz (crystal system: hexagonal; space group: P3221; a=b=4.912 Å, c=5.40 Å and α=β=90° γ=120°; JCPDS 78–1253) along with characteristic peak of SiC. The effects of MoO_3 content on the crystalline bond phase formation of the final ceramics are presented in Table 5.1.2. Rietveld analysis also confirmed the presence of crystalline sillimanite phase for the samples prepared with 1 and 3 wt% MoO_3 and mullite phase was detected when amount of MoO_3 was increased to 5 wt%. The conventional powder processing method for the preparation of mullite bonded SiC ceramics from SiC and alumina powder showed that mullitization reaction began at 1400°C due to reaction between Al_2O_3 and oxidation-derived SiO_2. However, the XRD patterns did not reveal obvious mullite peaks until 1450°C. It has been reported that extensive mullitization occurred at 1500°C, and at 1550ºC mullitization was

almost complete [1]. *Zhu et al*. found that the addition of MoO_3 altered the reaction path and decreased the mullitization temperature by 200°C during the formation of mullite whiskers from kaolin and $Al(OH)_3$ [2]. A wide body of evidence exists that mullite formation in diphasic aluminosilicate gels and quartz are controlled by "dissolution-precipitation reactions". The Al_2O_3 is dissolved into the SiO_2 rich liquid phase, and mullite nucleation occurs once the critical concentration value of Al_2O_3 in the SiO_2 rich liquid phase is reached [3]. According to literature reports, alkaline earth metal oxides, such as Y_2O_3, Sr_2O_3, etc. have been used as sintering aids in order to lower the mullitization temperature of porous SiC ceramics. The addition of these oxides increased the rate of solid state reaction and facilitated mullite formation at lower temperatures, presumably through the formation of eutectic liquid Y_2O_3–Al_2O_3–SiO_2 (1360°C), Sc_2O_3–Al_2O_3–SiO_2 (1450°C), MgO–Al_2O_3–SiO_2 (1355°C), CaO–Al_2O_3–SiO_2 (1170°C), SrO–Al_2O_3–SiO_2 (1358°C) [4]. Fly ash and MoO_3 combine to form mullite at relatively lower temperature in the present case. *Zhu et al.* [2] suggest that this could be explained by a solution-precipitation method. When the sample is heated to 500°C, MoO_3 begun to sublimate, which reacts with the Al_2O_3 present in the fly ash to form metastable $Al_2(MoO_4)_3$ phase. Above 800°C temperature, that $Al_2(MoO_4)_3$ phase decomposes to highly reactive Al_2O_3 and low melting MoO_3. That Al_2O_3 then dissolves in a viscous liquid SiO_2 phase derived from the oxidation of SiC, as a result, mullite crystal formed at a comparatively lower temperature of 850°C and the temperature is raised further to cause mullite crystal growth.

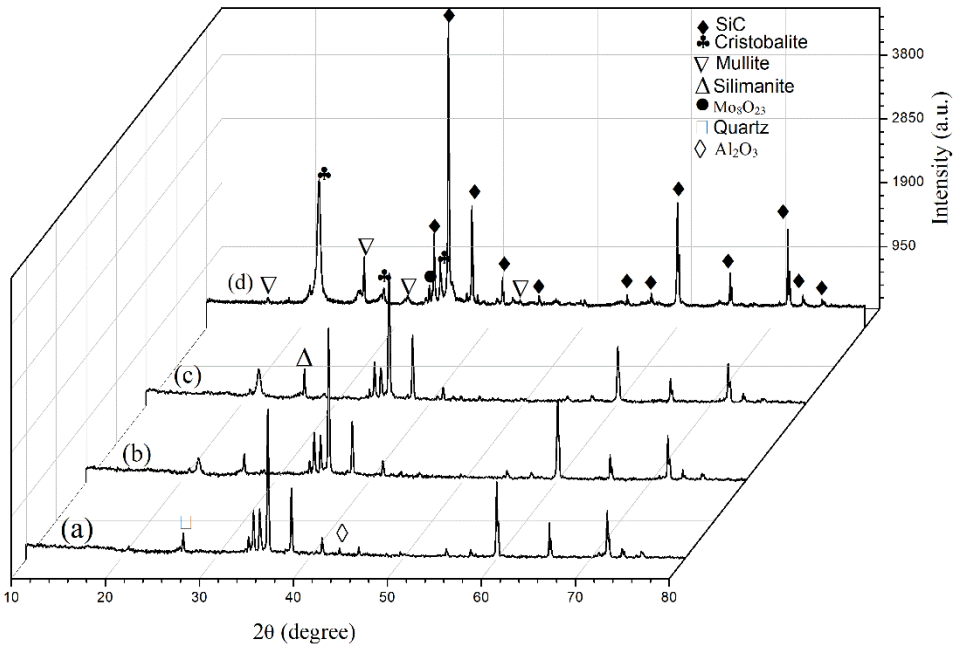

Figure 5.1.1. XRD plot of SiC ceramics prepared using SiC and fly ash with (a) 0 (b) 1 (c) 3 and (d) 5 wt% MoO_3.

Table 5.1.2 Effect of MoO_3 content on crystalline phases of porous SiC ceramic membranes prepared using SiC and fly ash in a weight ratio of 0.8:0.2.

MoO_3 (wt%)	Porosity (%)	Crystalline phases (%)							GOF
		SiC	Cristobalite	Mullite	Sillimanite	Quartz	Alumina	Mo_8O_{23}	
5	36.6	50.5	35.3	13.7	-----	----	----	0.5	1.53
3	37.8	68	16.2	----	15.4	----	----	0.5	1.42
1	41.3	77.1	8.3	----	14.5	----	----	0.1	1.31
0	----	95.4	----	----	----	4.5	0.2	----	----

5.1.3. SEM analysis

The representative microstructures of mullite bonded porous SiC ceramics SF, SF-G, SF-PC and SF-P samples along with overall pore morphology at higher and lower magnification are shown in Figure 5.1.2. An interconnected porous network were observed in the ceramics, along with a viscous layer on the SiC particle surface in the microstructures. Higher magnification showed that the SiC particles were bind with each other at the strut region. Figure 5.1.2 (right) shows an enlarged SEM image of the sample showing morphologies of

the different phases in more detail. Mullite crystals were found in rod shape in the microstructure. There have been several observations of mullite crystals with needle-shaped or rod-shaped crystals [2, 5-6]. Mullite whiskers with needle-like morphology and a smooth, rounded tip were synthesized from kaolin, $Al(OH)_3$ and $(NH_4)_6Mo_7O_{24}$ catalyst at different temperatures. With the increase of sintering temperature from 1100 to 1500°C, whisker length was reported to increase from ~0.8 to 10 μm [2]. Mullite whiskers obtained using AlF_3 and WO_3 as catalysts showed similar type morphology [5]. The sol-gel precursors used to obtain mullite ceramics sintered at 1300°C and 1600°C respectively were reported to produce needle-like mullite in the lengths of ~ 2 μm and ~20 μm by *Lee et al.* [6]. The effects of pore former on the microstructure of the porous ceramics were also clearly visible in Figure 5.1.2. Compared to SF-G and SF-P, the SF-PC showed most uniform porous structure with large number of necks between SiC particles. Microstructure in higher magnification clearly showed the changes in pore morphology from irregular to spherical with change of pore former from graphite to microbead to PVC.

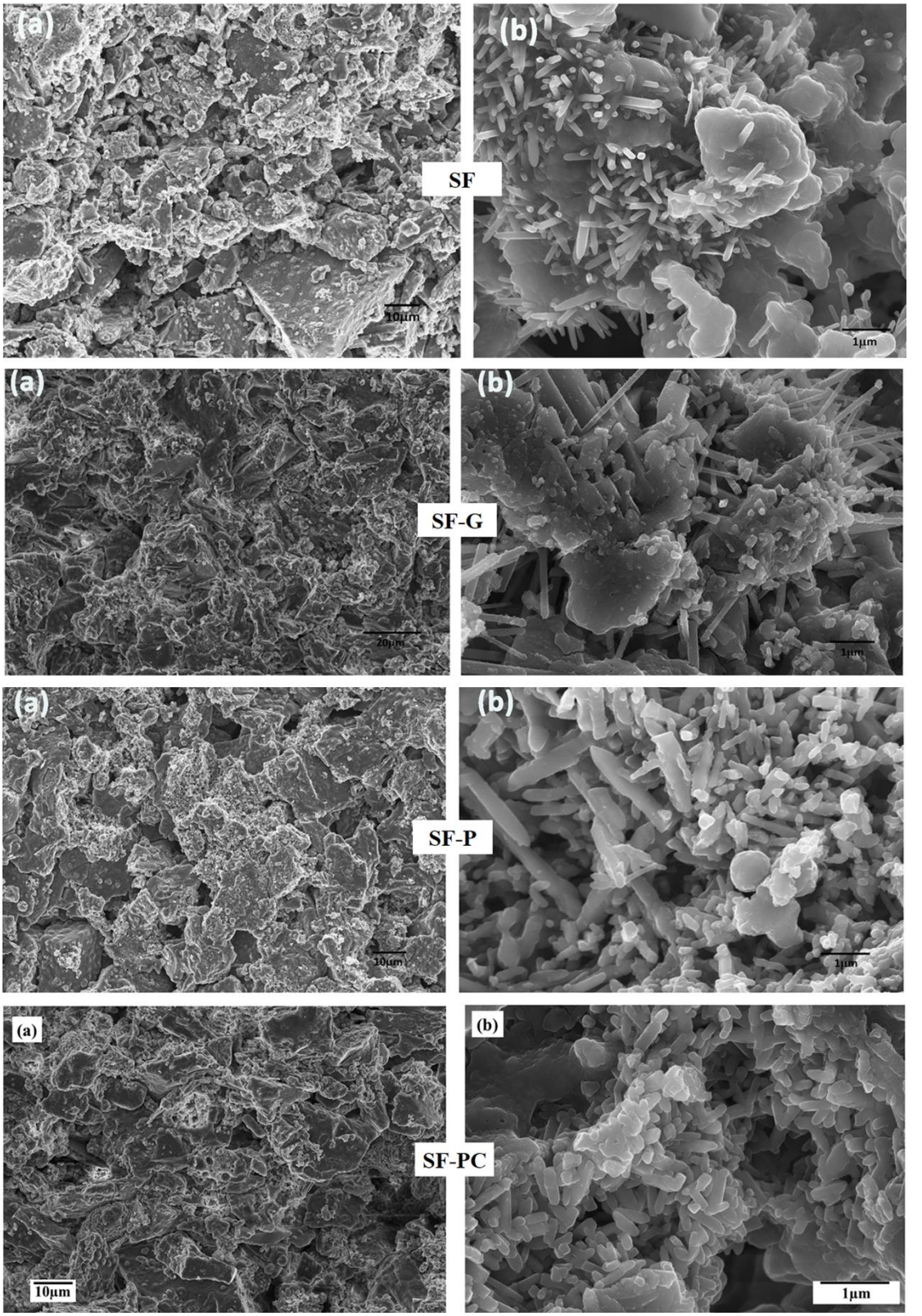

Figure 5.1.2. SEM micrographs of porous SiC samples prepared with different pore formers showing a) internal morphologies at low magnification and (b) mullite rods at high magnification.

Figure 5.1.3 shows some details about the presence of different elements in these areas revealed by Energy Dispersive X-ray (EDX) analysis under backswept electron (BSE) mode for the SF ceramics. According to the EDX result in the region "a", Si and O were detected, suggested that cristobalite could be present while in needle shaped grains in the area region "b" indicated the presence of Al, Si and O (the elemental constituents of mullite) suggested formation of mullite phase. In addition, the presence of Fe, Ti, and P element in the EDX, indicated that impurities came from fly ash. Presence of elemental Mo in EDX supported the XRD analysis result. There were no differences in the microstructures of the samples except for the different porosity.

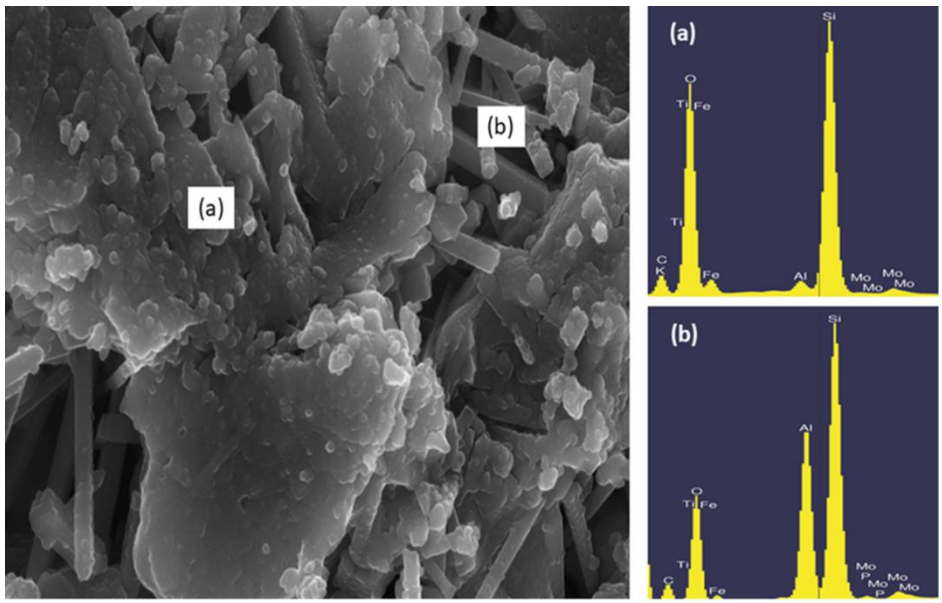

Figure 5.1.3. EDX results showing elemental information of different phases obtained during SEM microscopy of sample without pore former (SF).

5.1.4. PSD analysis

The monomodal pore size distribution with broad peak pattern profiles of the SiC ceramics sintered at 1000°C with change in pore former are presented in Figure 5.1.4. The PSD profiles indicated predominant presence of pores with diameters of 0.54–7.83 μm. The average pore diameters were found to be 2.9, 3.5, 4 and 3.7 μm for SF, SF-G, SF-P and SF-PC respectively, indicated that the pores were well dispersed around the average value. Pore diameter was the smallest for the samples without pore former, while the pore size increased with addition of pore former. It was predicted that the pore by stacking of SiC particles (d_{50}=22.4 μm) should be theoretically ~8 μm [7], provided that spherical SiC particles are in

dense cubic stack. In this study, pore formers with d_{50} ~10 μm were used. The sizes of the pore by burning out of pore former closely match with pores by stacking of SiC particles, therefore monomodal pore size distributions were obtained without any remarkable difference in the average pore diameter. But the average pore diameter is smaller (~3 μm) than predicted value (~8 μm) may be due to the irregular shape and wide particle size distribution of SiC particles, the variation in volume during the reaction bonding and the viscous flow of the oxidation derived silica. It was reported by several authors that pore diameter of porous SiC ceramics varied between ~2 and 8 μm for porous SiC ceramics prepared using SiC powder of d_{50}=22 μm, depending on processing parameters [8-10]. Due to the presence of MoO_3 in the present study, oxidation of SiC may have been enhanced, which might have led to formation of viscous silica liquid phase which can flows into the pores and reduces pore size. Thus, it was not possible to determine what accounted for the small differences in average pore sizes when pore former was added. The glassy melt, however, played a significant role in determining the pore diameter. The variation in pore diameters has also been reported in reaction-bonded ceramics and porous SiC ceramics, which was attributed to the formation of low viscous glassy melts in presence of sintering aids that flowed into the pores and caused the variation in pore diameters [7, 9].

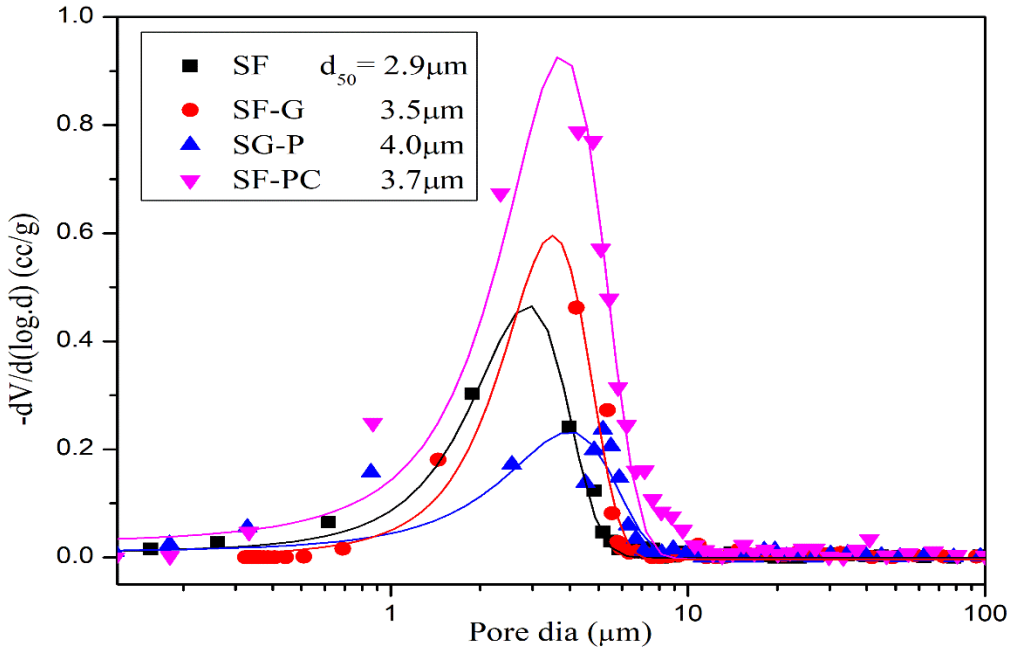

Figure 5.1.4. Pore size distribution pattern of porous SiC ceramic membrane prepared with and without pore formers.

5.1.5. Mechanical properties

The variation of three-point flexural strength with porosity of the final ceramics is shown in Table 5.1.1. The SiC ceramics prepared without pore former showed a flexural strength of ~38.4 MPa at a porosity of 36.4 vol% sintered at 1000°C. According to literature, the mullite bonded SiC ceramics were sintered at comparatively higher temperatures (1300-1550°C) for a longer time (2-4 hours) than the present work showed the variation of flexural strength from 9-44 MPa depending on the sintering additives (Al_2O_3, SrO, Y_2O_3, etc.) [11]. In a study by *Ebrahimpour et al.,* mullite-bonded SiC ceramics sintered at 1500°C for 3h, were strengthened by 30% by replacing some of the alumina powder with sol-gel alumina precursors [12]. Clay-bonded SiC ceramics prepared at 1200°C for 1h using SiC powder (d_{50}=14.5 µm), showed flexural strength of 5 MPa. These values increased to 36 MPa when the sintering temperature was raised to 1500°C [13]. Flexible glass-bonded SiC ceramics prepared with 5 and 15 wt% glass frit sintered at 850°C for 2h in air, had flexural strengths of 23 MPa, at 46% porosity and 75 MPa at 42% porosity respectively [14-15]. The superior strength of glass-bonded SiC membrane supports is explained by homogeneous microstructures and strong bonds between the SiC particles by glass frit. However, clay or glass bonded SiC ceramics degrade in harsh environments due to degradation of the binder phase under steam, alkali and heat conditions [16]. Mullite ceramics with whisker-interlocked structure were prepared using fly ash, bauxite, and 5 wt% MoO_3 sintered at 1200°C showed porosity 45.4 vol% and mechanical strength of 22.1 MPa [5]. In the present work, only fly ash was used as sintering aids and MoO_3 as catalyst and obtained SiC ceramics with higher mechanical strength even at low sintering temperature as low as 1000°C. Therefore, it is expected to reduce the processing cost as well as chemical stability of SiC ceramics in harsh condition due to formation of increased amount of mullite in the bond phase.

5.1.6. Air permeability study

Figure 5.1.5 shows the variation of normalised pressure drop (ΔP/L) with transmembrane pressure (TMP) along the membrane surface with air velocity (0– 0.20 m/s) for mullite bonded SiC ceramic membranes having different levels of porosity at room temperature. A high quality parabolic fitting of Forchheimer's equation were observed for all the membranes. The pressure drop shifted systematically upward with decreasing porosity for the same air velocity. The data in Figure 5.1.6 represents permeability coefficients k_1 and k_2 value and porosity of the sample prepared in this study in a comprehensive map that includes a large number of data on various types of porous membranes [17-18]. In general, the

permeability results of the samples examined in this study are similar to those found for other granular filters with similar porosities (Table 5.1.3).

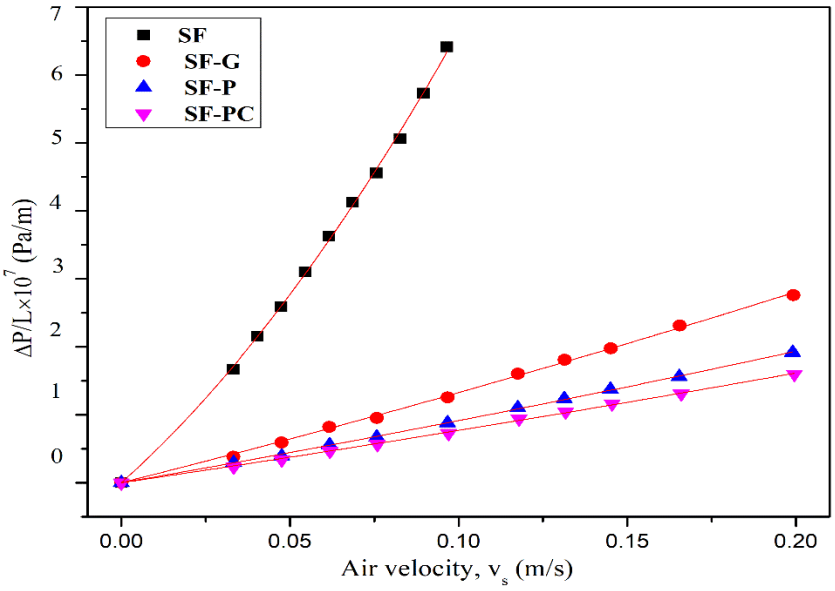

Figure 5.1.5. Permeation curves for SiC ceramic membranes with different porosities measured with airflow.

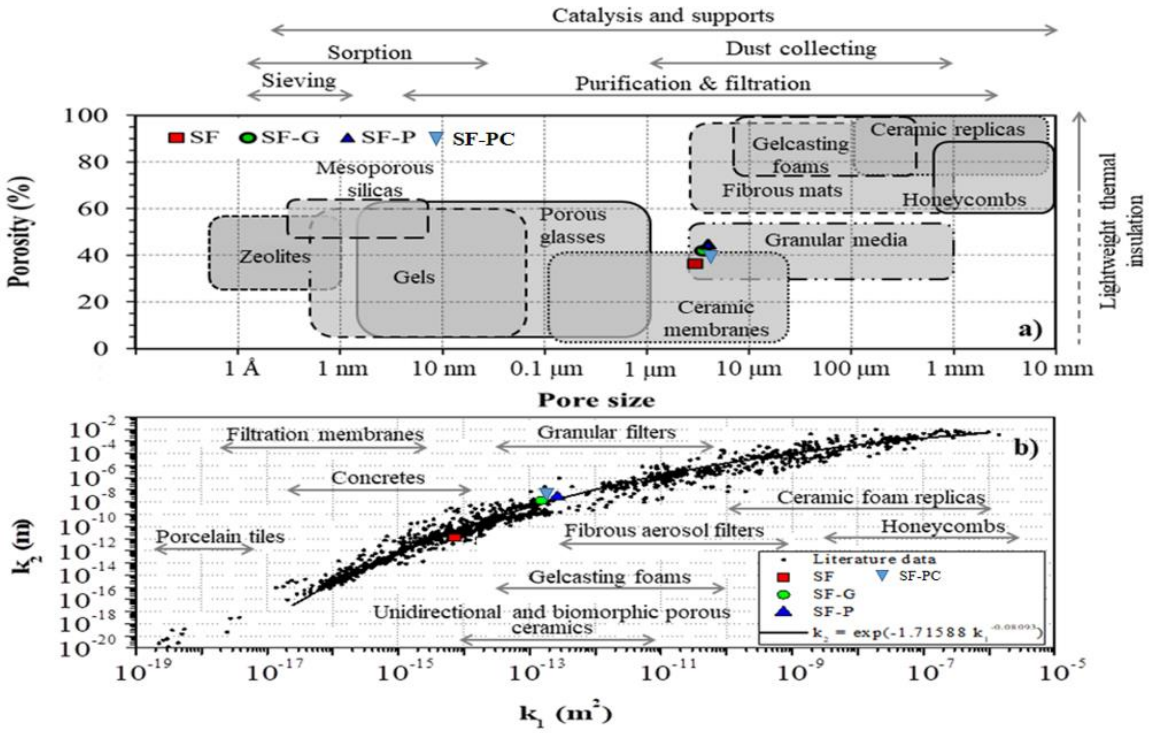

Figure 5.1.6. Maps of properties and applications of porous ceramics with location of SiC membranes SF, SF-G, SG-P and SF-PC: (a) porosity map adapted from *Okada et al.* [17]; (b) permeability map adapted from *Vakifahmetoglu et al.* [18].

Table 5.1.3. Comparison of air flow permeability and pore size data for the samples prepared with different pore formers.

Sample	d_{pore}(µm)*	k_1 (m^2)	k_2 (m)
SF	2.93	$(7.30\pm3.31)\times10^{-15}$	$(1.18\pm1.03)\times10^{-11}$
SF-G	3.49	$(1.52\pm0.03)\times10^{-13}$	$(1.37\pm0.04)\times10^{-8}$
SF-P	3.99	$(2.66\pm0.42)\times10^{-13}$	$(2.63\pm0.14)\times10^{-8}$
SF-PC	3.71	$(2.23\pm0.34)\times10^{-13}$	$(2.18\pm0.13)\times10^{-8}$

(*) from Hg porosimetry

5.1.7. Water permeation study

The parabolic relationship between pressure drop (ΔP) and superficial water velocity (v_s) of pure water permeation through the as prepared SiC membranes was observed in the same way as airflow tests. The permeability coefficients k_1 and k_2 obtained from high-quality fitting of Forchheimer`s equation to water permeation curves. The membrane resistance (R_m) and specific permeability (SP) were also calculated. Figure 5.1.7 shows the variation of pure water flux (J) as a function of transmembrane pressure (TMP) for all the membranes, and a high quality fitting is achieved in all cases (R^2>0.99). It was found that the flux of pure water increased with the increase in membrane porosity and transmembrane pressure across the membrane surface. The specific permeability of membrane prepared with PMMA, PVC and graphite as pore formers was 6113, 4843 and 3574 $Lm^{-2}h^{-1}bar^{-1}$ respectively, while the membrane prepared without a pore former had the lowest specific permeability of 1532 $Lm^{-2}h^{-1}bar^{-1}$. *Zhu et al.* reported pure water permeance of 700 LMH for clay bonded SiC support coated with 8 wt% SiC slurry of fine powder (d_{50}= 0.55 µm) sintered at 1000°C for 3h [13]. Clay-bonded flat tubular SiC membranes prepared by *Bukhari et al.* at 1400°C with 6.7 µm SiC powder, showed a pure water flux of ~5500 LMH at 1 bar with 16 inner holes and porosity at 47 vol% and pore diameter at 1.80 µm [19]. For alumina, silica, clay based membranes, the pure water flux rate has been reported to be 170, 1587, and 700 LMH [19-21].

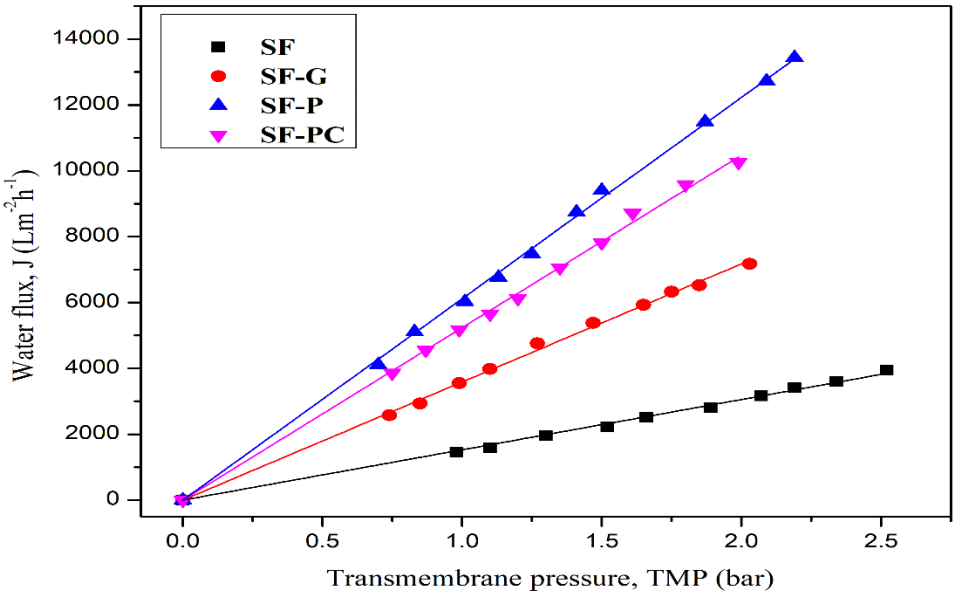

Figure 5.1.7. Plot of pure water flux against TMP for porous SiC membranes of different porosities.

As expected airflow permeability are consistently higher than those of water flow due to the hindrance of liquid percolation through the pores caused by high surface tension. The membrane resistance value increased with decrease in pore size and porosity of the filters and the SiC membranes showed membrane resistance of 27.3, 11.7, 6.8 and 8.93×10^{10} m^{-1} for SF, SF-G, SF-P and SF-PC membrane respectively. Figure 5.1.8 shows the contributions of inertia and viscous effect to membrane resistance. An intrinsic membrane resistance of 3×10^{12} m^{-1} was reported for zirconia based ceramic membranes with porosity of 22 vol% and an average pore size of 140 nm [22]. The zirconia based ultrafiltration and polyvinyl pyrrolidone (PVP) modified zirconia-based ultrafiltration membrane exhibited membrane resistance (R_m) of $2.6–5.3\times10^{12}$ m^{-1} for separation of oil water emulsion [23]. The ceramic membrane with pore diameter of 1.5 μm showed membrane resistance of 9.8×10^{10} m^{-1} for treating wastewater from dye based industry [24]. The above literature review indicates that depending on the type of membrane characteristics the membrane resistance and specific permeability results varied.

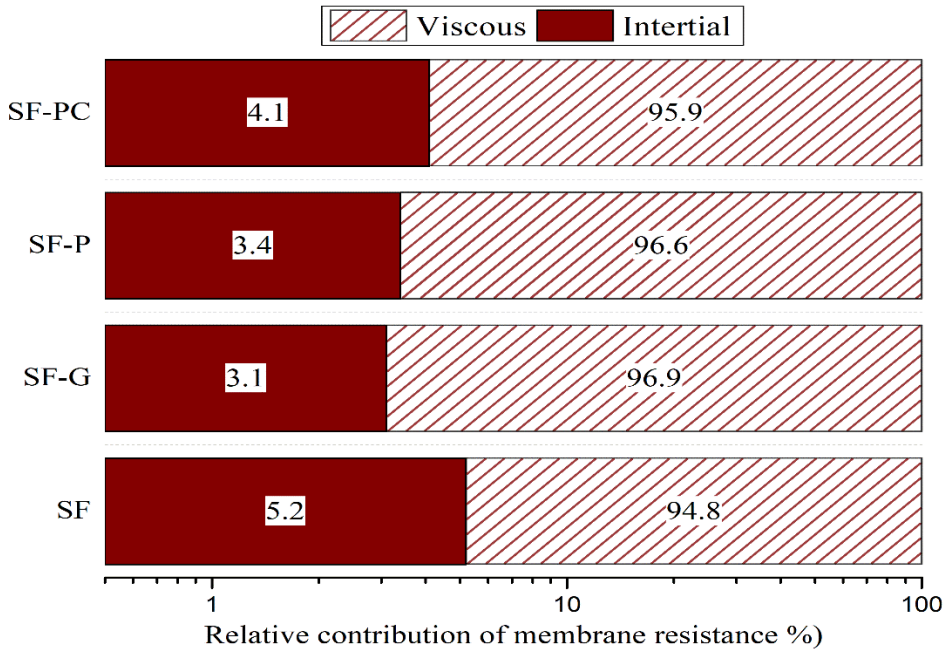

Figure 5.1.8. Relative contribution on membrane resistance in the interval 0.3–2.5 bar.

5.1.6. Wastewater filtration study

The results of removal efficiency in terms of COD, Oil, TSS, and turbidity from wastewater using as prepared membrane with different porosity levels are presented in Figure 5.1.9. The results showed that depending on the porosity of the filter material ~89-92% oil; 89–94% turbidity and 82–92% COD were removed from grey wastewater by the membranes prepared in this work.

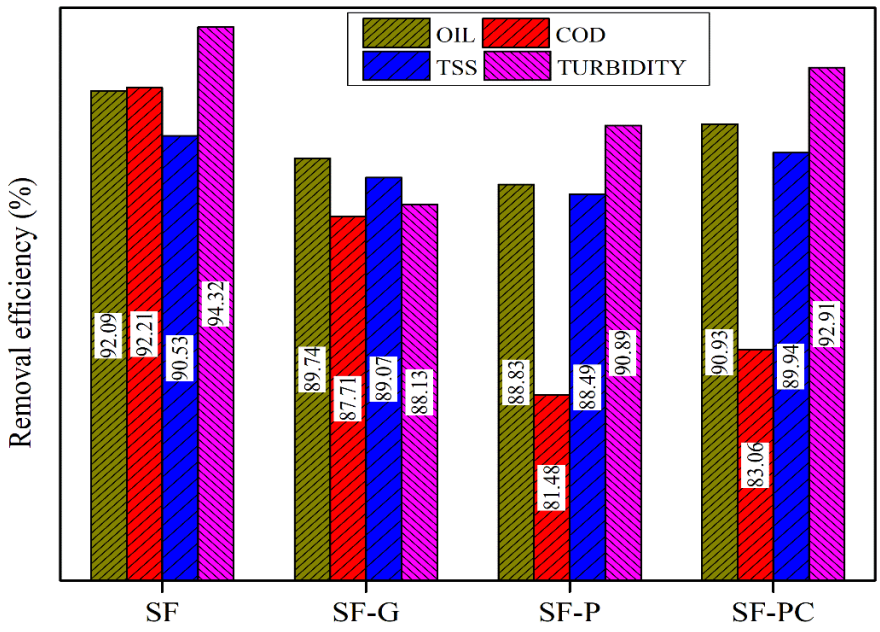

Figure 5.1.9. Evaluation of the effectiveness of different ceramic membranes for removing pollutant contaminants from wastewater.

The photographs of the permeate water after filtration through porous SiC filters and the feed wastewater are shown in Figure 5.1.10 showing high clarity of permeates after filtration. There has been little research on the effectiveness of clay, mullite, and alumina based membranes for removal of oil from synthetic oil-water emulsions or oily wastewater streams. However it has been reported that 84-99% of the oil can be removed depending on the membranes. On coating glass frit bonded SiC membrane with γ–Al_2O_3 the composite membrane showed oil rejection efficiency of 99.9% from water containing 600 mg/L oil and flux rate of $5.29\times10^{-5} m^3m^{-2}s^{-1}$ [15]. A comparative assessment of flux rate of pure water, contaminated feed water, oil rejection obtained for the ceramic membrane prepared in this work with literature data is presented in Table 5.1.4.

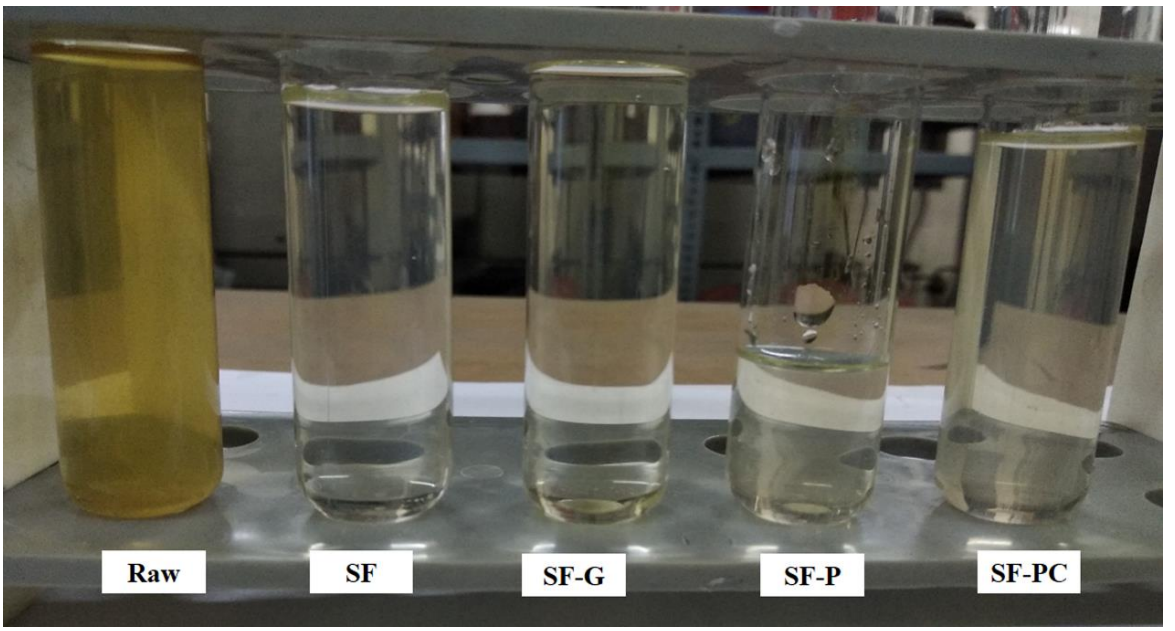

Figure 5.1.10. Photograph of wastewater filtered through porous ceramic membranes with varying porosities before and after filtering.

Table 5.1.4. Comparison of the performance of the ceramic membrane reported in the literature.

Ref.	Type of Membrane	Sint. Temp^{r}. (^{o}C)	Porosity (vol%)	Pore dia(µm)	Initial oil conc^{n}(mg/L)	Flux rate (L/m^2.h.bar)	Oil rejection rate (%)	Pure water flux L/m^2.h.bar)
[25]	clay	850	28	0.7	50	47.4	96.96	698.4
[26]	Clay	1000-1100	26	0.67	600	30	84.1	---
[27]	Fly ash	---	---	0.77	2000	92.99	98.2	---
[20]	Glass	850	---	1.47	1000	143.75	80	1587
[28]	Mullite	1350	41	0.25	600	34.83	90	109
[21]	Zeolite coated alumina	---	30-40	1-3	500	31	98.8	170
[29]	Commercial alumina	---	35	0.8	250	47.55	99.7	---
[19]	clay bonded SiC	1400	44-47	3.5-1.5	---	---	---	2500-3900
[30]	SiC coated with fine SiC	1100	---	0.093	---	---	---	400-210
[15]	γ-Al_2O_3 coated Glass bonded SiC	850	42-45	0.07-.41	600	64-190	99.9	---
[31]	γ-Al_2O_3 coatedcommercial α-Al_2O_3	550	45	0.02	69	240	84	---
This work	Mullite bonded porous SiC membrane	1000	36-45	3-4	1657	200-400	89-92	1500-6179

This research provides a new direction for the utilization of an industrial waste coal fly ash and a new low-cost method of porous mullite bonded SiC ceramic membrane preparation. Porous mullite bonded SiC ceramics were fabricated in air by an in situ reaction bonding process at 1000°C using SiC, fly ash, pore former as raw material and MoO_3 as catalyst. The permeation results of this work are comparable or even better than literature data, however based on the operating parameters like time, TMP, face velocity, etc. the performance of the membrane at best optimum operating conditions need to be evaluated. A potential benefit of this study is that it may provide an alternative method of recycling coal fly ash waste, not only to reduce its environmental impact, but also to produce high-valued porous ceramic membranes based on SiC for the separation of oily wastewater.

Chapter 5.2

5.2. Mullite bonded porous SiC ceramic membranes prepared using alumina as a bond forming additive and clay as sintering aid.

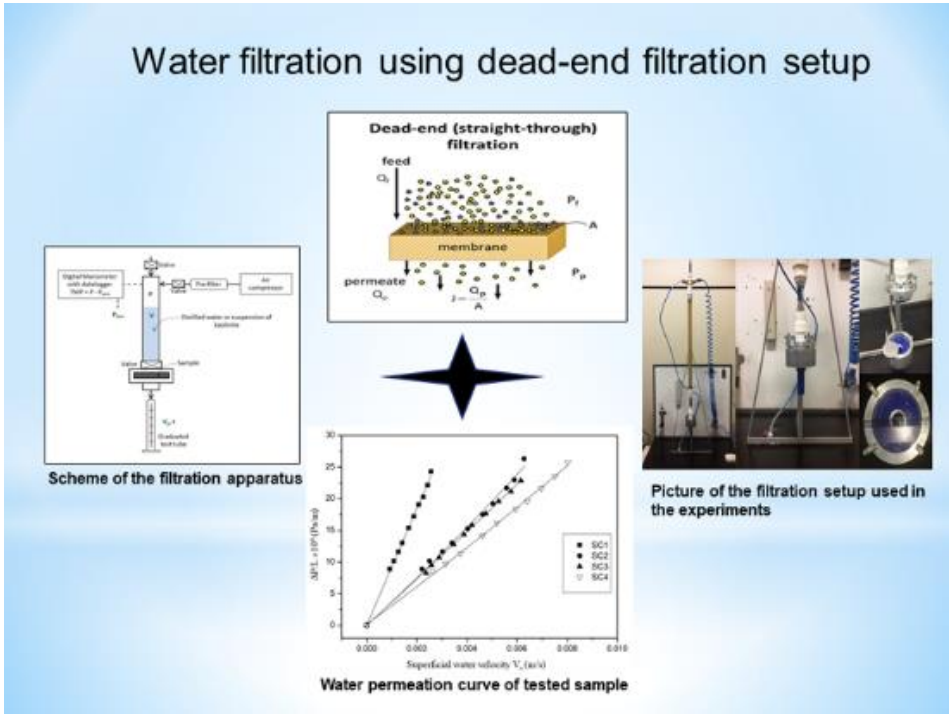

In this study efforts are made to select optimum amount of clay in green formulation for the preparation of mullite bonded porous SiC ceramics using alumina as bond forming additive. Based on the XRD and mechanical strength results, 1 wt% clay was chosen optimum amount for the preparation of mullite bonded SiC ceramics. The effect of different pore formers on the microstructure, mechanical strength, porosity and pore size distribution, air, and water permeability of porous SiC ceramics were investigated. The average pore diameter, porosities, and flexural strength of the final ceramics varied in the range 3.7-6.5 μm, 38-50 vol %, and 28-38 MPa, respectively, depending on the characteristics of pore former. The Darcian (k_1) and non-Darcian (k_2) permeability was found to vary from 1.48 to 4.64 $\times 10^{-13}$ m^2 and 1.46 to 6.51 $\times 10^{-8}$ m, respectively. All membranes showed high oil rejection rate (89-93%) from feed wastewater with oil concentration of 1557 mg/L.

Publications

1. D. Das, N. Kayal, et al., Int. J. App. Ceram. Tech., 17 (2020) 893-906.
2. D. Das, N. Kayal, M.D.M. Innocentini, Membr. Water Treat., 12 (2021) 133-138.

5.2.1. Effect of clay as a sintering additive in final SiC ceramics

In order to select optimum amount of clay on phase evolution and the properties of porous SiC ceramics, three different amounts of clay additive were added (i.e. 0, 1 and 2%) with SiC (d_{50}=22.4 μm) and alumina powder in the final composition and the ceramics sintered at 1400°C for 1h. A comparison of the characteristics of samples prepared without and with clay (1%) additive, as listed in the Table 5.2.1, allowed us to examine the effect of clay content on the properties of porous SiC ceramics after sintering.

Table 5.2.1. Effect of clay content on phase composition and flexural strength

Sample	Crystalline phases (%)				Porosity	Flexure
	SiC	**SiO_2**	**Mullite**	**Alumina**	(vol%)	strength(MPa)
S1(without clay)	66.30	24.40	—	9.30	38.92±0.19	31.11 ± 0.13
SC1(with 1 wt% clay)	68.85	19.05	12.10	—	36.58 ±0.44	57.07 ± 0.19

The samples prepared without clay additive, showed a signature alumina peak in XRD pattern, but no characteristic mullite phase peak present in the sample, indicated the presence of unreacted alumina in the sintered ceramics, as has also been evidenced by the Rietveld analysis. While the membranes prepared with 1 wt% clay (SC1) did not shown any signature peak of alumina but shown characteristic peak for mullite phase indicated, all the alumina is reacted with silica and formed mullite phase which is shown in Figure 5.2.1. The sample prepared without clay additives showed a flexural strength of 31 MPa at porosity 38.9 vol%, whereas with 1 wt% clay added, significant increase in strength of 57 MPa was observed. The change of flexural strength with clay addition due to variations in the composition of the bonding phases (silica, mullite, glassy phases), the Young's moduli of the phases, and porosity of the sample. Further increase in the clay content in the final ceramics, the amount of mullite bonding phases have increased and increases the strength of the ceramic but in literature, it is suggested to reduce the amount of clay during fabrication of porous SiC ceramics to increase the durability of the ceramics in harsh application conditions as it is alkaline in nature [32]. Because no unreacted alumina was obtained and the ceramic was mechanically strong enough due to the mullite phase as the primary bonding agent, therefore,

in this study 1 wt% clay selected as a minimum amount of clay in the total powder mixture for preparation of mullite bonded SiC membranes.

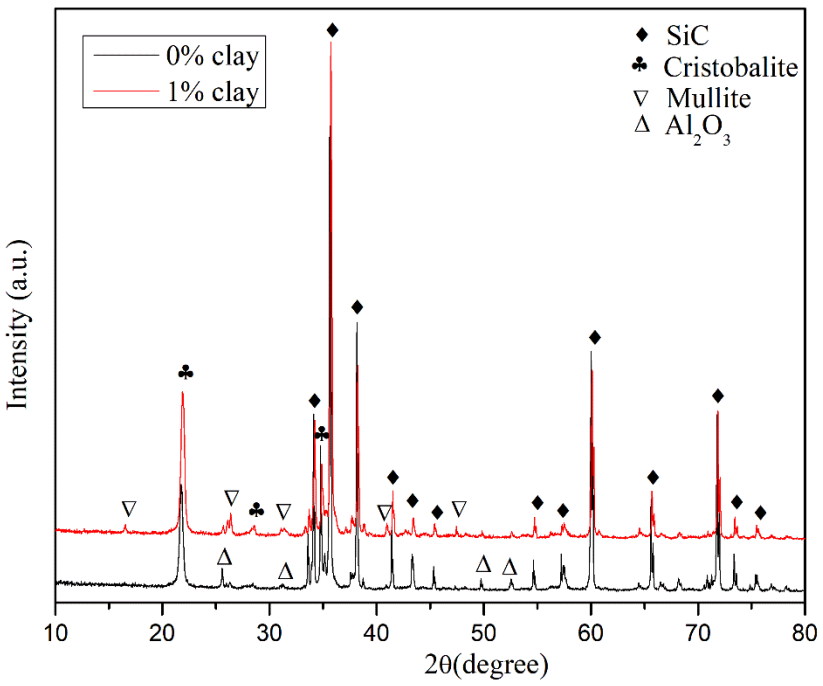

Figure 5.2.1. XRD pattern of porous SiC ceramics sintered at 1400°C showing the effect of clay addition on phase formation

No surface cracks or distortions in shape was observed in sintered SiC ceramic membranes prepared with 1 wt% clay after sintering at 1400°C for 1h in air. The volume expansion due to silica and mullite formation was compensated by the shrinkage in volume due to sintering, resulted no appreciable change in volume or dimensions for oxide-bonded ceramics. To observe the effect of variation in pore forming agent, on properties of final ceramics, three types of sacrificial pore forming agents (microbead, PVC and graphite) were employed to develop porous SiC structure. The samples obtained using graphite, PVC and polymer microbead named as SC2, SC3 and SC4 respectively. Addition of 10 wt% pore formers (graphite, PVC, PMMA) to the ceramics resulted in a significant increase in porosity from 38 vol% to 50 vol%, while the flexural strength decreased from 57 MPa to 28.5 MPa respectively and accordingly density of the samples was reduced from 1.8 to 1.5 g/cm^3. A small difference in porosity was found based on the decomposition temperatures of the pore formers (PVC at 500°C, PMMA at 550°C, and graphite at 750°C), the rate of decomposition and volume ratio of the pore formers to ceramic particles, and the particle size of the pore

formers. Table 5.2.2 summarizes the properties of porous ceramics and theoretically calculated bond phases containing both crystalline and amorphous states.

Table 5.2.2. Characteristics of porous SiC ceramic membranes.

Sample code	Pore former	Theoretical calculation (wt. %)			% oxidation	Porosity (vol. %)	Flexural strength (MPa)
		SiC	SiO_2	Mullite			
SC1	---	68.89	17.72	13.40	15.5	38.22±0.06	38.47±0.03
SC2	Graphite	72.63	15.05	12.31	14.6	48.56±0.20	31.86±0.13
SC3	PVC	72.17	14.27	12.21	13.9	49.90±0.10	28.53±0.17
SC4	PMMA	71.15	15.31	12.30	14.8	48.02±0.44	31.53±0.19

A theoretical calculation of the phase compositions of the sintered ceramics was done based on the mass change data for the various stages of the process [33]. Depending on the pore former, the % of SiC oxidation varied in the range of ~14-15.5 %. Samples prepared without pore former showed the highest amount of SiC oxidation, and those prepared using PVC as pore former showed the lowest amount. In the samples prepared without pore former, a faster diffusion of oxygen through the grain boundaries resulted in more silica [34]. The reduction of flexural strength was observed with the increase of porosity in this study, a common phenomenon observed by many authors and explained by a model based on minimum solid area (MSA) which predicts an exponential relationship between porosity and mechanical strength. The flexural strength decreased from 38.5 to 28.5 MPa with the increase in porosity from 38.2 to 50 vol% due to higher probability of pore coalescence with an increase of porosity [35]. The sample prepared with PVC as the pore former contained less silica content and showed the lowest flexural strength, which may be related to its high oxygen consumption during dehydrochlorination and slow thermal decomposition [36]. For SiC ceramics prepared at 1400°C using SiC powder of d_{50} = 14 µm, *She et al.* measured a flexural strength of 32.7 MPa, a porosity of 44%, and pore size of 3.44 µm [19]. *Kayal et al.* fabricated mullite bonded porous SiC ceramics by sol-infiltration technique sintered at 1400°C for 4 hours and characterized with a flexural strength of 36 MPa with a 33% porosity [33]. *Choi et al.* found that the candle ceramic made of ~180 µm size SiC powders and a clay based oxide binder had a strength of 28 MPa at a porosity of 28% [38]. Thus, the investigated ceramics provide flexural strength comparable or even superior to that of commercial filters from

Schumacher (Dia-Schumalith), Germany (39 MPa at 32.5% porosity), as well as other reported strengths for hot gas filters [35, 39-41].

5.2.2. XRD study

XRD analysis of sintered ceramics indicated the presence of α-SiC (crystal system: hexagonal; space group: P63mc; a=b=3.0817 Å, c=15.1183 Å and α=β=90°, γ=120°; with two polytypes 6H; JCPDS 029-1128 and 4H; JCPDS 029-1127), cristobalite (crystal system: tetragonal; space group: P41212; a=b=4.9934 Å, c=7.0055 Å and α=β=γ=90°; JCPDS 01-076-0939), mullite (crystal system: orthorhombic; space group: Pbam; a=7.5539 Å, b=7.6909 Å, c=2.8839 Å and α=β=γ=90°; JCPDS 79-1457) phases in the final ceramics as shown in Figure 5.2.2. No characteristic peaks of alumina and graphitic carbon were detected in the XRD profiles for the samples prepared using pore former and clay additive, which confirmed that complete conversion of alumina and removal of pore former during heat treatment. The mullite formation temperature was reduced by ~ 100^{o}C in presence of clay due to the formation of eutectic liquid $CaO–Al_2O_3–SiO_2$ at lower temperatures. The crystalline phase contents in the samples obtained by Rietveld analysis are presented in Table 5.2.3. Almost an equal quantity (~10 wt%) of mullite was found to be present in all samples prepared with and without pore former.

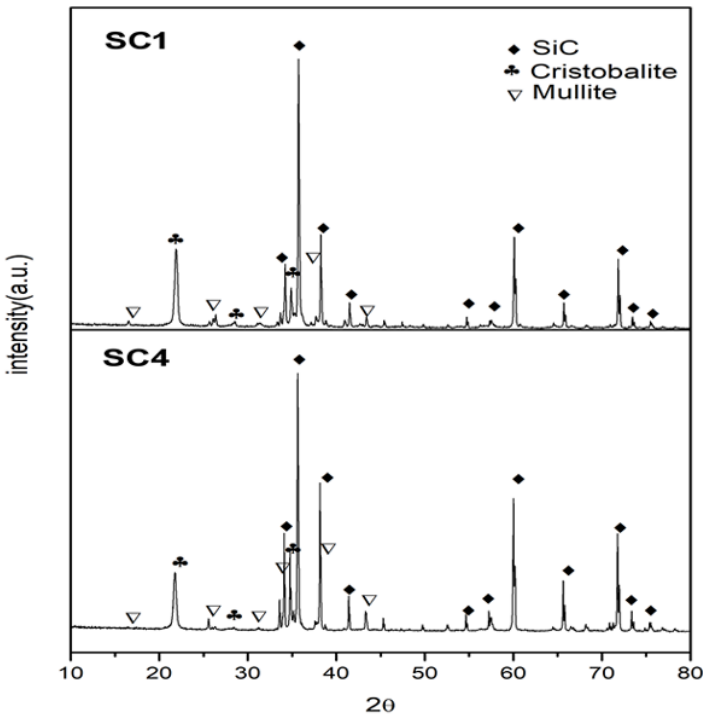

Figure 5.2.2. XRD pattern of mullite bonded SiC ceramics

Table 5.2.3. Rietveld analysis results of porous SiC ceramics.

Sample ID	Crystalline phases (%)				R_{wp}	GOF
	SiC		Cristobalite	Mullite		
	6H	4H				
SC1	60.9	3.6	25.2	10.3	11.50	2.03
SC4	62.1	2.7	25.0	10.2	11.37	1.83

5.2.3. Microstructure analysis

The representative microstructures of mullite bonded porous SiC ceramics along with overall pore morphology prepared with different pore formers, are shown in Figure 5.2.3. High magnification in-lens mode images showed well-developed necks between SiC particles and the changes in pore morphology from irregular to spherical with change in pore former from graphite to PMMA. The formation of needle-shaped and fish scale type phase in the neck region were also observed at higher magnification. Further EDX study revealed that the fish scale (assigned as area "a") and needle (assigned as "b") shaped phases are mainly cristobalite and mullite phases shown in Figure 5.2.4. The needle-shaped mullite crystals were found to be ~3-5 μm in length and 0.3-0.5 μm in width and the individual cristobalite grain size was found 0.5-1 μm in diameter for all the samples. Several other researchers [6, 42] have reported the needle shaped morphology of mullite phase and fish scale morphology of cristobalite.

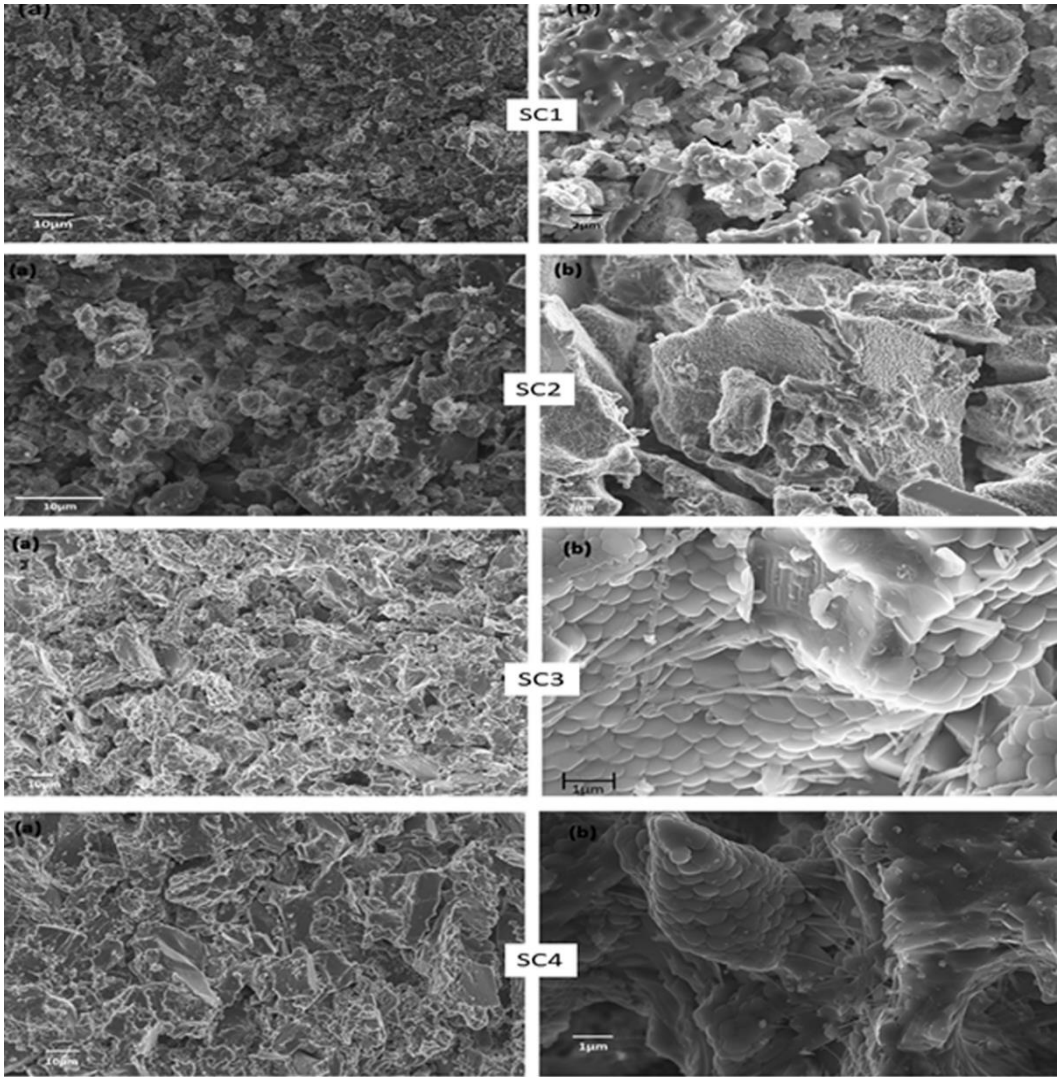

Figure 5.2.3. Representative microstructures of SiC microfiltration membrane prepared at 1400°C in (A) low and (B) high magnification.

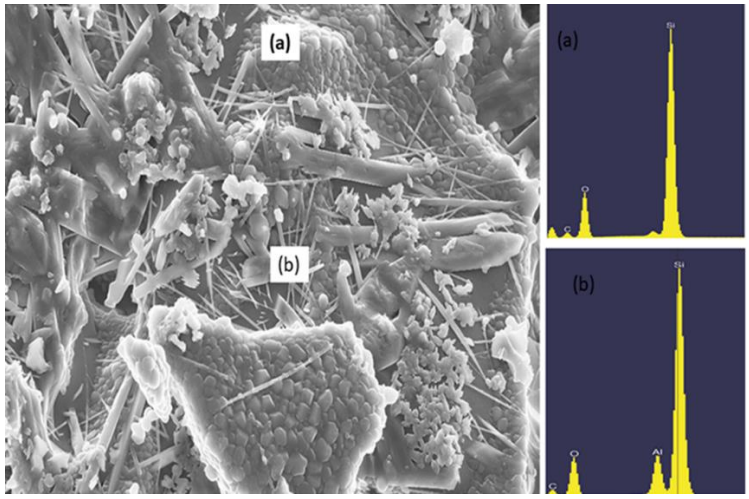

Figure 5.2.4. EDX analysis of the marked region of fish scale shaped (a) cristobalite and needle shaped (b) mullite crystal in SiC membranes.

5.2.4. PSD analysis

The monomodal pore size distribution pattern was obtained for all ceramics sintered at 1400°C and the variation of pore diameter of the ceramics are shown in Figure 5.2.5. The pore diameter of the final ceramics increased with the addition of pore former and the sample shows an average pore diameters of 3.7, 6.5, 4.2 and 4.3 μm, for SC1, SC2, SC3, and SC4 membranes respectively. Basically, pores are formed from stacking SiC particles into compacted powders and burning out the pores. Pore former is expected to have a less dramatic effect on the overall pore diameter of the ceramics since it was just 10 wt% of the whole powder mixture. The large pore size in the graphite-based SiC membrane might result from the combined effects of large variations in graphite particle size and agglomeration of graphite particles during processing.

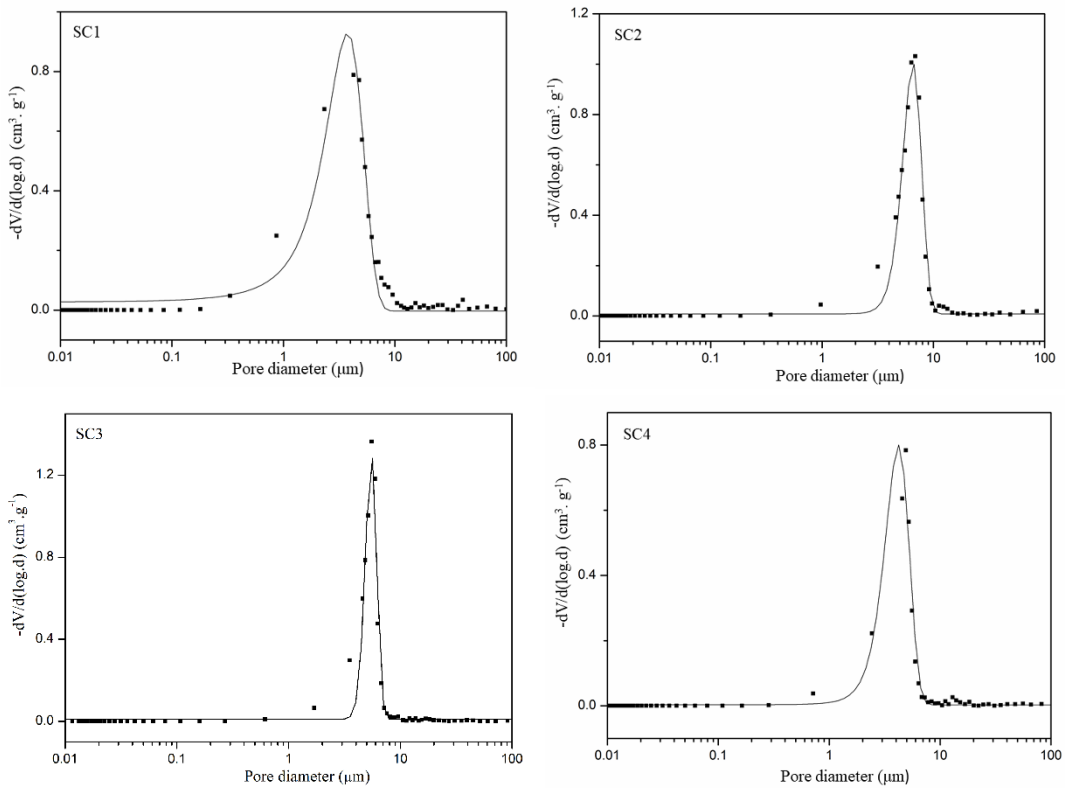

Figure 5.2.5. Distribution of pores in mullite-bonded porous SiC sintered at 1400°C.

5.2.5. Air permeability behaviour of the porous SiC membrane

The plots of pressure drop (ΔP/L) as a function of air velocity (v_s) for the as prepared mullite bonded porous SiC membranes are presented in Figure 5.2.6. Based upon the high-quality parabolic fitting of Forchheimer's equation, the permeability coefficients k_1 and k_2 and fluid

dynamic pore sizes are given in Table 5.2.4. A greater porosity led to an increase in permeability coefficient from 1.48 $\times 10^{-13}$ to 4.64 $\times 10^{-13}$ m^2 with an increase in porosity from ~38 to 48 vol% in this study. The pore diameters calculated from the Ergun equation were higher than those calculated from the experimental results, since Ergun equation is based on beds of loose particles. Thus, the Ergun equation can be expected to fail to provide reliable results for determining k_1 for sintered porous ceramic samples. As shown in Figure 5.2.7, the permeability data obtained for the SiC samples in this study are within the typical range for granular and fibrous filters.

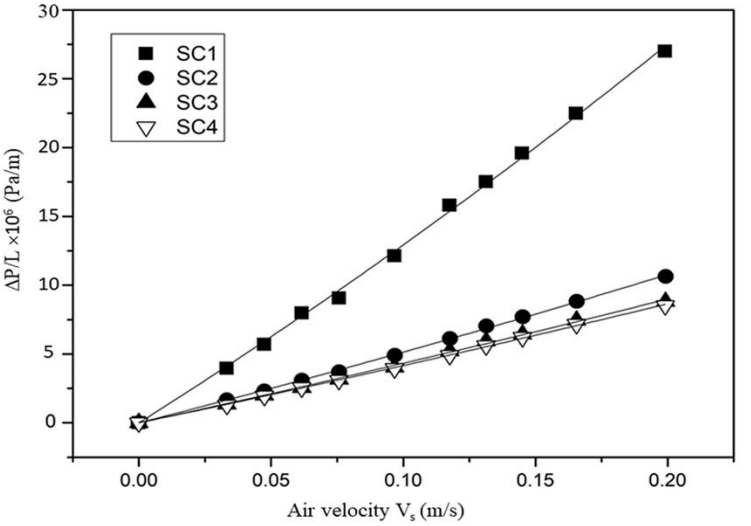

Figure 5.2.6. Experimental air permeation curves for SiC membranes prepared with different pore formers

Table 5.2.4. Effect of various pore former on the permeability coefficient value and pore size for as prepared SiC membranes obtained during air permeation.

Sample code	Pore former	$k_1(10^{-12}m^2)$	$k_2(10^{-8}$ m) *	d_{pore}(µm)
SC1	None	1.48±0.10	1.46±0.20	5.08±0.17
SC2	Graphite	3.75±0.12	4.94±0.87	7.17±0.13
SC3	PVC	4.53±0.02	6.29±0.21	7.77±0.02
SC4	PMMA	4.64±0.07	6.51±0.27	8.04±0.05

*Correlation coefficient R^2> 0.99 was observed for all samples

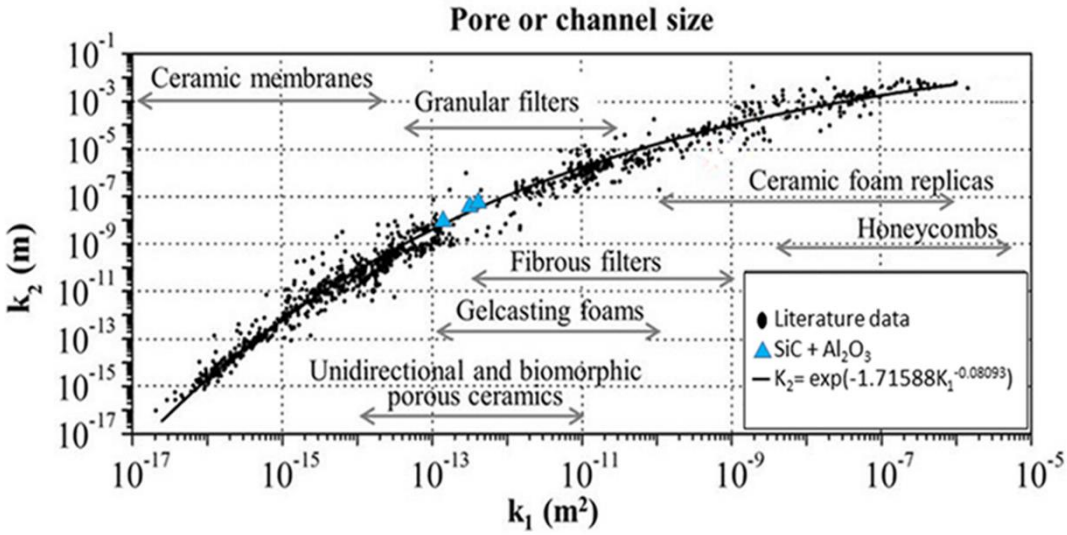

Figure 5.2.7. Location of experimental k_1 and k_2 data of SiC membranes obtained in this work in a comprehensive permeability map, adapted from References [43].

5.2.6. Water permeability behaviour of the SiC membrane

For all samples with varying porosities, a parabolic relationship between pressure drop (ΔP) and superficial water velocity (v_s) was obtained, and the Forchheimer's equation exhibited high correlation coefficients (R^2> 0.99) for clear water permeation through porous membranes. From the fitted curves of water permeation, the permeability coefficients k_1 and k_2, Specific permeability (SP), membrane resistance (R_m) are calculated and given in Table 5.2.5. The air flow values for porous SiC membranes were consistently higher than those of the water flow due to the surface tension, which interfered with liquid percolation through the pores and remained unchanged throughout the samples. In general, the permeability coefficients k_1 and k_2 are considered to be solely determined by the porous structure and independent of the flow conditions. In spite of this, if there is an interfacial tension in the pores during the percolation of liquids, the flow may be hindered and the coefficients will be reduced.

Table 5.2.5. Specific permeability (SP), membrane resistance (R_m) and permeability values obtained for tested membranes in the water flow experiments.

Sample code	Pore former	k_1 (10^{-13} m^2)	k_2 (10^{-8} m)	SP ($Lm^{-2}h^{-1}$ bar^{-1})		R_m (10^{10} m^{-1})	
				Min	**Max**	**Min**	**Max**
SC1	-	0.92±0.10	1.79±0.11	4417	4755	8.75±0.06	9.42±0.11
SC2	Graphite	2.62±0.26	1.85±0.10	11177	12344	3.45±0.27	3.82±0.32
SC3	PVC	2.34±0.11	4.95±0.20	9660	10992	3.67±0.23	4.19±0.38
SC4	PMMA	3.16±0.22	4.32±0.69	12516	14079	2.86±0.20	3.21±0.07

A plot of the water flux (J) versus the transmembrane pressure (TMP) across all samples is shown in Figure 5.2.8. The pure water flux increased as the porosity of the membrane and transmembrane pressure across the membrane increased. A more homogeneous microstructure in membranes prepared with PMMA as the pore former could account for the higher flux of the membrane than the other membrane. A porous SiC membrane supports were developed by *Kim et al.* using SiC and 15% glass frit sintered at 850°C and showed a flux rate variation from 600 to 1100 $Lm^{-2}h^{-1}$ depending on TMP [44]. The clay bonded SiC membrane exhibited a pure water flux rate of 25000 $Lm^{-2}h^{-1}bar^{-1}$ for 5h while maintaining a consistent number of inner channels [13]. The membrane has 44% porosity, a 3.3 µm pore diameter, and flexural strength of 32.7 MPa. *Bukhari et al.* reported that a ceramic membrane made from clay bonded SiC with a SiC filtration layer sintered at 1100°C had pure-water flux rates of 210 $Lm^{-2}h^{-1}bar^{-1}$ and exhibited very stable permeance over time [45]. The dead-end filtration system with pore size 250 nm showed pure-water permeability 240 $Lm^{-2}h^{-1}bar^{-1}$ [46-47]. Relative contributions due to inertia and viscous effect on membrane resistance in the interval 0.3-2.5 bar were calculated and found to be 1.5, 10.0, 11.2, and 5.8% for inertia and 98.5, 90.0, 88.8, and 94.2% due to viscous effects, respectively, for SC1, SC2, SC3, and SC4 membranes. In this study, with decrease of porosity from ~48 to 38 vol% the membrane resistance increased from 2.86×10^{10} to 8.75×10^{10} m^{-1}. Zirconia-based ultrafiltration membranes and polyvinylpyrrolidone (PVP) modified zirconia-based ultrafiltration membranes for separation of oil water emulsions demonstrated membrane resistance (R_m) of 2.6×10^{12}-5.3×10^{12} m^{-1} by *Faibish et al.* [48]. The membrane resistance of this ceramic membrane with a pore diameter of 1.5 µm was 9.8×10^{10} m^{-1} for the purification of wastewater of dye industry [24]. The above literature review indicates that depending on the

type of membrane characteristics the membrane resistance and specific permeability results varied.

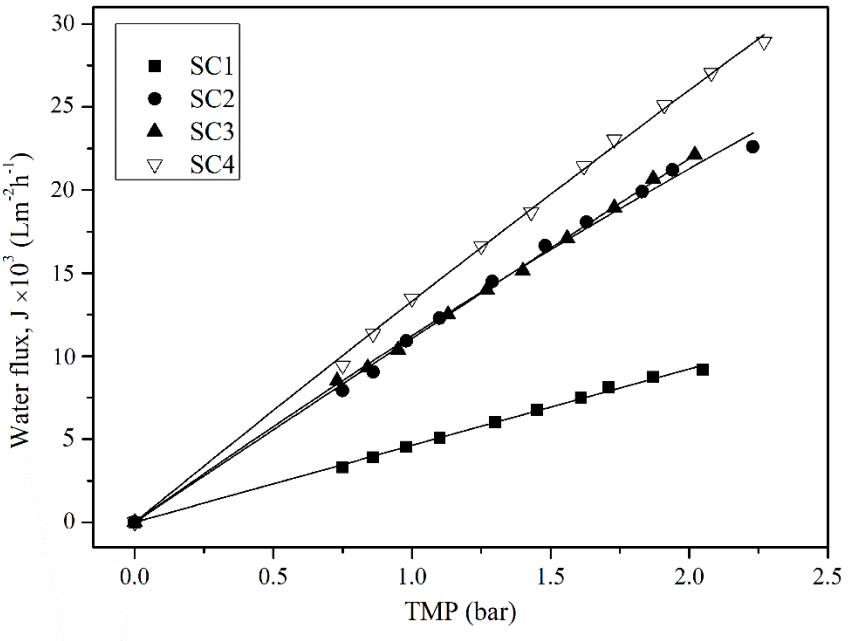

Figure 5.2.8. Experimental water permeation curves for SiC membranes prepared with different pore formers.

5.2.7. Wastewater filtration studies

In order to evaluate the effectiveness of the porous SiC membranes for filtering kitchen wastewater, the COD, TSS and oil concentrations of the permeate water were measured, and the results are summarized in Table 5.2.6. The as prepared SiC membranes showed oil rejection rates of 89-94% with a feed concentration of 1557 mg/L and a flux of 82-125 $Lm^{-2}h^{-1}$ at 1 bar. Based on the filtration tests, SiC membranes were found to remove ~ 85 to 90% of COD and 89 to 94% of turbidity from kitchen wastewater. The samples prepared without pore former showed the best results in terms of COD, oil removal efficiency from wastewater. The permeability of the membrane increased with increased porosity. Moreover, the results indicate that all the pore formers provide almost equivalent performance in terms of wastewater filtration. After cleaning with n-hexane followed by acid, alkali cleaning, the performance of the used membrane remained almost the same. This result suggested that ceramic membranes used for oily-wastewater filtration can be reused and recycled.

Table 5.2.6. Characterization of wastewater before and after filtration by the ceramic membranes.

Parameters	Values for wastewater	Values for permeate water after filtration using porous SiC membranes of varying porosity			
		SC1	SC2	SC3	SC4
Oil (mg/L) (% removal)	1557	110 (92.9)	162 (89.6)	160 (90.3)	151 (89.7)
TDS (mg/L)	941	663	701	721	719
TSS (mg/L)	1025	107	148	128	169
COD, mg/L (% removal)	1220	118 (90.3)	138 (88.7)	177 (85.5)	152 (87.5)
Turbidity, NTU (% removal)	123	7.03 (94.3)	10.9 (91.2)	8.82 (92.8)	13.2 (89.3)

Figure 5.2.9 presented the clearity of the permeate water after filtration through porous SiC membranes. The permeability, TDS, COD and oil rejection results of the membrane prepared in this present work are comparable to the reported membrane prepared from α-Al_2O_3, clay, mullite, etc. [49-52]. Compared to the conventional standard water treatment methods like flotation coagulation, biological water treatment, advanced oxidation processes [53], etc., the results of the present study indicated that similar quality water is possible to achieve by single step SiC based membrane filtration process.

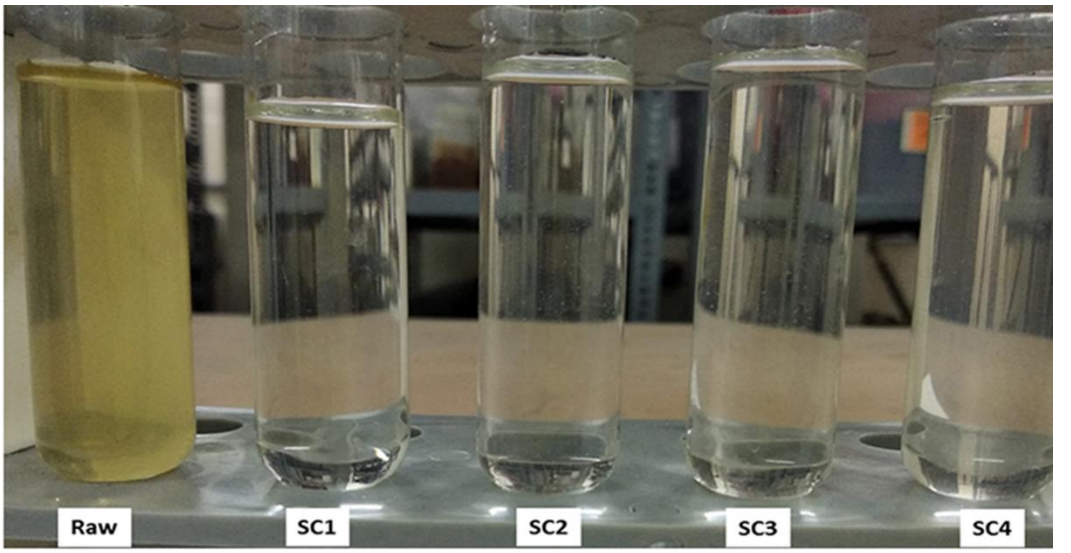

Figure 5.2.9. Photographs of the permeate water after filtration through porous SiC membranes.

5.2.8. Turbidity removal studies from kaolinite water

A study was conducted to determine the turbidity removal efficiencies of membranes prepared using different pore formers, from synthesized kaolinite water. The entire feed flow is forced perpendicularly through the membrane, and retained matter accumulates as a fouling layer (or cake) on the membrane's surface, while the permeate (or filtrate) is collected in the filter chamber as it passes through the membrane. In Figure 5.2.10, the picture of the membranes that have been tested based on filtration are shown. The cake's thickness therefore increased as it aged, and its permeation rate is correspondingly slowed. In Figure 5.2.11, plots of water flux (J) as a function of time are provided for all samples.

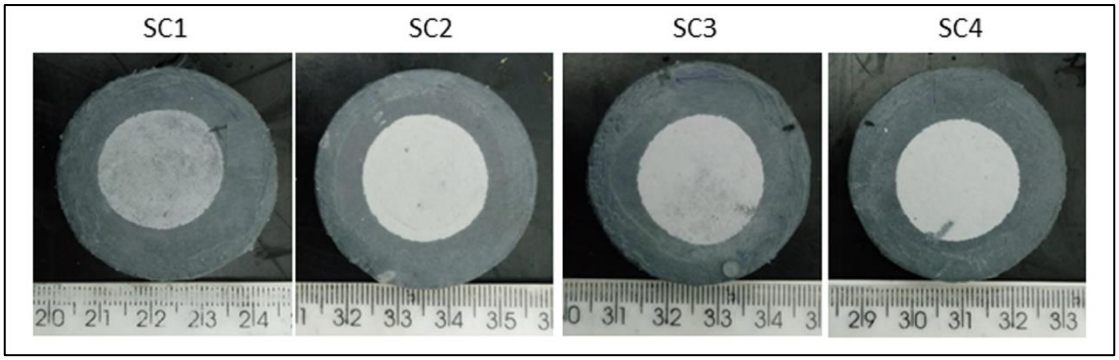

Figure 5.2.10. Photographs of different membranes after 300s of turbid water filtration.

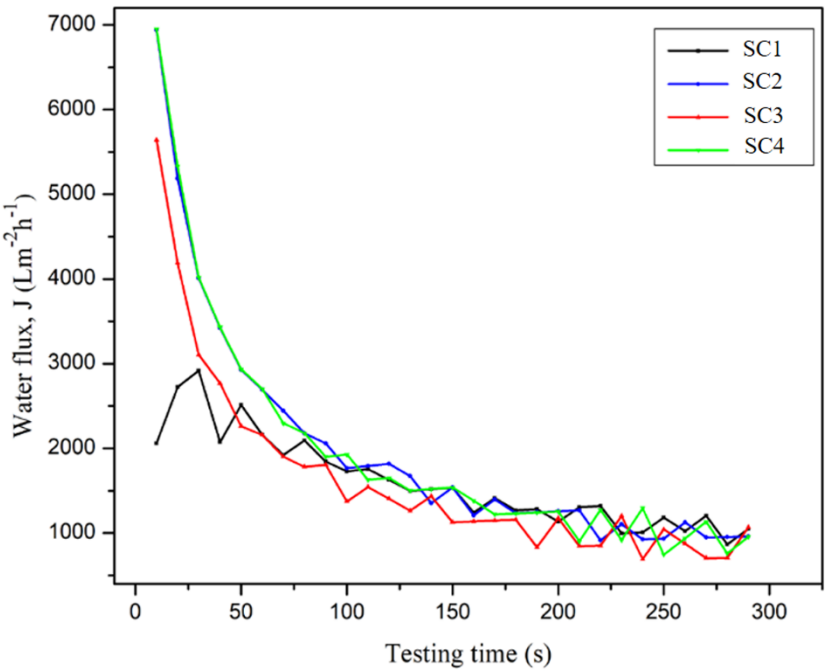

Figure 5.2.11. Variation of turbid water flux as a function of filtration time for porous SiC membranes.

Following 150 seconds of filtration, the flux for SC1, SC2, SC3 and SC4 membranes was reduced to 47.34, 77.88, 80.01 and 77.87%, respectively. Figure 5.2.12 shows the turbidity level of water before and after filtration (t=300 s) for all membranes. All ceramic membranes used in this study were found to remove more than 99% of turbidity under the same conditions. In case of turbidity removal, the small variation was due to the variation in green formulation, pore former and processing temperature, which resulted in variations in microstructure, porosity, and pore diameter of the final ceramics. In an experiment by *Hofs et al.*, using commercial ceramic tubes with pores of more than 0.2 µm and porosity > 70%, the tubes removed more than 95 % of turbidity from water containing 9.7 NTU [55]. *Park et al.* reported that the hollow ZrO_2-TiO_2 based tubes with pores larger than 0.2 µm removed 99% turbidity from water containing turbidity of 60 NTU [56]. A study using microfiltration of textile effluent water containing an initial turbidity of 167 NTU at 0.12 bar operating pressure demonstrated a reduction in turbidity removal efficiency from 96 to 80% after 60 minutes of filtration with a rise in porosity from 30.8 to 48.2% after microfiltration [57].

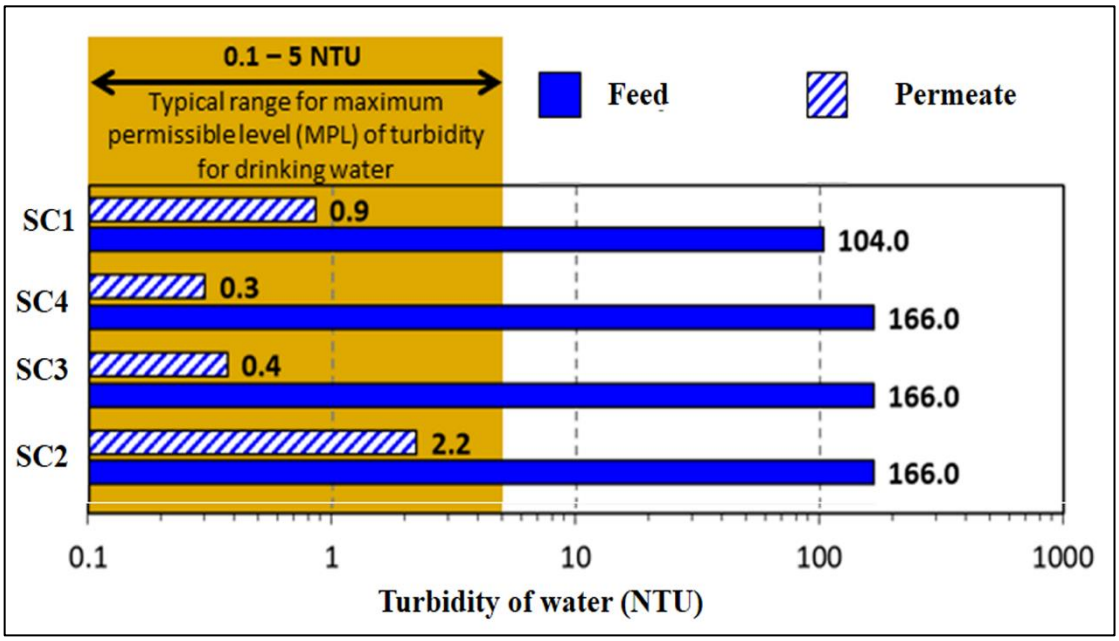

Figure 5.2.12. Turbidity level for all membranes before and after 300s of filtration.

Table 5.2.7 summarizes the percentage variations in turbidity removal after 300 seconds of filtration and flow reduction (FR%) due to fouling with varying membrane types. We can see that flow reduction increases as the membrane porosity and pore size increases. Increases in porosity from 38 to 50% result in an increase in FR from 19.2 to 67.5% for the as prepared

membrane. A decrease in flow is primarily due to two factors, the first being pore blockage and the second being concentration polarization. During microfiltration of turbid water, membranes with high porosity and pores experience increased pore blocking at the beginning of the process compared to the membranes with lower porosity and pore size, causing greater flux decline, and as microfiltration proceeds, more concentration polarization occurs. As microfiltration proceeds, pore blocking phenomenon becomes less significant and flux reduction will occur due to concentration polarization. However, this type of fouling is reversible in nature. Reports have shown that ceramic membranes can be cleaned easily by backwashing with water. They can also be reused for another filtration purpose [57]. According to *Vasanth et al.,* clay membranes with porosity 30 vol% and pore sizes 1.30 µm showed 83.2% flux decline during oil-water filtration, while membranes with porosity 23 vol% and pore sizes 0.45 µm witnessed 52.2% flux decline [58]. *Rajanna et al.* reported that the most significant flux decline ~83.8% was achieved after 24h filtration of industrial waste water using SiC ceramic membranes with pore sizes of 1.5 µm [59]. Furthermore, they reported a significant increase in the flux value recovery after simple backwashing, and the membrane could be reused. An above-average flux reduction of 95% was obtained using commercial ZrO_2-TiO_2 (Sterlitech Co., WA, USA) based ceramic membranes with average pore sizes of 0.20 µm during microfiltration of synthetic high turbid water with a turbidity of 60 NTU after 36 minutes of filtration [55]. A reduction in flux was attributed to fouling from particles present in the turbid water that caused cake to form during microfiltration.

Table 5.2.7. Performance parameters of prepared SiC membranes for turbidity removal

Sample	Porosity (vol %)	Turbidity removal (%)	Flow reduction after 300s (%)	Specific permeability for turbid water ($Lm^{-2}h^{-1}bar^{-1}$)
SC1	38.2	99.2	19.2	3422
SC2	48.5	98.7	61.1	8264
SC3	49.9	99.8	67.5	6617
SC4	48.0	99.8	62.1	8255

The excellent permeability and turbidity removal efficiency results of the porous SiC membrane prepared in this study will be helpful for the design low cost ceramic filter for water treatment.

Chapter 5.3

5.3. Properties of multiple oxide- bonded porous SiC ceramics prepared by an infiltration technique

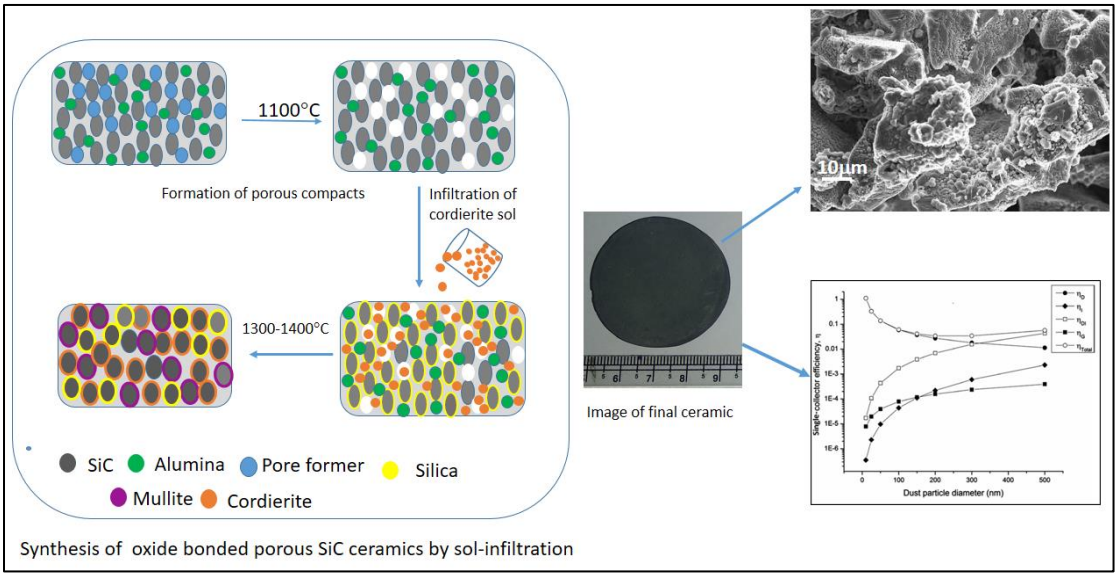

Synthesis of oxide bonded porous SiC ceramics by sol-infiltration

In this study efforts are made to fabricate porous SiC ceramics by infiltration bond phase precursor technique assuming to achieve homogenous distribution of bond phase, which is not obtained by powder processing method due to the agglomeration of fine sintering additives. In this chapter, multiple oxide- bonded porous SiC ceramics were fabricated by infiltrating a porous powder compact of SiC and alumina with cordierite sol followed by sintering at 1300- 1400°C in air for 3h. The microstructures, phase components, mechanical properties, and air permeation behaviour of the developed porous ceramics were examined and compared with materials obtained by the traditional powder processing route. The porosity, average pore diameter, and flexural strength of the ceramics varied from 33 to 37 vol%, ~12- 14 µm and ~23- 39.6 MPa, respectively, with variation in sintering temperature. To determine the suitability of the material in particulate filtration application, particle collection efficiency of the filter material was evaluated theoretically using single collector efficiency model.

Publications

1. D. Das, S. Baitalik, N. Kayal, Int. J. App. Ceram. Tech., 17 (2020) 476-483.

5.3.1. Characteristics of cordierite sol

Figure 5.3.1 showed particles sizes distribution result of prepared cordierite sol. Wide size of distribution was observed due to sol agglomeration of the sol particles. The sol exhibited trimodal size distribution with average particle diameters of 4.2, 17.6 and 190 nm. The sol viscosity was 14.2 mPa.s at 100 s^{-1} shear rate and the sol showed shear thinning nature as shown in Figure 5.3.2, indicated suitability of the sol for infiltration purpose according to proposed expression by *Martins et al.* [60].

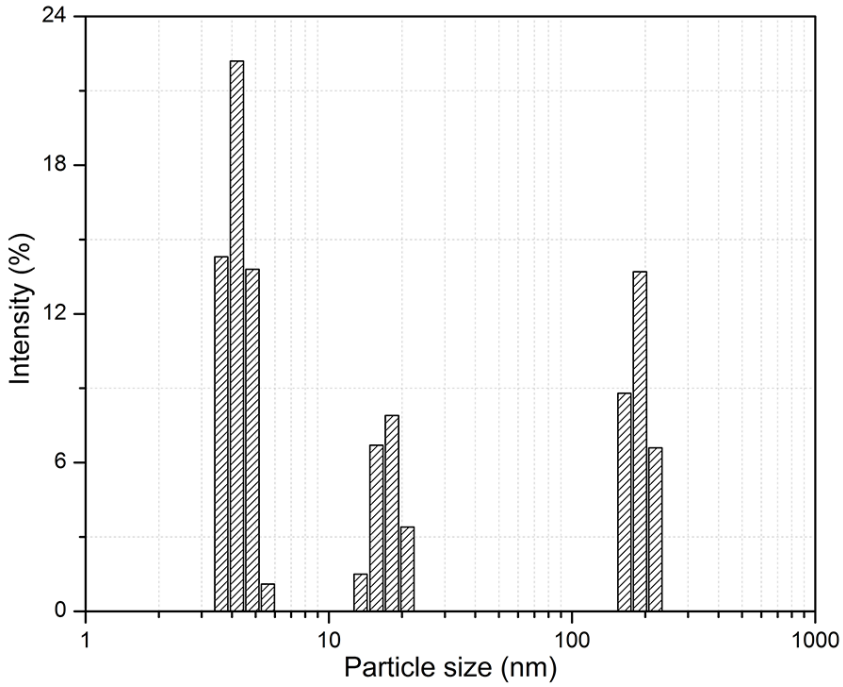

Figure 5.3.1. Particle size distribution of cordierite sol

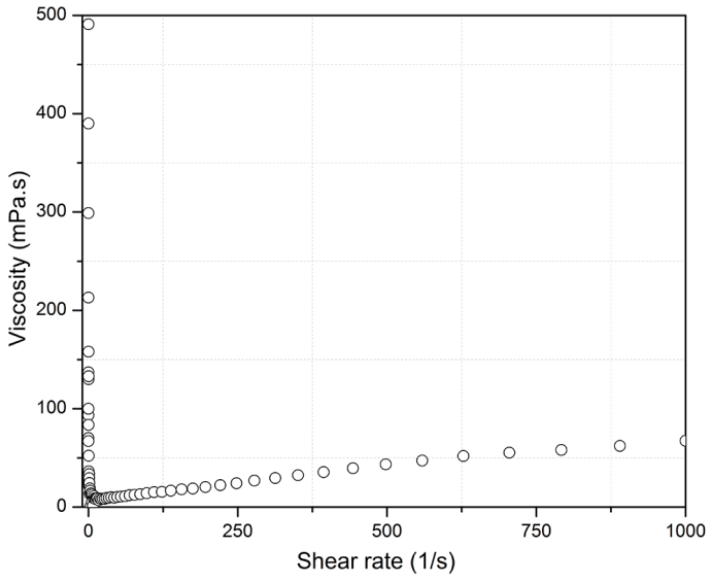

Figure 5.3.2. Viscosity *vs* shear rate changes of cordierite sol.

The pH of sol was found to be ~1 indicated highly acidic in nature. The result of TG-DTA analysis of cordierite gel as presented in Figure 5.3.3. About 16 % weight loss below 200°C was obtained within the endothermic peak region due to dehydration. The exothermic peak at ~390°C was corresponding to ~43% of weight loss which was responsible for oxidation of residual organic group followed by release of weakly bonded organic groups. Rapid weight loss was obtained up to ~400°C after that a slow reduction of weight was noticed which was found to be constant after 700°C. TG-DTA analysis of cordierite gel phase was reported [61] with an exotherm at ~967°C for µ-cordierite crystallization from its amorphous state. *El-Buaishi et al.* reported about cordierite crystallization reaction from its gel state which was prepared by nitrate precursors [62]. The crystallization occurred in several metastable phases of $MgO\text{-}SiO_2\text{-}Al_2O_3$ system by simultaneous heat release and absorptions with two exothermic peaks at 987 and 1305°C which were reported to be responsible for formation of µ-cordierite from spinel and cristobalite and for phase transformation of cordierite respectively. Three endothermic peaks at 850, 1225 and 1350°C were reported for gel to viscous liquid, structural changes to α-cordierite phase and liquid phase formation respectively [62]. In the present analysis, an exothermic peak appeared at around 973°C at constant mass retention region of TG analysis indicated crystallization of low temperature cordierite phase (µ-cordierite) from spinel and cristobalite phases. Structural changes of µ-cordierite phase to α-cordierite occurred at endothermic peak of 1231°C and liquid phase formation took place at 1350°C.

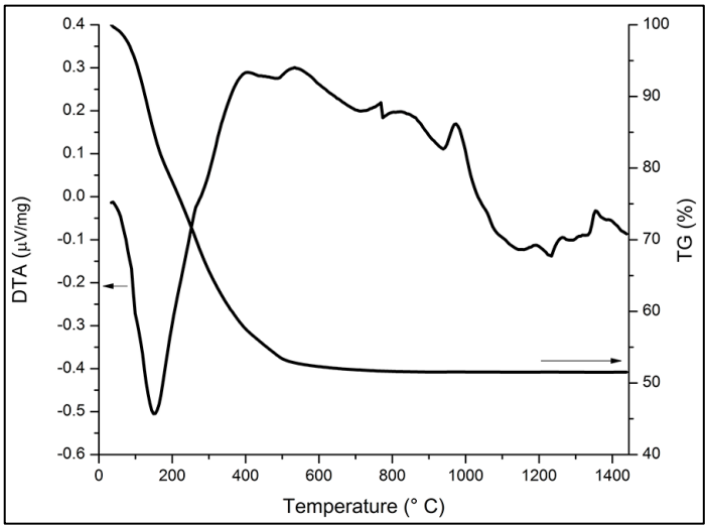

Figure 5.3.3. TG-DTA pattern of cordierite gel during heat treatment in air up to 1450°C

Figure 5.3.4 presented the XRD pattern of cordierite powder obtained after sintering at 1400°C for 2h. Phase of pure hexagonal α-cordierite crystalline state was obtained with space group of P6/mc (JCPDS: 84-1220) and crystalline parameters a=9.776Å, b=9.776Å, c=9.3448Å; α=β=90°, γ=120° and GOF (Goodness of Fit) value= 0.9.

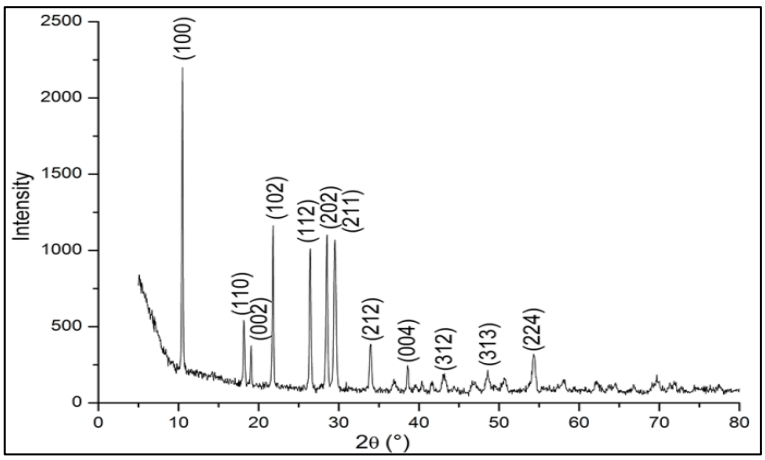

Figure 5.3.4. XRD pattern of cordierite powders obtained at 1400°C

5.3.2. Cordierite sol infiltration

Cordierite sol was infiltrated into powder compacts of SiC (d_{50}=22.4 µm) and Al_2O_3 heat treated at 1100°C/4h. Infiltration weight gain was observed with respect to time to measure the infiltration kinetics of cordierite sol into porous SiC compacts. A single pass of sol infiltration was not enough to achieve maximum sol infiltration, therefore multiple passes were used according to literature study [63]. But a new method for maximum sol infiltration was developed by establishing a single infiltration step followed by a complete evacuation of air from the sample by maintaining the sample at optimum vacuum pressure of 3 mm Hg in this work. As a result, the infiltration process in one step reduces the processing cost and time. The weight gain with single infiltration cycle is ~25%. There was no significant increase of weight after 2nd infiltration, indicated achievement of saturation level for bar samples by single infiltration cycle.

5.3.3. Structural and physical characterization of porous ceramics

After sintering of cordierite sol infiltrated porous SiC compacts at 1300-1400°C, weight gain was found due to formation of oxidation reaction derived silica, mullite and sol-gel derived cordierite in both glass and crystalline state as secondary oxide bonding phases in the final ceramics. These ceramics were shown to increase in length, width, and thickness by ~1% by

this method, which suggested that net shape and near-net dimension processing of porous ceramics were possible. The porosity, average pore diameter, and flexural strength of the ceramics varied from 37 to 33 vol%, ~14- 12 μm and ~23- 39.6 MPa, respectively, with variation in sintering temperature from 1300 to 1400°C. The pore size distribution patterns of the porous ceramics are shown in Figure 5.3.5. The final SiC ceramic specimens exhibited mono-modal pore size distribution patterns with average pore diameters of 14.5 and 11.9 μm sintered at 1300°C and 1400°C respectively. In general, the porosity of ceramics and the size of their pores are closely related to the packing arrangement of powders in a compact, so the pore diameter of these porous SiC ceramics is strongly influenced by the size of the raw materials, which are SiC, carbon, and alumina. The slight decrease in pore size with increased sintering temperature could be attributed to the change in glass and crystalline phases.

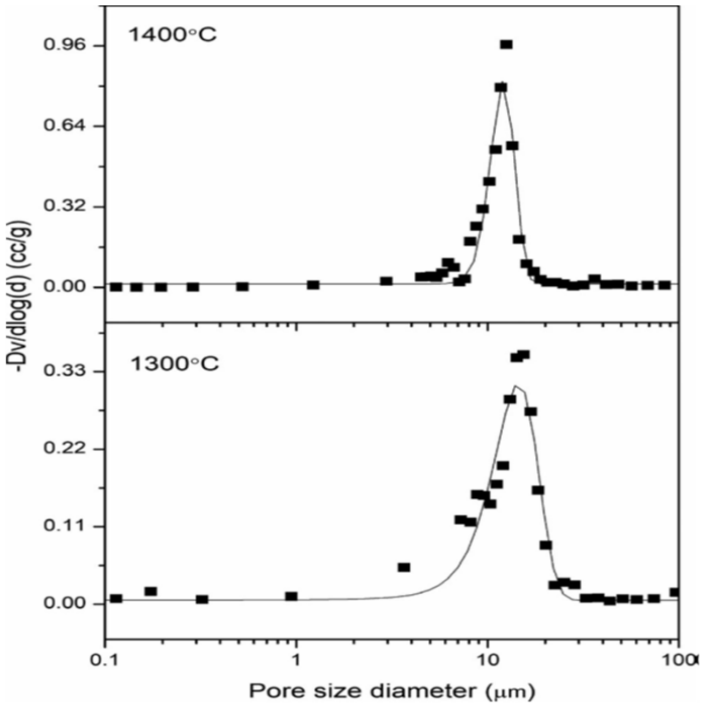

Figure 5.3.5. The pore size distribution patterns of SiC ceramics sintered in different temperatures with multiple oxide bonds.

5.3.4. XRD analysis

Figure 5.3.6 showed the characteristic XRD peaks of ceramics prepared at 1300-1400°C. The sintered ceramics developed with silicon carbide in hexagonal (SiC; 6H, JCPDS 29-1128), cristobalite in tetragonal (SiO_2; JCPDS 01-077-1317), alumina in hexagonal (Al_2O_3, JCPDS 081- 2267), mullite in orthorhombic ($3Al_2O_3.2SiO_2$, JCPDS 079- 1487) and α-cordierite in

hexagonal ($5SiO_2.2MgO.2Al_2O_3$; JCPDS 01-089- 1487) crystalline states. Quantitative analysis of crystalline phases was done using Rietveld analysis with XRD results is given in Table 5.3.1. The ceramics sintered at 1400°C obtained with higher amount of α-cordierite and cristobalite phases compared to the ceramics synthesised at 1300°C. The rearrangement of cordierite phase from glass to crystalline occurs near to its melting point (~1450°C) [64]; as a result the ceramics sintered at 1400°C produced more crystalline cordierite phases from 6 to 13 wt%. From the weight gain data, oxidation degree of SiC increased from 9.7% to 14.2% as the sintering temperature increased from 1300°C to 1400°C. With increase in temperature, mullite formation was accelerated, resulted an increase in the amount of mullite from 9.8 to 14.7 wt%. In conventional powder processing method, mullitization reaction starts at 1400°C due to reaction between alumina and silica and obvious peaks of mullite do not appear in the XRD until 1450°C [65]. However, in the present study, the temperature of mullite formation was reduced by nearly 100°C by incorporating amorphous Al- Mg- Si- O networks of cordierite generated from infiltrated sol.

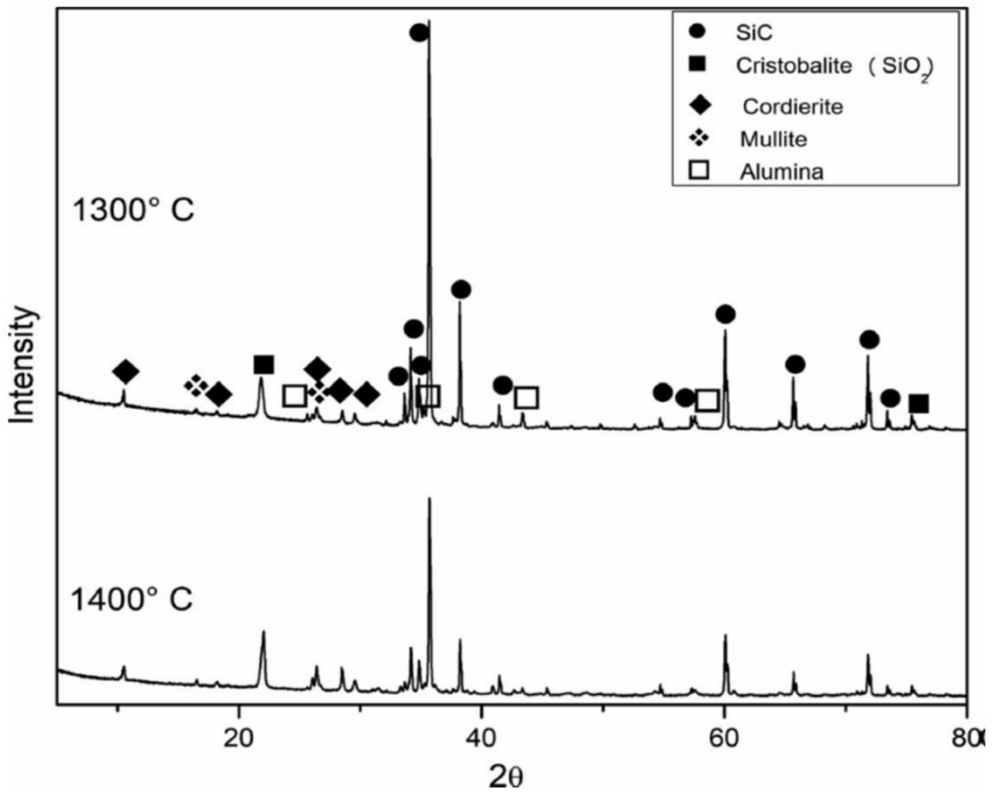

Figure 5.3.6. XRD pattern of multiple oxide bonded SiC ceramics sintered at various temperature.

Table 5.3.1. Rietveld phase analysis of multiple oxide bonded porous SiC ceramics sintered at 1300-1400°C

Sintering temp^{r} (°C)	Crystalline phases (%)					GOF
	SiC	SiO_2	alumina	mullite	cordierite	
1300	64.7	11.3	8.1	9.8	6.1	2.12
1400	51.5	14.3	6.5	14.7	13.0	2.03

5.3.5. SEM analysis

Figure 5.3.7 showed microstructures of porous SiC ceramics prepared at 1400°C. With increase of sintering temperatures, well developed necks were formed between SiC particles by sol-gel derived cordierite, oxidation reaction derived silica phases and reaction bonded mullite phases as evidenced in both SEM and XRD. The micrograph at high magnification also showed (Figure 5.3.7 (R)) various morphologies of different phases with spherical, rod, and plate- like morphologies indicated different phase transformation during sintering. Further EDS analysis showed (Figure 5.3.15) variation signals of Mg, Al, Si and O elements at various points and spherical (area "a"), rod- shaped (area "b") and plate like structures (area "c") morphologies were identified for cordierite, silica, and mullite, respectively.

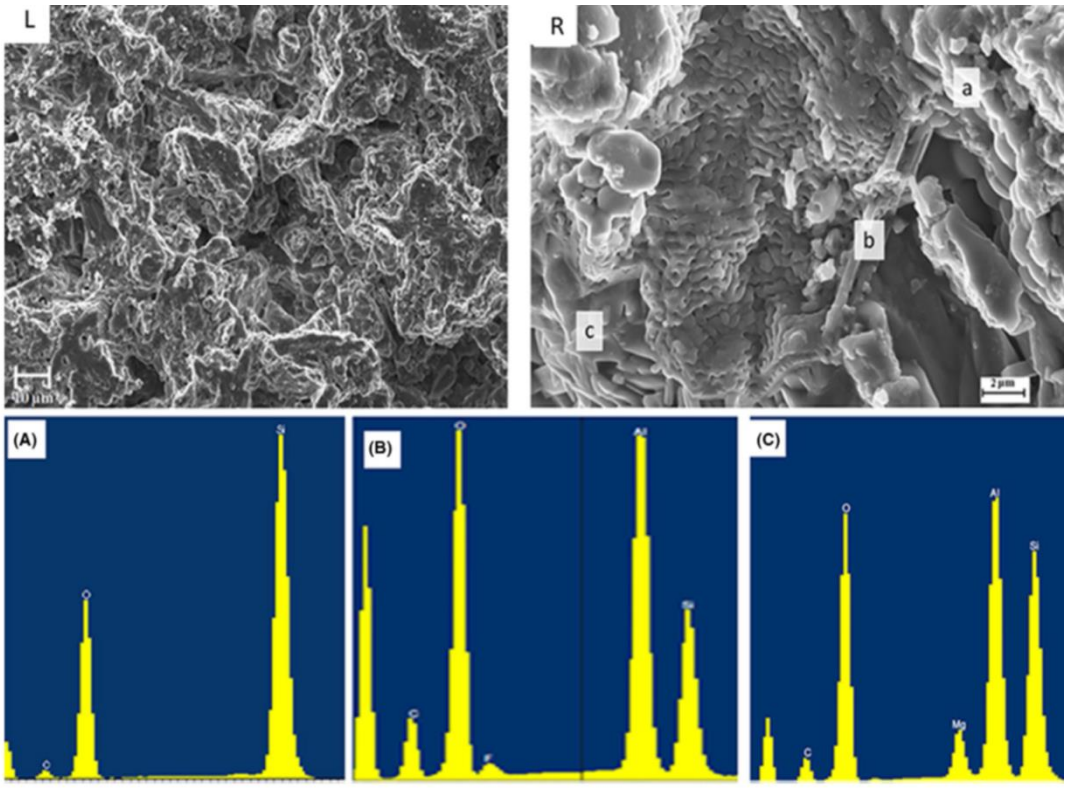

Figure 5.3.7. Microstructural view of multiple oxide bonded porous SiC ceramics sintered at 1400°C showing porous network at lower magnification (L) and various morphologies at different areas at high magnification (R) and their EDX analysis results.

5.3.6. Flexural strength analysis

The flexural strength values of porous SiC ceramics were increased with increase of sintering temperature. The SiC ceramics sintered at 1300°C and 1400°C exhibited flexural strength of 23.08 ± 0.42 MPa at a porosity 37 vol% and 39.63 ± 1.27 MPa at a porosity 33 vol%, respectively. Liquid phase formation and re-crystallisation of cordierite phase increased with increase of sintering temperature which was also evident in DTA result of cordierite gel with a sharp exotherm at 1350°C [62]. The diffusion of oxygen [66] through grain boundaries of SiC particles was enhanced by liquid phase formation during sintering, as a result, more crystalline phases of cordierite, mullite and cristobalite were formed with reduction of porosity which enhanced the mechanical strength of ceramics sintered at 1400°C. The formation of mullite due to alumina addition may explain the improvement in strength seen in the Young's modulus of SiC (450 GPa), mullite (150 GPa), cordierite (70 GPa), cristobalite (72 GPa), and glassy phase (72 GPa) [67-71].

According to the proposed minimum solid area (MSA) based model by *Rice* [72] for porous solid materials, the variations of mechanical properties with porosities of present system was explained with the help of exponential relationship between porosity and mechanical strength as:

$$\sigma = \sigma_0 \exp(-bp) \qquad (1)$$

Where, σ is flexural strength of porous ceramics, σ_0 is strength of ceramics with zero porosity, P is porosity of porous SiC ceramics and b is empirical constant depends on SiC particle stacking nature or pore structure. Depending on the type and size of the pore former, porosity of the final ceramics varied and accordingly flexural strength also varied. Based on equation-1, the strength-porosity relationship yields σ_0=195.04 MPa and b=5.05 corresponding to a cubic stack of SiC particles which was shown in Figure 5.3.8. According to the study by *Liu et al.*, the variations in flexural strength for cordierite bonded porous SiC ceramics were ~70-3 MPa for a variation in porosity of ~28-66 vol% with σ_0=501 MPa and b=6.97 [73]. For SiO_2 bonded porous SiC ceramic materials, *She et al.* reported b= 6.5 to 7.1 with porosity varying between 28 to 41 vol% for mullite-bonded porous SiC ceramics [74] and also obtained b=4.4 with porosity 28-44 vol% where graphite was used as pore former [10]. *Chun et al.* reported b=7.95 for silica bonded porous SiC ceramics where pore former was polymicrobead [75]. The cordierite bonded porous SiC ceramics prepared by conventional

powder mixing method showed σ_0=132 MPa and b=3.1 [66]. *Bai et al.* reported b=8.16 and σ_0=1237.04 MPa for cordierite-mullite bonded porous SiC ceramics [76]. Cordierite-mullite bonded porous SiC ceramics reported with b=8.16 and σ_0 =1237.04 MPa [77]. Literature data has indicated that the processing conditions have a great impact on b and σ_0 values of final porous SiC ceramics. In the present work, the evaluated values of b and σ_0 using equation-1 showed in good agreement with available literature values.

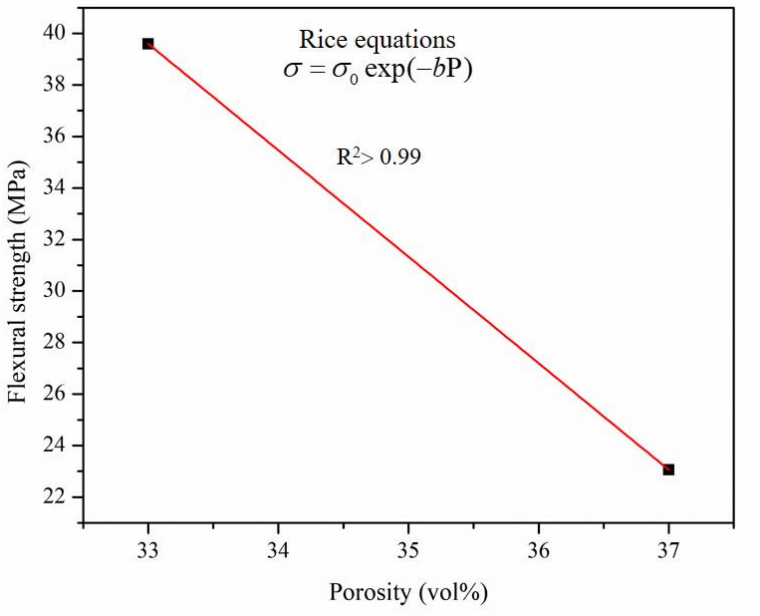

Figure 5.3.8. Flexural strength as a function of open porosity for the as prepared SiC ceramics sintered at various temperature.

Therefore, for the present study, it can be concluded that sintering temperature played important role to enhance flexural strength of final porous SiC ceramics. Though the amount of infiltrated sol was same in SiC powder compacts, but, the amount of cordierite in the final ceramics as crystalline phase was found to be increased with increase of sintering temperatures via a transformation of Al-Mg-Si-O glass to cordierite crystalline phase that resulted in neck growth between SiC particles and hence flexural strength was increased.

5.3.7. Permeability coefficients and pore related characteristics of porous SiC ceramics

It is known that Forchheimer's model best describes the air permeation characteristics of porous SiC ceramics at room temperature, which governs the nonlinear dependence of pressure drop on fluid velocity through a macroscopically homogeneous medium. The Figure 5.3.9 shows the variation of the normalized pressure drop ($\Delta P/L$) as a function of superficial

air velocity (v_s) for multiple oxide- bonded porous SiC ceramics. At any given porosity, the normalized pressure drop for ceramics increased with superficial fluid velocity, and this pressure drop further increased with the drop in porosity from 37 to 33 vol%. Forchheimer's equation was fitted to the experimental results using the list square method as described earlier [78]. Using the fitting constant of curves in Figure 5.3.9, the permeability coefficients k_1 and k_2 were evaluated. The as prepared porous SiC membrane sintered at 1400°C showed the permeability coefficients k_1 and k_2 values 1.3×10^{-13} m^2 and 0.34×10^{-8} m respectively, while the membrane sintered at 1300°C showed 4.09×10^{-13} m^2 and 0.71×10^{-8} m, respectively. The increase in sintering temperature resulted in more tortuous flow paths since more holes and pores were reduced, which enhanced inertia interaction between the flowing gas and pores, and reduced permeability coefficient values. *Liu et al.* reported room temperature k_1 values of 0.71 and 0.88×10^{-13} m^2, respectively, at 39 and 53% porosity for the cordierite bonded porous SiC ceramics [79]. Thus, the Darcian permeability coefficient values of the porous SiC ceramics investigated in the present work are improved in comparison with previously published results although very few information regarding permeability coefficient data for porous ceramic membrane are available in literature. To determine the suitability of the material as hot gas filter, pressure drop is considered as most important parameter. A pressure drop of 52990 and 15010 Pa was found for as prepared SiC membrane with flow velocity v_s = 0.05 m s^{-1} at porosity levels of ε = ~33% and ~37%, which is comparable to the value reported in literature for oxide-bonded porous SiC ceramics [8, 35, 78]. The pressure drop for cordierite bonded porous SiC ceramics prepared by powder processing method was reported to drop significantly from 22660 Pa to 5400 Pa with increase of porosity from 40% to 56% at a fluid velocity of 0.05 m/s^{-1} [78]. This pressure drop also further reduced to 550 Pa with increase of porosity to 74% under comparable conditions.

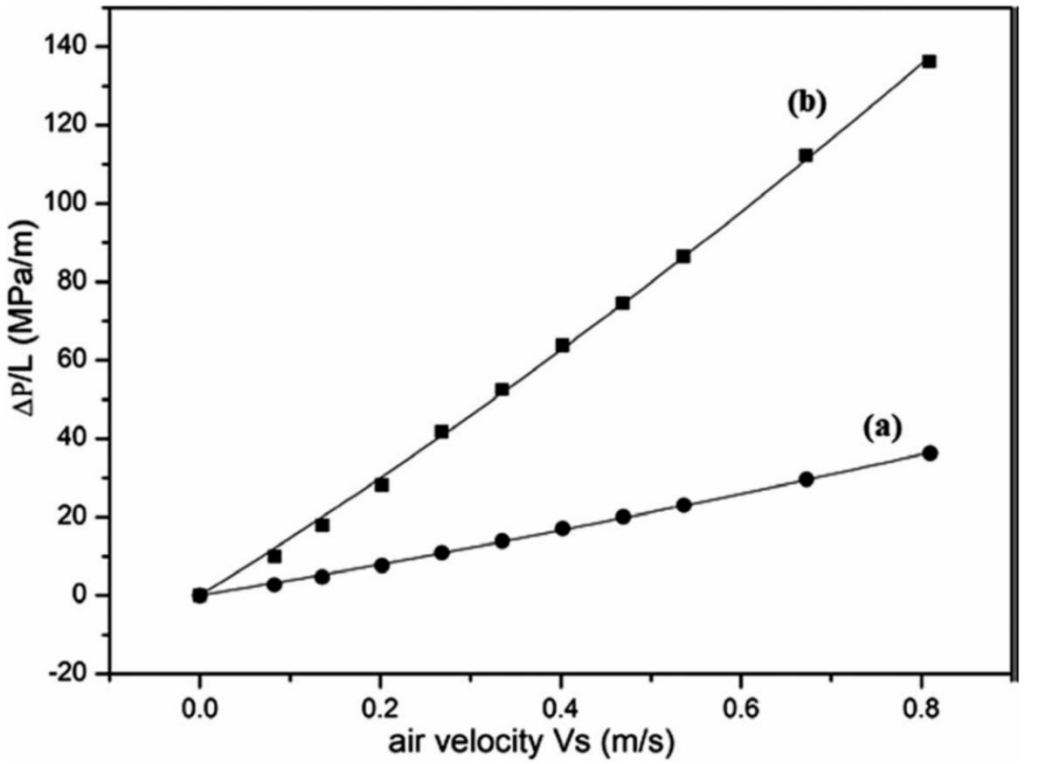

Figure 5.3.9. Permeation curves for multiple oxide bonded porous SiC ceramics prepared at (a) 1300°C and (b) 1400°C.

5.3.8. Filtration performance

The mechanisms by which particles are arrested by filter media are well-documented in the published literature. The expressions were derived in the literature on the basis of semi empirical correlations, considering the process of filtration to be time-independent–a condition valid for the first stage of a filtration process when no dust cake is present in the filter. In the present work, the fractional collection efficiency of a filter in the first filtration stages was calculated using the single-collector efficiency model derived for granular filters [80-83]. The relationship between total collection efficiency (E) and total single collector efficiency (η_{Total}) can be summarized as follows:

$$E = 1 - \exp\left[-\frac{\alpha K L(1-\varepsilon)\eta_{Total}}{d_c}\right] \qquad (2)$$

where L, ε, and d_c represent the thickness of the filter, porosity, and average collector diameter, respectively. The parameter "a" is fitting constant considered here as unity and K was proposed by *Yoshida* and *Tien* [83] in Equation (2):

$$K = \left[\frac{6}{(1-\varepsilon)^{2/3}}\right]^{1/3} \quad (3)$$

According to the model, the total collection efficiency of a single collector (η_T) is the combination of the individual contributions due to different collection mechanisms, diffusion (η_D), inertia (η_I), direct interception (η_{DI}), gravity (η_G), and electrophoresis (η_E). The single collector combined efficiency (η_T) is given by:

$$\eta_T = 1 - (1-\eta_D)(1-\eta_{DI})(1-\eta_I)(1-\eta_G)(1-\eta_E) \quad (4)$$

The diffusional collection arises from the random movement of suspended small particles in a gas, known as Brownian diffusion and the single-collector diffusional efficiency is given by

$$\eta_D = 4(1-\epsilon)^{2/3} {A_S}^{1/3} {N_{Pe}}^{-2/3} \quad (5)$$

where the *Happel's* parameter (A_S) is given by

$$A_S = \frac{2(1-(1-\epsilon)^{5/3})}{2-3(1-\epsilon)^{1/3}+(1-\epsilon)^{5/3}-(1-\epsilon)^2} \quad (6)$$

The Peclet number (N_{Pe}) and the diffusion coefficient (D) are given by

$$N_{Pe} = \frac{v_s d_{pi}}{D} \quad (7)$$

$$D = \frac{k_B T F_S}{3\pi\mu d_{pi}} \quad (8)$$

where d_{pi} is the nanoparticle dust size, k_B is the Boltzmann constant, T is the absolute temperature, μ is the air viscosity, and F_S is the slip correction factor which is given by *Allen* and *Raabe* as

$$F_S = 1 + \frac{\lambda}{d_{pi}}\left[2.34 + 1.05\exp\left(-0.39\frac{d_{pi}}{\lambda}\right)\right] \quad (9)$$

where λ is the mean free path of air. The single-collector inertia efficiency is given by

$$\eta_I = 0.2589 N_{St,eff} N_R \quad (10)$$

The interception parameter (N_R) and the effective Stokes number ($N_{St,eff}$) are

$$N_R = \frac{d_{pi}}{d_c} \quad (11)$$

$$N_{St,eff} = [A_S + 1.14 N_{Re} \varepsilon^{-1.5}] \frac{N_{St}}{2} \quad (12)$$

The Reynolds number (N_{Re}) and the Stokes' number (N_{St}) are given by

$$N_{Re} = \frac{\rho v_s d_c}{\mu} \quad (13)$$

$$N_{St} = \frac{\rho_p v_s F {d_{pi}}^2}{9 \mu d_c} \quad (14)$$

The expression for estimation of the collection efficiency due to direct interception is given by

$$\eta_{DI} = 6.3 \epsilon^{-2.4} {N_R}^2 \quad (15)$$

The collection efficiency due to gravitational effects is given by,

$$\eta_G = 3.75 \times 10^{-2} (\frac{v_t}{v_s})^{0.5} \quad (16)$$

where the terminal settling velocity (v_t) of the dust particle is obtained within the Stokes free-fall regime (N_{Re} <1) and g is the acceleration due to gravity

$$v_t = \frac{\rho_p g {d_p}^2}{18 \mu} \quad (17)$$

Based on dust particle size, Figure 5.3.10 shows the collection efficiencies associated with individual collection mechanisms. Dust particles with sizes smaller than 400 nm are dominated by diffusion, and dust particles larger than 400 nm are dominated by the direct interception mechanism. The efficiency of dust collection due to diffusion decreases with increasing particle size, but the efficiency of the other three mechanisms increases. *Choi et al.* also found that diffusion was the dominant collection mechanism for particles smaller than 0.7 µm, and that direct interception and inertial forces increased dramatically as particle sizes increased [8].

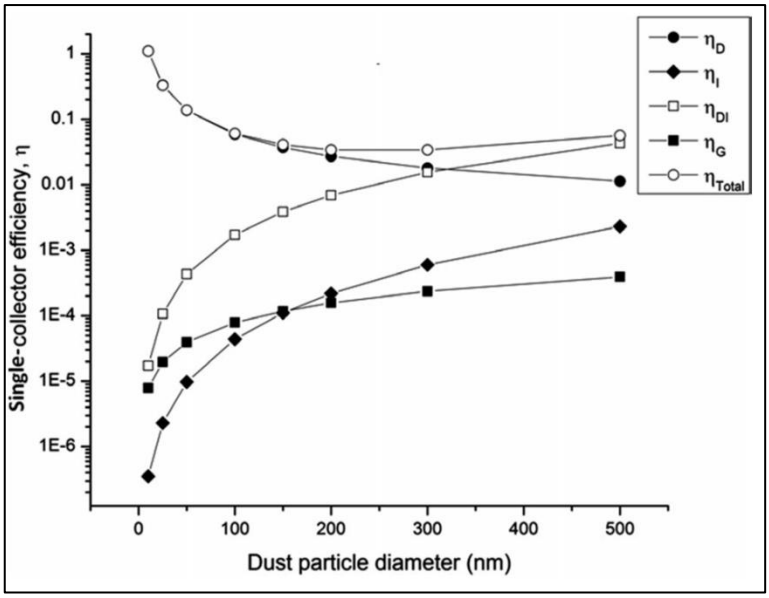

Figure 5.3.10. Effect of individual collection mechanisms on collection efficiencies with dust particle sizes for the porous SiC ceramics prepared at 1400°C.

The fractional filter efficiency (E_{frac}) was estimated as a function of dust particle size (d_{pi}) at different porosity levels by the sets of equation (2-17) and using experimental conditions (mean free path of air at room temperature and atmospheric pressure: $\lambda = 7.56 \times 10^{-8}$ m; viscosity of air, $\mu = 1.86 \times 10^{-5}$ kg $m^{-1}s^{-1}$; density of air, $\rho = 1.08$ kg m^{-3}; and face velocity of aerosol, $v_s = 0.1$ ms^{-1}). In Figure 5.3.11, the fractional efficiency (E) was determined at 0.1 m/s face velocity as a function of dust particle size (dp) at various porosity levels by the sets of equations [8,78]. *Freitas et al.* evaluated the filtration efficiency of a double-layered alumina based foam filter and found that the inertial mechanism was dominant for aerosol particles below 2 µm while in the range of 4- 8 µm, the bouncing/entrainment was predominating as detachment mechanism [84]. Based on the findings of the present study and previous studies, it can be concluded that the efficiency of filter media is highly dependent on the dust particle size and porosity of the filter media as well as the pore diameter and uniformity of the filter media. This study suggests that the ceramic filter made in this study can effectively filter fine dust particles based on theoretically predicted particle filtration results and experimental results of air permeability.

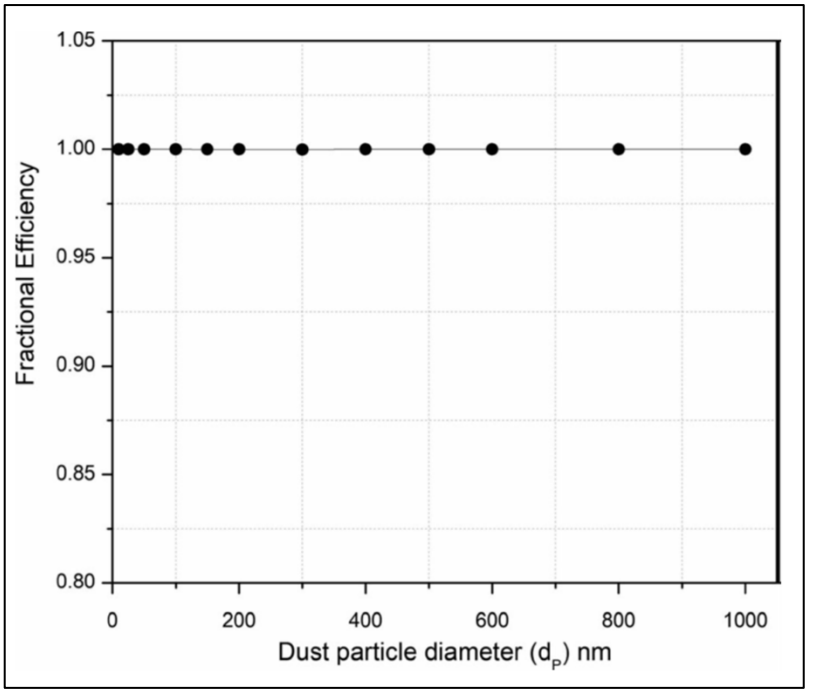

Figure 5.3.11. An estimate of the total single collector efficiency curve for porous SiC ceramics prepared at 1400°C.

These factors, along with their predicted overall particle filtration efficiency, permeability coefficients, and pressure drop values, suggest that these filters are highly effective in mitigating particulate emissions from industrial flue gases.

Chapter 5.4

5.4. The effect of sintering temperature and additives content on the chemical corrosion and thermal shock resistance properties of mullite bonded porous SiC ceramics.

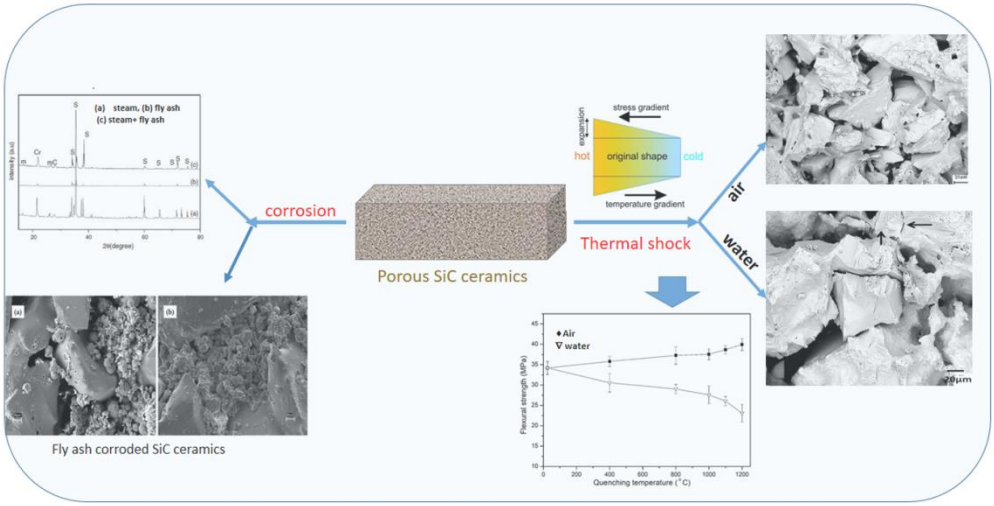

For hot gas filtration application, the stability of the filter in harsh environment condition need to evaluated to determine suitability of the filter materials. In this chapter, porous mullite bonded SiC ceramics prepared with various amount of alumina as bond phase additive and a mixture of clay based sintering aid by an in situ reaction bonding process. The effects of alumina additive, sintering temperature, and pore former addition on phase composition, microstructure and mechanical properties of the ceramics were studied. The corrosion behaviour of SiC ceramic filter materials in presence of steam, coal ash and both coal ash and steam was investigated at 1000°C for 96–240h. Thermal shock resistance of porous SiC ceramics due to cooling was evaluated as a function of quenching temperatures and quenching cycles using water- and air-quenching technique. The results showed that corrosion resistance and thermal shock resistance properties of the ceramics prepared with alumina are better than those of the ceramics prepared without alumina and the material was found suitable for hot gas filtration application.

Publications

1. D. Das, N. Kayal, Mat. Sci. Forum, 978, 2020.
2. D. Das, N. Kayal, Bol. Soc. Esp. Ceram. V, 58 (2019), 255-262.
3. D. Das, N. Kayal, Trans. Ind. Ceram. Soc., 78 (2019), 165-172.

5.4.1. Material properties of the porous SiC ceramic samples

The samples were prepared using various amount of alumina along with SiC powder (d_{50} = 212 µm) and a mixture of a clay mineral, Na salt of carboxy methyl cellulose and calcium carbonate in 3:2:1 weight ratio followed by pressing and sintering at 1300-1500°C. The detailed composition of different batch sample were shown in Table 5.4.1. According to the literature study, fabrication of porous granular filter for hot gas filtration, use of SiC powder with higher particle size is always beneficial as it largely increases the porosity of the filter and the filter shows higher collection efficiency due to higher inertial force [6, 9]. Thus in this study we have chosen SiC particles having higher particle size along with other additives. The samples prepared without and with 5 and 10 wt% alumina were named as MSC1, MSC2 and MSC3 respectively. To observe the effect of pore formers, 15 wt% graphite powder was added to the MSC1 and MSC2 composition, and named as MSC4 and MSC5 respectively. The ceramics MSC1 sintered at 1300-1500°C, samples of MSC2 composition sintered at 1300-1450°C and samples of MSC3 composition sintered at 1300-1400°C exhibited neither surface cracks nor distortion of shape and negligible dimensional changes indicated that near net dimension processing of porous ceramics was possible. Literature study indicated that the volume expansion due to formation of silica from oxidation of SiC and the formation of mullite by reaction bonding caused of ~108% and 13% respectively [87]. But here volume expansion is neutralized by shrinkage of the ceramics due to sintering, so there is no significant change in the dimensions or volume for oxide bonded ceramics sintered at 1300-1400°C. However the ceramics MSC2 and MSC3 sintered at 1500°C were found to be distorted/saggered due to volume expansion by formation of low viscous liquid glassy phase with expansion of volume ~30-40% as shown in Figure 5.4.1. The porosity of the sintered ceramics were decreased with increase in sintering temperature and alumina content in the final ceramics while the density of the ceramics followed reverse trend.

Table 5.4.1. Final composition of different samples.

Sample	**Batch compositions (wt %)**					
	SiC	Clay	$CaCO_3$	Na-CMC	Al_2O_3	Graphite
MSC1	94	3	2	1	---	---
MSC2	89	3	2	1	5	---
MSC3	84	3	2	1	10	---
MSC4	94	3	2	1	---	15
MSC5	89	3	2	1	5	15

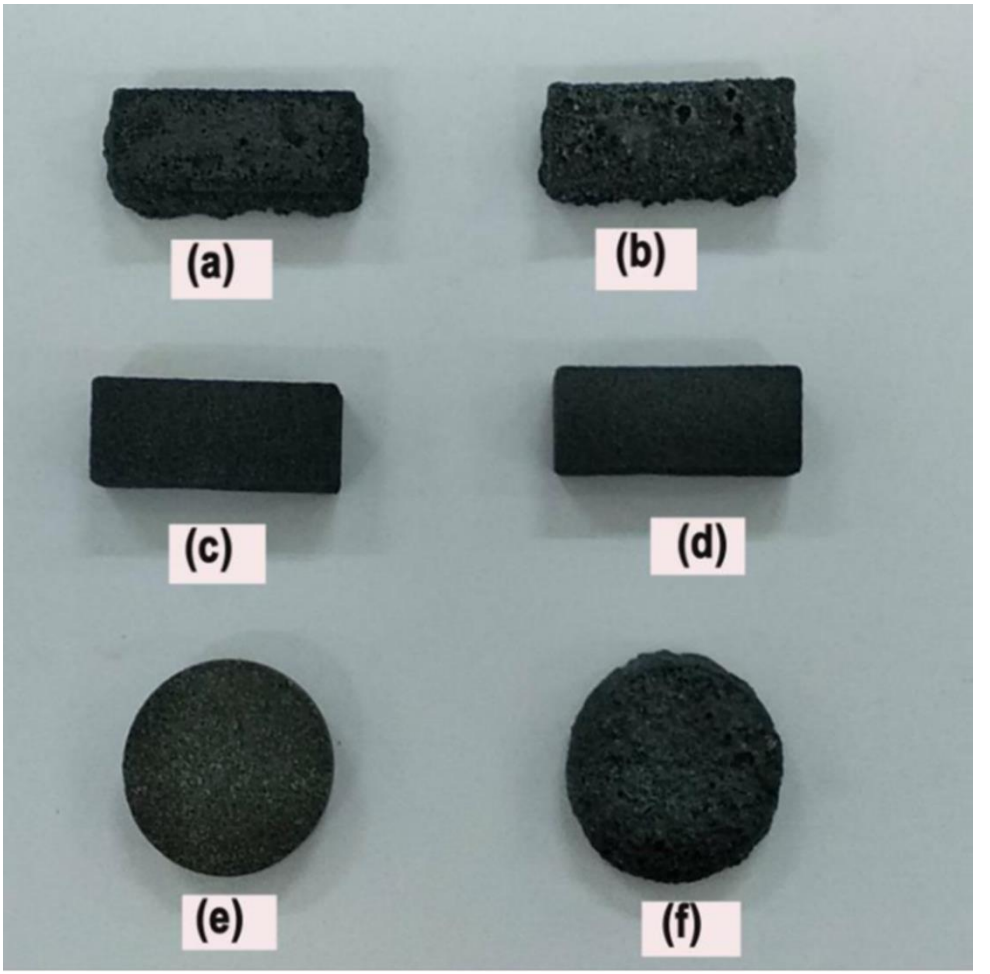

Figure 5.4.1. Photograph of sintered SiC ceramics [MSC2 sintered at (a) 1500 (c) & (e) at 1400] and [MSC3 sintered at (b) 1500 (d) 1400 (e) 1450°C]

Addition of pore former i.e. graphite powder to the ceramics increased the porosity of the membrane. With the addition of pore former to MSC1 sample the apparent porosity of the membrane increased from 38% to 41% in MSC4 ceramics while for MSC2 ceramics, porosity increased from 33 to 36% in MSC5 ceramics.

5.4.2. XRD analysis

Figure 5.4.2 shows the XRD pattern of the ceramics prepared with 5 wt% alumina (MSC2), the ceramics prepared without alumina (MSC1) sintered at 1400°C for 4h and the pure SiC powder. The effect of alumina additive on the crystalline phase formation in the sintered ceramics clearly seen from the XRD diffraction pattern. The ceramics prepared without

alumina additive (MSC1) shows the characteristics peaks of cristobalite and SiC phase but the addition of alumina to the sintered ceramics, resulted the formation of SiC, cristobalite and mullite crystalline phase and also indicated that all the alumina converted to mullite phase. Further Rietveld analysis of the ceramics shows the same trend. The amount of crystalline phase formed in the final sintered ceramics were shown in Table 5.4.2.

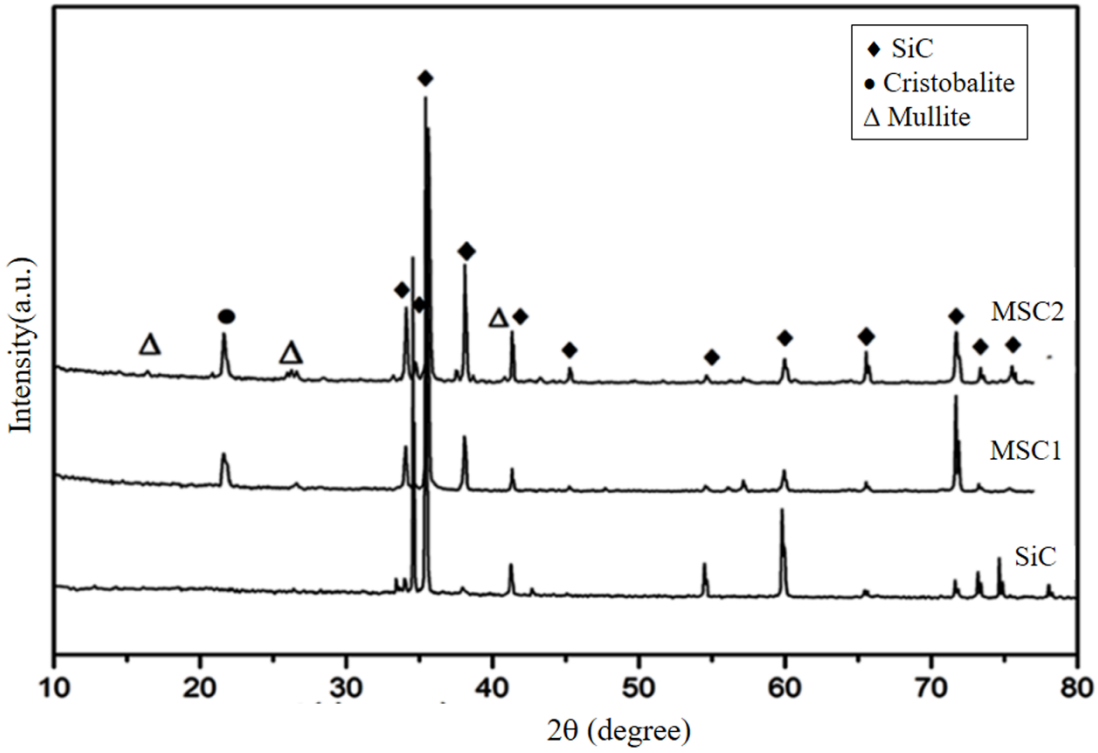

Figure 5.4.2. XRD diffraction patterns of oxide bonded porous SiC ceramics prepared without, with alumina additives sintered at 1400°C and pure SiC powder.

Table 5.4.2. Rietveld analysis data of sintered SiC ceramics

Sample	Crystalline phases (%)			Goodness of fitting
	SiC	Cristobalite	Mullite	
MSC1	80.2	19.8	---	1.72
MSC2	73	11.4	15.6	2.01

The effect of sintering temperature on the crystalline phase formation in final ceramics were seen by sintering MSC3 ceramics at three different temperature (i.e. 1300, 1400 and 1450°C). Figure 5.4.3 showed the typical XRD pattern of MSC3 ceramics sintered at different temperature. The MSC3 ceramic sintered at 1300°C shows the characteristic peaks of SiC,

cristobalite along with alumina phase. No mullite phase formed at this temperature but with increase in sintering temperature from 1300 to 1400°C, there was a formation of new crystalline mullite phase in the XRD pattern and the peak intensity of alumina gradually disappeared. Further increase in sintering temperature resulted increase in peak intensity of cristobalite phase while some of the crystalline mullite phase undergoes phase transition from crystalline to amorphous phase. The XRD analysis showed that mullite was completely formed at 1400°C, which means the temperature of mullitization was about 100°C lower because clay and $CaCO_3$ were present. Similarly *Ding et al.* has also shown that mullite is formed by the reaction between Al_2O_3 and oxidation-derived SiO_2 in the presence of 1.5% Y_2O_3 [9].

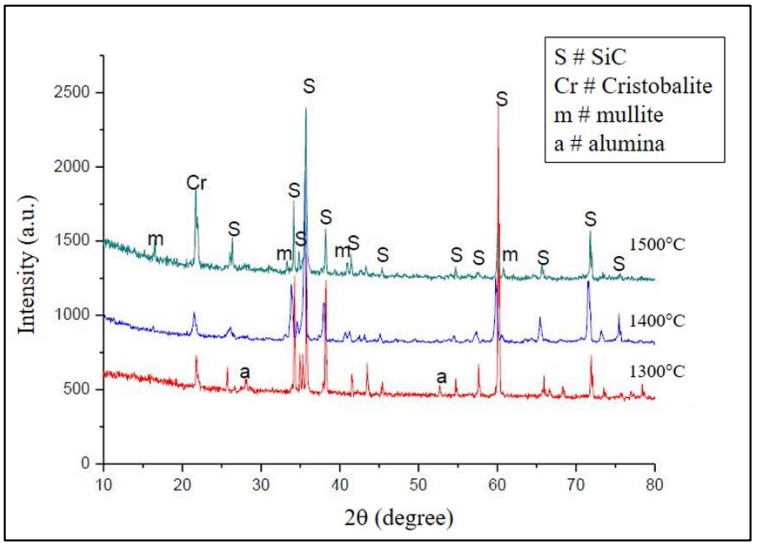

Figure 5.4.3. XRD pattern of mullite bonded porous SiC ceramic (MSC3) sintered at different temperature.

Table 5.4.3 provides a summary of the quantitative estimates of crystalline phases based on Rietveld analyses of XRD results. The amount of cristobalite increased from 7.9 to 15.9 % with increase in sintering temperature from 1300 to 1500°C for sample MSC3. At 1500°C, the sample MSC2 and MSC3 showed the characteristic peak of calcium aluminium silicate. In MSC2 and MSC3 samples, the amount of mullite phases decreased as the sintering temperature was raised from 1400°C to 1500°C, indicated the change in crystalline phases and glassy phase formation with rise in temperature could be responsible for the deformation of shape.

Table 5.4.3. Calculation of the crystalline phases for sintered samples at variable temperatures

Sintering temp^{r} (°C)	MSC1				MSC2				MSC3			
	SiC	cristobalite	alumina	mullite	SiC	cristobalite	alumina	mullite	SiC	cristobalite	alumina	mullite
1300	89.3	10.7	--	--	86.7	8.5	4.8	--	82.6	7.9	9.5	--
1400	80.2	19.7	--	--	73.0	11.4	--	15.6	74.2	5	--	20.8
1500	75.7	24.3	--	--	68.9	16.2	1.2	13.7	63.5	15.8	1.7	19

5.4.3. SEM analysis

Figure 5.4.4 presented the SEM images of MSC3 ceramic, showed the formation of porous network with well-developed necks between SiC particles sintered at (a) 1400 and (b) 1450°C in presence of air. The high resolution microstructures showed both needle, rod and fish scale morphologies after sintering at both temperature indicated formation of mullite, and cristobalite oxide bond phases at the neck region with their distinct morphological appearances which are shown in Figure 5.4.5. The microstructure analysis showed denser struts between SiC particles after sintering at 1450°C compared to the ceramics developed at 1400°C. Sintering temperatures increased the growth of mullite and cristobalite crystal in both the samples.

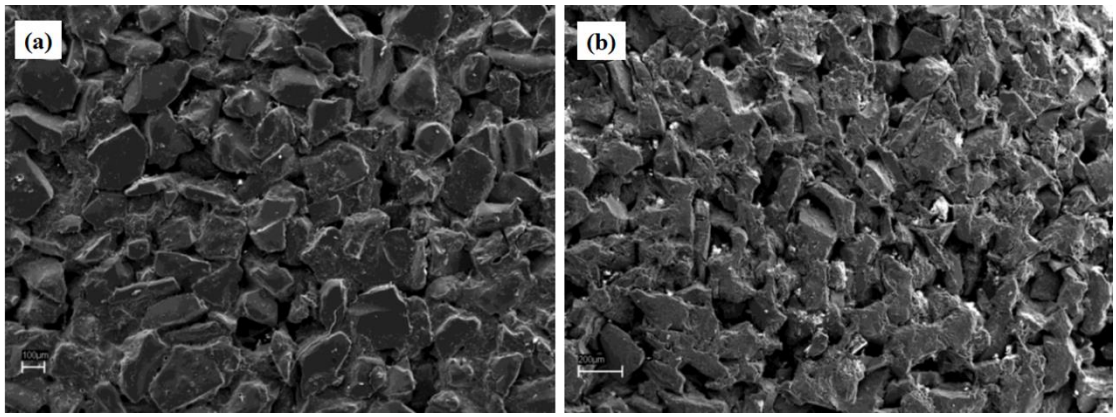

Figure 5.4.4. Microstructures of oxide bonded porous SiC ceramic (MSC3) sintered at (a) 1400 and (b) 1450°C.

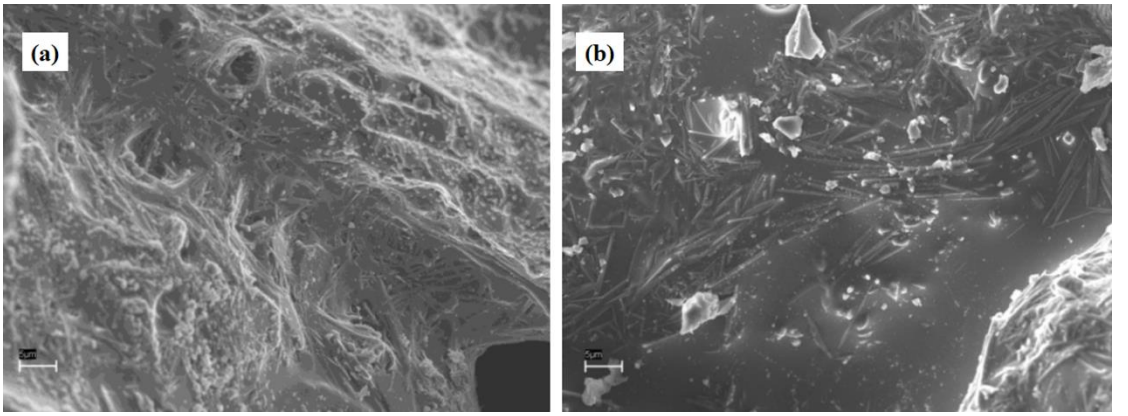

Figure 5.4.5. High resolution microstructural view of oxide bonded porous SiC ceramic (MSC3) sintered at (a) 1400 and (b) 1450°C.

The energy dispersive X-ray (EDX) analysis obtained during microstructure examination are presented in Figure 5.4.6, which provided details related to the presence of various elements in marked regions. As evident by EDX analysis, Al, Si, and O were found in the needle shaped grains (region "a"), suggesting that the needle shaped grains were composed of mullite. Si intensity increased in region "b" with a small amount of Al, indicating that the signal was coming from a region close to, or below, the fish scale morphology. It was found that each cristobalite grain measured ~1µm in diameter. Needle and rod shaped morphologies were reported for mullite crystals by many researchers [6]. *Viswabaskaran et al.* also reported mullite crystal with needle like morphology in heat treated compacts of reactive alumina, kaolinite clay, and magnesium oxide [88]. A mullite crystal with needle-like morphology was observed in calcined powder compacts of natural topaz by Miao [89]. At 1600°C, *Lee et al.* prepared mullite crystals from its precursor with width and length of nearly 1-2 µm and 10-20 µm respectively while the cristobalite grain size varied from 1 to 2.3 µm in diameter [6]. In the volcanic ash produced by dome-forming eruptions, *Damby et al.* observed of cristobalite phases having fish scale morphology with diameter 8 µm [42].

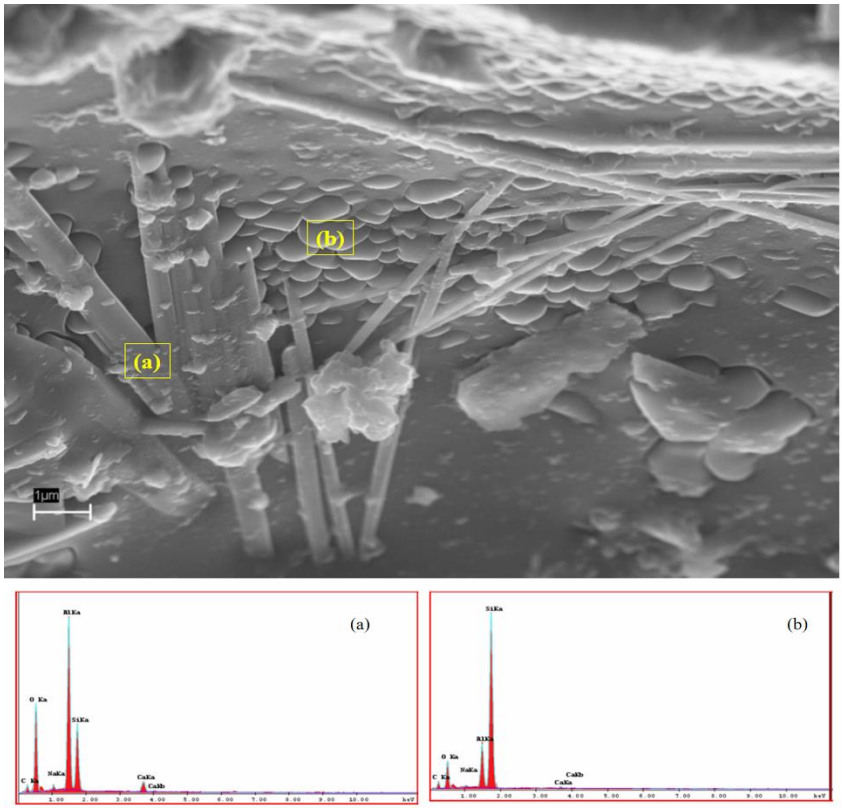

Figure 5.4.6. EDS analysis of different crystal phases formed different region (a) needle and (b) fish scale in MSC3 sample sintered at 1400°C

5.4.4. Pore size distribution analysis

Monomodal pore size distribution pattern was obtained for ceramics prepared without (MSC1) and with 5 wt% alumina additive (MSC2) sintered at 1400°C as shown in Figure 5.4.7. The wide distribution patterns obtained could be attributed to differences in the size of starting SiC powder. The pore diameter of the porous SiC ceramics was found to be strongly dependent on the addition of additives and pore former in the final ceramics. Addition of alumina additive in the final ceramics resulted the formation of high amount of liquid phase which flows into the pores as a result the average pore diameter of the ceramics decreased. The ceramics MSC1 and MSC2 showed the average pore diameter of 71 and 58 µm respectively. Addition of pore former to MSC1 and MSC2 ceramics, resulted increase in pore diameter of 87 and 63 µm respectively.

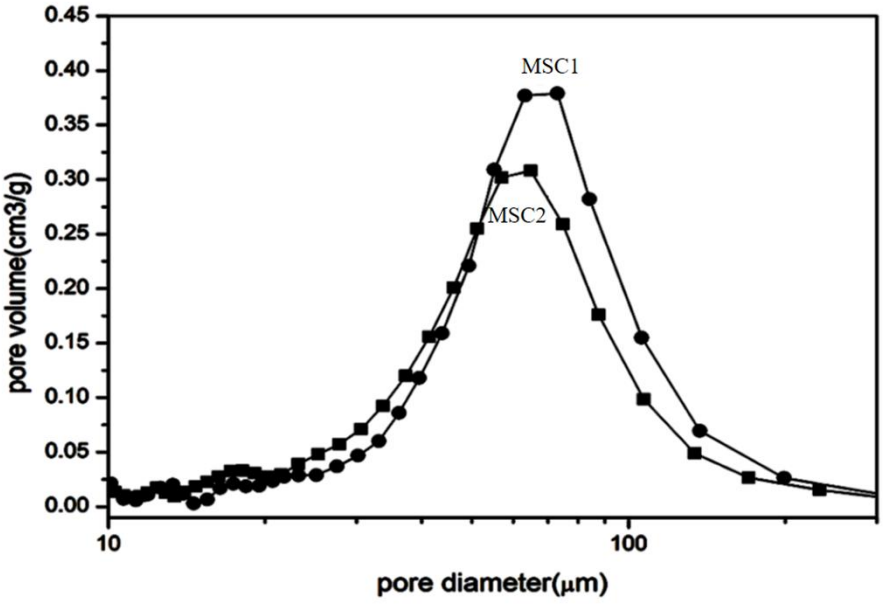

Figure 5.4.7. Pore size distribution pattern of MSC1 and MSC2 ceramics sintered at 1400°C in air.

A typical PSD-profile for samples MSC1 and MSC3 sintered at 1500^{o}C and 1300^{o}C, respectively, is shown in Figure 5.4.8. Observations on the microstructure and pore size of MSC1 and MSC3 were consistent with themselves, as MSC1 had an average pore size of 71.6 µm and MSC3 had an average pore size of 66.4 µm.

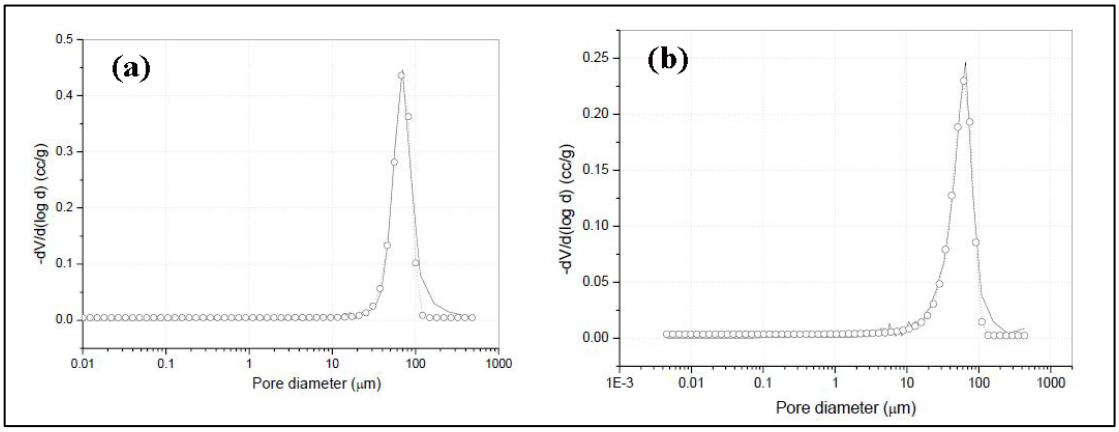

Figure 5.4.8. Pore size distribution pattern of oxide bonded porous SiC ceramics of (a) MSC1 sintered at 1500^{o}C and (b) MSC3 sintered at 1300^{o}C.

5.4.5. Mechanical strength analysis

Figure 5.4.9 showed the effect of alumina content on the room temperature mechanical strength of the porous SiC ceramic sintered at 1400°C. An increase in alumina content in the

final ceramics and sintering temperature increases the average flexural strength. The MSC1 sintered at 1500°C had a flexural strength of 32.5 MPa at a porosity of 33.3 vol%. With decreasing sintering temperature to 1300°C, the sample had a flexural strength of 23.7 MPa at a porosity of 39.8 vol%. Addition of bond phase additives resulted in a dramatic increase in average flexural strength and Young's modulus. The sample MSC3 sintered at 1400^{o}C had an average flexural strength of 57.69 MPa and a Young's modulus of 56.68 GPa at porosity of ~27 vol%. Since samples prepared at 1500^{o}C with 5-10 wt% Al_2O_3 were distorted, strength could not be determined for those samples.

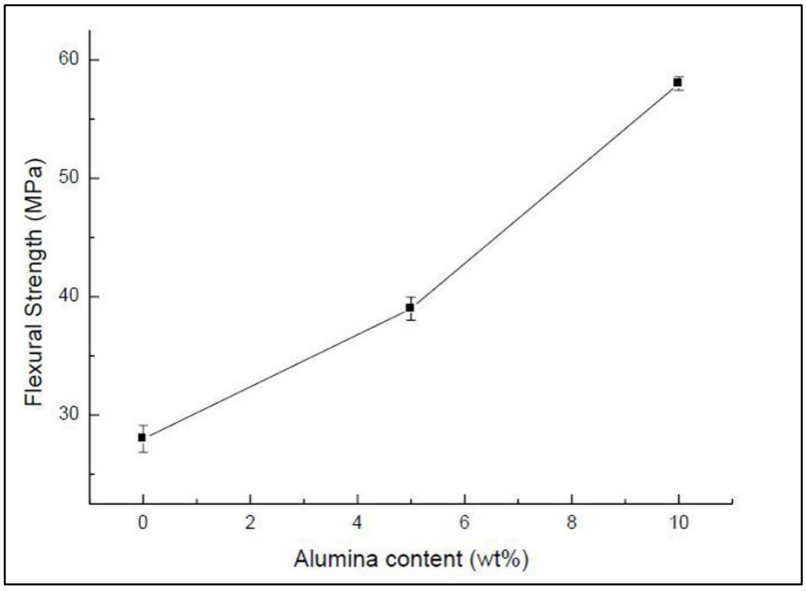

Figure 5.4.9. Effect of alumina content on the mechanical strength of the oxide bonded porous SiC ceramics

As porous ceramics are typically reported to exhibit a decreasing strength with increasing porosity, this is attributed to a higher probability of defects forming at higher porosities [90]. This results were similar for ceramic candle filters prepared by cold isostatic pressing from SiC powder with a d_{50} =180 µm obtained with a flexural strength of 20 MPa, a porosity of 35.8%, and an average pore diameter of 65 µm. Mullite bonded porous SiC ceramics synthesized from SiC (d_{50} =65 µm) and varying amounts of $Al(OH)_3$ content (14.5, 27.7, 39.6 and 47.3 wt%) at 1450-1550^{o}C showed flexural strength ranging from 3 to 14 MPa with porosity varying from 46 to 54 vol%. Mullitization becomes more rapid as $Al(OH)_3$ content increases, resulting in a decrease in porosity and an increase in flexural strength [91]. Several studies have shown that in presence of alkaline earth metals, such as yttria, a metastable eutectic liquid of low viscosity is formed at lower temperatures than SiO_2-Al_2O_3, and more

Al^{3+} ions are dissolved into the liquid, which accelerates mullite formation [89-92]. In the present study, clay accelerated the similar kind of mullite formation at low temperature with formation of low viscous eutectic phases. Mullite-bonded SiC ceramics prepared from SiC, Al_2O_3 and graphite pore former exhibited flexural strength of 10 MPa at 50% porosity and in presence of Y_2O_3 as sintering additive a flexural strength of 15 MPa was obtained at 48% porosity. The addition of alkaline earth metal oxides increased the strength significantly, compared to the mullite bonded SiC (MBSC) prepared with no additives [89]. The MBSC specimens showed the highest average strength of 44 MPa at 46% porosity, in contrast, the flexural strength of the MBSC without additives was ~6 MPa at ~49% porosity [92]. *Lee et al.* investigated the effects on porosity on flexural strength of porous SiC hot gas filters made of SiC powders of mean particle size of ~ 180 μm and a clay based oxide binder and reported a maximum strength of 28 MPa at a porosity of 28% [93]. *Han et al.* studied fabrication and properties of SiC hot gas filters by vacuum extrusion and ramming process using SiC powders of 85-100 μm average particle size with clay based oxide additives and obtained a maximum strength of 45 MPa at a porosity of 33% for the samples prepared by ramming method from 85 μm powder [94]. They observed decrease of strength with increase in average particle size of SiC powders. The mechanical property data of oxide bonded porous SiC ceramic samples of the present work are thus comparable to those mentioned by many researchers.

5.4.6. Effect of thermal shock on mechanical strength

A study has been conducted to investigate the flexural strength of porous SiC ceramics fabricated at 1400°C as a function of quenching temperatures and quenching cycles in air and water. Figure 5.4.10 showed the flexural strength of mullite bonded SiC ceramics (fabricated at 1400°C) as a function of number of quenching cycles in air. An analysis of thermal quenching cycles from 1000^{o}C to RT showed increases in flexural strength during the first few cycles due to healing of cracks caused by oxidized silica glass [95-96]. After the third cycle, cracks began to form around the weaker necks. This led to a decrease of flexural strength [97-99]. For sample MSC2 (in Figure 5.4.10(a)), the maximum strength of 44.5 MPa was achieved after the 2nd cycle; subsequently, the strength gradually decreased and eventually became almost constant after the 8th cycle. As can be seen in Figure 5.4.10(b), after the 1st cycle the strength of MSC4 sample increased from 24 to 26.5 MPa; after that a slow decay of strength was noticed; however, the strength did not decline beyond the initial

strength, even after 10th cycles. Upon reaching the seventh cycle, the strength was nearly constant, regardless of how many cycles had passed.

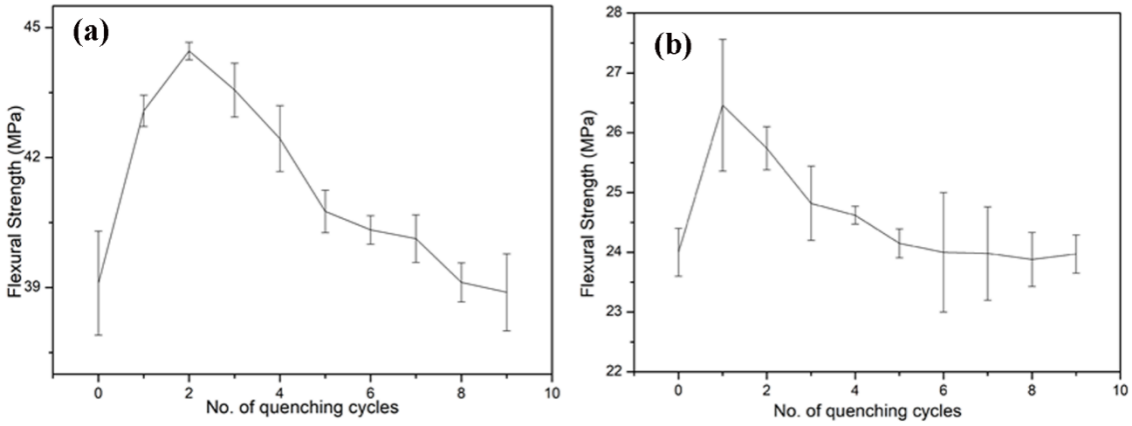

Figure 5.4.10. Effect of quenching cycle on the flexural strength of (a) MSC2 and (b) MSC4 ceramic sample quenched at 1000°C in presence of air medium.

Effect of quenching cycle on the flexural strength of MSC2 ceramics quenched at 1100°C in presence of air is shown in Figure 5.4.11. In MSC2 ceramics, the flexural strength gradually increased with quenching cycles, initially reaching 46 MPa, then decreased after the 3rd cycle, and becoming independent of quenching cycle after the 8th cycle. The flexural strength of MSC2 increased from 44.5 to 46 MPa with an increase in quenching temperature from 1000°C to 1100°C. An XRD analysis of the quenched MSC2 sample at 1100°C after 3rd cycles revealed a 5% increase in cristobalite, caused by the onset of oxidation of SiC and resulting in an increase in strength.

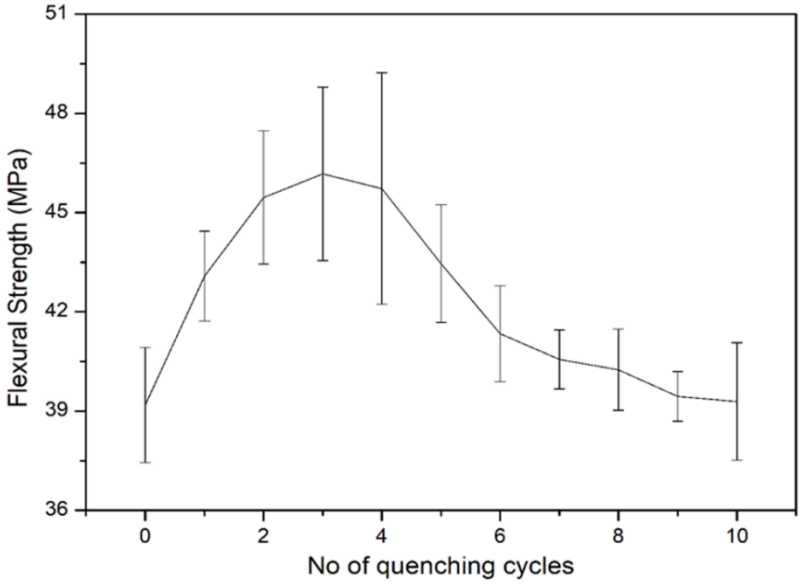

Figure 5.4.11. Variation of mechanical strength with quenching cycles for MSC2 sample by air quenching method heated at 1000°C.

An effect of cyclic thermal shock on the flexural strength of samples is shown in Figure 5.4.12, when the samples are cooled to room temperature from quenching temperatures of 1000^{o}C. After the third cycle, the quenched MSC4 and MSC5 samples showed residual strengths of 16.5 and 26.5 MPa, respectively. Following that point, strength became independent of cycle count. A similar phenomenon has been observed previously in oxide-bonded porous SiC ceramics [97].

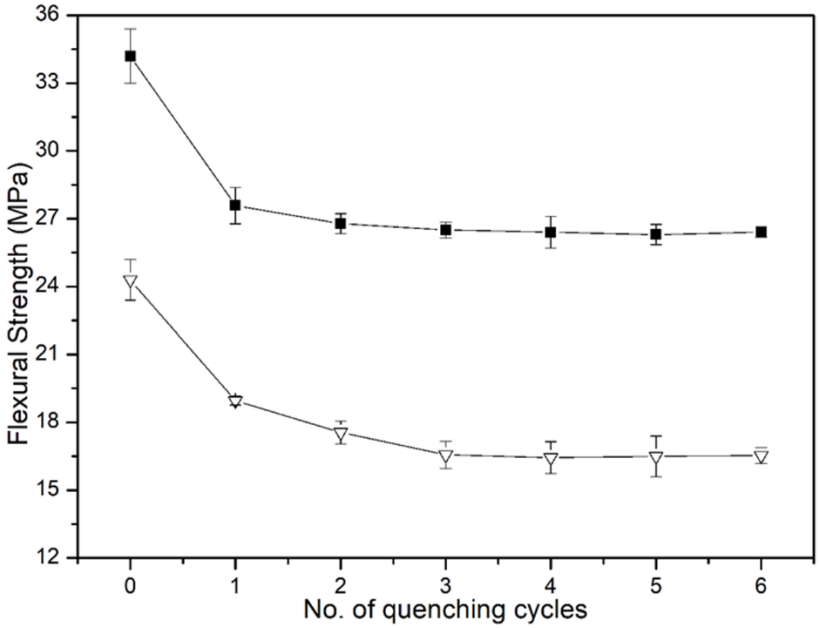

Figure 5.4.12. Flexural strength of (∇) MSC4 and (♦) MSC5 sample as a function of quenching cycle due to cooling in water at room temperature from 1000^{o}C

As a function of the quenching temperature in air or water, Figure 5.4.13 illustrates the variation in flexural strength of the MSC5 sample. As a result of increasing the quenching temperature from room temperature to 1200^{o}C, the residual strength of the quenched specimens decreased acutely from 34.2 to 23.08 MPa. The MSC5 ceramics faced steady decrease in strength up to 400°C during quenching in water medium but after this temperature, the strength sharply decreased from 400 to 1200^{o}C. This may be due to the nucleation of high number of cracks at the strut region increases as the quenching temperature increased, resulting in sudden decrease of strength. A subsequent rise in quenching temperature in water caused further thermal stress which accelerated the propagation of existing cracks and led to the formation of new cracks. As a consequence, a reduction in flexural strength was also observed. During quenching in presence water, the surface cooled almost immediately as soon as the sample came into contact with water, but the interior remained warm, causing an uneven thermal profile. Additionally, the mismatch between the growth of crystal phases during thermal shock and their different thermal expansion coefficients in the final ceramics also contributed to thermal stress. The combined effect created a large number of micro cracks in the sample, which resulted in a sudden reduction in flexural strength. On the other hand, with increasing quenching temperature in air the sample showed gradual increase in flexural strength from 34.2 to 39.95 MPa with increasing quenching temperature to 1200^{o}C. A gradual gain in mass was observed in the ceramic due to the onset of oxidation of SiC, and the healing of some cracks with oxidation-derived silica glass caused a strength increase with increasing thermal shock temperatures in air.

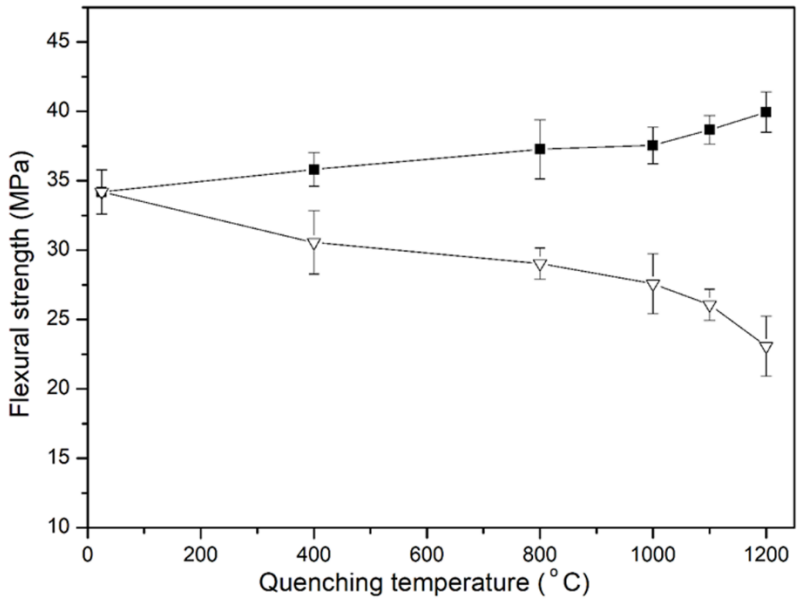

Figure 5.4.13. Change of flexural strength for MSC1 sample as a function of quenching temperature in (♦) air and (∇) water medium.

5.4.7. Effect of thermal shock on microstructure of porous materials

The samples did not exhibit any significant physical changes after the repeated thermal shock tests. A microstructural analysis of the samples revealed that they had been subjected to thermal shock as weak necks of porous SiC ceramics had cracked, as shown in Figure 5.4.14. As a result of crack formation, all elastic energy stores in cracks were transformed to effective surface energy, ensuring that porous SiC ceramics were stress-free. The effective surface energy gained by crack propagation was required to produce new cracks. By increasing the quenching temperature to 1200^{o}C, thermal tensile stress increased because of the large temperature gradient, which accelerated the propagation of initial cracks (Figure 5.4.15). Despite increasing the quenching temperature to 1200^{o}C, macroscopic cracks did not occur in the sample; hence, the sample was not fractured. A higher quenching temperature would result in more cracked necks. It was found that crack propagation was discrete and non-linear; cracks were arrested by pores which in turn reduced the effects of thermal shock on the quenched specimens. In order to crack the stronger necks, more thermal stress was required, which could not be achieved at the same quenching temperature. Therefore, flexural strength did not significantly decrease as the number of cycles increased. There were very few visible cracks in samples quenched in air which is shown in Figure 5.4.16. Based on microstructural examination and mechanical testing, the samples were found to be stable against thermal shock created by repeated cooling and heating in air. There have been similar

findings published in the literature for clay- and mullite-bonded SiC ceramics [96, 99-101]. However, the samples were less stable against thermal shock due to the cooling in water medium. A mullite-bonded SiC ceramic experienced less thermal shock damage compared to cristobalite bonded SiC ceramic due to the close match between the thermal expansion coefficients (CTE) of mullite and SiC. Thermal expansion coefficients of SiC, cristobalite and mullite are 4.7×10^{-6}, $14.5\times10^{-6}$and 5.3×10^{-6} K^{-1} respectively. The cumulative effect of crystalline and glass phases and differences in thermal expansion coefficient values resulted in more damage to MSC1 and MSC4 samples by thermal shock than MSC2 and MSC5.

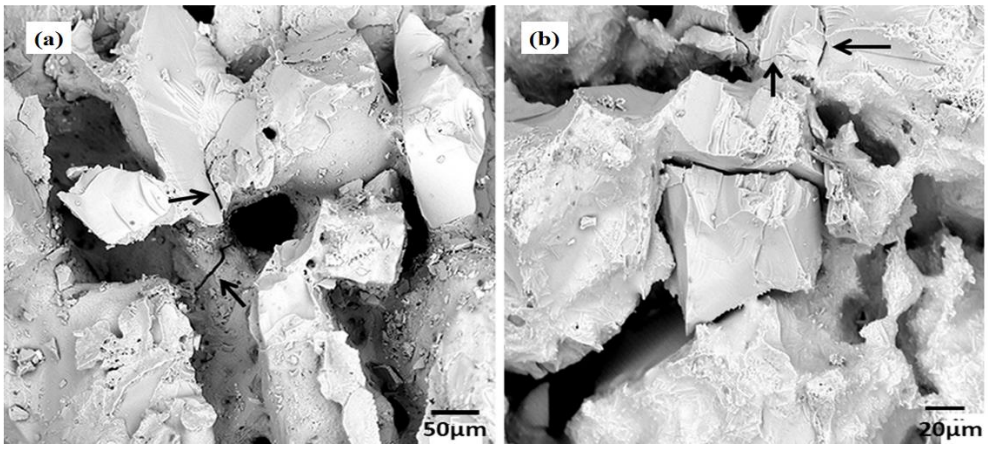

Figure 5.4.14. Microstructural view of (a) MSC4 and (b) MSC2 samples after 4th thermal cycle of cooling in water from 1000^{o}C.

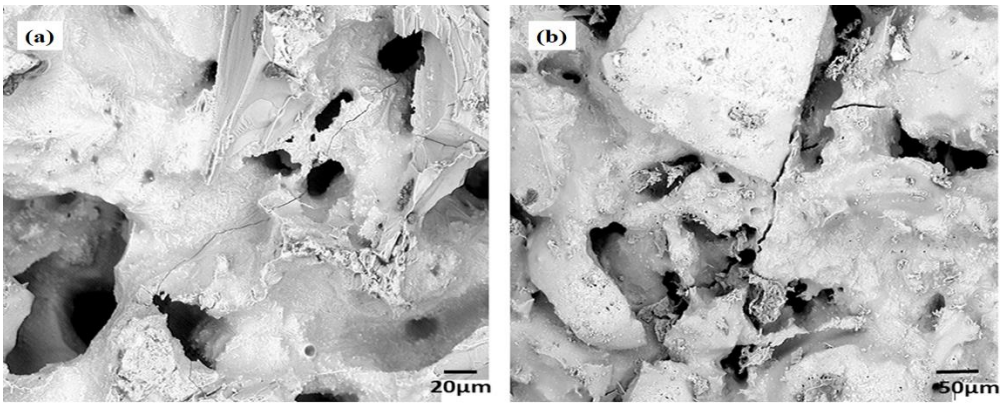

Figure 5.4.15. Fracture surface of MSC sample quenched in water from (a) 1000°C and (b) 1200°C to room temperature.

A material will fracture if its maximum thermal stress equals or exceeds its breaking strength, according to the theory of critical thermal stress promoted by *Kingery* [102]. The samples did

not fracture even with quenching temperatures increased to 1200°C, but their strength did decrease. These results indicate that the samples prepared in this study are excellent thermal shock resistant to fracture due to their low elastic modulus, which in turn produces low thermal stress [103]. Even though the quenched specimens were not fractured by thermal shock, there was damage. According to *Ding et al.* [98], the resistance (R″) to thermal shock damage in ceramic is given by

$$R'' = E/\tau_f^2\,(1-\mu) \qquad (4)$$

where Γ_f is the critical strength of materials, μ is the Poisson's ratio, E is the Young's modulus of elasticity. The thermal shock resistance of a material is directly proportional to its elastic modulus, and inversely proportional to its tensile strength [98]. For mullite bonded SiC ceramics with yttria addition, R″ was calculated to be 90.9 (M J m^{-3})$^{-1}$ whereas for dense magnesia-spinel composites, R″ was measured between 5 and 40 (M J m^{-3})$^{-1}$ [99].

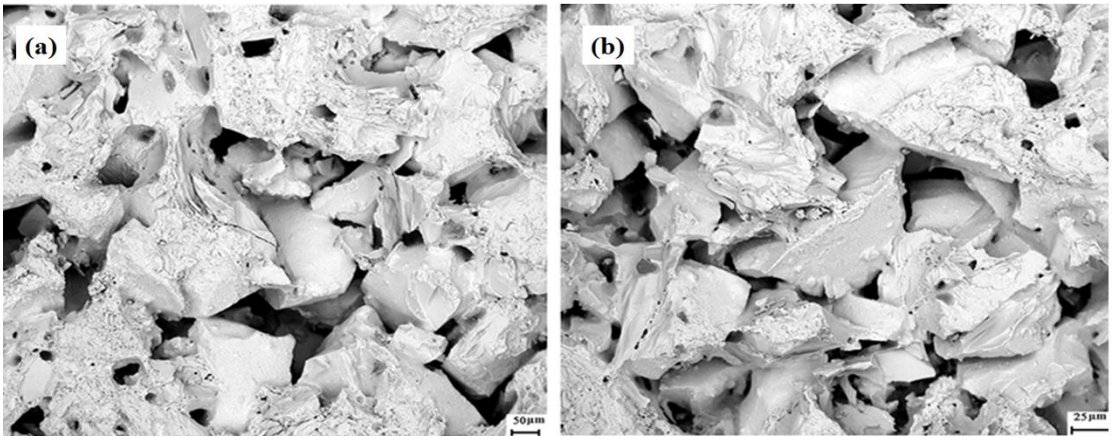

Figure 5.4.16. Fracture surface of (a) MSC1 and (b) MSC2 sample after 5th cycle of air quenching at 1000°C

Thermal quenching also induces surface oxidation, as demonstrated by the increase of cristobalite peak intensity (Figure 5.4.17) in the quenched samples. XRD analysis did not show any additional peaks after the third cycle of thermal shock. The amount of cristobalite and SiC were altered due to oxidation of SiC. The Rietveld analysis was used to find the changes in chemical composition caused by thermal shock. The quantitative phase analysis showed that the cristobalite content in MSC2 increased from ~10 to 13.2% while that in MSC1 increased from ~20 to 23.8%. However the mullite content remain unchanged during thermal shock. This study demonstrated that porous SiC ceramics prepared using a water

quenching method did not fracture under thermal shock; only strength was decreased due to the presence of cristobalite and mullite in the bond phase with reasonable flexural strength and elastic modulus. Hence, it can be concluded that the material possesses good thermal shock damage resistance.

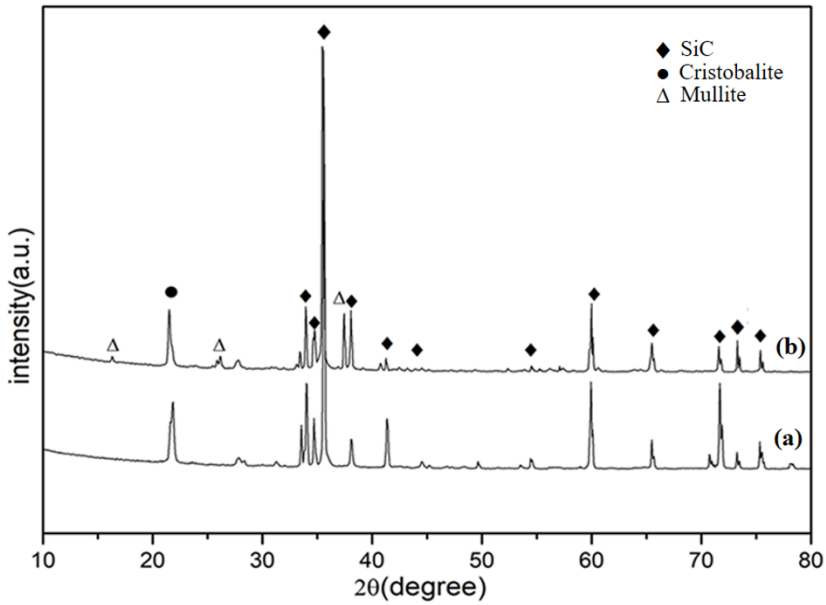

Figure 5.4.17. Effect of air quenching on XRD patterns of (a) MSC1 and (b) MSC5 samples quenched at 1000^{o}C.

5.4.8. Corrosion studies in presence of fly ash and steam

To see the effect of corrosion medium on the properties, microstructure and mechanical strength of porous SiC ceramics, the sample prepared without (MSC1) and with 5% alumina (MSC2) were covered with fly ash, placed in alumina boats and finally heat treated at 1000°C for 24–96 h in presence of air and for 96–240 h in water steam environment. A water dosing pump was used to inject 15 ml/min of water into the furnace at a rate of 15 ml/min when the furnace temperature reached 700°C for steam generation. After that, furnace temperature was allowed to increase up to 1000°C, keeping it for 96–240h.

Figure 5.4.18 shows the XRD pattern of the fly ash used for corrosion study as received and after calcination at 1000°C for 96h. The fly ash did not show any significant changes in crystalline phase after calcination. The sample was found to be free of surface cracks or shape distortion after corrosion tests. Table 5.4.4 summarizes the changes in mass and porosity of

the corroded samples after corrosion in presence of various corrosive environment for different time interval.

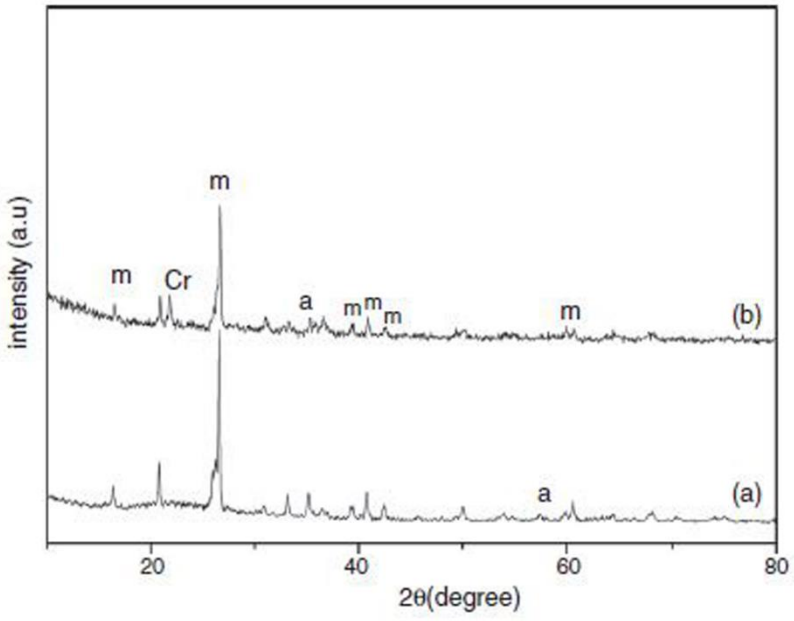

Figure 5.4.18. XRD pattern of fly ash received from industries (a) and calcined for 96 hours at 1000°C (b).

Table 5.4.4. Effect of corrosion media on the mass and porosity of the filter materials.

Sample code	Initial porosity (vol%)	Corrosion for 96h in presence of						Corrosion for 240 h in presence of			
		Fly ash		Fly ash + Steam		Steam		Fly ash + Steam		Steam	
		Porosity (vol %)	Mass gain (wt %)	Porosity (vol %)	Mass gain (wt%)	Porosity (vol%)	Mass gain (wt %)	Porosity (vol %)	Mas gain (wt %)	Porosity (vol %)	Mass gain (wt %)
MSC1	37.7	35.4	0.2	32.6	0.8	29.78	1.8	31.2	1.9	30	2.4
MSC2	33.0	30.6	0.3	28.9	0.65	27.2	0.9	30.6	1.1	28.3	1.7

XRD and SEM analysis indicate mass gains caused by cristobalite formation were counter balanced by the formation of crystalline phases and gaseous products. The most significant reduction in porosity was observed when the samples were corroded in the presence of steam due to increased oxidation of SiC. The XRD analysis of ash corroded samples did not only accentuate cristobalite, but it also revealed presence of alkaline alumina silicates as shown in Figure 5.4.19 and 5.4.20. Figures 5.4.21 and 5.4.22 demonstrate that the cristobalite peak increased further when the corrosion duration was increased to 240h. Nevertheless, it was impossible to precisely identify crystalline phases due to the overlap of many peaks of silicates with complex crystal structures. According to Table 5.4.5, the Rietveld analyses of XRD results provide a quantitative estimation of the amount of crystalline phases present.

After corrosion in the presence of steam, the amount of cristobalite increased from 19.6 to 25.2% for MSC1 sample, however the amount of cristobalite did not increase in presence of fly ash rather there was an increase in alkaline alumina silicate of 12.9%. In the same way, samples made with alumina additives (MSC2) showed increased cristobalite content after corrosion with steam. The results indicated that oxidation of SiC was reduced when samples was covered with fly ash.

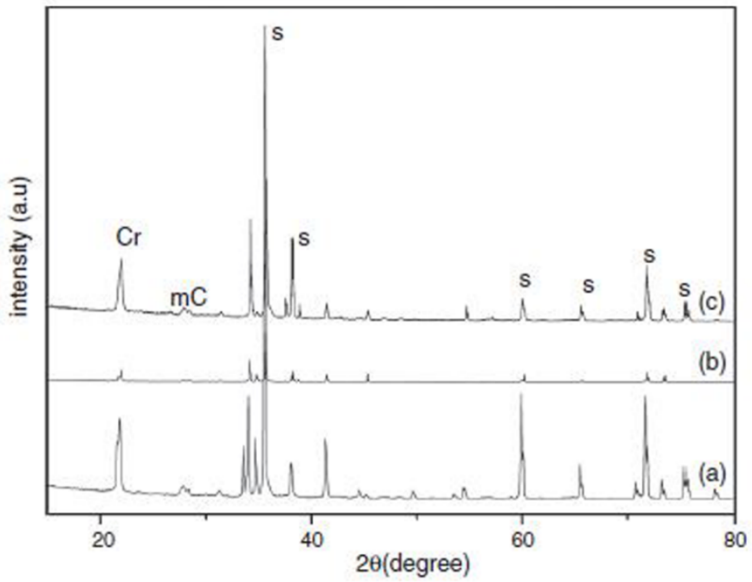

Figure 5.4.19. XRD pattern of MSC1 sample after corrosion with (a) steam, (b) ash, and (c) steam and ash. (Cr #cristobalite; m#mullite; s#SiC; C#alkaline alumina silicate).

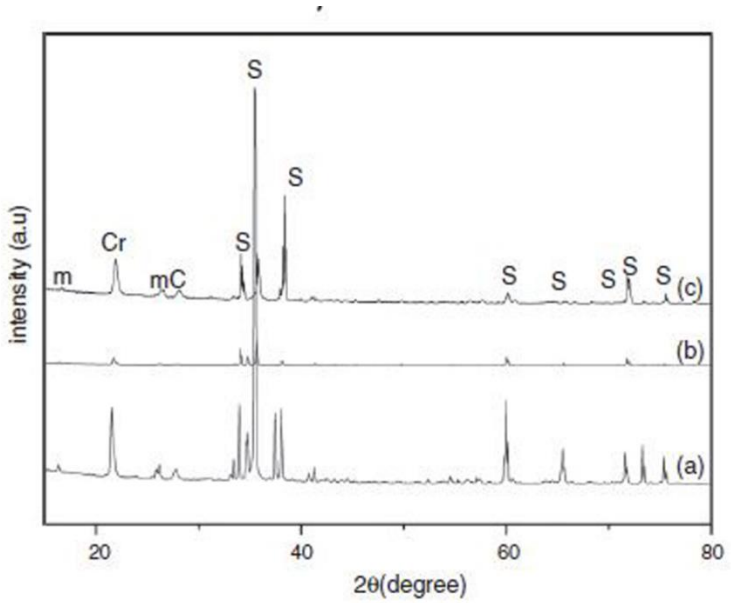

Figure 5.4.20. XRD pattern of MSC2 sample after corrosion for 96 h with (a) steam, (b) fly ash, (c) fly ash and steam.

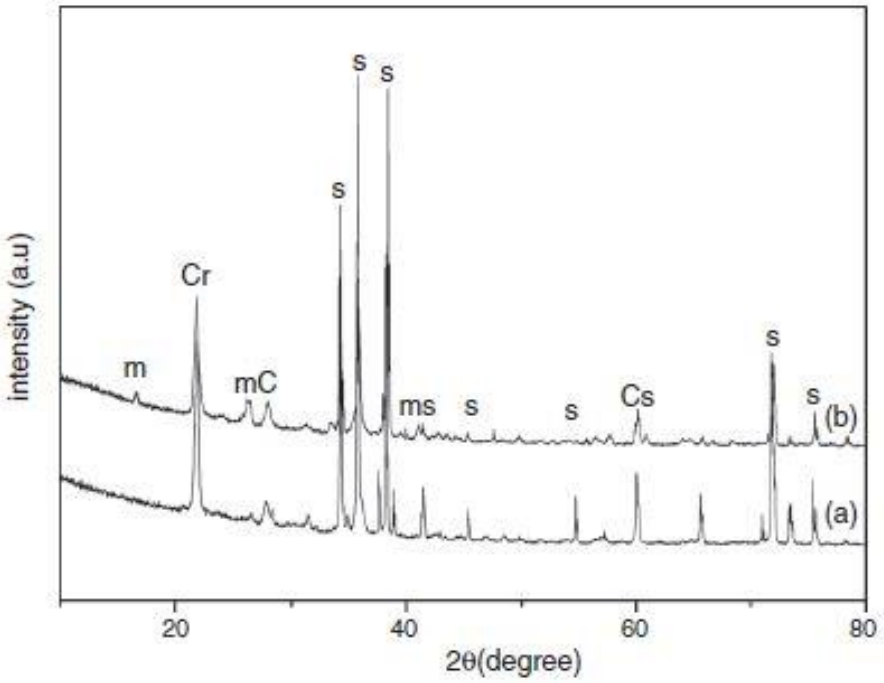

Figure 5.4.21. XRD plot of (a) MSC1 and (b) MSC2 samples after corrosion for 240 h with steam and fly ash.

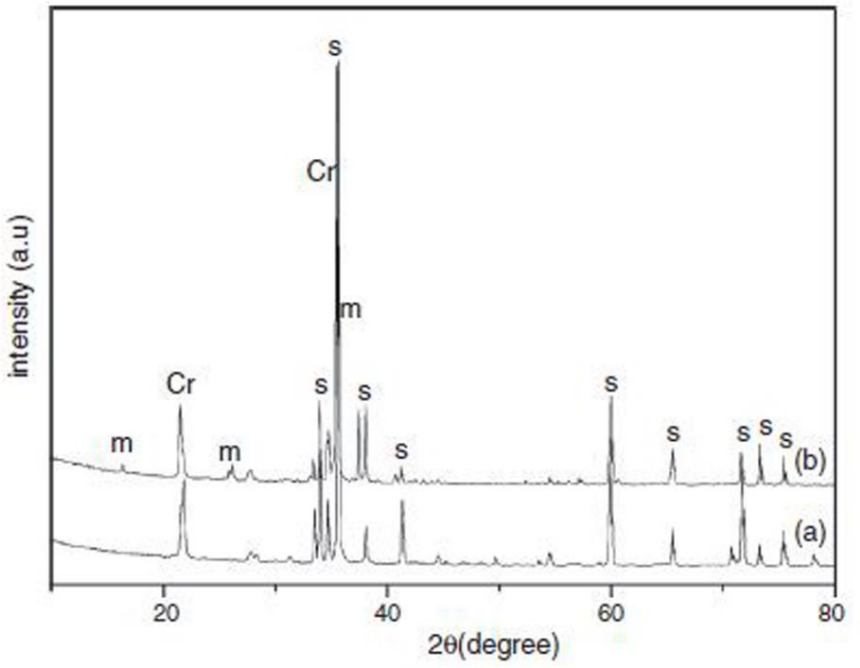

Figure 5.4.22. XRD pattern of (a) MSC1 and (b) MSC2 samples after corrosion for 240 h with steam.

Table 5.4.5. Quantitative estimation of the crystalline phases after corrosion with steam in presence or absence of fly ash for 96 h.

Sample	Initial composition of sample				After corrosion in presence of steam									
					With fly ash					Without fly ash				
	SiC	Cr	Mullite	GOF	SiC	Cr	Mullite	Ca-Al	GOF	SiC	Cr	Mullite	Ca-Al	GOF
MSC1	80.4	19.6	--	1.81	69.9	17.2	--	12.9	1.84	74.8	25.2	--	--	1.42
MSC2	73.7	10.5	15.8	1.68	55.3	22.0	11.1	11.6	2.22	64.7	22.3	13	--	1.98

In order to investigate any morphological changes caused by chemical interaction, SEM was used to examine the fly ash corroded samples. Figure 5.4.23 shows that particles of fly ash have been incorporated into the pore system. Alumina silicate crystals can be seen inside some pores under higher magnification. There are some grains of ash present in the interface with the surface of the sample that are particularly rich in the glassy phase, which causes them to stick permanently. There was a more noticeable change in microstructure in sample MSC1. The grain boundaries showed many pores mostly on the contacting bond phase region and also on the grain surfaces. Figure 5.4.24 displays the SEM microstructure of the corroded samples when they were exposed to steam. In both steam corroded samples, cracks were visible possibly caused by an increased amount of glass forming during the process. In a study published in 1999, water vapour was found to be a more severe oxidizer than oxygen [104].

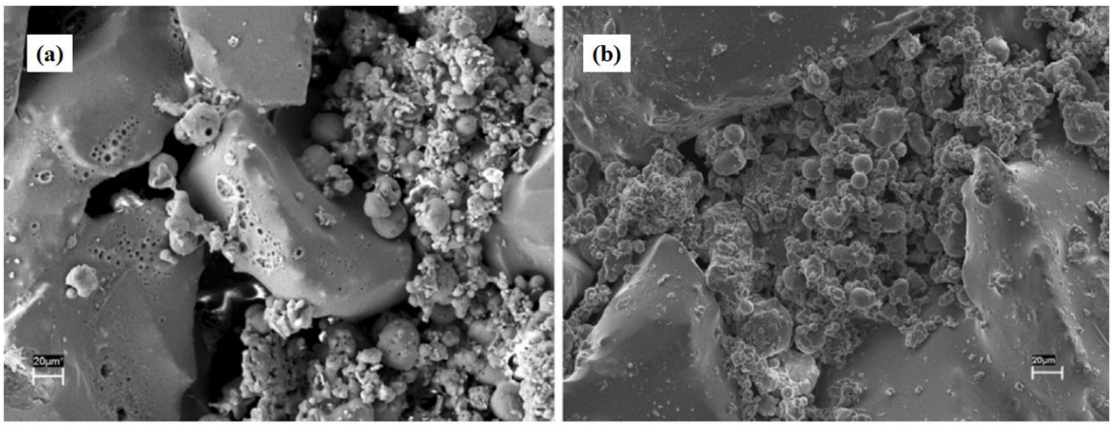

Figure 5.4.23. SEM images of top surface of sample (a) MSC1 and (b) MSC2 after exposure at 1000°C for 96h covered with fly ash.

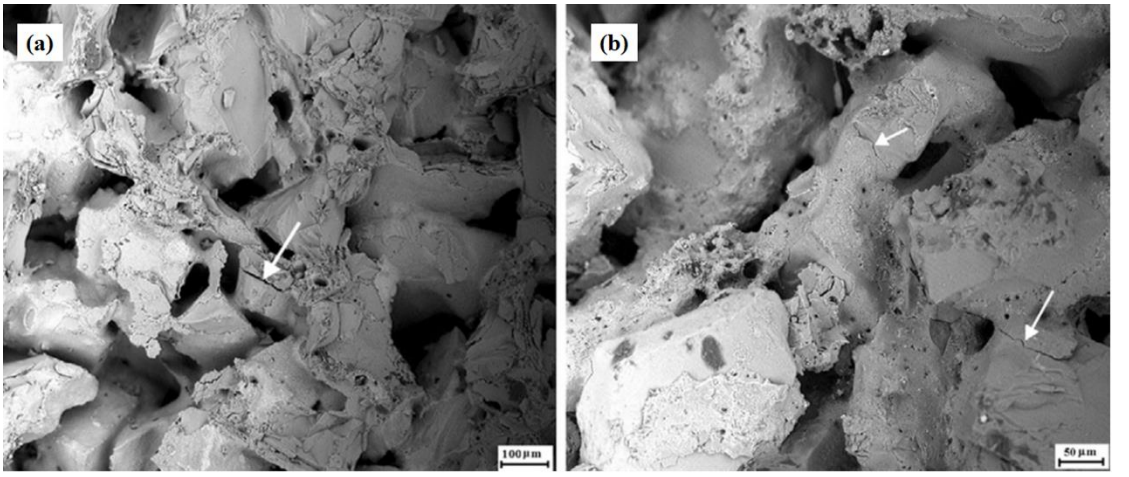

Figure 5.4.24. SEM images of corroded sample (a) MSC1 and (b) MSC2 in presence of steam for 96h.

Figure 5.4.25 shows SEM images of corroded sample in presence of steam and fly ash medium. Cracks were generated in the contacting bond phase and crack propagation was arrested by the pores. The formation of pitting on the surface of the glass layer may be caused by the removal of volatile agents during corrosion at 1000°C and the shrinkage of volume resulting from the transformation of crystalline state. During corrosion of SiC based filter material with fly ash, *Monatznaro et al.* [105] also observed the formation of pits at grain boundaries due to the breakdown of one or more components into gaseous products.

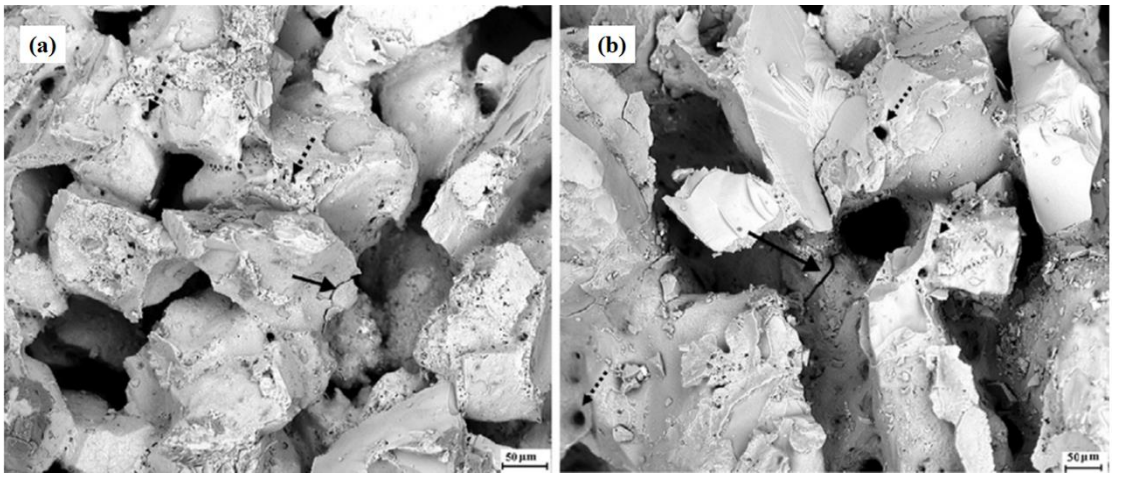

Figure 5.4.25. Microstructural view of top surfaces of filter material (a) MSC1 and (b) MSC2 after corrosion in presence of fly ash and steam for 96h.

The pore size distribution pattern of the MSC1 filter material in its corroded state after corrosion can be seen in Figure 5.4.26. The filter material initially possessed a pore size of 71

µm, but this was reduced by corrosion at 1000°C in fly ash and steam to a pore size of 64 µm. Due to glass formation during corrosion, porosity in the sample was found to be ~60 µm after corrosion with steam.

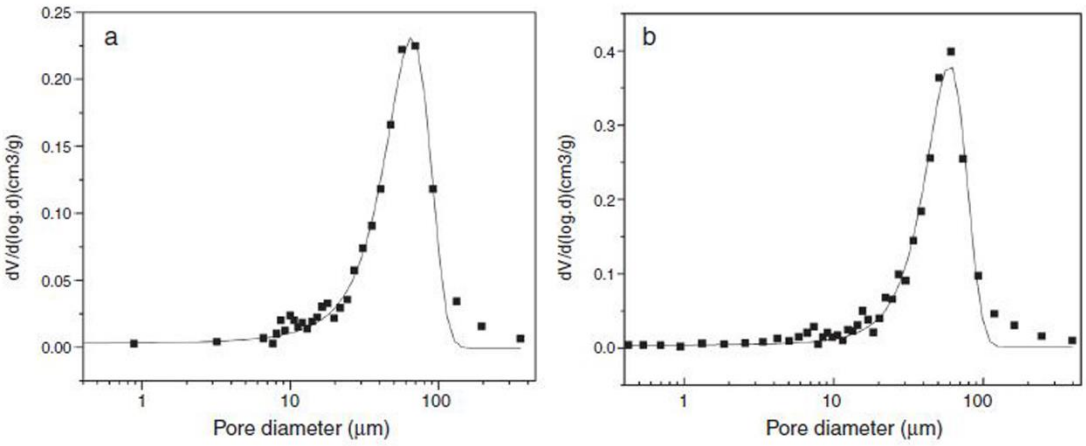

Figure 5.4.26. Pore size distribution pattern of MSC1 sample after corrosion in presence of (a) fly ash and steam, and (b) steam

Table 5.4.6 summarizes the change of strength on the filter material caused by exposure to fly ash, steam, and steam and fly ash together. The filter materials remained stable when exposed to fly ash alone and their strength has increased after 96 hours of corrosion. While in presence of steam, the mechanical strength of the filter materials were decreased. Following 96 hours of corrosion under steam, flexural strength for the MSC1 and MSC2 samples was reduced to 13.8 MPa and 23.6 MPa, respectively. Results show a good correlation between strength reduction and changes in microstructure and XRD spectrum. In samples that were corroded in the presence of water vapour or steam, the strength rapidly decreased after corrosion because of increased glass phase formation, associated with volume expansion, and crack formation. The presence of mullite in the bond phase for the samples prepared with alumina (MSC2) showed greater corrosion stability compared to MSC1 sample. Further increasing the corrosion duration to 240h resulted in a progressive decrease in flexural strength due to the formation of more glass phases and the depletion of crystalline phases. The residual strengths of MSC1 and MSC2 samples after 240 h of exposure to steam and fly ash were determined to be 9.4 MPa and 16.6 MPa, respectively. Filter material strength dramatically decreases as a result of the microstructural changes.

Table 5.4.6. Effect of corrosion on the room temperature mechanical strength of the filter materials after corrosion for 96h.

Sample	Room temperature mechanical strength							
	Initial strength of sample		After corrosion					
			In presence of fly ash		In presence of fly ash + steam		In presence of steam	
	Flexural strength (MPa)	Young's modulus (GPa)	Flexural strength (MPa)	Young's modulus (GPa)	Flexural strength (MPa)	Young's modulus (GPa)	Flexural strength (MPa)	Young's modulus (GPa)
MSC1	28.0	29.7	31.6	30.2	15.33	17.04	13.3	18.4
MSC2	39.1	40.2	42.54	46.9	27.5	32.6	23.6	26.6

Mullite bonded porous SiC ceramics were successfully prepared using alumina as bond phase additives and clay based material as sintering air by in-situ reaction bonding method. The addition of alumina to the ceramics lowered SiC oxidation in the ceramics and the presence of elongated mullite grains in the binder phase was possible because of the alumina addition and this could make the porous SiC ceramics exhibit better mechanical properties than the samples prepared without any alumina. On the basis of the corrosion studies, it turns out that samples prepared with alumina additives showed better corrosion resistance in presence of all three corrosive environment. Thermal shock studies of porous SiC prepared with alumina showed better thermal shock resistance compared to the ceramics prepared without alumina due to presence of mullite in the bond phase. The preliminary test result support the ability of the ceramic filter material to be used as hot gas filter material, however their durability in aggressive atmosphere must also be studied to predict the durability of the material.

References

1. S. Ding, S. Zhu, Y.P. Zeng, D. Jiang, Effect of Y_2O_3 addition on the properties of the reaction bonded porous SiC ceramics, Ceram. Int. 32 (2006) 461-466.
2. Z. Zhu, Z. Wei, J. Shen, L. Zhu, L. Ku, Y. Zhang, S. Sang, T Liu, Fabrication and catalytic growth mechanism of mullite ceramic whiskers using molybdenum oxide as catalyst, Ceram. Int., 43 (2017) 2871–2875.
3. B. Saruhan, W. Albers, H. Schneider, W.A. Kaysser, Reaction and sintering mechanism of mullite in the systems cristobalite/ α-Al_2O_3, J. Euro. Ceram. Soc. 16 (1996) 1075-1081.
4. E.F. Osborn, A. Muan, Phase equilibrium diagrams of oxide systems, The American Ceramic Society, 1960.
5. L. Zhu, Y. Dong, L. Li, J. Liu, S.J. You, With Coal fly ash industrial waste recycling for fabrication of mullite-whisker-structured porous ceramic membrane supports, RSC Adv., 5 (2015) 11163–11174.
6. J.E. Lee, J.W. Kim, Y.G. Jung, C.Y. Jo, U. Paik, Effects of precursor pH and sintering temperature on synthesizing and morphology of sol–gel processed mullite, Ceram. Int., 28 (2002) 935–940.
7. S. Liu, Y.P. Zeng, D. Jiang, S. Liu, Effects of preheated aluminosilicate addition on the phase development, microstructure and mechanical properties of mullitized porous OBSC ceramics, Intl. J. Appl. Ceram. Tech., 6 (2009) 617–625.
8. H.J. Choi, J.U. Kim, S.H. Kim, M.H. Lee, Preparation of granular ceramic filter and prediction of its collection efficiency, Aerosol Sci. Technol., 48 (2014) 1070–1079.
9. S. Ding, S. Zhu, Y.P. Zeng, D. Jiang, Fabrication of mullite bonded porous silicon carbide ceramics by in situ reaction bonding, J. Euro. Ceram. Soc., 27 (2007) 2095–2102.
10. J.H. She, T. Ohji, S. Kanazaki, Oxidation bonding of porous silicon carbide ceramics with synergic performance, J. Euro. Ceram. Soc., 24 (2003) 331–334.
11. Y.H. Choi, Y.W. Kim, I.S. Han, S.K. Woo, Effect of alkaline earth metal oxide addition on flexural strength of porous mullite bonded silicon carbide ceramics, J. Mat. Sci., 45 (2010) 6841-6844.
12. O. Ebrahimpour, C. Dubois, J. Chaouki, Fabrication of mullite-bonded porous SiC ceramics via a sol–gel assisted in situ reaction bonding, J. Euro. Ceram. Soc., 34 (2014) 237-247.

13. S. Zaighum, A. Bukhari, J.H. Ha, J. Lee, I.H. Song, Fabrication and optimization of a clay-bonded SiC flat tubular membrane support for microfiltration application, Ceram. Int., 43 (2017) 7736–7742.
14. S.H. Chae, Y.W. Kim, I.H. Song, H.D. Kim, J.S. Bae, S.M. Na, S. Kim, Low temperature processing and properties of porous frit-bonded SiC ceramics, J. Korean Ceram. Soc., 46 (2009) 488-492.
15. S.C. Kim, H.J. Yeom, Y.W. Kim, I.H. Song, J.H. Ha, Processing of alumina-coated glass-bonded silicon carbide membranes for oily wastewater treatment, Int. J. Appl. Ceram. Technol., 14 (2017) 692-702.
16. P. Pastila, V. Helanti, A.P. Nikkila, T. Mantyla, Enviromental effects on microstructure and strength of SiC-based hot gas filters, J. Euro. Ceram. Soc., 21 (2000) 1261–1268.
17. K. Okada, T. Isobe, K. Katsumata, Y. Kameshima, A. Nakajima, K.J.D. Mackenzie, Porous ceramics mimicking nature preparation and properties of microstructures with unidirectionally oriented pores, Adsorp. Sci. Technol., 12 (2011) 6.
18. C. Vakifahmetoglu, D. Zeydanli, M.D.M. Innocentini, F.S. Ribeiro, P.R.O Lasso, G.D. Soraru, Gradient hierarchic aligned porosity SiOC ceramics, Sci. Rep., 7 (2017) 41049.
19. S.Z.A. Bukhari, J.H. Ha, J. Lee, I.H. Song, Effect of different heat treatments on oxidation-bonded SiC membrane for water filtration, Ceram. Int., 44 (2018) 14251-14257.
20. C.H. Ohya, J. Kim, A. Chinen, Effects of pore size on separation mechanisms of microfiltration of oily water, using porous glass tubular membrane, J. Membr. Sci., 145 (1998) 1-14.
21. J. Cui, X. Zhang, H. Liu, S. Liu, K.L. Yeung, Preparation and application of zeolite/ceramic microfiltration membranes for treatment of oil contaminated water, J. Membr. Sci., 325 (2008) 420-426.
22. I.J. Kang, S.H. Yoon, C.H. Lee, Comparison of the filtration characteristics of organic and inorganic membranes in a membrane-coupled anaerobic bioreactor, Water Res., 36 (2002) 1803–1813.
23. S.R. Faibish, Y. Cohen, Fouling and rejection behaviour of ceramic and polymer modified ceramic membranes for ultrafiltration of oil-in-water emulsions and micro emulsions, Colloids Surf, A Physicochem. Eng. Asp., 191 (2001) 27–40.
24. L. Xu, W. Li, S. Lu, Z. Wang, Q. Zhu, Y. Ling, Treating dyeing waste water by ceramic membrane in cross flow microfiltration, Desalination, 149 (2002) 199–203.

25. B.K. Nandi, R. Uppaluri, M.K. Purkait, Treatment of oily waste water using low-cost ceramic membrane: flux decline mechanism and economic feasibility, Sep. Sci. Tech., 44 (2009) 2840-2869.
26. J. Eom, H. Yeom, Y. Kim, I. Song, Ceramic membranes prepared from a silicate and clay-mineral mixture for treatment of oily wastewater, Clays Clay Miner., 63 (2015) 222-234.
27. J. Fang, G. Qin, W. Wei, X. Zhao, L. Jiang, Elaboration of new ceramic membrane from spherical fly ash for microfiltration of rigid particle suspension and oil-in-water emulsion, Desalination, 311 (2013) 113–126.
28. M. Abbasi, M. Mirfendereski, M. Nikbakht, M. Golshenas, T. Mohammadi, Performance study of mullite and mullite-alumina ceramic MF membranes for oily wastewaters treatment. Desalination, 259 (2010) 169-178.
29. J. Mueller, Y. Cen, R. Davis, Crossflow microfiltration of oily water, J. Membr. Sci., 129 (1997) 221-235.
30. S.Z.A. Bukhari, J.H. Ha, J. Lee, I.H. Song, Oxidation-bonded SiC membrane for microfiltration, J. Euro. Ceram. Soc., 38 (2018) 1711-19.
31. A. Bayat, H.R.M. Kazemimoghaddam, T. Mohammadi, Preparation and characterization of γ-alumina ceramic ultrafiltration membranes for pre-treatment of oily wastewater, Desalination Water Treat., 57 (2016) 24322-24332.
32. P. Pastila, V. Helanti, A.P. Nikkila, T. Mantyla, Environmental effects on microstructure and strength of SiC based hot gas filters, J. Euro. Ceram. Soc., 21 (2000) 1261-1268.
33. N. Kayal, A. Dey, O.P. Chakrabarti, Synthesis of mullite bonded porous SiC ceramics by a liquid precursor infiltration method: Effect of sintering temperature on material and mechanical properties, Mater. Sci. Eng., 556 (2012) 789-795.
34. J.H. Eom, Y.W. Kim, I.H. Song, Effects of the initial α-SiC content on the microstructure, mechanical properties and permeability of macroporous silicon carbide ceramics, J. Eur. Ceram. Soc., 32 (2012) 1283-1290.
35. S.K. Woo, K.S. Lee, I.S. Han, D.W. Seo, Y.O. Park, Role of porosity in dust cleaning of silicon carbide ceramic filters. J. Ceram. Soc. Jpn., 109 (2001) 742-747.
36. C.L. Beyler, M.M. Hirschler, Thermal decomposition of polymers. In SFPE Handbook of Fire Protection Engineering, MA, USA. (2001) 1-110.
37. J.H. She, J.F. Yang, N. Kondo, T. Ohji, S. Kanzaki, Z.Y. Deng, High strength porous silicon carbide ceramics by an oxidation-bonding technique, J. Am. Ceram. Soc., 85 (2002) 2852-2854.

38. J.H. Choi, S.M. Keum, J.D. Chung, Operation of ceramic candle filter at high temperature for PFBC application, Korean J. Chem. Eng., 16 (1999) 823-828.
39. Future filtraton silicon carbide ceramic membranes. LiqTech International Ballerup, Denmark, 2014.
40. Pall Dia-Schumalith N Product Catalogue. http://www.pall.com/pdfs/Fuels-and-Chemicals/PIDIASCHUMALNEN.pdf
41. J.H. Eom, Y.W. Kim, S. Raju, Processing and properties of macroporous silicon carbide ceramics: A review, J. Asian Ceram. Soc., 1 (2013) 220–242.
42. D.E. Damby, E.W. Llewellin, C.J. Horwell, B.J. Williamson, J. Najorka, G. Cressey, M. Carpenter, The α–β phase transition in volcanic cristobalite. J. App. Cryst., 47 (2014) 1205-1215.
43. C. Vakifahmetoglu, D. Zeydanli, M.D.M. Innocentini, F.D.S. Ribeiro, P.R.O. Lasso, G.D. Soraru, Gradient hierarchic aligned porosity SiOC Ceramics, Scientific Reports, 7 (2017) 41049.
44. S.C Kim, Y.W. Kim, I.H. Song, Processing and properties of glass-bonded silicon carbide membrane supports, J. Euro. Ceram. Soc., 37 (2017) 1225-1232.
45. S.Z.A. Bukhari, J.H. Ha, J. Lee, I.H. Song, Oxidation-bonded SiC membrane for microfiltration, J. Euro. Ceram. Soc., 38 (2018) 1711-1719.
46. A.K. Bakshi, R. Ghimire, E. Sheridan, M. Kuhn, Treatment of produced water using SiC membrane filters. In: Narayan R, Colombo P, editors. Advances in bio ceramics and porous ceramics VIIII. Florida: Wiley, 2015; p. 91.
47. R. Neufert, M. Moeller, A.K. Bakshi, Dead-end silicon carbide micro-filters for liquid filtration. In: Narayan R, Colombo P, editors. Advances in bio ceramics and porous ceramics VI: ceramicengineering and science proceedings. Hoboken, NJ: John Wiley & Sons, 2013; 34: p. 115–26.
48. S.R. Faibish, Y. Cohen, Fouling and rejection behaviour of ceramic and polymer-modified ceramic membranes for ultrafiltration of oil-in-water emulsions and micro emulsions, Colloids and Surfaces A: Physicochem. Eng. Asp., 191 (2001) 27-40.
49. X.F. Zhang, S.M. Lai, R.M. Aranda, K.L. Yeung, An investigation of Knoevenagel condensation reaction in microreactors using a new zeolite catalyst, Appl. Catal., 261 (2004) 109-118.
50. J. Eom, H. Yeom, Y. Kim, I. Song, Ceramic membranes prepared from a silicate and clay-mineral mixture for treatment of oily wastewater, Clay Clay Miner., 63 (2015) 222-234.

51. M. Abbasi, M. Mirfendereski, M. Nikbakht, M. Golshenas, T. Mohammadi, Performance study of mullite and mullite-alumina ceramic MF membranes for oily wastewaters treatment, Desalination, 259 (2010) 169-178.
52. F.L. Hua, Y.F. Tsang, Y.J. Wang, S.Y. Chan, H. Chua, S.N. Sin, Performance study of ceramic microfiltration membrane for oily wastewater treatment, Chem. Eng. J., 128 (2007) 169–175.
53. L. Yu, M. Han, F. He, A review of treating oily wastewater, Arab J. Chem., 10 (2017) 1913-1922.
54. B. Hofs, J. Ogier, D. Vries, E.F. Beerendonk, E.R. Cornelissen, Comparison of ceramic and polymeric membrane permeability and fouling using surface water, Sep. Purif. Tech., 79 (2011) 365-374.
55. W. Park, S. Jeong, S. JuIm, A. Jang, High turbidity water treatment by ceramic microfiltration membrane: Fouling identification and process optimization, Environ. Technol. Innov., 17 (2020) 100578.
56. H. Elomari, B. Achiou, A. Karim, M. Ouammou, A. Albizane, J. Bennazh, S.A. Younssi, I. Elamrani, Influence of starch content on the properties of low cost microfiltration membranes, J. Asian Ceram. Soc., 5 (2017) 313-319.
57. B. Chakrabarty, A.K. Ghoshal, M.K. Purkait, Ultrafiltration of stable oil-in-water emulsion by polysulfone membrane, J. Membr. Sci., 15 (2008) 427-437.
58. D. Vasanth, G. Pugazhenthi, R. Uppaluri, Cross-flow microfiltration of oil-in-water emulsions using low cost ceramic membranes, Desalination, 320 (2013) 86-95.
59. S.S. Rajanna, G.M. Madhu, C.D. Madhusoodana, A. Govindarajan, Silicon carbide-coated ceramic membrane bioreactor for sustainable water purification, Membranes, 9 (2019) 47.
60. G. Martins, D. Olson, G. Edwards, Modeling of infiltration kinetics for liquid metal processing of composites, Metall. Mater. Trans. B, 19 (1988) 95-101.
61. I.J. Častvan, S. Lazarević, D. Tanasković, A. Orlović, R. Petrović, D. Janaćković, Phase transformation in cordierite gel synthesized by non-hydrolytic sol–gel route, Ceram. Int., 33 (2007) 1263-1268.
62. N.M. El-Buaishi, I.J. Častvan, B. Jokić, D. Veljović, D. Janaćković, R. Petrović, Crystallization behavior and sintering of cordierite synthesized by an aqueous sol–gel route, Ceram. Int., 38 (2012) 1835-1841.
63. S. Baitalik, N. Kayal, Processing and properties of cordierite- silica bonded porous SiC ceramics, Ceram. Int., 43 (2017) 14683-92.
64. E. Rabinovich, Preparation of glass by sintering, J. Mat. Sci., 20 (1985) 4259-4297.

65. S. Ding, Y.P. Zeng, D. Jiang, Gas permeability behaviour of mullite- bonded porous silicon carbide ceramics, J. Mater. Sci., 42 (2007) 7171-7175.
66. W. Shi, B. Liu, X. Deng, J. Li, Y. Yang, In-situ synthesis and properties of cordierite-bonded porous SiC membrane supports using diatomite as silicon source, J. Euro. Ceram. Soc., 36 (2016) 3465-3472.
67. R.W. Carnahan, Elastic properties of silicon carbide, J. Am. Ceram. Soc., 51 (1968) 223–224.
68. P. Pastila, A.P. Nikkila, T. Mantyla, E.L. Curzio, Effect of thermal cycling to the strength and fracture of SiC–based candle filters, Ceram. Eng. Sci. Proc., 23 (2002) 607–613.
69. E.Z. Hayati, O.M. Moradi, M.G. Kakroudi, Investigation the effect of sintering temperature on Young's modulus evaluation and thermal shock behaviour of a cordierite–mullite based composite, Mater. Des., 45 (2013) 571-575.
70. T. Tsuzuki, N. Mitamura, Glass composition, US Pat. 0273635 A1; 2010.
71. R.W. Rice, Extension of the exponential porosity dependence of strength and elastic moduli, J. Am. Ceram. Soc., 59 (1976) 536–537.
72. R.W. Rice, Evaluation and extension of physical property-porosity models based on minimum solid area, J. Mater. Sci., 31 (1996) 102-118.
73. S. Liu, Y.P. Zeng, D. Jiang, Fabrication and characterization of cordierite- bonded porous SiC ceramic, Ceram, Int., 35 (2009) 597–602.
74. J. She, J.F. Yang, N. Kondo, T. Ohji, S. Kanzaki, Z.Y. Deng, High- Strength Porous Silicon Carbide Ceramics by an Oxidation- Bonding Technique, J. Am. Ceram. Soc., 85 (2002) 2852-2854.
75. Y.S. Chun, Y.W. Kim, Processing and mechanical properties of porous silica-bonded silicon carbide ceramics, Met. Mater. Int., 11 (2005) 351-355.
76. C.Y. Bai, X.Y. Deng, J.B. Li, Y.N. Jing, W.K. Jiang, Z.M. Liu, Y. Li, Fabrication and properties of cordierite–mullite bonded porous SiC ceramics, Ceram. Int., 40 (2014) 6225-6231.
77. J.H. Eom, Y.W. Kim, Effect of initial α-phase content on microstructure and flexural strength of macroporous silicon carbide ceramics, Met. Mater. Int., 18 (2012) 379-383.
78. A. Dey, N. Kayal, O.P. Chakrabarti, R.F. Caldato, C.M. Andre, M.D.M. Innocentini, Permeability and nanoparticle filtration assessment of cordierite- bonded porous SiC ceramics, Ind. Eng. Chem. Res., 52 (2013) 18362–18372.

79. S. Liu, Y.P. Zeng, D. Jiang, Effects of CeO_2 addition on the properties of cordierite- bonded porous SiC ceramics, J. Euro. Ceram. Soc., 29 (2009) 1795–1802.
80. M.D. Allen, O.G. Raabe, Slip correction measurements of spherical solid aerosol particles in an improved Millikan apparatus, Aerosol Sci. Technol., 4 (1985) 269–286.
81. E. Gal, G. Tardos, R. Pfeffer, A study of inertial effects in granular bed filtration, AIChE J., 31 (1985) 1093–1104.
82. Y.M. Kuo, S.H. Huang, W.Y. Lin, M.F. Hsiao, C.C. Chen, Filtration and loading characteristics of granular bed filters, J. Aerosol Sci., 41 (2010) 223–229.
83. H. Yoshida, C. Tien, A new correlation of the initial collection efficiency of granular aerosol filtration, AIChE J., 31 (1985) 1752–1754.
84. N.L. Freitas, J. Gonçalves, M. Innocentini, J.R. Coury, Development of a double- layered ceramic filter for aerosol filtration at high temperatures: the filter collection efficiency, J. Hazard. Mater., 136 (2006) 747–56.
85. H.J. Choi, J.U. Kim, S.H. Kim, M.H. Lee, Preparation of granular ceramic filter and prediction of its collection efficiency, Aerosol. Sci. Technol., 48 (2014) 1070-1079.
86. S.C. Shamkuwar, D.N. Malkhede, S. Ugile, Critical study on rotary fluidized bed as a diesel particulate filter using SiC particles, Mater. Today: Proc., 4 (2017) 653-659.
87. S. Wu, N. Claussen, Reaction bonding and mechanical properties of mullite/silicon carbide composites, J Am. Ceram. Soc., 77 (2005) 2898-2904.
88. V. Viswabaskaran, F.D. Gnanam,Mullite from clay–reactive alumina for insulating substrate application, Applied Clay Sci., 25 (2004) 29-35.
89. X. Miao, Porous mullite ceramics from natural topaz, Mater. Lett., 38 (1999)167-172.
90. J.H. Eom, Y.W. Kim, I.H. Song, H.D. Kim, Microstructure and properties of porous silicon carbide ceramics fabricated by carbothermal reduction and subsequent sintering process, Mater. Sci. Eng., 464 (2007) 129-134.
91. B.V.M. Kumar, J.H. Eom, Y.W. Kim, I.H. Song, H.D. Kim, Effect of aluminum hydroxide content on porosity and strength of porous mullite-bonded silicon carbide ceramics, J. Ceram. Soc. Jpn., 119 (2011) 367–370.
92. Y.H. Choi, Y.W. Kim, I.S. Han, S.K. Woo, Effect of alkaline earth metal oxide addition on flexural strength of porous mullite-bonded silicon carbide ceramics, J. Mat. Sci., 45 (2010) 6841-6844.

93. K.S. Lee, S.K. Woo, I.S. Han, D.W. Seo, S.J. Park, Y.O. Park, Filtering characteristics of porous SiC filter with high surface area, J. Ceram. Soc. Jpn., 110 (2002) 656-661.
94. I.S. Han, D.W. Seo, S. Kim, K.S. Hong, S.K. Woo, Y.W. Kim, Fabrication and properties of SiC candle filter by vacuum extrusion and ramming process (II), J. Korean Ceram. Soc., 47 (2010) 515-523.
95. F. Zhai, S. Li, J. Sun, Z. Yi, Microstructure, mechanical properties and thermal shock behavior of h-BN-SiC ceramic composites prepared by spark plasma sintering, Ceram. Int., 43 (2017) 2413-2417.
96. J.H. She, T. Ohji, S. Kanazaki, Oxidation bonding of porous silicon carbide ceramics with synergistic performance, J. Eur. Ceram. Soc., 24 (2003) 331-334.
97. J. She, T. Ohji, Z.Y. Deng, Thermal shock behaviour of porous silicon carbide ceramics, J. Am. Ceram. Soc., 85 (2002) 2125-2127.
98. S. Ding, Y.P. Zeng, D. Jiang, Thermal shock resistance of in situ reaction bonded porous silicon carbide ceramics, Mater. Sci. Eng. A, 425 (2006) 326-329.
99. S. Ding, Y.P. Zeng, D. Jiang, Thermal shock behaviour of mullite-bonded porous silicon carbide ceramics with yttria addition, J. Phys. D: Appl. Phys., 40 (2007) 2138-2142.
100. P. Pastila, A.P. Nikkila, T. Mantyla, L. Curzio, Effect of thermal cycling to the strength and fracture of SiC- based candle filters, Ceram. Eng. Sci. Proc., 23 (2002) 607-613.
101. G. Li, H. Chen, Effect of repeated thermal shock on mechanical properties of ZrB2-SiC-BN ceramic composites, Sci. World J., 11 (2014).
102. W. Kingery, Factors affecting thermal stress resistance of ceramic materials, J. Am. Ceram. Soc., 38 (1955) 3-15.
103. R.M. Orenstein, D.J. Green, Thermal shock behaviour of open- cell ceramic foams, J. Am. Ceram. Soc., 75 (1992) 1899-1905.
104. J.O. Elizabeth, Variation of the oxidation rate of silicon carbide with water–vapor pressure, J. Am. Ceram. Soc., 82 (1999) 625–636.
105. L. Montanaro, A. Negro, O. Frantz, P. Billard, R. Rezakhanlou, Corrosion of ceramic filters for hot cleaning in thermal power plants, 21 (2008) 561.

Chapter 6

Conclusions and Future Scopes

6.1. Concluding remarks

The present research investigated the effect of different processing parameters on the properties of microporous silicon carbide membrane and explored the application possibilities of the developed membrane in air and water filtration applications. Mullite bonded SiC ceramic (MBSC) membranes were synthesized by a facile solid-state reaction process, using SiC, solid waste fly ash as raw materials and MoO_3 as catalyst followed by sintering at 1000^{o}C. The effect of MoO_3 catalyst on mullitization reaction and mullite morphology was investigated. In another approach, mullite bonded SiC ceramic membranes were synthesized using SiC, alumina and optimum amount of clay or mixture of sintering additives (clay, NaCMC and $CaCO_3$) at 1400^{o}C. The effect of different organic and inorganic pore formers on the microstructure, mechanical strength, porosity and pore size distribution, air and water permeability of porous SiC ceramics were investigated. To determine the suitability of the developed membrane in industrial air and water filtration application, the chemical resistance (at high pH) and thermal shock resistance properties of the membranes were evaluated. The corrosion behaviour of SiC ceramic filter materials in presence of steam, coal ash and both coal ash and steam was investigated at 1000°C for 96–240h to determine the suitability of the material in hot gas filtration. In order to obtain final ceramics with homogeneous distribution of bond phase with improved physical and mechanical properties infiltration assisted technique was used for processing of oxide bonded SiC ceramics followed by infiltrating a porous powder compact of SiC and alumina with cordierite sol followed by sintering at 1300–1400^{o}C in air for 3h and compared their properties with the ceramic prepared by powder processing method. To determine the suitability of the material in particulate filtration application particle collection efficiency of the filter material was evaluated theoretically using single collector efficiency model.

Following conclusions are summarized from the work:

1. A new low-cost method of mullite bonded porous SiC ceramic membrane was developed and showed a new direction for the utilization of an industrial waste coal fly ash. It was observed that by addition of MoO_3, mullitization reaction temperature was significantly reduced and promoted the growth of elongated mullite crystals in the final ceramics and hence improved the flexural strength. The air water permeability and wastewater filtration efficiency results indicated that MBSC membrane prepared by this new method has strong application possibilities in various

fields. This study also suggested an alternative method of recycling the coal fly ash waste not only to reduce its environmental impacts but also to produce high-valued SiC-based porous ceramic membranes for potential oily wastewater separation.

2. The effect of amount of clay content, alumina and sintering temperature on the material properties, microstructure and flexural strength of in situ reaction bonded porous SiC ceramics were investigated. It was found that only 1 wt% clay additive was sufficient to initiate mullitization reaction and formation of MBSC ceramic membrane at 1300^{o}C with considerable mechanical strength. The air permeation results of porous SiC ceramic membrane prepared in this work were within the range of granular and fibrous filters applied for hot gas filtration, indicated application possibility in air filtration. The membrane prepared without pore former showed best result in respect to wastewater filtration efficiency and the membrane prepared with PMMA as pore former showed best permeability results.
3. The % SiC oxidation degree was found to be almost invariant with porosity when porosity was not very high. At higher porosities (> 35%), the % SiC oxidation degree showed a slight increasing trend because of availability of high surface for oxidation of SiC due to burning of the pore former. It was also observed that oxidation of SiC was significantly reduced using optimum amount of clay and alumina content, which resulted better chemical corrosion resistance properties.
4. It was found that mechanical properties of porous SiC ceramics were strongly influenced by three factors: pore size, pore shape, and binder phase. Porosity dependence of the flexural strength was found to follow exponential relation (exponential decay) which could be explained by the empirical model based on minimum solid area (MSA) concept. In comparison to the other types of porous materials with comparable porosity, porous SiC ceramics with a silica bond had the lowest flexural strength. The better mechanical properties of the mullite and cordierite bonded porous SiC ceramics was due to formation of strong neck between SiC particles by the needle-shaped mullite and plate like cordierite grains in the binder phase.
5. It was noticed that the porosity and pore size of porous ceramics could be altered by varying powder size of SiC, sintering temperature, size and shape of the pore former. The size of the pores of the porous SiC ceramics were defined mostly by the primary SiC particle size and the amount of glassy phase formed during the oxide bonding systems. Mostly monomodal distributions of pore sizes were obtained for all

the membranes synthesized using various processing methods and processing parameters, indicated strong interconnection between void spaces and between SiC particles.

6. Parabolic relationship between pressure drop and air velocity for the oxide bonded porous SiC ceramics was confirmed through high quality fitting of experimental data to the Forchheimer's equations. Darcian and non-Darcian permeability coefficients (k_1 and k_2) values for the oxide bonded porous SiC ceramics indicated that they were well within the typical range of permeability coefficients of granular filters (hot gas filters). Permeability coefficient value for the ceramics could be increased by several orders of magnitude by increasing porosity through the use of sacrificial pore former. Thus it was concluded that as per the needs of specific application, desired permeability parameter could be achieved by selection of porosity of filter and corresponding processing parameters.
7. The results of oily wastewater filtration (containing higher than 1500 mg/l oil) test of the as prepared porous SiC membranes showed high removal efficiency (>90%) in terms of oil, TDS, turbidity and COD along with high water flux value. Membrane regeneration was studied by chemical cleaning method and nearly >80% of flux recovery was obtained. Based on these experimental investigations, it was concluded that the prepared membrane could be used to treat oily wastewater and can meet stricter environmental regulations.
8. The present research developed an improved method of preparation multiple oxide bonded porous SiC ceramics by an infiltration of cordierite sol into porous powder compact of SiC and alumina by single infiltration step followed by reaction bonding technique in air at 1300-1400^{o}C. It was observed that using optimum vacuum pressure full saturation of porous body with precursor sol could be achieved by single step infiltration instead of multiple infiltration steps, hence the processing cost was reduced. The amount of cordierite and mullite was found to increase with the increase of sintering temperature which improved the bonding between SiC particles and thus the strength of the sample was improved. The Permeability coefficients of the ceramics were found to increase with porosity and the values of k_1 and k_2 varied in the ranges of 1.3-4×10^{-13} m^2 and 0.3-0.7×10^{-8} m respectively. To determine the suitability of the material in particulate filtration application, particle collection efficiency of the filter material was evaluated theoretically using single collector efficiency model. The

predicted overall particle filtration efficiency of the investigated SiC samples, permeability coefficients and pressure drop values indicated their strong application possibilities in mitigating particulate emissions from industrial flue gases.

9. The corrosion of SiC ceramic filter materials at 1000^{o}C for 96-240h in presence of steam, coal ash and both coal ash and steam were investigated. SEM and XRD results indicated diffusion of fly ash particles into the filter material and formation of additional phase of calcium aluminosilicate after exposure in ash. Ash particles were seen to be present in the interface with the sample surface particularly rich in glassy phase which induced permanent sticking of these grains. Many pores were appeared at the grain boundaries mainly in the contacting bond phase region and also on the glassy surface of the grains. In presence of steam, oxidation degree of SiC was increased and resulted higher amount of cristobalite. Significant reduction of flexural strength was obtained due to corrosion in steam due to formation of cracks at the bonding necks between SiC particles. The further crack propagation was arrested by the pores which opposed further damage. But corrosion was less for samples coated with fly ash. On the basis of the present studies, it turns out that samples prepared with alumina additives showed the best corrosion resistance. Thus corrosion studies indicated that the MBSC ceramics synthesized in this work are stable for long period even in strong aggressive environment and at high temperature which is suitable for many industrial applications.
10. Thermal shock resistance studies as a function of quenching of temperature in water and against number of quenching cycles in air, indicated the porous SiC ceramics synthesized in this study are quite stable due to healing of thermally induced cracks by silica glass phase formed during air oxidation. In summary, the mullite bonded SiC ceramic showed better residual strength values upon thermal shock analyses due to increase of fracture toughness compared to the silica bonded SiC ceramic

All the above results indicated that the membrane prepared in this study are cost effective compared to the reported published results. The membranes obtained with homogeneous distribution of bond phase, narrow pore size distribution, high porosity and flexural strength. The permeability results and wastewater filtration results suggested that the developed membranes can be up scaled for liquid separation processes such as wastewater from various industries, oil/water separation, food, pharmaceutical, etc. and air filtration.

6.2. Future scope

The permeation results OBSC membranes are comparable or even better than literature data. However based on the operating parameters like time, TMP, face velocity, etc., the performance of the membrane at best optimum operating conditions fouling and flux decline, need to be investigated. There is high probability for the integration of OBSC membranes with high permeability and a long lifetime for process intensification and the purification of products in various industries. The demand of SiC membranes are increasing particularly in the liquid separation processes such as wastewater from various industries, oil/water separation, food, pharmaceutical, etc. SiC membranes are envisaged to have a great potential for particulate separation from hot gas, control of pollutant gases (VOC, SOx, NOx), catalytic membrane reactor for generation and separation of hydrogen (clean energy production), conversion of greenhouse gases to value added product, catalyst support, etc. The processing of porous ceramics by oxidation bonding technique has been continuously improving to meet the requirement of microstructure, pore characteristics and properties as per the need of application areas. Further improvement of their processes, functionalization of support SiC membrane will definitely meet the growing demand of SiC based filter in the near future in new applications. The deployment of the oxide bonded SiC ceramic membrane in industrial scale need to be started immediately.

Journal of the European Ceramic Society 40 (2020) 2163–2172

Contents lists available at ScienceDirect

Journal of the European Ceramic Society

journal homepage: www.elsevier.com/locate/jeurceramsoc

Original Article

Recycling of coal fly ash for fabrication of elongated mullite rod bonded porous SiC ceramic membrane and its application in filtration

Dulal Das[a], Nijhuma Kayal[a,*], Gabriel Antonio Marsola[b], Daniel Gonçalves Parra Filho[b], Murilo Daniel de Mello Innocentini[b]

[a] CSIR, Central Glass and Ceramic Research Institute, CSIR, Kolkata, 700 032, West Bengal, India
[b] Course of Chemical Engineering, University of RibeirãoPreto (UNAERP), 14096-900 RibeirãoPreto, SP, Brazil

ARTICLE INFO

Keywords:
Recycling of fly ash
SiC membrane
Mechanical strength
Wastewater treatment
Permeability

ABSTRACT

Mullite bonded SiC ceramic membranes were synthesized by a facile solid-state reaction process, using SiC, solid waste fly ash as raw materials and MoO_3 as catalyst for growth of mullite at 1000 °C. The effect of MoO_3 catalyst on mullitization reaction and mullite morphology was investigated. Different pore formers were used to enhance the porosity and to observe its effects on the permeability parameters and filtration characteristics. At room temperature Darcian (k_1) and non-Darcian (k_2) in both water and air flow were measured and clean water flux was determined. The porous SiC ceramics with addition of 5 wt.% MoO_3 exhibited a flexural strength of 38.4 MPa at porosity 36.4 vol% and showed 92% oil removal efficiency from oily wastewater. This technique, combining low-cost materials and the co-sintering at low temperature, can serve as a cost-effective method for the production of high-performance porous SiC ceramic membrnaes for filtration application.

1. Introduction

Porous silicon carbide (SiC) ceramics have been considered as an ideal candidate for several industrial applications, such as hot gas cleanup, water and wastewater filtration, melt metal filtration, catalytic support in some typical catalytic processes both for gas-phase and liquid-phase reactions, etc., owing to their low bulk density, high permeability, high temperature stability, corrosion resistance, medium thermal conductivity, etc. [1–6]. SiC membranes have a high potential for oil separation and oily wastewater treatment applications because of their excellent corrosion resistance, hydrophilicity, superb fouling resistance due to negative charge on the material surface [7], low water contact angle [8], high water permeability, etc. Therefore, longer membrane lifetime is expected using SiC based membranes [9]. The literature barely mentioned the application of oxide bonded SiC membranes for oily wastewater treatment. In practical applications, the permeability of porous media needs to be quantified to investigate the efficiency of the filter material. However, very limited information about the permeability of porous SiC ceramics exists in the literature [10,11].

The direct fabrication of SiC ceramics is rather difficult below 2100 °C due to the strong covalent nature of the Si—C bond [12]. To decrease the processing temperature, the most common solutions is the oxidation-bonding technique that involves heating the powder compact of SiC and sintering additives in air instead of an inert atmosphere [13,14]. Therefore, the oxide bonded SiC ceramics exhibit good oxidation resistance.

Further membrane structure modifications maintaining the SiC membrane performance are needed to reduce production time and costs. One option is the use of low-cost raw materials. For instance, coal ash is generated worldwide in large amounts as a by-product from thermal power plants. Environment-friendly utilization of coal fly ash is an important subject because of the measures needed for the prevention of environmental pollution. Currently coal ash is used in brick manufacturing, road and dam construction, backfill, etc., although large amounts are still disposed without environmental concern [15]. During the last decade, several researchers have used coal ash for the processing of oxides composite materials, sialon, zeolites, sorbents, etc. [16–18]. So far, there are a few documents about the preparation of porous ceramics [16,19–21] especially, preparation of porous SiC ceramic from coal ash [22,23]. The present study aims at recycling industrial waste fly ash for processing of a porous SiC ceramic support at low temperature with increased mechanical resistance and permeability to fluid flow.

In this work, mullite bonded SiC ceramics (MBSC) with porous structure composed of elongated mullite rod was prepared using

* Corresponding author.
E-mail address: nijhuma@cgcri.res.in (K. Nijhuma).

https://doi.org/10.1016/j.jeurceramsoc.2020.01.034
Received 30 October 2019; Received in revised form 8 January 2020; Accepted 16 January 2020
Available online 17 January 2020
0955-2219/ © 2020 Elsevier Ltd. All rights reserved.

Trans. Ind. Ceram. Soc., vol. 80, no. 3, pp. 186-192 (2021).
© 2021 Indian Ceramic Society
ISSN 0371-750X (Print), ISSN 2165-5456 (Online)
http://dx.doi.org/10.1080/0371750X.2021.1934122

Permeability Behavior and Wastewater Filtration Performance of Mullite Bonded Porous SiC Ceramic Membrane Prepared Using Coal Fly Ash as Sintering Additive

Dulal Das,[a] Nijhuma Kayal[a,*] and Murilo Daniel de Mello Innocentini[b]

[a]CSIR-Central Glass and Ceramic Research Institute, CSIR, Kolkata–700032, West Bengal, India
[b]Course of Chemical Engineering, University of RibeirãoPreto (UNAERP), 14096-900 RibeirãoPreto, SP, Brazil

[MS received December 31, 2020; Revised copy received April 30, 2021; Accepted April 30, 2021]

ABSTRACT

With SiC as starting powder, waste fly ash as sintering additive and metal oxide as catalyst, mullite bonded SiC ceramic membrane was prepared at 1000°C using the conventional solid-state reaction method. Permeability parameters in both air and water flow tests were obtained using laboratory made set-up and the pure water permeability was measured at variable transmembrane pressures. The membrane exhibited excellent pure water flux of 5261 $L.m^{-2}.h^{-1}.bar^{-1}$ with open porosity of 44.7% and mean pore size of 3.7 μm. With this membrane a high oil removal efficiency of 91% was achieved from the kitchen wastewater having initial oil concentration of 1657 $mg.L^{-1}$. The method developed here is technologically benign and addressed prevention of environmental pollution by utilizing hazardous waste material for fabrication of porous SiC ceramic membrane at a reduced cost with good mechanical, permeability characteristics and wastewater filtration efficiency. Hence, the proposed method for SiC membranes has good sustainability and is scalable for oily wastewater treatment.

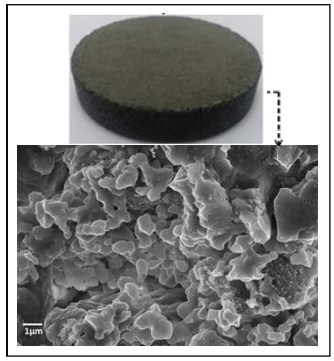

[Keywords: Microfiltration membrane, Microstructure, Air permeability, Wastewater treatment]

Introduction

Rapid industrialization and urbanization leads to the production of highly concentrated (100-1000 $mg.L^{-1}$) oil-water (O/W) emulsion mainly from metallurgical, petroleum and food processing industry.[1] Separation of oil from oil-wastewater has been considered as an urgent need for many industrial processes as well as for domestic purpose because of its destructive impact on ecosystem and harmful effect on human life and it is very difficult to separate.[2, 3] Initially several methods, such as coagulation, electro-coagulation, dissolved air flotation, gravity separation, de-emulsification, skimming and flocculation, etc[4–7] were employed for separation but these methods are not efficient for separation and they also produced secondary waste product in large quantities.

Therefore in recent decades there has been increasing interest on the use of porous ceramic membrane in the separation field, e.g. oily wastewater filtration, hot gas filtration, separation of hydrogen, etc due to its high chemical stability, low fouling properties and long life time compared to polymeric membrane.[8–10] The ceramic membrane materials used for the separation of oil wastewater are mainly oxides, such as Al_2O_3, TiO_2, SiO_2 and ZrO_2, however, SiC is considered as a more suitable membrane material for separation of oily wastewater as it has strong hydrophilic nature, superb fouling resistance property, better chemical stability, high flux value, etc.[11–13] SiC membranes have various configurations, such as flat, tubular and hollow fibers.[14] For large scale applications, the hollow fiber configuration has higher packing density and higher water flux than that of the flat membrane.[15] However, most oil-in-water (O/W) emulsion separation studies were carried out using SiC ceramic membrane sintered at ~2100°C owing to the strong covalent nature of Si-C bond.

So far few reports are available on oxide bonded SiC membrane prepared at low temperature for wastewater filtration.[16, 17] Recently SiC membrane has been prepared in an air atmosphere at 1000°C using zeolite residues and its performance has been examined in O/W emulsion separation process.[18] Oxide-bonding is considered as one of the most simple and cost effective techniques for fabrication of macroporous SiC membrane where the oxidized silica reacts with some additives leading to the formation of a bonding phase between the SiC particles at a very low temperature, which enhances its mechanical strength. Moreover, the oxidized SiC surface could lower the water contact angle, improve the hydrophilic property

*Corresponding author; email: nijhuma@cgcri.res.in

Received: 19 December 2019 | Revised: 19 December 2019 | Accepted: 26 December 2019

DOI: 10.1111/ijac.13463

Check for updates

International Journal of Applied Ceramic Technology

ORIGINAL ARTICLE

Permeability behavior of silicon carbide-based membrane and performance study for oily wastewater treatment

Dulal Das[1] | **Nijhuma Kayal**[1] | **Gabriel Antonio Marsola**[2] | **Leonardo Augusto Damasceno**[2] | **Murilo Daniel de Mello Innocentini**[2]

[1]CSIR-Central Glass and Ceramic Research Institute, CSIR, Kolkata, India

[2]Course of Chemical Engineering, University of Ribeirão Preto (UNAERP), Ribeirão Preto, Brazil

Correspondence
Nijhuma Kayal, CSIR-Central Glass and Ceramic Research Institute, CSIR, Kolkata-700 032, West Bengal, India.
Email: nijhuma@cgcri.res.in

Funding information
Science and Engineering Research Board, Grant/Award Number: GAP0261; SERB; Department of Science and Technology; CNPq, Grant/Award Number: 307259/2018-8

Abstract

Porous SiC ceramic is considered as a suitable material for hot gas filtration, microfiltration, and many others industrial applications. However, full utilizations of porous SiC ceramics have been limited by high-processing costs. In this study, mullite-bonded porous SiC ceramics membranes were prepared using commercial SiC powder, alumina, clay, and different sacrificial pore formers. The effect of different pore formers on the microstructure, mechanical strength, porosity and pore size distribution, air, and water permeability of porous SiC ceramics were investigated. The average pore diameter, porosities, and flexural strength of the final ceramics varied in the range 3.7-6.5 μm, 38-50 vol. %, and 28-38 MPa, respectively, depending on the characteristics of pore former. The Darcian (k_1) and non-Darcian (k_2) permeability evaluated from air permeation behavior at room temperature was found to vary from 1.48×10^{-13} to 4.64×10^{-13} m^2 and 1.46×10^{-8} to 6.51×10^{-8} m, respectively. All membranes showed high oil rejection rate (89%-93%) from feed wastewater with oil concentration of 1557 mg/L. The membrane with porosity ~48 vol% and mechanical strength 31.5 MPa showed and highest pure water permeability of 13 298 $Lm^{-2}h^{-1}bar^{-1}$.

KEYWORDS

fluid flow properties, membrane, microstructure, silicon carbide

1 | INTRODUCTION

Silicon carbide (SiC) is one of the most promising membrane materials for various applications, such as particulate filtration from hot flue gases, water treatment, hydrogen separation, etc, because of its excellent mechanical and chemical stability, high-temperature corrosion resistance, high thermal conductivity, and high thermal shock resistance.[1–8] Oily wastewater emulsions are one of the main industrial pollutants emitted into aquatic environments, which are difficult to treat. The metallurgical, petrochemical, textile, oil-refinery industries produce oily wastewater emulsions in the concentration range of 50-1000 mg/L.[9] Whether it is for disposal or reuse, oily water treatment has become a major focus in industries during the past decade. Ceramic membranes technology has been widely used and suggested for treatment of oily wastewater.[10–15] Membrane technology has several advantages over conventional treatment methods, as it produces lower variation in permeate quality by variation in feed water quality, does not require to add chemicals prior to separation, requires small space, produces lower sludge, produces high-quality permeate, etc. On the other hand, SiC-based ceramic gas filters raise new hopes and bring new opportunities as they show possibilities of mitigating particulate emissions in many advanced power production technologies, chemical industries, etc. Most of the previous high-temperature dust removal studies were carried out with commercial SiC

 © 2019 The American Ceramic Society

Membrane and Water Treatment, *Vol. 12, No. 3 (2021) 133-138*
DOI: https://doi.org/10.12989/mwt.2021.12.3.133

Effect of processing parameters on mullite bonded SiC membrane for turbid water filtration

Dulal Das[1], Nijhuma Kayal*[1], Murilo D.M. Innocentini[2] and Daniel G.P. Filho[2]

[1]*CSIR-Central Glass and Ceramic Research Institute, CSIR, Kolkata-700 032, West Bengal, India*
[2]*Course of Chemical Engineering, University of RibeirãoPreto (UNAERP), 14096-900 RibeirãoPreto, SP, Brazil*

(Received August 7, 2020, Revised June 2, 2021, Accepted June 3, 2021)

Abstract. A water-filtration membrane made of SiC possesses some excellent properties, but its application is limited by high fabrication cost. In this study, two sets of mullite bonded porous SiC ceramics membranes were prepared at reduced temperature by oxidation bonding method using different processing conditions. Dead-end filtration mode was utilized for the determination of permeability and their efficiency towards removal of turbidity. It was found that all the membranes prepared using different composition, pore formers (graphite, PVC and PMMA) and sintering temperature exhibited high turbidity removal efficiency (> 99%). This study provides an efficient method to prepare porous SiC ceramics with excellent permeability and turbidity removal efficiency, which will be helpful for the design of low cost SiC ceramic filters for water treatment.

Keywords: membrane; microfiltration; SiC ceramic; turbidity

1. Introduction

In the rainy season, high-turbidity water has been reported as a challenge for water treatment facilities and turbidity is the most problematic factor in water treatments (Kan *et al*. 2002, Mann *et al*. 2007, Bilotta and Brazier 2008). The higher turbidity level in drinking water causes risk to human health due to the suspended solids contaminated with viruses, bacteria etc. (Mann *et al*. 2007, Bilotta and Brazier 2008). Ceramic membranes are mainly used to remove particles contained in drinking water; however, they have recently been gradually expanded to other water treatments (Chang and Liao 2003, Ciora and Liu 2003, Cha *et al*. 2019, Jang and Lee 2018). Coagulation/flocculation pre-treatments, combined with ceramic MF membrane filtration, are nowadays seen as an alternative, less energy-consuming membrane process for microbial, natural organic matter and turbidity removal (Li *et al*. 2010, Meyn and Leiknes 2010, Maddah and Chogle 2015). Membranes used in MF/UF operations are very similar to conventional filters, with a rigid, highly porous structure of randomly distributed and interconnected voids. However, these pores differ from those in a conventional filter by being extremely small, in the order of 0.01–10 μm in diameter (Baker 2012, Gitis and Rothenberg 2016). According to the pore size distribution of the membrane, all particles larger than the largest pores are completely rejected by the membrane and particles smaller than the largest pores but larger than the smallest pores are partially rejected (Baker 2012). Ceramic membranes are mainly made from inorganic ceramic materials (zirconia, alumina, titania, SiC etc.) and consist of several layers of one or more expensive ceramic material with direct bearing on the commercial ceramic membrane price (Li 2007, Mulatu 2014, LiqTech International 2014). Therefore development of low cost ceramic membrane is highly demanding in separation and purification technologies. SiC based ceramic filters promote new opportunities as they show possibilities of wastewater treatment in many advanced chemical and oil industries but again are limited by high fabrication cost. To reduce high sintering temperature and costly inert atmosphere, oxide-bonding technique is accepted as a simple technique for fabrication of macro porous SiC membrane (Kim *et al*. 2017, Bukhari *et al*. 2017, Das *et al*. 2020a, b). In the oxide bonding technique, powder mixtures of SiC, with and without oxide additives (Al_2O_3, MgO, etc.) and pore former are heated in air instead of an inert atmosphere. At the heating stage, the oxidation derived SiO_2 glass from surface oxidation SiC particles crystallize to cristobalite and simultaneously reacts with oxide additive to form secondary oxide bond phases like, mullite, cordierite, etc., depending on the types of additive used.

The detailed studies on applicability of oxide bonded SiC ceramic membrane for treatment of waste water with high turbidity are very few. The aim of the present work is to explore the applicability of porous SiC ceramic membrane in removal of turbidity from drinking water. The membranes used in this study were prepared using two different sintering aids, e.g., (a) small amount of clay and (b) fine industrial waste fly ash. The effect of organic (PMMA and PVC) and inorganic (graphite) pore formers on the pore structures of ceramics and efficiency of turbidity removal are evaluated.

*Corresponding author, Ph.D.
E-mail: nijhuma@cgcri.res.in

Copyright © 2021 Techno-Press, Ltd.

ISSN: 2005-8624 (Print), 2092-7037 (Online)

Received: 15 July 2019 | Revised: 15 July 2019 | Accepted: 27 September 2019

DOI: 10.1111/ijac.13402

Check for updates

International Journal of Applied Ceramic TECHNOLOGY

ORIGINAL ARTICLE

Properties of multiple oxide-bonded porous SiC ceramics prepared by an infiltration technique

Dulal Das | **Sanchita Baitalik** | **Nijhuma Kayal**

CSIR-Central Glass and Ceramic Research Institute, Kolkata, India

Correspondence
Nijhuma Kayal, CSIR-Central Glass and Ceramic Research Institute, 196, Raja S. C. Mullick Road, Kolkata 700 032, India.
Email: nijhuma@cgcri.res.in

Funding information
SERB, Department of Science and Technology, Government of India, Grant/Award Number: GAP-0261

Abstract

Multiple oxide-bonded porous SiC ceramics were fabricated by infiltrating a porous powder compact of SiC and alumina with cordierite sol followed by sintering at 1300-1400°C in air for 3 hours. The microstructures, phase components, mechanical properties, and air permeation behavior of the developed porous ceramics were examined and compared with materials obtained by the traditional powder processing route. The porosity, average pore diameter, and flexural strength of the ceramics varied from 33 to 37 vol%, ~12-14 μm and ~23-39.6 MPa, respectively, with variation in sintering temperature. The X-ray diffraction results reveal that both the amount of cordierite and mullite as the binder increased with increase in sintering temperature. In addition, it was found that the addition of alumina in powder form effectively enhanced the strength due to formation of mullite in the bond phase in contrast to the samples prepared without alumina additive. To determine the suitability of the material in particulate filtration application, particle collection efficiency of the filter material was evaluated theoretically using single collector efficiency model.

KEYWORDS

cordierite, permeability, porous material, silicon carbide

1 | INTRODUCTION

Increasing particle pollution in industrial waste has led to increasing regulations in order to control and to limit these atmospheric pollutants. Hot gas filtration from industrial flue gases not only improves the process efficiencies but also increases heat recovery and protects the plant from corrosion. In advanced coal-fueled processes, flues coming out from gasifiers or combustion boilers at high temperatures are cleaned from entrained particles by ceramic filters and fed to downstream turbines.[1–5] Porous SiC ceramics are most recommended materials for filtration of hot flue gas especially for pressurized fluidized bed combustion, integrated gasification combined cycle processes, industrial wastes management processes, etc.[6–15] The advantageous properties such as high temperature strength, low thermal expansion coefficient, excellent thermal shock resistance, high abrasion, and erosion resistance and extreme inertness even at high temperatures make porous SiC bodies useful for such applications. For hot gas filtration process, the ceramic filters need to resist the chemical attack at high temperature (600-900°C) and high pressure (6-10 atm) by variety of gases and also need to withstand the mechanical stress or thermal shock in the pulse cleaning process.[16,17] Low pressure drop values are always useful, as they can decrease the pumping power required in filtration processes. Permeability is also important in filter designing, as it ultimately determines the type and power of blowers or compressors to be used to force the fluid through the filtering medium. Literature survey indicates that processing of suitable SiC material for such application is still challenging. Oxide bonding is one of the major techniques that has been used for the synthesis of porous SiC ceramics at low temperatures (1300-1550°C) under an ambient atmosphere using commercial-grade raw powders.[18–23] The

Materials Science Forum
ISSN: 1662-9752, Vol. 978, pp 454-462
doi:10.4028/www.scientific.net/MSF.978.454
© 2020 Trans Tech Publications Ltd, Switzerland
Submitted: 2019-01-14
Accepted: 2019-07-01
Online: 2020-02-19

The Effect of Bond Phase Additive and Sintering Temperature on the Properties of Mullite Bonded Porous SiC Ceramics

Dulal Das, Nijhuma Kayal*

CSIR-Central Glass and Ceramic Research Institute, 196, Raja S. C. Mullick Road, Kolkata 700 032, India

*Corresponding author. Tel.: +91-33-23223241; FAX: +91-33-24730957

*Corresponding author: nijhuma@cgcri.res.in

Keywords: Porous SiC; mullite; mechanical properties; microstructure

Abstract. Porous mullite-bonded silicon carbide (SiC) ceramics were prepared from SiC and alumina powders along with other sintering additives. The alumina content was varied from 5-10 wt%, and porous SiC ceramics were fabricated via reaction sintering at 1300-1500°C for 4 h. The microstructure showed large SiC grains embedded in a matrix of small mullite and silica particles. It was demonstrated that the porosity decreased and flexural strength increased with increase in alumina content. The porosity varied from 27-38 vol% and flexural strength varied from 25 to 58 MPa with the variation in alumina content and sintering temperature. Typically, porous mullite-bonded SiC ceramics prepared at 1400^{o}C with 10 wt% alumina additive exhibited highest mechanical strength of ~ 58 MPa at porosity level ~27 vol. %.

1. Introduction

Currently, porous SiC ceramics have been a focus of interesting research in the field of porous materials due to their excellent structural properties, high strength, high hardness, and superb mechanical and chemical stabilities even at high temperatures and hostile atmospheres. Porous SiC ceramics have been considered as suitable candidate materials for catalyst supports [1-2], hot gas or molten metal filters [3], high temperature membrane reactors [4], thermal insulating materials [5], gas sensors [6] etc. Porous SiC ceramics are fabricated by various methods including partial sintering [7], carbothermal reduction [8-9], replication or pyrolysis of polymeric sponge [10-12], reaction bonding [13] etc. In all these methods SiC needs to be sintered which requires a very high temperature due to the strong covalent nature of the Si-C bond, selective sintering additives, expensive atmosphere, costly and delicate instrumentation. Processing of porous SiC ceramics at low temperature using a simple technique thus becomes necessary. Bonding of SiC can be done at low temperatures by use of different oxide and non-oxide secondary phases. They include silica, mullite, cordierite, silicon nitride, etc. Various sintering additives are used for the formation of variety of secondary oxide bond phases for formations for porous SiC [14-19] Choice of mullite as a bond for SiC has many advantages. Mullite possesses a high melting point (T_m= 1850^{o}C) and a low oxygen diffusion coefficient (5.6 x 10^{-14} m^2/sec at 50^{o}C). It has a matching thermal expansion coefficient with SiC ($CTE_{mullite}$= 5.3 ×10^{-6}/K; CTE_{SiC} = 4.7 ×10^{-6}/K at RT-1000 ^{o}C) and a high strength that can be retained up to a very high temperature. Different sources of aluminum, such as Al_2O_3, Al, AlN, and $Al(OH)_3$ powders were used for the formation of mullite bonded porous SiC ceramics (MBSC) [20-21]. However, the mullitization temperature of 1550^{o} C is still necessary. In this work, mullite bonded porous SiC ceramics were fabricated by an in situ reaction-bonding process; the mixture of clay and $CaCO_3$ were chosen as sintering additives to lower the mullitization reaction between Al_2O_3 and oxidation-derived SiO_2. The effect amount of alumina, sintering temperature and other sintering aids on material property such as porosity/pore size distribution mechanical and micro structural properties of porous oxide bonded SiC ceramics were studied.

All rights reserved. No part of contents of this paper may be reproduced or transmitted in any form or by any means without the written permission of Trans Tech Publications Ltd, www.scientific.net. (#539697997, University of Warwick, Coventry, United Kingdom-24/05/20,09:19:49)

BOLETIN DE LA SOCIEDAD ESPAÑOLA DE
Cerámica y Vidrio
www.elsevier.es/bsecv

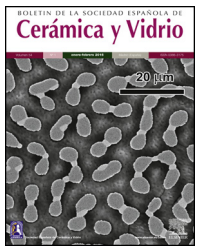

Influence of fly ash and steam on microstructure and mechanical properties of oxide bonded porous SiC ceramics

*Dulal Das, Nijhuma Kayal**

CSIR-Central Glass and Ceramic Research Institute, 196, Raja S.C. Mullick Road, Kolkata 700 032, India

ARTICLE INFO

Article history:
Received 9 October 2018
Accepted 29 May 2019
Available online 22 June 2019

Keywords:
SiC filter
Corrosion
Microstructure
Mechanical strength

ABSTRACT

Ceramic filters specially SiC filters are used in advanced coal combustion and gasification processes to remove fine dust particles from the fuel gas at high temperatures and high pressure for protection of turbine blades and other downstream components from corrosion and erosion and to meet the environmental regulations. Processing of corrosion resistant porous SiC ceramics at low temperature using a simple technique is still challenging. In this study oxide bonded porous SiC ceramics were synthesized by cost effective method. The corrosion behaviour of SiC ceramic filter materials in presence of steam, coal ash and both coal ash and steam was investigated at 1000 °C for 96–240 h. The apparent changes in mass, porosity and density with corrosion duration and environment were recorded. Finally SEM, XRD and mechanical tests of the corroded samples were carried out. The corrosion test results indicated water vapour is the perpetrator for strength degradation.

© 2019 SECV. Published by Elsevier España, S.L.U. This is an open access article under the CC BY-NC-ND license (http://creativecommons.org/licenses/by-nc-nd/4.0/).

Influencia de las cenizas volantes y el vapor de agua en la microestructura y las propiedades mecánicas de las cerámicas porosas de SiC ligadas mediante óxidos

Palabras clave:
Filtro de SiC
Corrosión
Microestructura
Resistencia mecánica

RESUMEN

Los filtros cerámicos, especialmente los filtros de SiC, se utilizan en procesos avanzados de combustión y gasificación de carbón para eliminar las de polvo fino partículas en suspensión del gas combustible, a altas temperaturas y altas presiones, para proteger los álabes de las turbinas, y otros componentes aguas abajo, de la corrosión y la erosión y para cumplir con las regulaciones ambientales. El procesamiento de cerámicas porosas de SiC resistentes a la corrosión a baja temperatura utilizando una técnica simple sigue siendo un desafío. En este estudio, las cerámicas porosas de SiC ligadas mediante óxidos se sintetizaron mediante un método rentable. El comportamiento a la corrosión de los filtros cerámicos de SiC en presencia de vapor de agua, ceniza de carbón y ceniza de carbón y vaporde agua se investigó a 1000° C durante 96-240 horas. Se registraron los cambios aparentes en masa, porosidad

* *Corresponding author.*
E-mail address: nijhuma@cgcri.res.in (N. Kayal).
https://doi.org/10.1016/j.bsecv.2019.05.003
0366-3175/© 2019 SECV. Published by Elsevier España, S.L.U. This is an open access article under the CC BY-NC-ND license (http://creativecommons.org/licenses/by-nc-nd/4.0/).

Trans. Ind. Ceram. Soc., vol. 78, no. 3, pp. 165-171 (2019).
© 2019 Indian Ceramic Society
ISSN 0371-750X (Print), ISSN 2165-5456 (Online)
http://dx.doi.org/10.1080/0371750X.2019.1665478

Thermal Shock Resistance of Porous Silicon Carbide Ceramics Prepared Using Clay and Alumina as Additives

Dulal Das and Nijhuma Kayal*

CSIR-Central Glass and Ceramic Research Institute, 196, Raja S. C. Mullick Road, Kolkata – 700032, India

[MS received November 26, 2018; Revised copy received September 04, 2019; Accepted September 04, 2019]

ABSTRACT

Porous silicon carbide ceramics were prepared by an *in situ* reaction bonding process using clay and alumina as additives. The effects of alumina additive, pore former on phase composition, microstructure, flexural strength and thermal shock resistance of the ceramics were studied. Thermal shock resistance of porous SiC ceramics due to cooling was evaluated as a function of quenching temperatures and quenching cycles using water- and air-quenching technique. It was observed that residual strength of the quenched samples in water decreased with increase in the quenching temperature but was almost independent of quenching cycles. In water quenching, the surface of the sample cooled almost instantly but the inside remained hot which created an uneven thermal profile and generated microcracks in the sample; as a result sudden reduction of flexural strength was observed. The results showed that flexural strength and thermal shock resistance properties of the ceramics prepared with alumina are better than those of the ceramics prepared without alumina and the material was found suitable for hot gas filtration application.

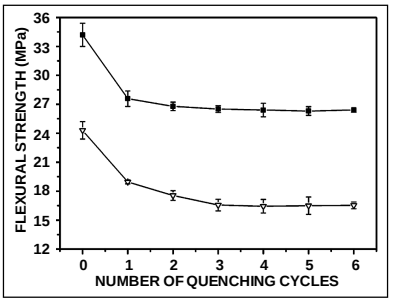

[Keywords: Porous ceramics, Thermal shock, Mechanical strength, Microstructure]

Introduction

The growing needs for energy and the necessity of decreasing carbon dioxide emissions from power plants are enforcing efficient solutions in power generation. New technologies such as gasification systems are being successfully introduced. Composition of the released gas and solid phases depends on the processing parameters, air and/or oxygen content, biomass or coal feed and additive compositions.[1] For further use, the raw gas mixture needs to be cleaned from pollutants like tars, NH_3, H_2S, heavy metal compounds and particulate matter.[2] In the mid-1980s, advanced filtration systems for removal of char and ash fines were developed, installed and operated in pilot or demonstration plants.[1] Porous silicon carbide (SiC) ceramics have been considered as one of the most promising candidates for hot-gas filtration due to its large specific surface, high temperature stability, high permeability, low thermal expansion coefficient and excellent mechanical properties.[3–7] However, SiC ceramics, because of the strong Si–C bond, are usually sintered in inert gas at extremely high temperature above 2000°C.[8] An *in situ* reaction bonding process was developed by She *et al.*[3] to fabricate reaction bonded porous SiC ceramics in air at 1400°-1550°C. In the common clay-bonded SiC ceramic materials, the clay binder content can be around 20%.[9] Creep resistance, corrosion resistance and structural stability of the clay bonded SiC got deteriorated because of degradation of the binder phase at high temperature service environments including steam and alkali, badly affecting the long term durability and reliability of the filter materials.[10–12] Careful selection and use of the additives for binder phase formation have thus become necessary. For hot gas filtration applications, porous SiC ceramics are usually applied under conditions of severe and repeated thermal shock. To check the suitability of the material for any high temperature application, such as metal melting, casting, insulating, light weight structural component, etc, it is necessary to investigate the thermal shock behavior of porous materials. However, very limited information exists in the literature on the effect of thermal shock on mechanical and microstructural properties.[13–16] Theories about thermal shock behavior of the ceramics mainly include the theory of critical thermal stress[17] and the unified theory of fracture initiation and crack propagation.[18]

In the present work, thermal shock resistance of oxide bonded porous SiC ceramics with and without 5.0 wt% Al_2O_3 addition along with reduced amount of clay binder was evaluated by water and air quenching technique as a function of quenching temperature and quenching cycles. Flexural strength of the samples before and after thermal shock tests was measured and the effect of thermal stress on microstructure was evaluated. The mechanism of thermal shock damage was also analysed.

*Corresponding author; email: nijhuma@cgcri.res.in

Author's personal copy

J Porous Mater
DOI 10.1007/s10934-017-0528-5

Preparation and characterization of macroporous SiC ceramic membrane for treatment of waste water

Dulal Das[2] · Sanchita Baitalik[1] · Barun Haldar[1] · Rajnarayan Saha[2] · Nijhuma Kayal[1]

© Springer Science+Business Media, LLC, part of Springer Nature 2017

Abstract Porous SiC based materials present high mechanical, chemical and thermal robustness and thus have been largely applied to water-filtration technologies. In this study, circular disc shaped SiC microfiltration membranes were prepared by dry pressing of commercially available SiC powder with yttria and alumina as additives followed by a low-cost oxide bonding technique. The membranes fabricated were characterized using standard characterization techniques like Scanning Electron Microscopy (SEM), Powder X-ray Diffraction (PXRD), porosity and pore size distribution analysis and compared with the membrane prepared by liquid phase sintering route from the same powder composition. Finally, water permeation studies were carried out in a standard membrane module and clean water flux was determined. These membranes were found well suited for treatment of oily waste water and grey water. The membrane prepared by oxide bonding method effectively removed ~ 89–93% of COD, ~ 77–86% of oil/grease and 88.4–92% of TSS from kitchen waste water and the removal efficiency are better compared to the membrane prepared by liquid phase sintering method. The effects of corrosions on the membranes were investigated in strong acid and alkali solution at 90 °C. The membranes prepared by oxide bonding method showed better corrosion resistance with retention of mechanical strength.

Keywords Macroporous · SiC membrane · Corrosion · Filtration

1 Introduction

Today our water resources are threatened worldwide more than ever due to rapid population growth and industrialization. Water is used in huge quantities in manufacturing industries to process goods [1]. Recently FICCI Water Mission undertook a survey with its member companies to gauge the importance Indian companies attach to water, its conservation and management, risks associated with water, its availability, quality and the subsequent impact on the businesses [2]. To meet the increasing demand of water, waste water needs to be purified and recycled. The domestic waste water or grey water from shower, basin, kitchen sink, washing machine are potentially different from industrial wastewater as they might contain high organic load, soap and detergents, with the main contaminants being proteins, carbohydrates, oil, dissolved and suspended other compounds and harmful pathogens. Ceramic membrane based filtration system (CMS) is the latest technology in the effluent and waste water treatment [3–10]. CMS operates various filtration ranges includes microfiltration, ultrafiltration, fine ultrafiltration and nanofiltration. Though ceramic membranes are more prone to breakage than polymeric membranes, they are extremely suitable to withstand the backwash pressure due to their higher mechanical stability also the ceramic membranes have higher hydrothermal stability, high fluxes at low pressures. Ceramic membrane may be expensive than polymeric membranes; however, these advantages offer adequate benefits in the long run [11, 12]. The application of SiC membranes for water cleaning and liquid separation processes has received recent attention of

✉ Nijhuma Kayal
nijhuma@cgcri.res.in

[1] CSIR-Central Glass and Ceramic Research Institute, 196, Raja S. C. Mullick Road, Kolkata 700 032, India

[2] National Institute of Technology, Mahatma Gandhi Avenue, Durgapur 713209, India

Published online: 09 November 2017

Materials Today: Proceedings xxx (xxxx) xxx

Contents lists available at ScienceDirect

Materials Today: Proceedings

journal homepage: www.elsevier.com/locate/matpr

Influence of clay content on microstructure and flexural strength of in situ reaction bonded porous SiC ceramics

Dulal Das, Nijhuma Kayal *

CSIR-Central Glass and Ceramic Research Institute, 196, Raja S. C. Mullick Road, Kolkata 700 032, India

ARTICLE INFO

Article history:
Received 14 January 2020
Received in revised form 17 February 2020
Accepted 24 February 2020
Available online xxxx

Keywords:
Porous ceramic
Mullite
Reaction bonding
Microstructure

ABSTRACT

The aim of the present study is to reveal the effects of clay contents on in situ reaction bonding of SiC, phase development, microstructure, porosity and mechanical properties of porous SiC ceramics. Porous silicon carbide (SiC) ceramics are prepared in air at 1400 °C for 1 h using alumina as bond phase additive and variable amount of clay as sintering aids and compared their properties. The ceramics prepared with only alumina additive obtained with flexural strength of 28 MPa at porosity 38 vol% without any characteristic peak for mullite. The mullitization was almost completed at 1400 °C with addition of 3 wt% clay. It was found that the addition of clay strongly promoted the phase transformation towards mullite at lower temperature. A high flexural strength of 72 MPa was achieved at porosity level of 33 vol% in the sample prepared with 5 wt% clay due to the enhancement of necks at the contacting points.
© 2020 Elsevier Ltd. All rights reserved.
Selection and Peer-review under responsibility of the scientific committee of the 2nd International Conference on Processing and Characterization of Materials.

1. Introduction

There has been increasing attention on fabrication of porous ceramic membrane because of its versatile applications like catalytic supports, diesel particulate filter, gas burner media, water filtration, gas separation, etc [1–5]. For such applications, the ceramic filter material must be able to withstand the chemical attack by different corrosive atmosphere and mechanical stress. Porous SiC is considered as one of the best membrane material because of its unique combination of properties such as low thermal coefficient value, high chemical resistance, high temperature melting point, high hardness, high thermal shock resistance value, etc. However due to its strong covalent Si-C bond, fabrication of SiC ceramics is quite difficult as it requires very high sintering temperature ~2100 °C [6]. Various processing methods are reported on fabrication of porous SiC ceramics by several researchers such as partial sintering, replica method, sacrificial template, direct foaming, reaction bonding, etc. [7]. Among these methods reaction bonding technique is the easiest and cost effective method for fabrication of SiC ceramics [8]. However, only very limited information about the processing details of SiC based ceramic filters and the influence of different processing parameters on materials properties, mechanical characteristics, microstructure, gas permeation behaviour, etc. are available in the published literature [8–12]. In the common clay-bonded SiC ceramic materials, the clay binder content was kept around 20% [13,14]. The most disadvantages of the clay bonded SiC are they deteriorate because of degradation of the binder phase at the high temperature service environments including steam and alkali. The creep resistance, corrosion resistance and the structural stability of clay bonded SiC ceramic badly affecting the long term durability and reliability of the filter materials [15]. Therefore, careful selection and use of the additives for binder phase formation thus becomes necessary. It is also important to examine the role of SiC oxidation in binder phase formation. Any addition of alumina or aluminium containing materials to the clay binder can promote mullite formation and improve mechanical and corrosion resistance of filter materials. Possible effects of mullitization on binder phase formation need to be investigated. The purpose of the present investigation was to study the exact role of the clay based additive in the formation of the oxide binder phase for SiC; how the binder phase formation is influenced by addition of alumina and finally material and mechanical properties of the oxide bonded porous SiC ceramics.

* Corresponding author.
E-mail address: nijhuma@cgcri.res.in (N. Kayal).

https://doi.org/10.1016/j.matpr.2020.02.862
2214-7853/© 2020 Elsevier Ltd. All rights reserved.
Selection and Peer-review under responsibility of the scientific committee of the 2nd International Conference on Processing and Characterization of Materials.

Please cite this article as: D. Das and N. Kayal, Influence of clay content on microstructure and flexural strength of in situ reaction bonded porous SiC ceramics, Materials Today: Proceedings, https://doi.org/10.1016/j.matpr.2020.02.862

Materials Today: Proceedings xxx (xxxx) xxx

Contents lists available at ScienceDirect

Materials Today: Proceedings

journal homepage: www.elsevier.com/locate/matpr

Permeability and dust filtration behaviour of porous SiC ceramic candle filter

Dulal Das, Nijhuma Kayal *

CSIR-Central Glass and Ceramic Research Institute, 196, Raja S. C. Mullick Road, Kolkata 700 032, India

ARTICLE INFO

Article history:
Received 6 February 2020
Received in revised form 1 April 2020
Accepted 6 April 2020
Available online xxxx

Keywords:
Candle filter
Ramming
Air permeability
Mechanical strength
Dust particle filtration

ABSTRACT

Porous SiC candle filter (~660 mm L and 75 mm OD) were fabricated by ramming process using commercially available SiC powder (d_{50} = 212 μm), with and without alumina and small amount (3 wt %) of clay as the major binder phase additives, following heat treatment at 1400 °C in air. Depending on the composition, porosity of the candle filters varied from 36 to 39 vol% and C-ring strength varied from 15 to 23 MPa. The air permeability and dust filtration efficiency of the candle filter were evaluated using laboratory made test set up. At room temperature, Darcian (k_1) and non-Darcian (k_2) permeability parameters varied from 1.9 to 2.2 × 10^{-12} m^2 and 5.4–9.72 × 10^{-8} m, respectively. Airborne fly ash particle filtration tests showed good performance of SiC candle filter with filtration efficiency of >97%.
© 2020 Elsevier Ltd. All rights reserved.
Selection and Peer-review under responsibility of the scientific committee of the 2nd International Conference on Recent Trends in Metallurgy, Materials Science and Manufacturing.

1. Introduction

Porous SiC ceramic filters are mostly recommended for hot gas cleaning processes [1–4] as they possesses several advantageous properties such as low thermal expansion coefficient, excellent thermal shock resistance, high abrasion and erosion resistance, extreme inertness and mechanical strength even at high temperatures. Oxide bonding technique has been shown to be a very simple, low-temperature and cost-effective processing method for fabrication of porous SiC ceramics. Permeability is also important to filter design, as it ultimately determines the type and power of blowers or compressors used to force the fluid through the filtering medium. In advanced coal-fueled processes for power production (IGCC and PFBC processes) and in biomass gasification/combustion, flues coming out from gasifiers or combustion boilers at high temperatures must be cleaned from entrained particles by ceramic filters and fed to downstream turbines [5–8]. Typical candle filters are cylindrical tubular types, one side is closed and the other side is open. Hundreds of candle filters are set in a large hot gas filter unit and cleaning operations are periodically done to spate and remove dusts from the surface of filter element. The commercial filter candle lengths range from 1000 to 3000 mm with outer diameters between 60 and 150 mm and wall thicknesses between 10 and 20 mm. The useful filtering area (based on the outer candle surface) varies from 0.19 to 1.42 m^2 per element [3,7].

High-pressure drop during filtration means loss of energy and decrease in turbine efficiencies. Low-pressure drop values are always useful, as they can decrease the pumping power required in filtration processes. Permeability is an important property of porous ceramics because it directly correlates with the initial pressure drop of clean filters [9–10].

Fluid dynamical characterization of porous ceramics for filters thus becomes necessary to understand their permeation behavior. Most of the previous high temperature dust removal studies were carried out with commercial SiC ceramic candle filters in advanced power generation process [2–4,7,8]. Filtration performance in terms of collection efficiency and pressure drop of laboratory made samples are also evaluated using the laboratory test set up to filter nano aerosol particles [8–12]. Very few studies were reported in literature on evaluation of filtration performance of the ceramic candle filter using laboratory made test set up to filter coal fly ash particles in actual power generation conditions [13,14]. In this paper, we have fabricated SiC candle filter using a small amount of clay and alumina as the binder phase additives. The formation of the oxide binder phase in final ceramics was examined, the microstructural features of the candle filter were explained and the mechanical strength was determined. The air permeation

* Corresponding author.
E-mail address: nijhuma@cgcri.res.in (N. Kayal).

https://doi.org/10.1016/j.matpr.2020.04.090
2214-7853/© 2020 Elsevier Ltd. All rights reserved.
Selection and Peer-review under responsibility of the scientific committee of the 2nd International Conference on Recent Trends in Metallurgy, Materials Science and Manufacturing.

Please cite this article as: D. Das and N. Kayal, Permeability and dust filtration behaviour of porous SiC ceramic candle filter, Materials Today: Proceedings, https://doi.org/10.1016/j.matpr.2020.04.090

Available online at www.sciencedirect.com

ScienceDirect

Materials Today: Proceedings 21 (2020) 1069–1077

materialstoday: PROCEEDINGS

www.materialstoday.com/proceedings

ICRACM-2019

Processing of Si-Mo-SiC composite by infiltration of silicon metal alloy into coir fibre derived bio-preform

Pulak Sardar, Dulal Das and Nijhuma Kayal*

CSIR-Central Glass and Ceramic Research Institute, 196, Raja S.C.mullick Road, Kolkata-700 032, West Bengal, India

* Corresponding author. Tel. : +91-33-2473469/3496 Extn. 3241; FAX: +91-33-24730957

Abstract

Fibreboards made of coir fibres were converted to carbon templates by controlled thermal processing which were further infiltrated and reacted with Mo-Si alloy containing 90.4wt% Si, at 1400-1550°C in vacuum. Depending on infiltration temperature the composition of the final composite varied containing mainly SiC, $MoSi_2$, unreacted Si and C. Morphology and the phase distribution of the final Si-Mo-SiC composite determined by scanning electron microscopy and X-ray diffraction technique. Micro- hardness test at different loads was carried out using a Vicker's micro-hardness tester. The sample prepared at 1400°C showed best hardness property.

Keywords:Coir fibre;morphology;SiC composite;microhardnes; infiltration

1. Introduction:

SiC ceramics and SiC based composites exhibit unique combination of properties, such as, high strength, excellent oxidation, corrosion and wear resistance, high thermal conductivity, high hardness, good thermal shock resistance, etc. These properties make SiC ceramics suitable for a wide range of engineering applications, such as kiln furniture, mechanical pump seals, rocket nozzle components, satellite mirrors, armours, molten metal filters, gas filters, catalyst support structure, bio-medical implants, etc.[1-4]. However processing of SiC ceramics requires very high

*Corresponding author. Tel. : +91-33-2473469/3496 Extn. 3241; FAX: +91-33-24730957
E-mail address: nijhuma@cgcri.res.in

2214-7853© 2019 Elsevier Ltd. All rights reserved.
Selection and peer-review under responsibility of SIXTH INTERNATIONAL CONFERENCE ON RECENT ADVANCES IN COMPOSITE MATERIALS, ICRACM-2019.

Journal of Materials Science Research and Reviews

2(2): 1-25, 2019; Article no.JMSRR.46033

Review on Oxide Bonded Porous SiC Ceramics: Processing, Properties and Applications

Dulal Das[1] and Nijhuma Kayal[1*]

[1]Central Glass and Ceramic Research Institute, CSIR, 196, Raja S. C. Mullick Road, Kolkata-700 032, India.

Authors' contributions

This work was carried out in collaboration between both authors. Both authors read and approved the final manuscript.

Article Information

DOI: 10.9734/JMSRR/2019/46033
Editor(s):
(1) Dr. Anjanapura V Raghu, Professor, Department of Basic Science, Centre for Emerging Technology, Jain Global Campus, Jain University, India.
Reviewers:
(1) Yuan-Tsung Chen, National Yunlin University of Science and Technology, Taiwan.
(2) Ahmad Adlie Shamsuri, Universiti Putra Malaysia, Malaysia.
Complete Peer review History: http://www.sciencedomain.org/review-history/27940

Review Article

Received 09 October 2018
Accepted 12 December 2018
Published 24 December 2018

ABSTRACT

Recently the use of porous SiC ceramics is increasing tremendously for various industrial applications due to its excellent properties. Various processing techniques are tried to develop porous SiC ceramics. The fabrication of porous SiC ceramics by an oxidation bonding technique offers several advantages like good oxidation resistance because of air sintering of the ceramics, low sintering temperature, cost effectiveness and easy control over the porosity and other properties of the resultant ceramics. This review deals with processing strategies of oxidation bonding technique. The effect of pore former, powder size, sintering temperature and sintering additives on the properties of the oxide bonded porous SiC ceramics are discussed in detail. The available literatures are thoroughly reviewed with emphasis on mechanical properties, thermal shock resistance properties, gas permeability behavior and separation of particulate from off gas. This review has also enlightened future scope on processing of oxide bonded porous SiC and its usage in various applications.

Keywords: Porous SiC; oxide bond; mechanical properties; gas permeabilty; thermal shock resistance.

**Corresponding author: Email: nijhuma@cgcri.res.in;*